NOVEMBER 1960 VOLUME 9 (1960) No. 2

GEORGE M. SINCLAIR LIBRARY
UNIVERSITY OF HAWAII
8-7-63

NUCLEAR INSTRUMENTS & METHODS

A JOURNAL ON ACCELERATORS, INSTRUMENTATION AND TECHNIQUES IN NUCLEAR PHYSICS

EDITOR: K. SIEGBAHN - UPPSALA

CONTENTS

H. JUNG, PH. PANUSSI und J. JÄNECKE, Reversible Verstärkungsänderungen von Photomultipliern bei unterschiedlichen Zählraten 121
HELMUT PAUL, Higher order chance coincidences in a fast-slow coincidence arrangement 131
É. KISDI-KOSZÓ and L. TURI, Phase- and vertical stability of microtrons 137
T. WESTERMARK, L. DEVELL and N. A. GHANEM, On the use of bremsstrahlung for the determination of tritium in aqueous and organic systems 141
S. RABOY and C. C. TRAUL, A note on the background in NaI scintillation counters 145
R. S. WEAVER and R. E. BELL, Method of evaluating delayed coincidence experiments . . . 149
M. SAKAI, H. IKEGAMI and T. YAMAZAKI, Sector-type double-focusing beta-ray spectrometer 154
O. J. ORIENT, On the mechanism of multiple discharges in halogen-quenched G.M. counters 165
H. R. E. TJIN A DJIE, F. J. DE HEER and L. A. CH. KOERTS, Small scattering chamber for large angular region 172
L. C. THOMPSON, A method for the measurement of gamma-ray spectra in omnidirectional gamma-ray fields 175
C. H. VINCENT, The rapid recognition of a significant increase in the rate of arrival of pulses occurring at random 181
G. CAGLIOTI, A. PAOLETTI and F. P. RICCI, On resolution and luminosity of a neutron diffraction spectrometer for single crystal analysis. 195
W. L. RAUTENBACH, A high temperature sputtering ion source for a laboratory isotope separator 199
L. G. PREUSS et J. P. ESCARFAIL, De la décomposition des intensités spectrales en courbes de Gauss 212
R. W. FINDLEY, R. A. REITER and T. A. ROMANOWSKI, A precision clock for measuring time intervals 221
S. S. GLICKSTEIN and R. G. WINTER, Nuclear reactions from recoil protons in a reactor . 226
W. R. DIXON and J. H. AITKEN, Pulse shape discrimination and energy response of calcium tungstate crystals 229
P. GRIVET et H. HAHN, La stabilisation du champ magnétique par un maser à résonance magnétique nucléaire 233
BOOK REVIEWS 242
NEWS ITEM 243
ERRATA 244

NORTH-HOLLAND PUBLISHING COMPANY — AMSTERDAM

NUCLEAR INSTRUMENTS AND METHODS

A journal on accelerators, instrumentation and techniques in nuclear physics

EDITOR: K. SIEGBAHN, UPPSALA

EDITORIAL BOARD:

J. B. ADAMS (CERN)
F. A. ALSINA (Buenos Aires)
E. AMALDI (Rome)
H. L. ANDERSON (Chicago)
K. T. BAINBRIDGE (Cambridge, Mass.)
P. R. BELL (Oak Ridge)
R. E. BELL (Montreal)
A. BERTHELOT (Saclay)
H. BRINKMAN (Groningen)
E. H. COOKE–YARBOROUGH (Harwell)
S. DE BENEDETTI (Pittsburgh)
M. DE HEMPTINNE (Louvain)
A. DE-SHALIT (Rehovoth)
M. DEUTSCH (Cambridge, Mass.)
S. DU TOIT (Pretoria)
B. S. DŽELEPOV (Leningrad)
W. GENTNER (Heidelberg)
P. C. GUGELOT (Amsterdam)
H. HALBAN (Paris)
O. HAXEL (Heidelberg)
P. HUBER (Basel)
S. KIKUCHI (Tokyo)
J. KOCH (Copenhagen)
M. S. KOZODAEV (Moscow)
S. LIVINGSTON (Cambridge, Mass.)
E. M. MCMILLAN (Berkeley)
M. G. MEŠČERJAKOW (Moscow)
P. B. MOON (Birmingham)
M. L. OLIPHANT (Canberra)
W. PAUL (Bonn)
A. S. RAO (Bombay)
G. SALVANI (Rome)
P. SAVIĆ (Belgrade)
P. SCHERRER (Zürich)
CH. SCHMELZER (CERN)
R. TANGEN (Oslo)
D. TAYLOR (Northampton)
V. I. VEKSLER (Moscow)
G. VON DARDEL (CERN)
O. WERNHOLM (Stockholm)
R. R. WILSON (Cornell)
S. D. WINTER (Saclay)

INSTRUCTIONS FOR CONTRIBUTORS

Contributions may be sent to the Editor, Professor K. Siegbahn, Institute of Physics, University of Uppsala, Sweden, either directly or through the intermediation of one of the members of the Editorial Board Contributions may be written in English, French or German but should always, except for very short papers, be supplied with a brief abstract in English. Figures should be in inked original drawings or glossy prints and they should be sufficiently large. Contributors should make sure that important details in drawings and photographs will show up clearly in the diminished copy used by the publisher.

Books for review should be sent to Professor Siegbahn.

Objective and descriptive material on endeavours and product developments from the industry for the section "Spotlight on Industry" should be sent directly to the publishers, North-Holland Publishing Company, P.O. Box 103, Amsterdam.

Nuclear Instruments and Methods is published monthly. The subscription price of a volume of 360 pages is $ 17.00 (130 s), postage free.

Subscription should be sent to the publishers, North-Holland Publishing Company. P.O. Box 103. Amsterdam or to any subscription-agent.

No part of this issue may be reproduced in any form, by print, photoprint, microfilm or any other means without written permission from the publisher.

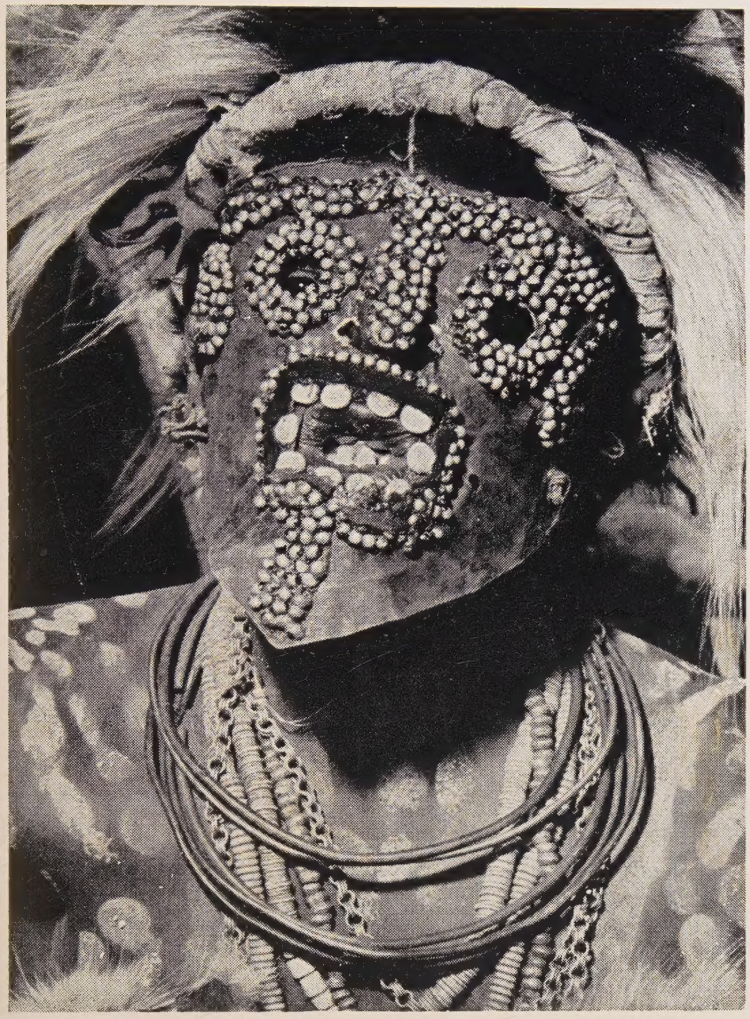

PHILIPS

NDO

Even against the seemingly mysterious threats to human life which radioactivity can entail, health physics does not make use of the magic invariably resorted to by the witch doctor.

For the detection and measurement of radioactive radiation a great variety of methodically developed equipment is available to provide an effective health protection service.

The increasing application of radioactive sources in industrial processes and the growing number of nuclear reactors which are coming into use, call for constantly intensified care on the part of Health Physics Officers in their efforts to protect the growing numbers of people coming daily into close contact with ionizing radiation.

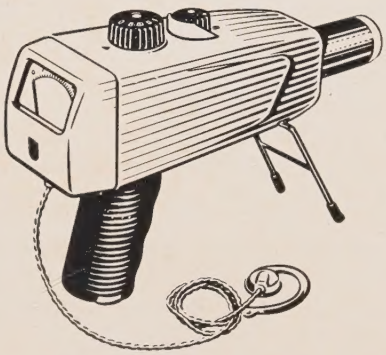

modern witchcraft

Philips produce indispensable aids in a range extending from small monitors and dosimeters for the protection of individual workers to permanent monitoring, multi-channel installations for the coverage of buildings and surroundings of reactors, nuclear research laboratories or "hot labs".

N.V. PHILIPS' GLOEILAMPENFABRIEKEN - EINDHOVEN - HOLLAND

PHILIPS
nuclear equipment

Particle accelerators ● Reactor control instrumentation ● Health protection and monitoring equipment ● Radiation measuring and detection equipment ● Geiger counter tubes ● Photomultipliers ● Radio-active isotopes ● Vacuum measuring equipment ● Air and gas liquefiers.

Eldorado

DECIMAL SCALERS
FOR THE NUCLEAR PHYSICIST

...and Fast

Eldorado solid state all-electronic scalers count random events at a maximum rate of over one million counts per second. Resolving time is less than 1.0 microsecond. Especially well-suited for accelerator counting room service, these compact instruments weigh just 13 pounds and use ⅓ fewer transistors than comparable models. They can be used wherever the advantages of complete transistorization are important.

Eldorado offers three standard models in the SC-750 series, each with built-in regulated power supply. Two models provide full electronic storage of 10^7 and 10^8 counts. The third has 3 decades of electronic storage and a 4-digit mechanical register. Special versions can be furnished with other counting combinations and provisions for readout to a printer or tape punch.

KEY SPECIFICATIONS

SCALER	
Resolution	Better than 1.0 microsecond
Max. Counting Rate	Greater than 1 megacycle
AMPLIFIER (optional)	
Minimum Input Signal	10 millivolts
Overload Recovery	10 X, 7 microsecond
DISCRIMINATOR TYPE	Integral
RANGE	1 to 11 volts
SIZE	19 x 3¼ x 10½ inches

Eldorado can furnish scalers and counters to fit your specific application. For more details, please address Dept. **79**

Eldorado
Electronics
2821 Tenth Street
Berkeley 10, California

nuclear physics

FOR PULSED NEUTRON & TIME-OF-FLIGHT STUDIES • GAMMA AND COINCIDENCE PAIR SPECTROSCOPY

health physics

FOR WHOLE BODY COUNTERS • BIOLOGICAL ASSAYS • FALLOUT ANALYSES

radiochemistry

FOR QUALITATIVE AND QUANTITATIVE ANALYSES

reactor engineering

FOR REACTOR CONTROL DESIGN • FUEL ROD ANALYSIS

mass spectroscopy

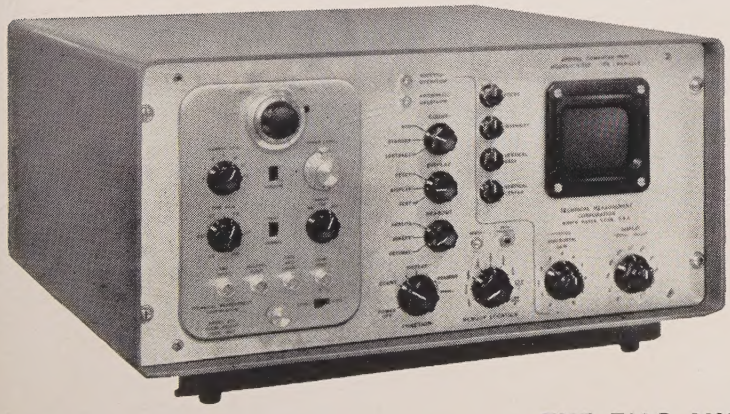

and for other areas of research involving pulse or time measurements . . .

THE TMC MULTICHANNEL ANALYZER
MODEL CN-110

First and finest of all transistorized multichannel analyzers, the CN-110 is now widely used throughout the U.S., Canada and Europe. Its interchangeable plug-in logic, 256-channel basic computer and associated data handling units are unconditionally guaranteed for one full year and backed by an unequalled service policy. Call or write for complete specifications.

TMC **TECHNICAL MEASUREMENT CORPORATION**
441 WASHINGTON AVE., NORTH HAVEN, CONN. • CE 9-2501

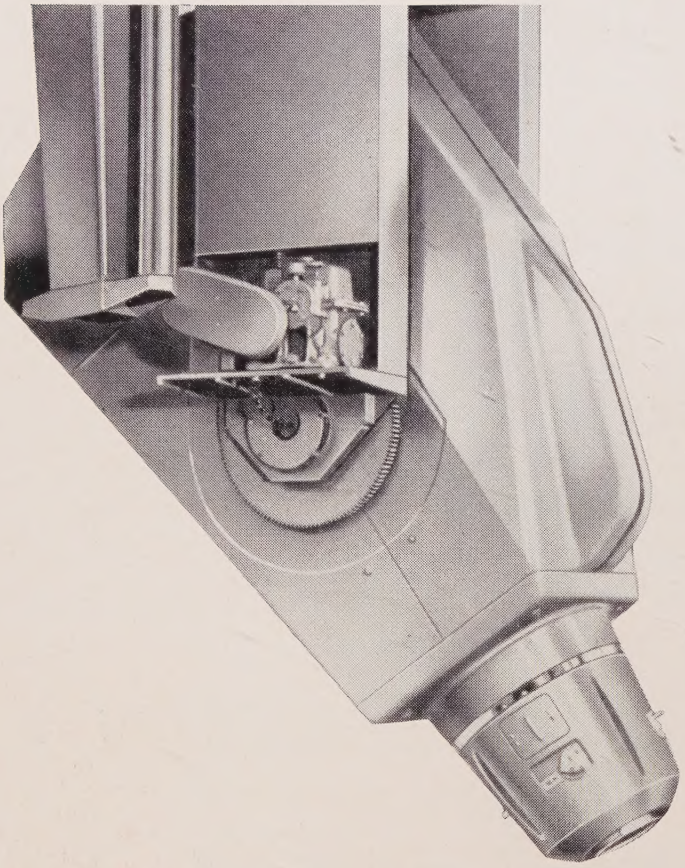

electron linear accelerators for research, industry and medicine

by Mullard Equipment Limited

Electron Linear Accelerators manufactured by Mullard Equipment Ltd. are the logical result of wide and detailed experience in this field. Machines for all types of applications are available, from the standard 4.3 MeV model to equipments specially built to meet individual requirements with electron beam energies up to 50 MeV.
The units are designed for continuous operation, ease of control and high reliability.

STANDARD MACHINE OPERATING AT 4.3 MeV

Mean power output at 500 pulses per second	850 W (electrons)
Maximum pulse repetition frequency.....	500 p.p.s.
Electron pulse length.....	1.65 microseconds
When used as an X-Ray source maximum X-Ray output is approximately.....	600 röntgens per minute at 1 metre

MULLARD EQUIPMENT LIMITED

Mullard House · Torrington Place
London W.C.1 · Tel: LANgham 6633

RESEARCH Now regarded as indispensable in many research laboratories Linear Accelerators can be fitted with supplementary heads to provide X-Rays or neutrons. Present day applications include investigation of properties of irradiated materials; preservation of food; basic studies on structure of organic molecules; modification of the properties of plastics.

INDUSTRIAL RADIOGRAPHY The compact accelerator design with wide range of movements and precision positioning enables radiographs of complicated heavy metal sections to be taken with minimum setting-up times. The high X-Ray output gives short exposure time and the extremely small (2mm) focal spot gives the highest possible definition. Penetration is sufficient to radiograph steel sections up to 12 inches thick.

MEDICAL THERAPY The use of Linear Accelerators for X-Ray and Electron Medical Therapy is well established. These machines give rapid treatment times with precisely defined fields and negligible 'penumbra' effects. Skin and exit dosages are minimised.

ME 664

DYNAMITRON

Dynamitron ion accelerator, featuring high beam current, constant potential, and "industrial" reliability, for fundamental and applied research.

RADIATION DYNAMICS, INC.

FOR FURTHER INFORMATION ..... WRITE DEPT. RSI-6

Westbury Industrial Park
Westbury, Long Island, N.

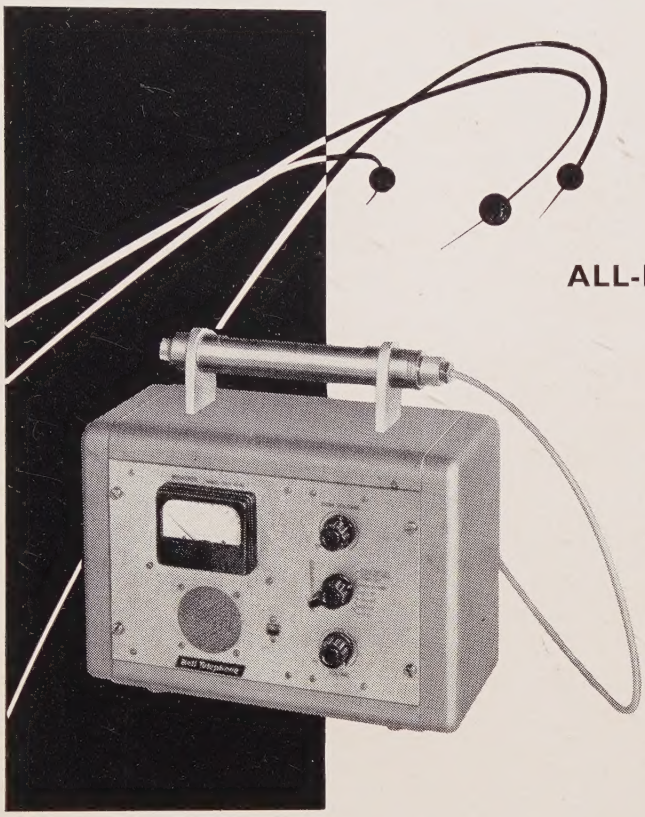

ALL-ROUND, LOW PRICED MONITOR

Typically developed as a laboratory equipment the monitor 111-A1 combines quality and high performance with low cost.

- Completely transistorized
- Designed as portable type
- Very low count rate: 0 to 5 c.p.s. full scale
- Highest count rate: 0 to 5000 c.p.s. full scale
- Equalizing accumulators
- Automatically recharged from A.C. mains
- Priced $ 410 F.O.B. Antwerp

For further information on this and other applications in the field of "Electronics for Nucleonics" ask :

AN ITT ASSOCIATE

Bell Telephone Mfg Co

"NUCLEAR ENERGY DIVISION"
33, Berkenrodelei
HOBOKEN-Antwerp
Belgium

NORTH-HOLLAND BOOKS

Paul Ehrenfest

COLLECTED SCIENTIFIC PAPERS

XII + 632 pages

Guilders 45,00 (90s.)

This volume makes widely scattered publications readily available. All Dutch articles appear here in English; the German publications are in the original language.

Sole Agency for U.S.A.:

Interscience Publishers Inc. — New York

NORTH-HOLLAND PUBLISHING COMPANY - AMSTERDAM

FOR SCINTILLATION & PROPORTIONAL COUNTING

Non-overloading Linear Amplifiers

MODELS 108 and 108 p

* GAIN–40,000, continuously variable
* RISE TIME–0.2 microsecond
* ACCEPTS + AND — PULSES

Tremendous Dynamic Range

EXCEEDS 1,000,000 (0.1 mV to 100 V)

Excellent linearity for small pulses in the presence of tremendous overloads that paralyze other amplifiers.
Model 108 P includes precision trigger type Pulse-Height Selector.

Model 413 Mercury relay precision sliding Pulser

The **one** pulser that fills **every** need
of the Nuclear Physics Laboratory
0 to 100 Volts

10 full scale ranges from 1 mV to 100 volts
Fast rise and exponential decay of 1, 3, 10. 30, and 100 microsec simulate pulses from scintillation, proportional and Geiger counters.
Incorporates both manual control and precision motor drive.
The ideal instrument for precise calibration and test of pulse-height analyzers and other nuclear instrumentation.

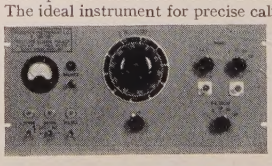

Window widths are determined AUTOMATICALLY, 10 × more ACCURATELY, 40 × FASTER than with conventional pulsers.

Model 108 Amplifier . . . . . $ **545.00**
Model 108 P Amplifier (includes pulse-height selector) $ **595.00**
Model 413 Precision Sliding Pulser . . . . . $ **630.00**
Prices f.o.b. Silver Spring. Md.

RADIATION INSTRUMENT CO.

P.O. BOX 733 SILVERSPRING, MARYLAND, U.S.A.

Let's Talk About RATEMETERS . . .

Pictured left to right: Transistorized Dual Ratemeter; SC-80 Ratemeter Spectrometer; SC-79 Tracermatic Ratemeter and Model SC-91 Scaler-Ratemeter.

One glance at the vast array of ratemeters on the market today and you can readily realize the growing importance of these instruments for use in radioisotope laboratories and clinics. To help select the one best ratemeter for you from this bewildering variety of models, a simple seven-point check list has been developed. Before making a decision, consider these points carefully:

1. Range and Number of Scales
2. Range and Number of Time Constants
3. Stability and Range of the High Voltage Supply
4. Stability of Calibration
5. Low Zero Drift
6. Functional Design
7. Cost

When you examine the Tracerlab line, we believe you will find that for versatility, quality, ease of operation, precision and real value, you simply can't beat Tracerlab Ratemeters.

For example, Tracerlab's standard laboratory ratemeters offer a choice of nine full-scale ranges from 0-100 c.p.m. all the way up to 0-1,000,000 c.p.m. with intermediate ranges in multiples of 3 and 10. This extremely wide choice of ranges provides the versatility you require in selecting the optimum range for any given application.

Number and range of time constants is important, too (Tracerlab's standard laboratory ratemeter has eight). Very short time constants on the upper range scales permit rapid response with no significant increase in probable error while longer time constants on the lower ranges will damp out most of the statistical fluctuations common to these count rates. On the higher ranges a minimum time constant of 0.05 seconds is provided, while for low count rates, a 40 seconds time constant is available. Tracerlab Ratemeters have stability of calibration and zero drift is virtually eliminated.

The ratemeter you select should have a precision high voltage power supply with a high degree of regulation to insure negligible output voltage changes when input voltage varies. The power supply output voltage of Tracerlab Ratemeters changes less than 0.003% for a 1% change in input voltage. As a result, they can be used with scintillation as well as geiger detectors. What's more, you don't need to buy an additional power supply when you use a Tracerlab Ratemeter with a Spectrometer. Why? Because standard equipment on all Tracerlab Spectrometers includes a super regulator that provides all the additional stability your Tracerlab Ratemeter power supply needs for precision spectrometry.

Should you require an unusually compact, low power, dual channel Ratemeter with the operating benefits of solid state circuitry, Tracerlab offers an all-transistor instrument. This light weight precision built unit provides both linear or log response, plug-in construction, dual power supply and, when desirable, a Spectrometer input. Very low power consumption and heat dissipation contribute substantially to the long life and reliability of these fully transistorized units.

Tracerlab also offers a Basic Ratemeter and Laboratory Monitor, a compact instrument of simple circuitry designed for laboratory use and 24-hour-per-day operation.

Last, but by no means least, Tracerlab Ratemeters are low in cost, yet they incorporate numerous hidden plusses and extra values. Their inherent quality and advanced design is the result of years of specialization in nuclear instrumentation. A large staff of nuclear applications engineers and a world-wide network of authorized service representatives back up all claims made for satisfactory and lasting performance.

For further information on Tracerlab Ratemeters and the complete line of Tracerlab nuclear instruments, write for General Catalog F.

Tracerlab *first in radiation measurement*

TRACERLAB, INC. • 1610 Trapelo Rd., Waltham 59, Mass. • 2030 Wright Ave., Richmond, Calif.

European Office: TRACERLAB (Holland) N.V. 119 Singel, Amsterdam, Netherlands

maximum accessibility for servicing...
maximum flexibility of data presentation...

AEI PULSE HEIGHT ANALYSER

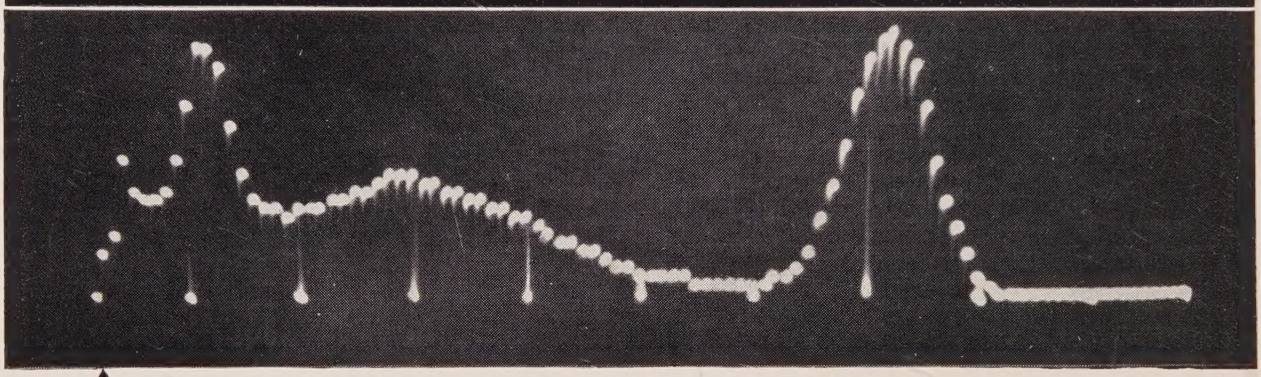

Typical presentation of analogue count on the CRT. This is the gamma spectrum of gold foil irradiated for 30 minutes at a neutron flux of 2×10^8 n/cm²/S. The curve and two significant peaks are due to ^{198}Au.

* Unit construction for easy servicing
* Analogue presentation on cathode ray tube or chart recorder
* Decimal presentation on Dekatrons or 3″ paper tape
* Ferrite memory prevents loss of count if mains fail
* Circuitry largely transistorised for reliability
* 100 Channels, capacity 65,535 pulses per channel
* Console or rack-mounted versions.

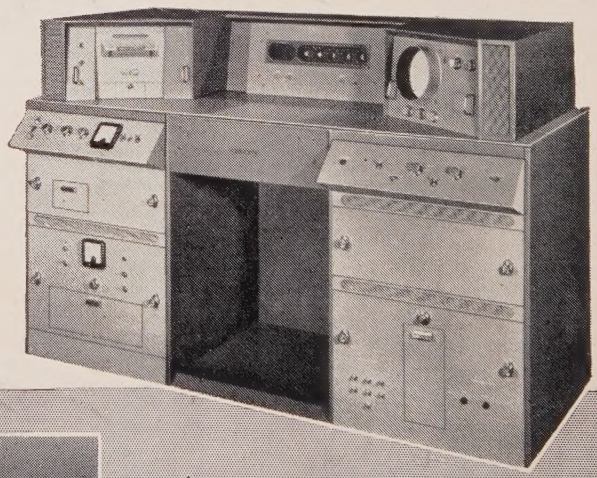

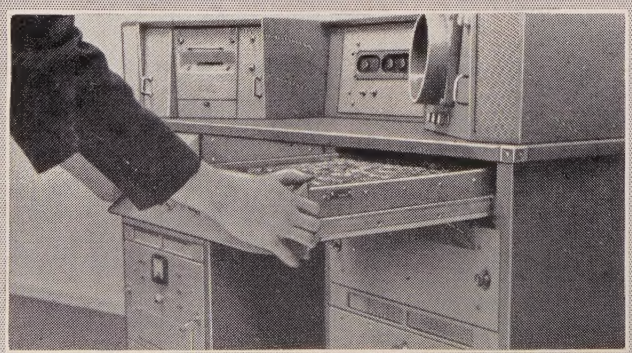

All units draw out on runners so that servicing and setting up can be accomplished without switching off power or removing inter-connecting cables.

A full technical specification of the P.H.A. is given in publications 2451-70 available from:

AEI

Instrumentation Division
Associated Electrical Industries Limited
P.O. BOX 1 - Harlow - Essex - ENGLAND

sc/10

Fewer components . . . greater reliability

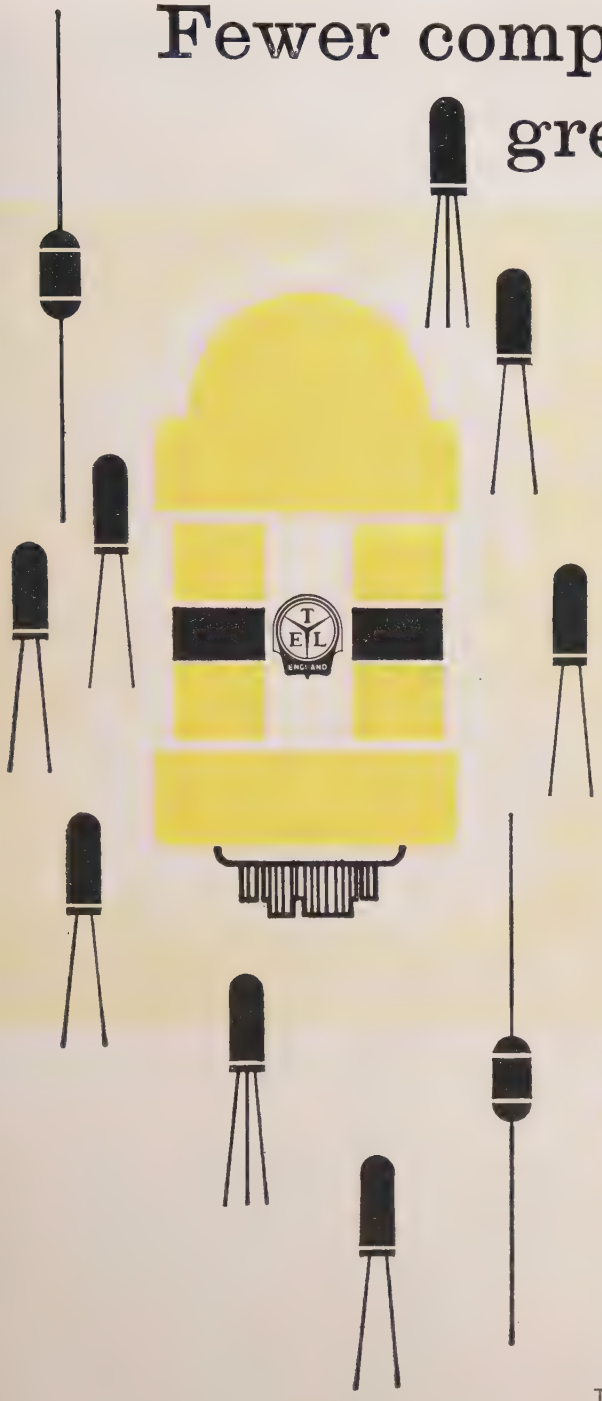

Reliability is not the easiest of terms to define—someone else's definition inevitably takes no account of your own requirements. Yet on one thing all agree, there are only two ways to get greater circuit reliability, one is to choose only the best components and the other to reduce the numbers used. Here difficulties arise for although there are many excellent component alternatives it is only rarely that there becomes available a device which will, without sacrificing performance, allow big component saving.
Trochotron Beam Switching Tubes are such devices.
With the 28V VS.10.K, the Ericsson range has been further extended to give Trochotron reliability at low voltage working and here again component saving is remarkable. For instance, in conventional transistorized decade counters with visual readout, transistors and diodes may number about 90, whereas using the VS.10.K Trochotron this total is reduced by about *ninety percent.*
If, therefore you are concerned with counting, frequency dividing, timing, programming, gating etc., make sure you get greater reliability with fewer components by using Etelco Trochotron Beam Switching Tubes.

28V TROCHOTRON VS.10.K

Heater.....6.3 or 28.0 V
Max. spade to cathode voltage.....30 V
Min. spade to cathode voltage.....24 V
Target current.....2.0 mA nom.
Counting speed.....1 Mc/s

The whole range of Trochotrons is being colour coded for ease of identification. VS.10.G-Red. VS.10.H-Yellow. VS.10.K-Green.

For booklet and leaflets please write to:-

TUBE DIVISION
BEESTON NOTTINGHAM

ETELCO

ETELCO LIMITED · HEAD OFFICE · 22 LINCOLN'S INN FIELDS LONDON W.C.2
TR.11a

Elcor inc.
1225 W. BROAD ST.
FALLS CHURCH, VA.

MODEL A 309
CURRENT INDICATOR AND INTEGRATOR

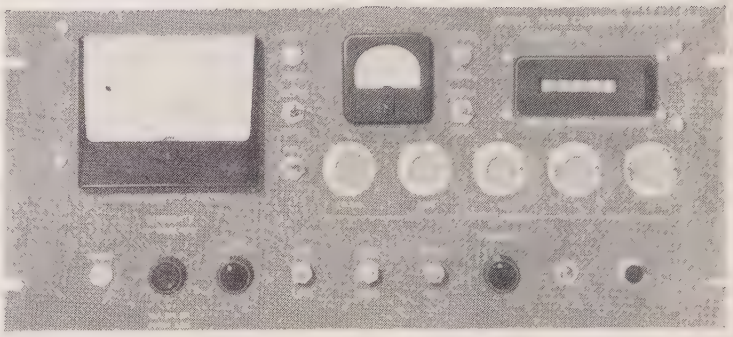

MODEL A 309 A

FEATURES

- Wide current range: 1 x 10^{-3} to 3 x 10^{-9} amp. in 12 switch settings.
- High accuracy: 1% of full scale.
- Internal calibrating current source to check proper operation.
- Front panel switch allows instrument to be used with current of either polarity.
- Pre-setting feature provides means of safeguarding against over-exposure.
- Developed especially for use with Van de Graaff and other high-voltage accelerators.
- Permits many experiments with particle accelerators that would otherwise be difficult or impossible.
- Register readout gives digital accuracy on charge measurement.

The versatility and accuracy of two instruments in one!

1. Measures currents from 1 milliampere to 3 milli-microamperes.
2. Integrates input current and registers accumulated charge.

GENERAL DESCRIPTION –The Model A309 Current Indicator and Integrator is a sensitive current indicator that also measures the total charge collected in a given length of time. Developed especially for use with high-voltage particle accelerators such as the Van de Graaff generator, the instrument is also ideally suited for other applications requiring the measurement of accumulated charge or the integration of a variable current.

The full-scale sensitivity of the instrument can be varied from 1 milliampere to 3 milli-microamperes in twelve ranges. For convenience in checking the performance and accuracy of the instrument, an internal calibrating current source is provided for each range. The accumulated charge is indicated on a 5-decimal digit register. Any number up to 99,999 can be preset into the instrument, and upon reaching the corresponding charge a relay closes to actuate a warning device or control auxiliary equipment. In applications where X-rays are being generated, this feature affords protection against accidental over-exposure.

Input current of either polarity can be measured and integrated, and a front panel switch enables the instrument to be immediately changed from one polarity to the other. Advanced circuit techniques have been employed to achieve low input impedance, negligible drift, and a high overall accuracy and reliability.

Two models are available with the same specifications except for the method of presetting. In the Model A309A the presetting means consists of five front-panel switches. Presetting in the Model A309B is accomplished by manual adjustment of five presetting wheels that are accessible through the hinged cover of the register used in this model.

SPECIFICATIONS

1. Input current for full-scale meter deflection — 1 x 10^{-3} to 3 x 10^{-9} ampere in twelve switch settings.
2. Polarity of input current — positive or negative, controlled by front-panel switch.
3. Current indicating means — 4½" meter.
4. Charge indicating means — 5-decimal-digit register and 2½" meter
5. Maximum charge indicating capacity — 99,999 units.
   Note: Each unit is equal to one coulomb multiplied by the numerical value of the full-scale current.
6. Maximum integrating time — 28 hours.
7. Integrating rate for full-scale current — 1 unit per second.
8. Method of presetting:
   Model A309A — five front-panel switches.
   Model A309B — five presetting wheels in register.
9. Accuracy (Indicating and integrating accuracy, based on full-scale current) — 1%.
10. Maximum drift — .01% per hour.
11. Maximum input voltage for full-scale current — 2 millivolts.
12. Minimum signal-source impedance for 1% accuracy — 1 ohm divided by numerical value of full-scale current.
13. Calibration — Internal reference current provided for each current range.
14. Power Input — 110–125 volts, 50-60 cps.
15. Dimensions — 19" wide x 8¾" high x 13¼" deep.
16. Mounting — standard 19" relay rack.
17. Weight — approximately 25 lbs.
18. Price: Model A309A — $1674.00.
    Model A309B — $1524.00.

ELCOR, — INC. • 1225 W. BROAD STREET • FALLS CHURCH, VA.

Telephone JEfferson 2-7718 A subsidiary of Fairfax Manufacturing Co., Inc. Bulletin No. 24-1258

LOW BETA

new
low level
counting
system

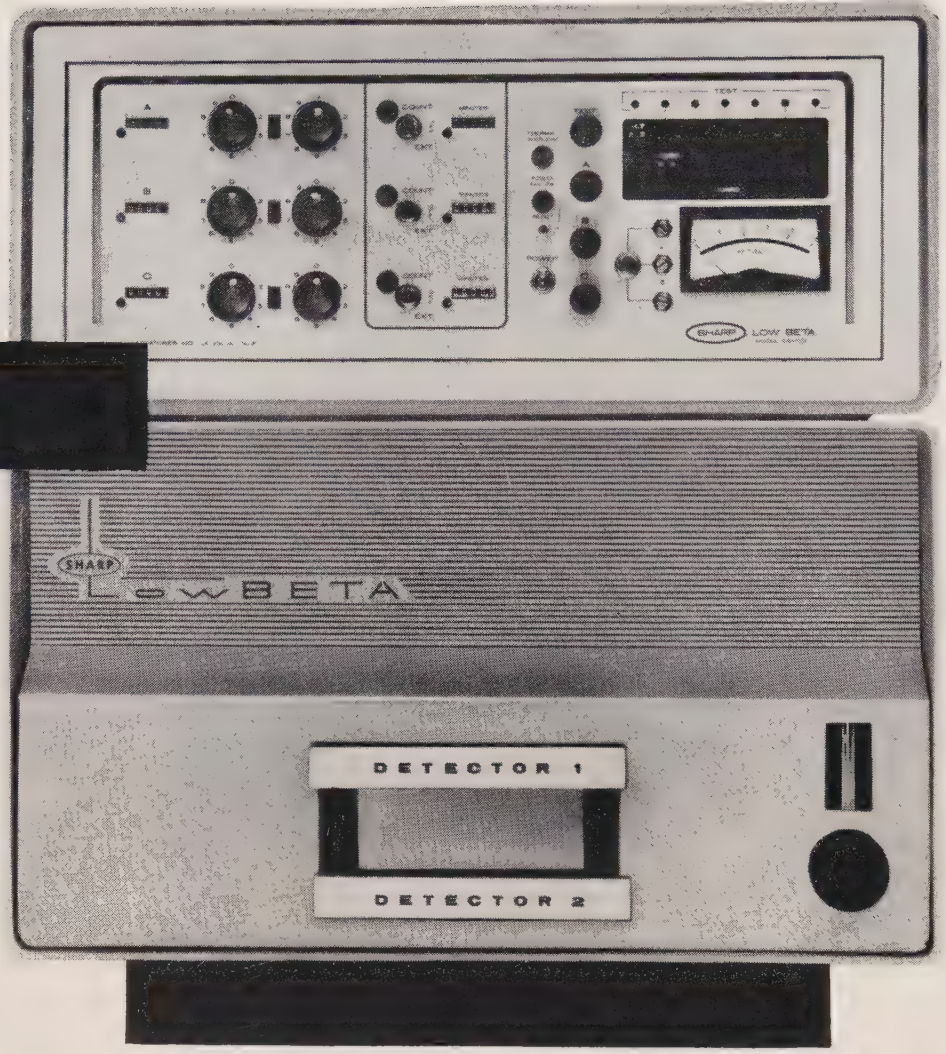

Background less than ¼ count per minute!

Sharp Laboratories has revolutionized the low-level counting field with an instrument with such advanced characteristics that it obsoletes previous designs. Look at these specifications:

- Background less than 0.25 counts per minute for a 1-inch diameter detector.
- Shield size only 18 inches square.
- Shield weight only 1500 lbs.
- All transistorized electronics.
- Plug-in printed circuit cards.
- Illuminated programming panel for simplified control.
- Electronics ideal for carbon dating.

The system pictured is a two-detector, manual, low background beta detection system. Sharp equipment lends itself well to the "building-block" approach. You can convert this basic system to simultaneous alpha-beta measurements on a single sample. Fully automatic operation may be added.

You get the option of simultaneous alpha and beta counting with four channels of readout and two detectors. Automatic readout may be provided in the form of simple printing timers or a complete pre-set count—pre-set time readout system with over-riding control. Available in standard detector sizes of ½″, 1″, 2″ and 3″. Other sizes on special order.

Represented exclusively by BAIRD ATOMIC, INC. See your BAIRD Representative, or write or call Sharp Laboratories, Inc., Dept. NIM-1, Box 1302, La Jolla, Calif., for literature.

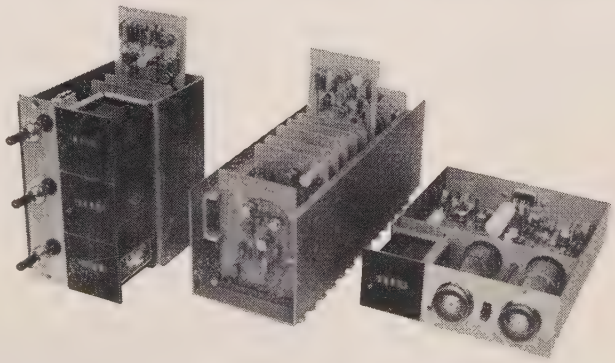

The modular construction of the Sharp low background system is shown here. Shown left to right are the timing module, the printed circuit card file containing the amplifiers and logical circuitry, and one of the three scaler modules.

SHARP

LABORATORIES, INC.

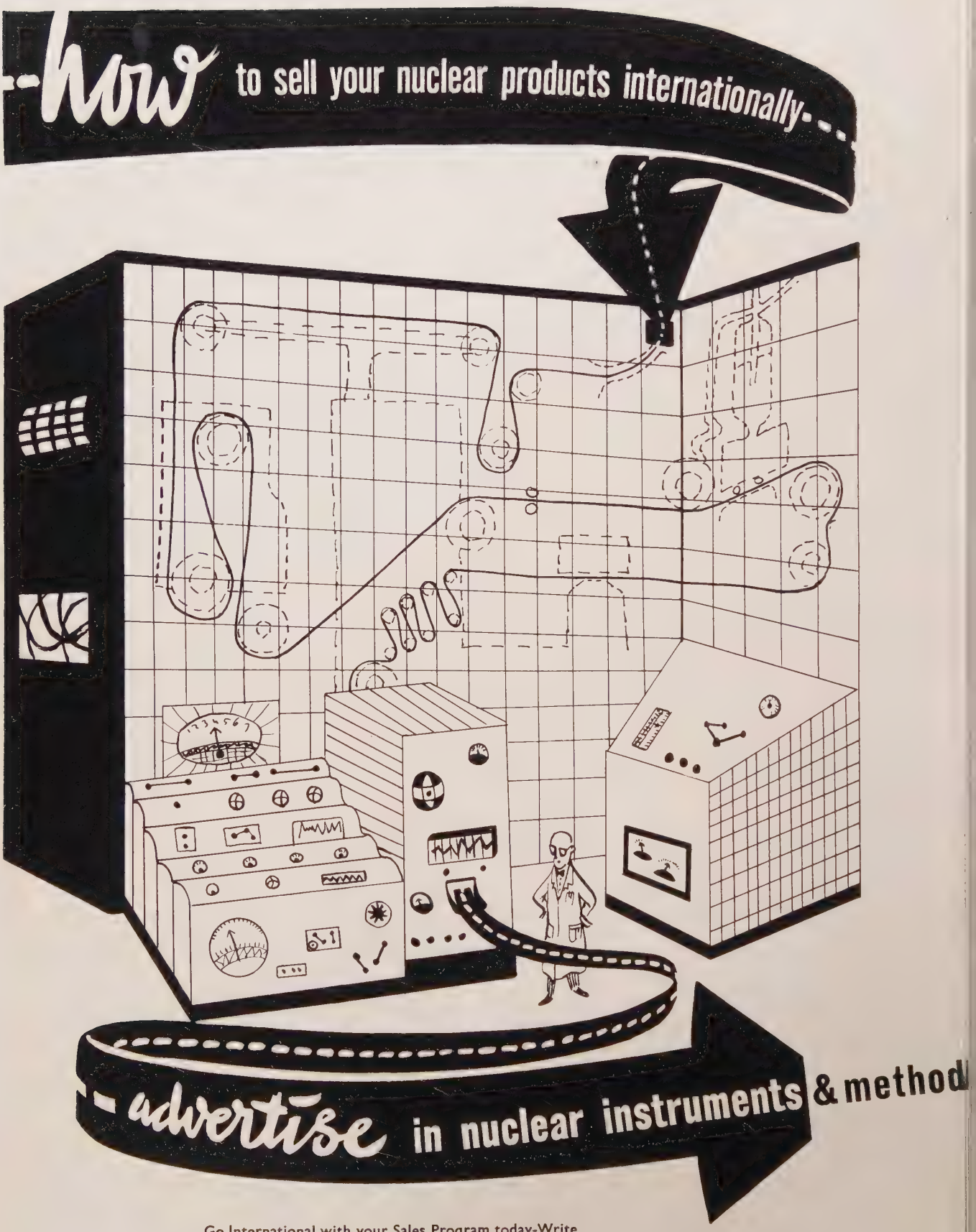

Go International with your Sales Program today-Write

William F. Baars-Advertising Manager, North-Holland Publishing Company

P.O. Box 103, Amsterdam, The Netherlands

Transistorized . . . . . Multichannel Analyzers

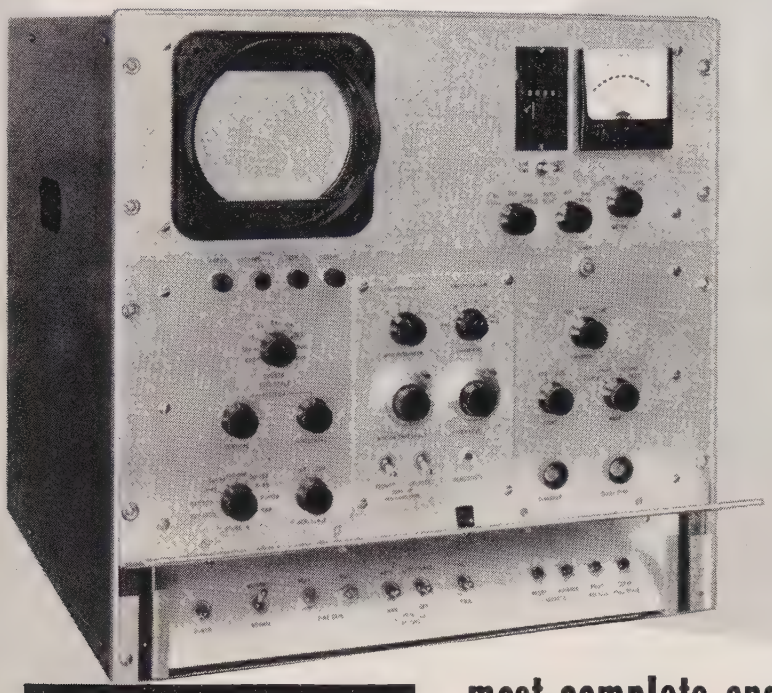

Model 34-8

200-Channel

Model 34-12

400-Channel

- automatic programming including
  - Auto-Print
  - Auto-Record
  - Auto-Transfer
- weight less than 80 pounds
- NOT microminiaturized
- ALL coincidence features
- ferrite core memory
- memory subgrouping
- 10^5 count capacity (10^6 OPT.)
- external programming
- LIVE display
- time analyzer mode
- CRYSTAL controlled live timer
- FAILSAFE channel identification
- simultaneous print and record (OPT.)
- 0.5 percent linearity
- dead time meter
- spectrum transfer circuit

most complete and available line of *TRANSISTORIZED* analyzers

FULLY TRANSISTORIZED . . . Most of the Pulse Height Analyzers produced today are transistorized units, and fully transistorized units have long been in production at RIDL. Full production of complete system RIDL transistorized multi-channel analyzers has allowed RIDL to put many units in the field and to produce additional available 200-channel Model 34-8s and 400-channel Model 34-12s. All models may be operated as **one, two** or **four** independent analyzers, or as multi-channel scalers (time analyzers). All models have **all** the best features of RIDL's best analyzers.

AUTOMATION IN THE LAB . . . RIDL designed the Model 34-8 and Model 34-12 analyzers to save valuable technical man hours through providing such features as **Auto-Print, Auto-Record** and an automatic transfer circuit. A built-in crystal-controlled Live Timer allows automatic **dead time correction.** The addition of automatic **background correction** allows final data readout without laborious manual corrections or replotting of curves.

AUTOMATIC DATA PROCESSING . . . RIDL builds on its maximum development of automatic **data gathering** and **analysis** further possibilities for **automatic data processing.** To normal printing and recording is added readout on **magnetic tape, punched tape,** and parallel or serial entry printers. This allows full control over programming, internal and external data format, and data processing. Whatever your data readout and processing needs may be, our staff is ready at all times to discuss them with you.

SIXTY DAY DELIVERY ON ANALYZERS IN ANY PART OF THE WORLD

Light weight makes AIR SHIPMENT economical.
Chicago to Europe — for example — approximately $150.00
RIDL Representatives are located in most areas of the world.
Contact the RIDL home office for prompt service in locating the sales office nearest you.

RIDL INC.

Radiation Instrument Development Laboratory, Inc.

61 EAST NORTH AVENUE • NORTHLAKE, ILLINOIS

PHONE: MUrray 1-2323 • Cable Address: RADILAB

SETTING NEW STANDARDS

at 99.98% of the speed of light

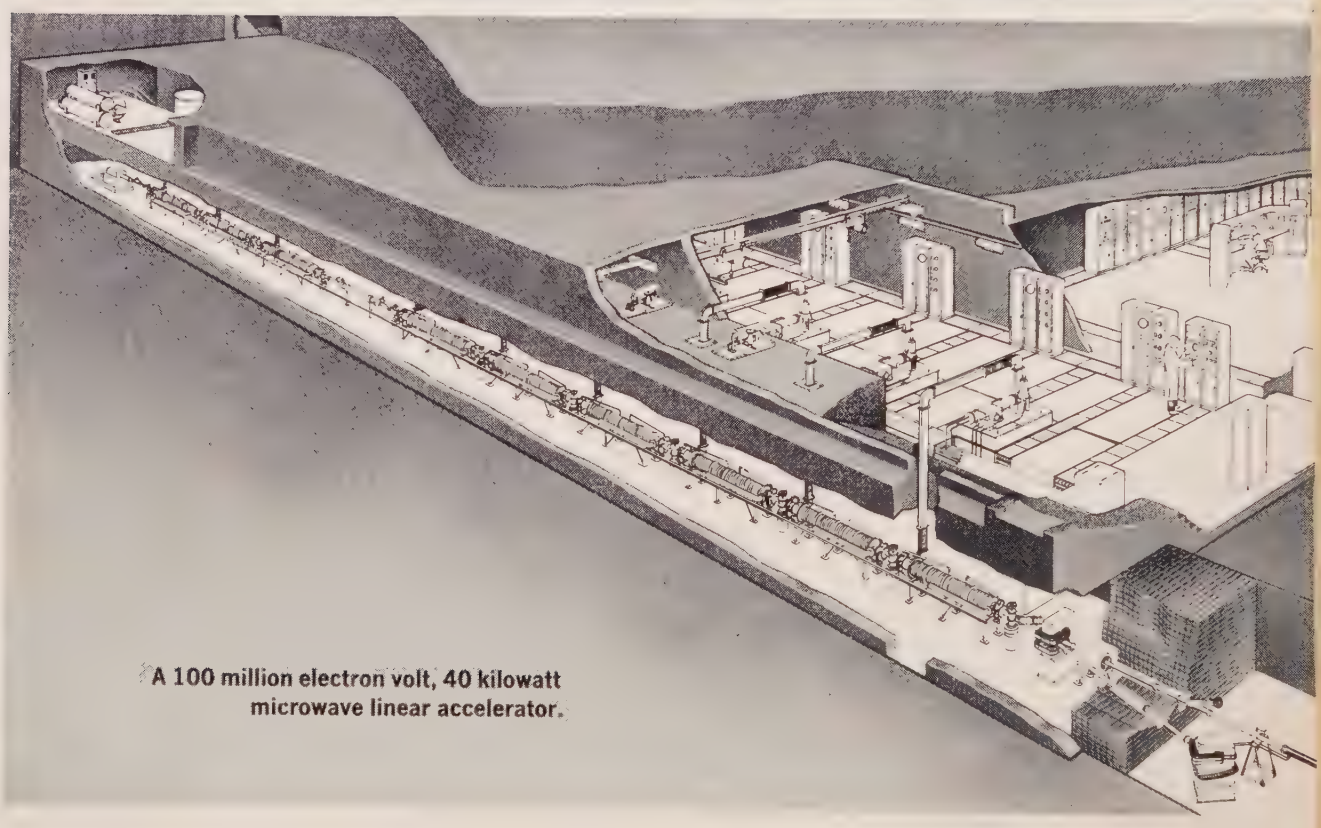

A 100 million electron volt, 40 kilowatt microwave linear accelerator.

One of the world's most powerful when completed, this high-energy electron accelerator will enable the U.S. National Bureau of Standards to carry out extensive programs in:

- ***Nuclear Physics Research***
- ***Radiation Effects***
- ***Dosimetry Standards***

. . . to meet the need for new data in the growing field of applied radiation.

The linear accelerator (Linac) is under construction at the manufacturing and test facility of Applied Radiation Corporation, Walnut Creek, California.

Particle accelerators for science and industry

High Voltage Servicing Company, Ltd.
London, England

High Voltage Engineering (Europa) N.V.
Amersfoort, The Netherlands

HVEC arco

HIGH VOLTAGE ENGINEERING CORPORATION

BURLINGTON, MASSACHUSETTS • U. S. A.

APPLIED RADIATION CORPORATION HIGH VOLTAGE ENGINEERING (EUROPA) N.V.

NUCLEAR INSTRUMENTS AND METHODS 9 (1960) 121–130; NORTH-HOLLAND PUBLISHING CO.

REVERSIBLE VERSTÄRKUNGSÄNDERUNGEN VON PHOTOMULTIPLIERN BEI UNTERSCHIEDLICHEN ZÄHLRATEN†

H. JUNG, PH. PANUSSI und J. JÄNECKE††

Max-Planck-Institut fur Kernphysik, Heidelberg

Eingegangen am 5 August 1960

The time dependence of the gain of several RCA, DuMont and EMI photomultiplier tubes has been measured prior to, during, and after a constant illumination of the photocathode. The light source was a NaI (Tl) crystal irradiated with γ-rays of Cs^{137} or Co^{60}. A change in the counting rate results in rapid and slow variations in the gain.

The rapid gain variations take place within an interval of less than 10 seconds. The amplitude is dependent upon the change in counting rate and the tube chosen. Moreover the sign may be positive or negative for individual tubes of the same type. It may be assumed that a sudden reversible sensitization or desensitization of the photocathode explains the effect.

The slow gain variations after a change in counting rate are made up of two exponential components. The respective saturation value after an increase in counting rate is approached faster than after a decrease in counting rate. The amplitude is dependent upon the average anode current and the high voltage. The slow gain variations of all examined RCA tubes (6342, 6342A, 5819) were found to be negative, whereas the changes of the DuMont 6292 and EMI 6255 tubes were found to be positive. It may be assumed that reversible dynode effects explain the changes.

The different behaviour of the various types of photomultiplier tubes is not correlated to the dynode material. The absolute value of the gain variations of all tubes examined were approximately of the same magnitude under comparable conditions.

1. Einleitung

Für viele Untersuchungen mit Photomultipliern benötigt man eine konstante Verstärkung. Es ist bekannt, dass die Verstärkung eines Multipliers von der Zählrate abhängen kann. Diese Abhängigkeit macht sich besonders bei kernspektroskopischen Untersuchungen an abklingenden Aktivitäten und beim Auswechseln von Präparaten störend bemerkbar. Es liegen aber relativ wenig quantitative Messungen[1–5]) dieses Effektes vor. Auch scheinen sich die verschiedenen Resultate teilweise zu widersprechen.

Caldwell und Turner[1]) stellten 1954 beim Bestrahlen einer Szintillations-Messanordnung (NaJ-Kristall) mit γ-Strahlung erstmals solche Effekte fest. Sie fanden bei DuMont 6292 Multipliern reversible Verstärkungsänderungen nach einer Änderung der Zählrate. Die untersuchten RCA 5819 Multiplier zeigten diesen Effekt nicht. Eine Vergrösserung bzw. Verkleinerung der Zählrate führte bei den DuMont Multipliern zu einem zeitlichen Anwachsen bzw. Absinken der Verstärkung über Zeiten von einer Stunde und mehr.

Bell, Davis und Bernstein[2]) fanden dagegen bei DuMont 6292, 6363 und 6364 Multipliern zählratenabhängige Verstärkungsänderungen, die sich weit schneller einstellten. Nach einer Vergrösserung der Zählrate war bereits nach einer halben Minute und nach einer Verkleinerung nach 2 bis 3 Minuten ein konstanter Verstärkungswert erreicht. Die Verstärkungsänderungen waren bei den DuMont 6292 Multipliern mit wachsender Zählrate teils positiv, teils negativ. Auch sie fanden bei RCA 5819 Multipliern keinen Effekt.

† Vorgetragen auf der Physikertagung in Heidelberg am 28. April 1960; vgl. Phys. Verh. **11** (1960) 69.

†† Jetzt: The University of Michigan, Ann Arbor (USA).

[1]) R. L. Caldwell und S. E. Turner, Nucleonics **12** (1954) No. 12, 47.

[2]) P. R. Bell, R. C. Davis und W. Bernstein, Rev. Sci. Instr. **26** (1955) 726.

[3]) L. Cathey, IRE Transact. Nucl. Sci. **5** (1958) 109.

[4]) R. D. Connor und M. K. Husain, Nucl. Instr. and Meth. **6** (1960) 337.

[5]) W. E. Mott und R. B. Sutton, Handbuch der Physik **45** (1958) 89.

Cathey[3]) untersuchte Verstärkungsänderungen und Ermüdungserscheinungen an einer grösseren Anzahl DuMont 6292 und RCA 6655 und 5819 Multiplier über mehrere Tage. Die von ihm gemessenen Kurven enthalten ausser irreversiblen möglicherweise noch reversible Anteile. Er fand auch Effekte bei RCA 5819 Multipliern.

Die Messungen von Connor und Husain[4]) ergaben für DuMont 6292, 6364 und 6291 Multiplier bei einer plötzlichen Vergrösserung bzw. Verkleinerung der Zählrate eine momentane und eine langzeitige Verstärkungszunahme bzw. -abnahme. Die Abweichung hatte jeweils nach 2 bis 3 Stunden einen Sättigungswert erreicht.

Ziel dieser Arbeit war es, weitere Aussagen über das Verhalten von Multipliern bei veränderlichen Zählraten zu gewinnen. Die Messungen mit verschiedenen Präparaten und variierter Hochspannung sollten Hinweise auf die Ursachen der einzelnen Effekte geben. Ausserdem sollten die Untersuchungen an verschiedenen Exemplaren und Typen von Multipliern die Auswahl der günstigsten Typen und Betriebsbedingungen erleichtern.

2. Versuchsanordnung und Messmethode

Abb. 1 zeigt das Blockschaltbild der verwendeten Szintillations-Messanordnung. Als Lichtquelle wurde ein NaJ (Tl)-Kristall von 25 mm Dicke und 38 mm Durchmesser (Harshaw 6D4) benutzt. Die elektrischen Impulse aus dem jeweiligen Photomultiplier wurden über einen White-Kathodenfolger einem Linearverstärker nach Fairstein[6]) (Victoreen Type DD2) mit Einkanaldiskriminator[7]) zugeleitet. Die Zählimpulse wurden in zwei Zählgeräten (-hp-523 B und -dy-5159) abwechselnd gezählt und die Resultate sofort gedruckt (-hp-560 A mit-dy-5243). Ein quarzgesteuerter Zeitgeber schaltete die beiden Zählgeräte in Zeitintervallen von 10, 100 oder 1000 sec um. Ein stabilisiertes Hochspannungsgerät (Knott NSHV-1.5) lieferte eine positive Anodenspannung. Der Querstrom im Spannungsteiler betrug meistens 0.4 mA. Bei allen Messungen wurde außerdem der mittlere Anodenstrom des Multipliers mit einem Nano-Amperemeter gemessen.

Zur Anzeige der momentanen Verstärkung des Multipliers wurde die energiereiche Linie eines intensitätsschwachen γ-Präparates (Testpräparat) benutzt. Hierzu diente die Linie bei 2.76 MeV von Na^{24} oder die Linie bei 3.41 MeV = (4.43–1.02) MeV von C^{12*} (Po-Be Quelle). Zu

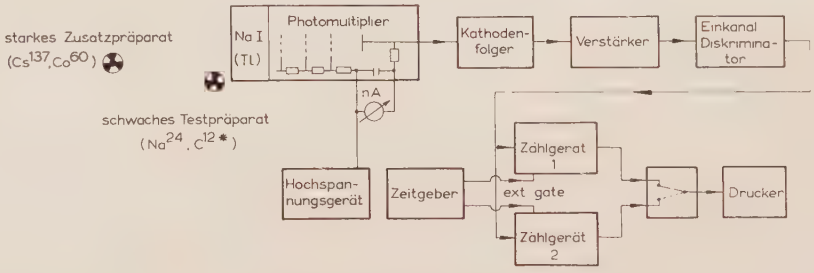

Abb. 1. Blockschaltbild der Messanordnung.

Beginn jeder Messung wurde die Linie des Testpräparates ausgemessen und der Einkanaldiskriminator differentiell auf eine Flanke der Linie eingestellt. Um die integrale Zählrate (Diskriminierung bei 60 keV) bzw. den mittleren Anodenstrom zu erhöhen, wurde dann der Kristall zusätzlich mit einer Cs^{137}- oder Co^{60}-Quelle (Zusatzpräparat) bestrahlt. Die Änderung der Zählrate am Ausgang des Einkanaldiskriminators gestattete die zeitliche Verschiebung des Maximums der Testlinie zu bestimmen. Da sich die relative Linienbreite bei hoher Zählrate etwas vergrössert, wurde nach Erreichen einer konstanten Verstärkung die Form der Testlinie nochmals ausgemessen (vgl. Abb. 2). Bei der Auswertung

[6]) E. Fairstein, Rev. Sci. Instr. **27** (1956) 475.
[7]) E. Fairstein, Rev. Sci. Instr. **27** (1956) 549.

wurde diese Linienverbreiterung berücksichtigt.

Eine Reihe von Kontrollmessungen ergab, dass die gefundenen Verstärkungsänderungen (vgl. Abb. 2) auf Einflüsse des Photomultipliers (Photokathode und/oder Dynoden) zurückzuführen sind, während ausserhalb des Multipliers liegende Effekte höchstens Verstärkungsänderungen von 1 oder $2^0/_{00}$ verursachen oder vortäuschen können. Die Kontrollmessungen betrafen die Auswirkungen von sich aufstockenden Impulsen, den Einfluss der Elektronik und verschiedener Spannungsteiler mit Querströmen bis zu 5 mA sowie den Einfluss des Spannungsabfalles am Anodenwiderstand des Multipliers bei hohen Anodenströmen.

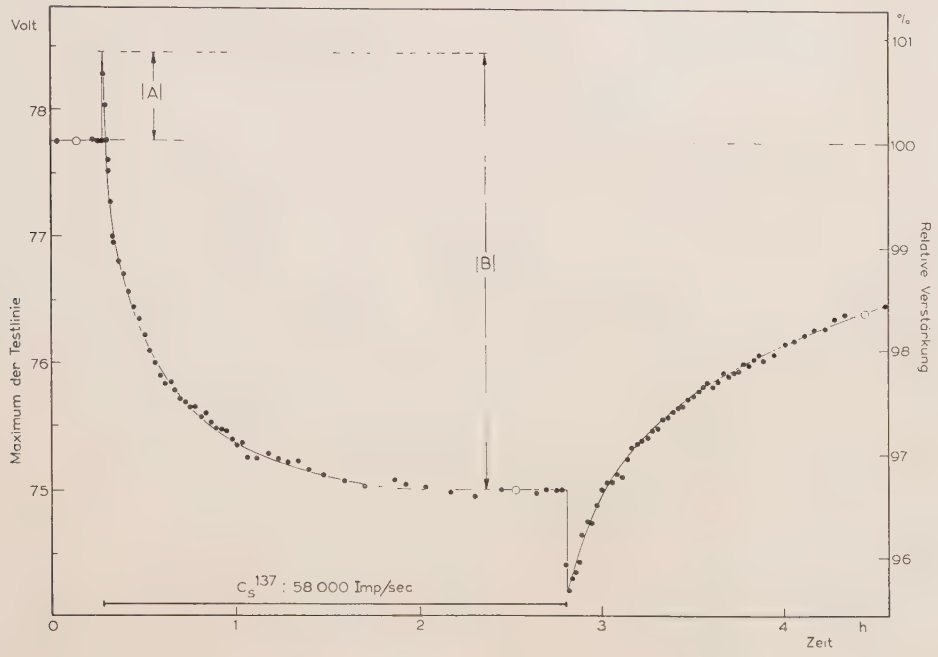

Abb. 2. Charakteristischer Verlauf der Verstärkung eines RCA 6342 Photomultipliers vor, während und nach einer Belichtung der Photokathode. Bei O wurde die Testlinie vermessen.

3. Beeinflussung der Verstärkung durch unterschiedliche Zählraten bei verschiedenen Präparaten und Hochspannungen

Es wurde zunächst ein einzelner Multiplier der Type RCA6342 bei sehr unterschiedlichen Bedingungen untersucht. Dieser Multiplier hat eine SbCs-Photokathode und AgMg-Dynoden. Es wurden 30 Messreihen mit verschiedenen Test- und Zusatzpräparaten (vgl. Abschnitt 2) bei Zählraten bis zu 90000 Imp/sec und bei Hochspannungen zwischen 600 und 900 V durchgeführt. Bei einer Reihe von Messungen wurden die Spannungsteilerwiderstände variiert (vgl. Abschnitt 2).

Abb. 2 zeigt eine charakteristische Messung mit dem Na^{24}-Testpräparat. Während des angegebenen Zeitintervalls wurde der Kristall zusätzlich mit einer Cs^{137}-Quelle bestrahlt. Die plötzliche Erhöhung der Zählrate durch das Zusatzpräparat bewirkte zunächst ein sprunghaftes Ansteigender Verstärkung um $|A|$ in einem Zeitintervall von weniger als 10 Sekunden. Anschliessend verringerte sich die Verstärkung sehr schnell, unterschritt bereits nach etwa einer Minute den Anfangswert und erreichte nach 2 bis 3 Stunden einen Sättigungswert. Dieser Sättigungswert liegt um etwa 3.3% ($= |B| - |A|$) unter dem Anfangswert. Beim Entfernen des Zusatzpräparates verliefen die Verstärkungsänderungen ähnlich, nur mit umgekehrten Vorzeichen. Nach einem sprunghaften Absinken der Verstärkung um etwa den gleichen Betrag wie zu Anfang, stieg die Verstärkung langsam wieder an

und erreichte innerhalb von 8 bis 10 Stunden den ursprünglichen Wert. Die beobachteten Verstärkungsänderungen waren praktisch völlig reversibel.

Die zeitabhängigen Verstärkungsänderungen während bzw. nach der Bestrahlung des Kristalls lassen sich jeweils durch eine Funktion mit zwei exponentiellen Komponenten beschreiben. In

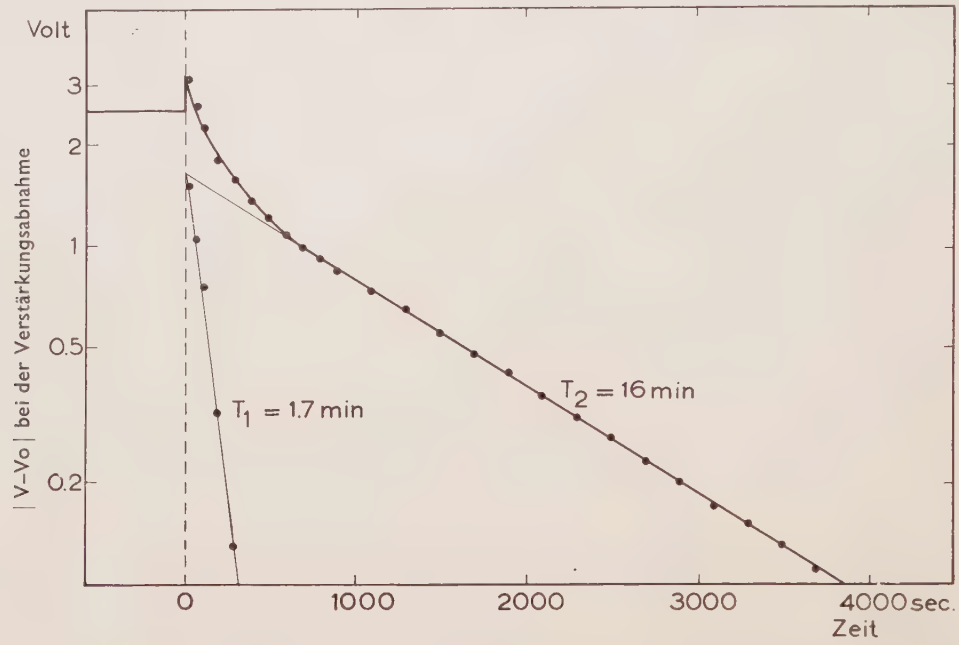

Abb. 3. Verlauf der Verstärkung während der konstanten Belichtung der Photokathode. Die Abweichung von Sättigungswert ist halblogarithmisch gegen die Zeit aufgetragen.

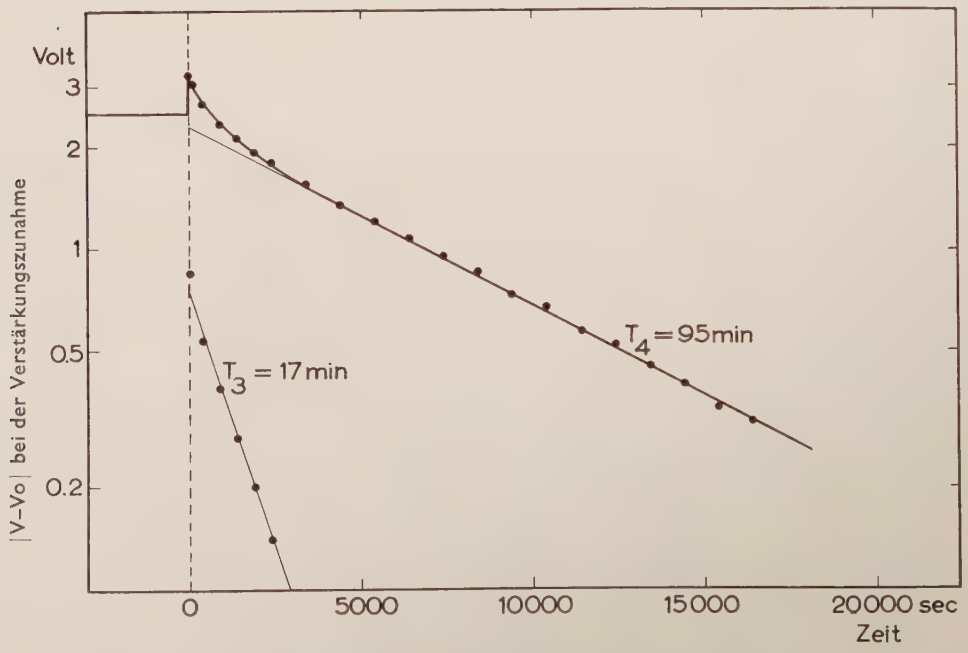

Abb. 4. Verlauf der Verstärkung nach der Belichtung der Photokathode. Die Abweichung vom Sättigungswert ist halblogarithmisch gegen die Zeit aufgetragen.

Abb. 3 und 4 ist die Differenz zwischen augenblicklicher Verstärkung und dem zugehörigen Sättigungswert halblogarithmisch gegen die Zeit aufgetragen. Die gefundenen Halbwertszeiten wegen der notwendigen kurzen Messzeitintervalle nur relativ ungenau zu messen. Abb. 5 zeigt den Betrag von A in Abhängigkeit von der Zählrate eines Cs-Zusatzpräparates. Die Hochspannung

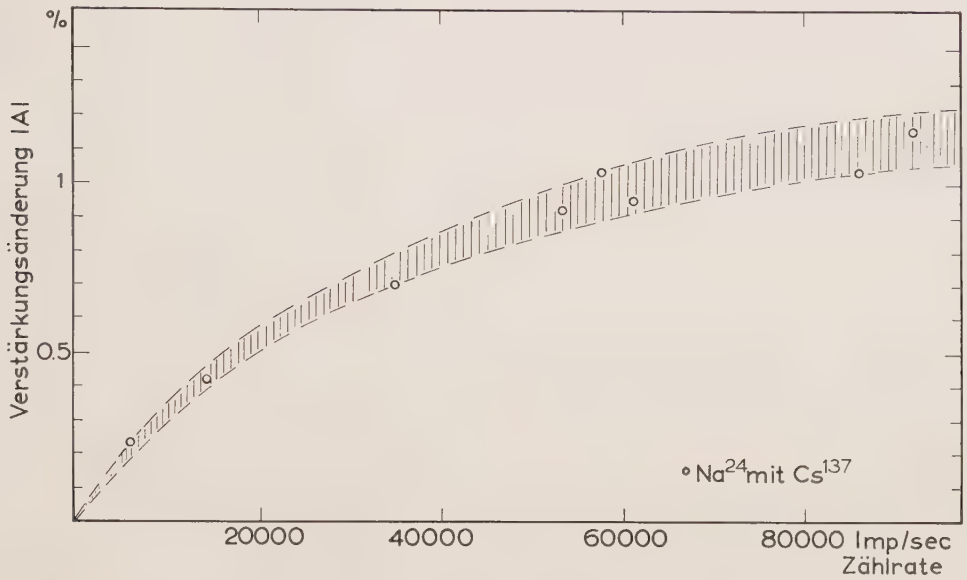

Abb. 5. Betrag der Verstärkungsänderung A als Funktion der Zählrate eines Cs^{137}-Zusatzpräparates.

sind in den Abbildungen angegeben. Die Analyse von 10 unter verschiedenen Bedingungen aufgenommenen Kurven ergab folgende Mittelwerte:

$$\begin{aligned} T_1 &= 1.7 \pm 0.1 \text{ min} \\ T_2 &= 17.8 \pm 2.2 \text{ min} \\ T_3 &= 16.0 \pm 3.4 \text{ min} \\ T_4 &= 105 \pm 8 \text{ min} . \end{aligned} \quad (1)$$

Der Verlauf der relativen Verstärkungsänderungen bei Vergrösserung bzw. Verkleinerung der Zählrate lässt sich somit durch folgende Beziehungen beschreiben:

$$\frac{\Delta V}{V} = A + B_1(1 - e^{-\alpha_1 t}) + B_2(1 - e^{-\alpha_2 t})$$

$$\frac{\Delta V}{V} = -A - B_3(1 - e^{-\alpha_3 t}) - B_4(1 - e^{-\alpha_4 t}) . \quad (2)$$

Dabei ist $\alpha_i = \ln 2/T_i$ und $B = B_1 + B_2 = B_3 + B_4$. A ist positiv und B negativ. Die Messungen ergaben, dass A und B von der Zählrate, der Hochspannung und dem Spektrum des verwendeten Präparates abhängig sind.

Die momentane Verstärkungsänderung A ist betrug 900 V. A strebt bei grösseren Zählraten einem Sättigungswert von etwas über 1% zu.

In Abb. 6 ist der Betrag des momentanen Verstärkungssprunges A zu Beginn bzw. nach Beendigung der Bestrahlung als Funktion der Hochspannung aufgetragen. Die Werte wurden jeweils bei einer zusätzlichen Bestrahlung mit etwa 36000 Imp/sec aus einer Cs^{137}-Quelle gewonnen. Die Abbildung zeigt, dass A bei konstanter Zählrate von der Hochspannung praktisch unabhängig ist.

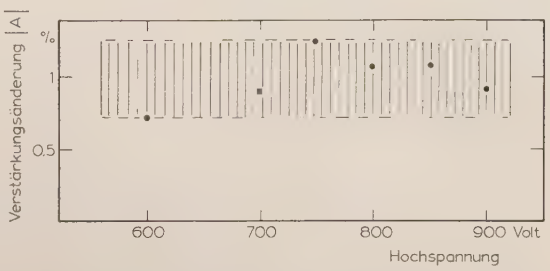

Abb. 6. Betrag der Verstärkungsänderung A als Funktion der Hochspannung bei etwa konstanter Zählrate des Zusatzpräparates.

In Abb. 7 ist die Abhängigkeit zwischen dem Betrag von B und der Zählrate des Zusatzpräparates wiedergegeben. Bei einer konstanten Hochspannung von 900 V erhält man mit Cs^{137} bzw.

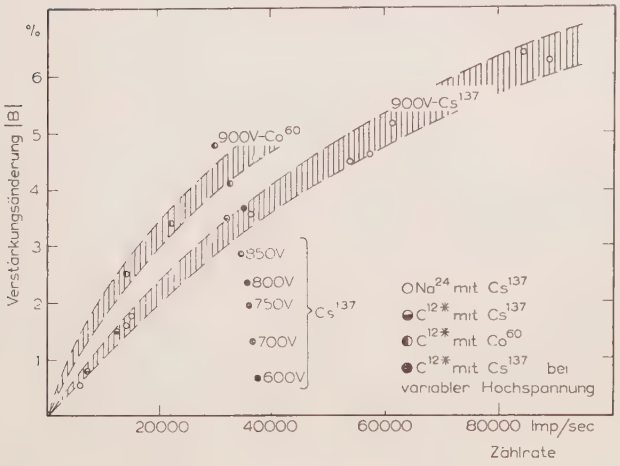

Abb. 7. Betrag der Verstärkungsänderung B als Funktion der Zählrate eines Cs^{137}- oder Co^{60}-Zusatzpräparates.

Co^{60} als Zusatzpräparat Messpunkte innerhalb der schraffierten Bereiche. Bei gleicher Zählrate ist die durch das energiereichere Spektrum von Co^{60} verursachte Abweichung stets grösser als für Cs^{137}. Bei einer Zählrate von etwa 36000 Imp/sec zeigen die schwarzen Punkte den Einfluss der Hochspannung. Mit abnehmender Hochspannung wird der Effekt bei gleicher Zählrate kleiner.

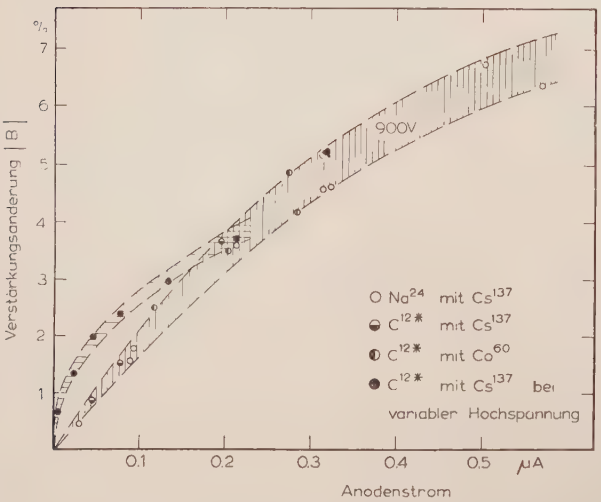

Abb. 8. Betrag der Verstärkungsänderung B als Funktion des durch das Zusatzpräparat hervorgerufenen mittleren Anodenstromes.

Trägt man die Messpunkte nicht als Funktion der Zählrate sondern als Funktion des gemessenen mittleren Anodenstromes auf (Abb. 8), so liegen die bei 900 V mit Cs^{137} und mit Co^{60} gemessenen Punkte auf einer gemeinsamen Kurve (senkrecht schraffierter Bereich). Die Abhängigkeit ist bis zu Anodenströmen von etwa 0.2 μA linear und strebt dann exponentiell einem Sättigungswert von etwa 9.5% zu. Die bei reduzierter Hochspannung gemessenen Werte liegen nicht auf dieser Kurve (horizontal schraffierter Bereich). Bei jeweils gleichem Anodenstrom ist der Effekt umso grösser, je kleiner die Hochspannung ist. Gleicher Anodenstrom erfordert bei verminderter Hochspannung eine Vergrösserung der Zählrate.

Die Beziehung zwischen B und der Hochspannung ist nochmals in Abb. 9 dargestellt (schraffierter Bereich). Ausserdem ist der Verlauf des mittleren Anodenstromes mit der Hochspannung eingezeichnet. Der Anodenstrom ist bei konstanter Zählrate der Verstärkung des Multipliers proportional. Für alle Messpunkte betrug die Zählrate des Cs-Präparates etwa 36000 Imp/sec. Aus der Abbildung geht hervor,

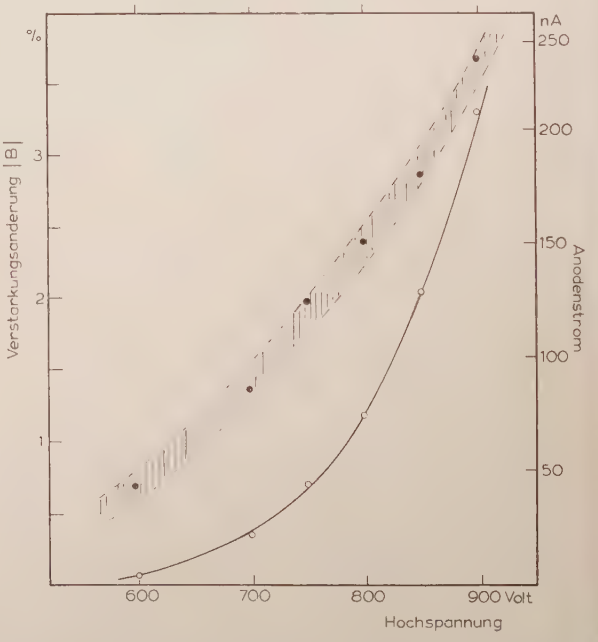

Abb. 9. Betrag der Verstärkungsänderung B und mittlerer Anodenstrom als Funktion der Hochspannung bei etwa konstanter Zählrate des Zusatzpräparates.

daß die langzeitige Verstärkungsänderung B mit zunehmender Hochspannung langsamer ansteigt als der mittlere Anodenstrom.

Eine weitere Messung lieferte zusätzliche Hinweise auf die Ursachen der verschiedenen Effekte. Dabei wurde für 30 Minuten die Hochspannung am Multiplier abgeschaltet, das Na^{24}-Testpräparat aber nicht entfernt. Die Photokathode blieb also weiterhin belastet, es floss aber kein Anoden- und Dynodenstrom. Nach dem Wiederanlegen der Hochspannung lag das Maximum der Testlinie höher. Die Verstärkung verringerte sich anschliessend und erreichte nach etwa 2 Stunden wieder den Ausgangswert. Die Halbwertszeiten T_1 und T_2, die dabei gefunden wurden, stimmen mit den entsprechenden Werten (Glch. 1) der übrigen Messreihen überein. Das Einschalten der Hochspannung am Multiplier hatte also bezüglich der langzeitigen Verstärkungsänderungen dieselben Folgen wie das Hinzubringen eines Präparates.

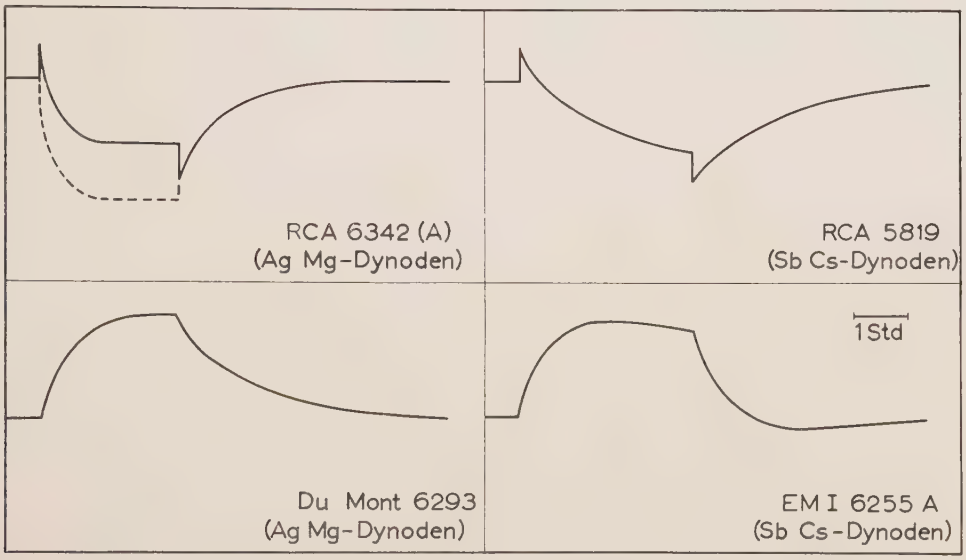

Abb. 10. Charakteristischer Verlauf der Verstärkung von RCA-, DuMont- und EMI-Photomultipliern vor, während und nach einer konstanten Belichtung der Photokathode. Die Verstärkungsänderungen betragen je nach Exemplar 0.5 bis 2% bei einem mittleren Anodenstrom von 100 nA.

4. Verstärkungsänderungen bei verschiedenen Typen und Exemplaren

Nach dem in Abschnitt 2 beschriebenen Messverfahren wurden ausserdem eine Reihe anderer Multiplier getestet. Es waren dies 6 Exemplare RCA 6342 bzw. 6342 A, 3 Exemplare RCA 5819, 2 Exemplare DuMont 6292 und 1 Exemplar EMI 6255 A. Die Photokathode besteht bei allen Typen aus SbCs[8]). Das Dynodenmaterial ist jedoch verschieden. RCA 6342 (A) und DuMont 6292 besitzen AgMg-Dynoden[8]). RCA 5819 und EMI 6255 besitzen SbCs-Dynoden[8]). Ausserdem unterscheiden sie sich sehr in der geometrischen Anordnung des Dynodensystems. Pro Exemplar wurden 2 bis 3 Messungen unter vergleichbaren Bedingungen durchgeführt. Abb. 10 zeigt das charakteristische Verhalten der vier Multipliertypen.

Bei allen RCA-Multipliern traten momentane Verstärkungsänderungen A bei einer Änderung der Zählrate auf. Bei den getesteten DuMont- und EMI-Multipliern wurden hingegen praktisch keine Sprünge gefunden. Die geringe Anzahl der untersuchten Multiplier dieser Typen lässt jedoch keine allgemeine Aussage zu. Die Sprünge bei den RCA-Multipliern sind beim Vergrößern der

[8]) Der tatsächliche Aufbau von Photokathode und Dynoden ist weit komplizierter, als aus der vereinfachten Schreibweise zu ersehen ist. Vgl. z.B. S. C. Curran, Luminescence and the Scintillation Counter (London, 1953).

Zählrate teils positiv (Abb. 2), teils negativ (Abb. 11). A liegt bezogen auf 10000 Imp/sec aus einer Cs^{137}-Quelle zwischen — 0.5 und + 0.5 %.

Bei allen Multipliern wurden ausserdem langzeitige Verstärkungsänderungen B gefunden. B

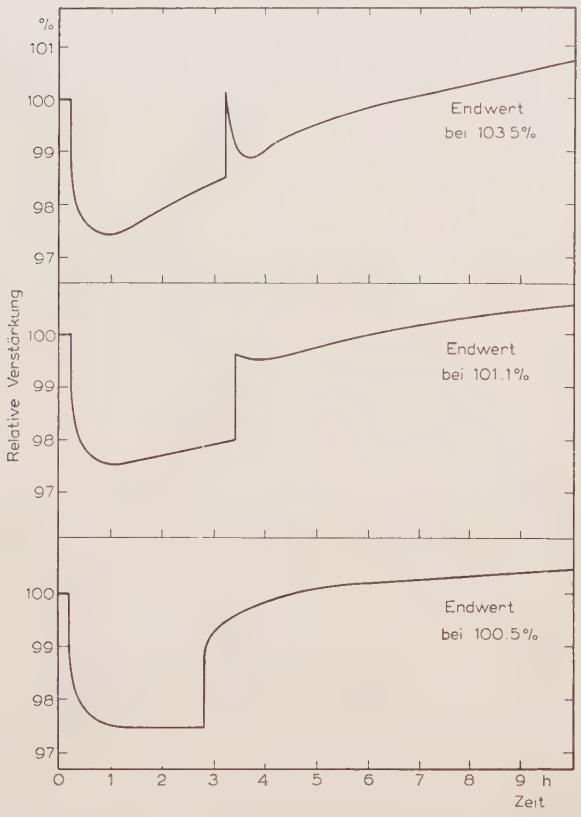

Abb. 11a bis c. Verhalten eines fabrikneuen RCA 6342 Multipliers. Nach einer Bestrahlung mit 36000 Imp/sec. während 10 Std. (zwischen a und b) bzw. 35 Std. (zwischen a und c) stellte sich der bei den anderen Exemplaren dieser Type beobachtete Verlauf der Verstärkungsänderung ein.

hat für alle getesteten RCA Multiplier negatives Vorzeichen, während dieser Wert für die DuMont- und EMI-Multiplier positiv war. Es besteht also keine Korrelation zwischen dem Dynodenmaterial und dem Vorzeichen von B. Bei allen Multipliertypen (auch für RCA 5819) ist der Betrag von B von ähnlicher Grösse. Er liegt je nach Exemplar zwischen 0.5 und 2% bei einem mittleren Anodenstrom von 100 nA. Bei den RCA 5819 Multipliern stellt sich der Sättigungswert beim Vergrössern der Zählrate wesentlich langsamer ein als bei den anderen Typen.

Ein besonders ungewöhnliches Verhalten wurde bei einem fabrikneuen RCA 6342 Multiplier festgestellt[9]). Abb. 11 zeigt drei Messungen bei derselben Hochspannung und denselben Zählraten. Der zunächst irreguläre Verlauf der Verstärkung (Abb. 11a) geht in den bekannten charakteristischen Verlauf über (Abb. 11c), wenn Kristall mit Multiplier einer intensiven Bestrahlung ausgesetzt werden. Ausserdem verringerte sich durch diese Bestrahlung der anfängliche irreversible Anteil von 3.5% auf 0.5%. In dem Zeitraum zwischen den Messungen Abb. 11a und 11b bzw. Abb. 11a und 11c betrug die Anodenbelastung des Multipliers 4 $\mu A \cdot h$ bzw. 14 $\mu A \cdot h$ (etwa 36000 Imp/sec während 10 bzw. 35 Stunden).

5. Diskussion

Unsere Ergebnisse lassen sich in einer Reihe von Punkten mit den bisher bekannten Messungen vergleichen:

1. Langzeitige Verstärkungsänderungen mit positiven B wurden bei DuMont 6292 Multipliern (vgl. Abb. 10) bereits von einigen Autoren[1,4]) gefunden. Bei verschiedenen Messungen[2,4]) zeigte sich auch ein momentaner Sprung A, der bei den beiden von uns getesteten Exemplaren nicht festgestellt werden konnte.

2. Das teils positive, teils negative Vorzeichen von A bei Bell *u.a.*[2]) stimmt mit dem von uns bei RCA-Multipliern beobachteten Verhalten überein.

3. Bell *u.a.*[2]) fanden keine langzeitigen Verstärkungsänderungen B. Ein entsprechendes Verhalten zeigten unsere Multiplier bei kleinen Hochspannungen. Während nämlich bei gleicher Zählrate A von der Hochspannung praktisch unabhängig ist, nimmt B mit kleiner werdender Hochspannung stark ab.

4. Das bei RCA 5819 Multipliern gefundene Verhalten ist widerspruchsvoll. Von uns und von Cathey[3]) wurden Effekte registriert, von anderen Autoren[1,2]) nicht.

5. Irreversible Verstärkungsänderungen treten

[9]) vgl. R. B. Linden, F. W. Schenkel und P. A. Snell, IRE Transact. Nucl. Sci. **7** (1960); zit. nach Nucleonics **18** (1960) No. 5, 90.

in Uebereinstimmung mit Cathey[3]) bei Anodenströmen bis zu einigen 100 nA praktisch nicht auf.

Es zeigte sich, dass der Sprung A in der Verstärkung bei gleicher Zählrate praktisch nicht von der Hochspannung abhängt (Abb. 6). Da sich die Belastung der Anode und der Dynoden mit der Hochspannung jedoch stark ändert (vgl. Abb. 9), hat man anzunehmen, dass eine reversible Sensibilisierung oder Desensibilisierung der Photokathode diesen Effekt verursacht. Es wäre denkbar, dass sich durch den Austritt von Elektronen aus der Photokathode Cs-Atome in Cs-Ionen umwandeln[10]). Die Oberfläche verarmt dadurch an lichtelektrisch wirksamen Zentren, die Austrittsarbeit erhöht sich und beeinflusst damit die Verstärkung. Allerdings ist dadurch eine Erhöhung der Verstärkung kaum zu erklären. Die Photokathode kann sich auch als Halbleiter aufladen[11,12]). Eine Verkleinerung der Spannung zwischen Photokathode und erster Dynode führt aber stets nur zu einer Verkleinerung der Verstärkung. Ebenso würden Sättigungsstromeffekte an der Anode des Multipliers nur zu einem negativen Verstärkungssprung führen, der ausserdem von der Hochspannung abhängig sein müsste.

Die langzeitigen Verstärkungsänderungen B sind vom mittleren Anodenstrom bzw. Dynodenstrom und von der Hochspannung abhängig (Abb. 8 und 9). Bei gleicher Zählrate ändert sich B im Gegensatz zu A mit der Hochspannung bzw. dem Dynodenstrom. Es ist deshalb wahrscheinlich, dass der Sekundäremissionsfaktor der Dynoden mit ihrer Strombelastung variiert. Der Einfluss der letzten Dynode mit der höchsten Strombelastung ist am grössten. Die vorhergehenden Dynoden liefern jedoch auch einen Beitrag. Dieser ist bei gleichem Anodenstrom umso grösser, je kleiner die Hochspannung und damit der Sekundäremissionsfaktor ist. Dies erklärt, weshalb in Abb. 8 die bei verminderter Hochspannung gemessenen Werte über der Kurve für 900 V liegen und weshalb in Abb. 9 der Effekt mit zunehmender Hochspannung langsamer ansteigt als der Anodenstrom.

Einen weiteren Hinweis dafür, dass die langzeitigen Verstärkungsänderungen B von den Dynoden verursacht werden, liefert die am Ende von Abschnitt 3 beschriebene Messung. Durch das Abschalten der Hochspannung bei fortdauernder Bestrahlung wurde der Dynoden- und Anodenstrom unterbrochen, nicht aber die Belastung der Photokathode. Der zeitliche Verlauf der Verstärkungsänderung nach Wiederanlegen der Hochspannung war ähnlich wie bei einer Vergrösserung der Zählrate, was auf einen Zusammenhang mit den Dynoden hinweist. Einen ähnlichen Versuch unternahmen Caldwell und Turner[1]). Sie bestrahlten Kristall mit Multiplier ohne Hochspannung mehrerer Stunden lang mit insgesamt 9 r. Nach dem Wegnehmen des Präparates und Wiederanlegen der Hochspannung zeigte die Verstärkung den ursprünglichen Wert.

Cathey[3]) führt die irreversiblen langzeitigen Verstärkungsänderungen auf Dynodeneffekte zurück. Er diskutiert Strukturänderungen und Verunreinigungen in den Dynodenoberflächen, die ihrerseits von der Stromdichte, der Temperatur und der Vorgeschichte abhängen. Als Ursache für irreversible Verstärkungsänderungen betrachtet er die Verringerung der Cs-Konzentration auf den Dynodenoberflächen. Mit dieser speziellen Annahme lassen sich wohl langzeitige irreversible Prozesse beschreiben, kaum aber die von uns beobachteten reversiblen Aenderungen. Diese können nicht durch Strukturänderungen erklärt werden. Eine mögliche Deutung ist folgende: der Austritt oder Aufprall von Elektronen bewirkt eine Zerstörung oder "Ausheizung" von wirksamen Zentren. Diese werden durch Diffusion von Elektronen durch die schlecht leitenden Zwischenschichten aus MgO oder $SbCs_3$ zurückgebildet, wobei sich ein Gleichgewicht einstellt[10]). Mit einer solchen Vorstellung lassen sich auch die unterschiedlichen Zeitkonstanten (Glch. 1) einigermassen verstehen.

Das Vorzeichen von B ist nicht mit dem Dynodenmaterial korreliert. Möglicherweise

[10]) z.B. J. H. de Boer, Elektronenemission und Adsorptionserscheinungen (Leipzig, 1937).

[11]) E. Breitenberger, Progr. Nucl. Phys. **4** (1955) 87.

[12]) N. Schaetti und W. Baumgartner, Helv. Phys. Acta **24** (1951) 614.; Le vide **6** (1951) 1041; Z. angew. Math. Phys. **4** (1953) 159.

besteht aber ein Zusammenhang mit der Konzentration freier Cs-Atome auf der Oberfläche der Dynoden. Die Sekundärelektronenemission überschreitet mit zunehmender Cs-Konzentration ein Maximum, das dem optimalen Bedeckungsgrad der Oberfläche entspricht[13]). Cathey[3]) unterscheidet bei den irreversiblen Verstärkungsänderungen zwischen Dynoden mit geringer und hoher Cs-Konzentration. Eine Abnahme der Cs-Konzentration kann danach sowohl eine Abnahme als auch eine Zunahme der Verstärkung zur Folge haben. Aehnlich könnten sich auch reversible Dynodeneffekte auf die Sekundäremission und damit auf die Verstärkung auswirken. Je nach Cs-Konzentration erhält man dann ein positives B (DuMont 6292 und EMI 6255) oder ein negatives B (RCA 6342 (A) und RCA 5819).

Eine vollständige Klärung der Ursachen für die verschiedenartigen Effekte kann nur durch weitere Messungen erreicht werden. Dabei sollte man eine Isolierung der einzelnen Effekte anstreben.

Wir danken Herrn Prof. W. Gentner für sein förderndes Interesse an dieser Arbeit.

Bei den Messungen wurden Geräte der Deutschen Forschungsgemeinschaft mitbenutzt.

[13]) z.B. H. Bruining, Sekundär-Elektronen-Emission fester Körper (Berlin 1942).

NUCLEAR INSTRUMENTS AND METHODS 9 (1960) 131–136; NORTH-HOLLAND PUBLISHING CO.

HIGHER ORDER CHANCE COINCIDENCES IN A FAST-SLOW COINCIDENCE ARRANGEMENT

HELMUT PAUL

Physics Department, Purdue University, Lafayette, Indiana

Received 6 September 1960

In this paper, we consider an ordinary fast-slow coincidence measurement with two radiation detectors. In addition to the chance coincidences due to two pulses (one from each detector) there are higher order chance coincidences which require a total of three or four pulses and whose relative contributions to the counting rate increase with source strength. Formulas for these effects are given, and methods for measuring the corrections are discussed. For a source with a simple decay scheme, and for the special cases of either very narrow or very wide analyzer channels it is shown that the higher order corrections may be neglected if the single counting rates are small compared to the reciprocal resolving time of the slow coincidence circuit.

1. Introduction

The fast-slow coincidence method was introduced by Bell, Graham, and Petch in 1949 and has found wide application in nuclear spectroscopy[1]). Under many conditions, chance coincidence corrections are easily applied or even unnecessary, but if the source strength is large, higher order corrections may become necessary. In the following, these corrections are calculated under certain assumptions often fulfilled in practice: We consider two radiation detectors which subtend relatively small solid angles at the source. We also assume, in order not to complicate the formulas, that the triple coincidence circuit can be described by one resolving time T, and that there are no crystal summing or dead-time effects. Granting these assumptions, however, the higher order corrections given below are complete.

Consider two detectors in fast coincidence (resolving time τ) looking at a radioactive source. For simplicity, let the source emit β particles and γ quanta, and let one of the detectors be a β-, the other a γ-detector. Their single counting rates are S_β, S_γ; they produce a coincidence rate ${}_2C$ in the fast coincidence circuit which consists of true and chance (random) coincidences:

$$ {}_2C = {}_2C^{\mathrm{t}} + {}_2C^{\mathrm{r}} . \tag{1} $$

If ${}_2C^{\mathrm{t}} \ll S_\beta$, S_γ, and if S_β, $S_\gamma \ll (2\tau)^{-1}$, then the chance rate is given by[2])

$$ {}_2C^{\mathrm{r}} = 2\tau S_\beta S_\gamma . \tag{2} $$

Let both counters be connected to pulse height analyzers. If, in the $\beta(\gamma)$ channel, the probability for a pulse—picked at random from the single spectrum—to be accepted by the $\beta(\gamma)$ analyzer is p_β (p_γ), then the output counting rate $S'_\beta(S'_\gamma)$ of the analyzer is given by

$$ S'_\beta = p_\beta S_\beta $$

and

$$ S'_\gamma = p_\gamma S_\gamma . \tag{3} $$

The fast coincidence output and the analyzer outputs are fed into a (slow) triple coincidence circuit (resolving time T) of the symbolic block diagram in fig. 1.

The triple coincidence rate ${}_3C$ will contain true coincidences ${}_3C^{\mathrm{t}}$ (due to a true double coincidence with both β and γ pulse of proper pulse height) and chance coincidences of various types. These chance coincidences may be conveniently divided, in order of decreasing importance, into three types depending on whether they are due

[1]) Cf. R. E. Bell in: K. Siegbahn, Beta- and Gamma-Ray Spectroscopy (North-Holland Publishing Co., Amsterdam 1955) p. 502.

[2]) J. V. Dunworth, Rev. Sci. Instr. 11 (1940) 167.

to two, or three, or four particles†, and designated by ${}_3C'$, ${}_3C''$, and ${}_3C'''$††.

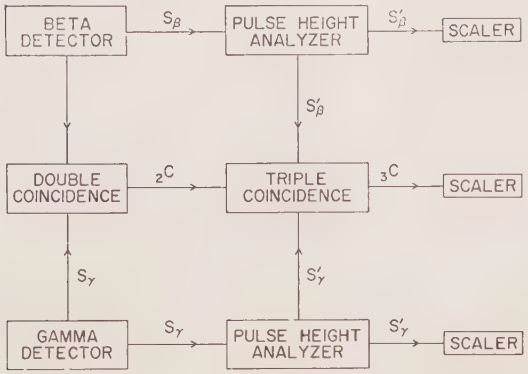

Fig. 1.

2. Triple Chance Coincidences of First Type, and True Triple Coincidences

As per definition, these require only one β and one γ particle. Clearly then, a triple coincidence can occur only if the particles produce a double coincidence, and if their energies are such that both the β and γ pulse pass through the respective pulse height analyzers. If the double coincidence is a chance coincidence, then the $\beta(\gamma)$ pulse has a probability p_β (p_γ) of passing through the analyzer, hence the resultant rate is

$$ {}_3C' = {}_2C^r p_\beta p_\gamma = 2\tau S'_\beta S'_\gamma . \tag{4}$$

If, on the other hand, the double coincidence is a true coincidence, then the triple coincidence becomes a true coincidence also. Given such a true double coincidence, we could again define, say, the probability q^*_β that the β pulse will be accepted by the β analyzer. q^*_β will in general be different††† from p_β. But since, in general, the probability of acceptance for the β pulse will be different if it is known that the γ pulse has, or has not been, accepted*, the probability q^*_β (which presupposes complete lack of knowledge about the γ pulse) is not useful for our purposes. We therefore introduce the following definitions which all refer to a true double coincidence randomly selected from all true double coincidences:

$q_{\beta\gamma}$ = probability for both β and γ pulse to be accepted,

q_β = probability for β pulse to be accepted while γ pulse is rejected,

q_γ = probability for γ pulse to be accepted while β pulse is rejected.

Evidently, the probability for neither pulse to be accepted is given

$$ 1 - q_\beta - q_\gamma - q_{\beta\gamma} . $$

The following relations hold for q^*_β, q^*_γ (i.e., the see probability of acceptance for a $\beta(\gamma)$ pulse that has given rise to a true coincidence, if nothing is known about the amplitude of the $\gamma(\beta)$ pulse):

$$ \begin{aligned} q_\beta^* &= q_\beta + q_{\beta\gamma} \\ q_\gamma^* &= q_\gamma + q_{\beta\gamma} . \end{aligned} \tag{5}$$

Then we have for the rate of true coincidences:

$$ {}_3C^t = {}_2C^t q_{\beta\gamma} . \tag{6}$$

3. Triple Chance Coincidences of Second Type

These require three particles, for example one β and two γ particles. The β and one of the γ's have to produce a double coincidence. While the β pulse is accepted by the analyzer, the γ pulse is not**. A second γ pulse has to come within T and to be accepted by the analyzer so that a triple coincidence is produced. There are then two types of such events:

a. Type ${}_3C''_r$: events due to random double coincidences. The number of random double coincidences whose β pulse is accepted while the γ pulse is not, is given by:

$$ {}_2C^r p_\beta (1 - p_\gamma) . $$

† "Particle" here means a β particle or γ quantum.

†† Upper indices t and r distinguish true and random coincidences. The upper index r has, however, been omitted from all primed symbols, for simplicity.

††† If, e.g., the analyzer window sits on a non-coincident peak, q^*_β will be zero but p_β will not be zero.

* Consider, e.g., a decay scheme that gives rise to two types of coincidences, β_1–γ_1 and β_2–γ_2, where γ_1 and γ_2 have different energies. Consider further a particular true coincidence whose γ pulse has been accepted by the analyzer. If this analyzer is set so as to accept only γ_1 pulses, then we know that the coincidence must be of the first type, and this knowledge influences, of course, the acceptance probability for the β pulse. If the β analyzer happens only to accept β_2 pulses, that probability might be zero even though p^*_β would not be.

** If it were accepted, the coincidence would be of the first type already considered.

If such a pulse arrives within time T from any selected γ pulse (rate S'_γ), a chance coincidence is produced. Taking also the symmetrical effect (two β's and one γ) one obtains the rate:

$$
\begin{aligned}
{}_3C''_{\mathrm{r}} &= 2T\,{}_2C^{\mathrm{r}}\{\,p_\beta\,(1-p_\gamma)\,S'_\gamma + p_\gamma\,(1-p_\beta)\,S'_\beta\,\} \\
&= 2T\,{}_3C'\{\,(S_\gamma - S'_\gamma) + (S_\beta - S'_\beta)\,\}\,. \qquad (7)
\end{aligned}
$$

b. Type ${}_3C''_{\mathrm{t}}$: events due to true double coincidences. The derivation here is similar to the one above, but one has to take into account that the pulse height selection is not independent of time selection. Now, the number of true coincidences whose β pulse is accepted while the γ pulse is not, is given by

$$
{}_2C^{\mathrm{t}}q_\beta
$$

and these should be in coincidence with independent selected γ's (rate S'_γ). Including the symmetrical effect, the rate becomes:

$$
{}_3C''_{\mathrm{t}} = 2T\,{}_2C^{\mathrm{t}}\{\,q_\beta\,S'_\gamma + q_\gamma\,S'_\beta\,\}\,. \qquad (8)
$$

4. Triple Chance Coincidences of Third Type

These require four pulses to be produced. Two (a β and a γ pulse) have to produce a double coincidence, but neither is accepted by the respective analyzer, so that both an additional β and an additional γ pulse of the proper height are required within T to produce a triple coincidence.

a. Type ${}_3C'''_{\mathrm{r}}$: events due to random double coincidences. Here, entirely independent pulses have to arrive at the three inputs, whose rates are ${}_2C^{\mathrm{r}}\,(1-p_\beta)\,(1-p_\gamma)$, S'_β, and S'_γ, respectively. Assuming that all three pulses have to arrive within T to produce a coincidence, the rate becomes

$$
\begin{aligned}
{}_3C'''_{\mathrm{r}} &= 3T^2\,{}_2C^{\mathrm{r}}\,(1-p_\beta)(1-p_\gamma)\,S'_\beta\,S'^{\gamma} \\
&= 3T^2\,{}_3C'\,(S_\beta - S'_\beta)\,(S_\gamma - S'_\gamma)\,. \qquad (9)
\end{aligned}
$$

b. Type ${}_3C'''_{\mathrm{t}}$: events due to true double coincidences. In analogy to the preceding formula, one obtains

$$
{}_3C'''_{\mathrm{t}} = 3T^2\,{}_2C^{\mathrm{t}}\,(1-q_\beta-q_\gamma-q_{\beta\gamma})\,S'_\beta\,S'_\gamma\,. \qquad (10)
$$

c. Other effects. Considering, e.g., a coincidence due to a β and three γ pulses, it can be seen that this would be an effect of the type considered in section 3, but with one additional γ which is unnecessary to produce a coincidence unless one considers summing effects. Such a combination of pulses would therefore not lead to any additional chance rate, nor would combinations of five or more pulses. The total measured triple coincidence rate is therefore

$$
{}_3C = {}_3C^{\mathrm{t}} + {}_3C' + {}_3C''_{\mathrm{r}} + {}_3C'''_{\mathrm{r}} + {}_3C''_{\mathrm{t}} + {}_3C'''_{\mathrm{t}}\,. \qquad (11)
$$

5. Relative Importance of the Various Contributions

The rates ${}_3C''_{\mathrm{r}}$ and ${}_3C'''_{\mathrm{r}}$ can be easily compared to the well known rate, ${}_3C'$, of chance coincidences of the first kind. One gets

$$
\begin{aligned}
{}_3C' : {}_3C''_{\mathrm{r}} : {}_3C'''_{\mathrm{r}} &= 1 : 2T\,\{\,(S_\beta - S'_\beta) + \\
&\quad + (S_\gamma - S'_\gamma)\,\} : 3T^2\,(S_\beta - S'_\beta)\,(S_\gamma - S'_\gamma)\,. \qquad (12a)
\end{aligned}
$$

If both rates of rejected particles are small compared to $1/T_3$ ${}_3C''_{\mathrm{r}}$ will be small compared to ${}_3C'$, and ${}_3C'''_{\mathrm{r}}$ will be even smaller.

The rates ${}_3C''_{\mathrm{t}}$ and ${}_3C'''_{\mathrm{t}}$ are best compared to the true rate, ${}_3C^{\mathrm{t}}$. For simplicity, let us assume that $p \ll 1$ (narrow windows) and $p \approx q$ for both β and γ channel, and further let us consider a simple decay scheme that has only one excited state capable of producing β–γ coincidences. Then $q_{\beta\gamma} = q^*_\beta\,q^*_\gamma \approx q_\beta\,q_\gamma$, and we obtain

$$
{}_3C^{\mathrm{t}} : {}_3C''_{\mathrm{t}} : {}_3C'''_{\mathrm{t}} = 1 : 2T\,(S_\beta + S_\gamma) : 3T^2\,S_\beta S_\gamma\,, \qquad (12b)
$$

i.e., under this approximation the relative magnitudes are the same as above.

If the windows are not narrow, then the comparison is more complicated than eq. (12b). However, for the same type of decay scheme, if the above approximation holds for one window, and if the other window is very wide ($p = q^* = 1$), e.g., if (in the γ branch, say) there is a multichannel analyzer, then one term in the expressions for ${}_3C''_{\mathrm{r}}$ and ${}_3C''_{\mathrm{t}}$ drops out, and one has (approximately)

$$
{}_3C^{\mathrm{t}} : {}_3C''_{\mathrm{t}} : {}_3C'''_{\mathrm{t}} = 1 : 2T\,S_\beta : 0\,. \qquad (13)
$$

In this case, the triple coincidence work essentially as a double coincidence, and hence there are no triple coincidences of third type.

If both windows are opened completely ($p_\beta = q^*_\beta = p_\gamma = q^*_\gamma = 1$), the chance coincidences of second type also vanish, and one is left with an ordinary fast coincidence arrangement.

It may be noted that the various types of coincidences have the following dependence upon source strength N:

$$
\begin{aligned}
&{}_3C^{\mathrm{t}} \sim N \\
&{}_3C' \,,\, {}_3C''_{\mathrm{t}} \sim N^2 \\
&{}_3C''_{\mathrm{r}} \,,\, {}_3C'''_{\mathrm{t}} \sim N^3 \\
&{}_3C'''_{\mathrm{r}} \sim N^4 \,.
\end{aligned}
$$

The importance of the higher order chance coincidences increases therefore with increasing source strength.

6. Experimental Determination of Chance Coincidences

6.1. MEASUREMENTS BY INSERTING DELAYS

6.1.1. *Delay in a fast channel*

Normally, without any delays, one measures the triple coincidence rate ${}_3C$ given by eq. (11). But if, e.g., the pulse from the γ counter is delayed by an amount $> \tau$, then all true coincidences will be destroyed, and the measured rate will be

$$D = {}_3C' + {}_3C''_{\mathrm{r}} + {}_3C'''_{\mathrm{r}} \,. \tag{14}$$

Delaying the β pulse gives the same result.

6.1.2. *Delay in a slow channel*

If the pulse from the γ analyzer is delayed by an amount $> T$, two particles will not be able to produce a triple coincidence. For they would have to produce a double coincidences, but the γ pulse from the analyzer would be too late with respect to the double coincidence and the beta pulse. To produce a triple coincidence, a second (earlier) γ pulse of the right energy is needed.

One would therefore expect to measure in this way essentially chance coincidences of second and third type. The only difference with respect to those rates (cf. equations (7)–(10)) is the following: in the derivation of ${}_3C''_{\mathrm{r}}$, e.g., we had to consider the rate of random double coincidences whose β pulse is accepted while the γ pulse is not, but here we do not have to require anything about the γ pulse, since only unrelated γ pulses will be able to produce a triple coincidence. This changes the probability factors in every term. We have, for the rates of double coincidences accompanied by a selected β pulse:

$${}_2C^{\mathrm{r}}\, p_\beta \text{ (random doubles), and}$$
$${}_2C^{\mathrm{t}}\, q^*_\beta = {}_2C^{\mathrm{t}}\,(q_\beta + q_{\beta\gamma}) \text{ (true doubles)}$$

and, for the rates of double coincidences not accompanied by a selected β pulse:

$${}_2C^{\mathrm{r}}\,(1 - p_\beta) \text{ (random doubles), and}$$
$${}_2C^{\mathrm{t}}\,(1 - q^*_\beta) = {}_2C^{\mathrm{t}}\,(1 - q_\beta - q_{\beta\gamma}) \text{ (true doubles).}$$

The measured rate is therefore

$$D'_\gamma = 2T\,\{\,{}_2C^{\mathrm{r}}\, p_\beta + {}_2C^{\mathrm{t}}\,(q_\beta + q_{\beta\gamma})\,\}\,S'_\gamma + \\ + 3T^2 S'_\beta S'_\gamma\,\{\,{}_2C^{\mathrm{r}}\,(1 - p_\beta) + {}_2C^{\mathrm{t}}\,(1 - q_\beta - q_{\beta\gamma})\,\}\,. \tag{15}$$

Delaying only the pulse from the β analyzer, one gets similarly

$$D'_\beta = 2T\,\{\,{}_2C^{\mathrm{r}} p_\gamma + {}_2C^{\mathrm{t}}\,(q_\gamma + q_{\beta\gamma})\,\}\,S'_\beta + \\ + 3T^2 S'_\beta S'_\gamma\,\{\,{}_2C^{\mathrm{r}}\,(1 - p_\gamma) + {}_2C^{\mathrm{t}}\,(1 - q_\gamma - q_{\beta\gamma})\,\}\,. \tag{16}$$

6.1.3. *Delay both in a fast and in a slow channel*

This will be like the previous case except that now ${}_2C^{\mathrm{t}} = 0$. Hence the measured rates will be

$$D''_\gamma = 2T\,{}_2C^{\mathrm{r}}\, p_\beta\, S'_\gamma + 3T^2\, S'_\beta S'_\gamma\,(1 - p_\beta)\,{}_2C^{\mathrm{r}}$$
(slow γ delayed) (17)

and

$$D''_\beta = 2T\,{}_2C^{\mathrm{r}}\, p_\gamma S'_\beta + 3T^2\, S'_\beta S'_\gamma\,(1 - p_\gamma)\,{}_2C^{\mathrm{r}}$$
slow β delayed). (18)

Evidently, from eqs. (7), (9), (17), and (18):

$${}_3C''_{\mathrm{r}} + 2\,{}_3C'''_{\mathrm{r}} = (1 - p_\gamma) D''_\gamma + (1 - p_\beta) D''_\beta \,. \tag{19}$$

Similarly, from eqs. (15–(18):

$$D'_\gamma - D''_\gamma = 2T\,{}_2C^{\mathrm{t}}(q_\beta + q_{\beta\gamma})\,S'_\gamma + \\ + 3T^2\, S'_\beta S'_\gamma\,(1 - q_\beta - q_{\beta\gamma})\,{}_2C^{\mathrm{t}}$$

$$D'_\beta - D''_\beta = 2T\,{}_2C^{\mathrm{t}}\,(q_\gamma + q_{\beta\gamma})\,S'_\beta + \\ + 3T^2\, S'_\beta S'_\gamma\,(1 - q_\gamma - q_{\beta\gamma})\,{}_2C^{\mathrm{t}} \tag{20}$$

and hence, using eqs. (6), (8) and (10):

$$ {}_3C''_t + {}_3C'''_t = (D'_\beta - D''_\beta) + (D'_\gamma - D''_\gamma) - $$
$$ - 2T\,{}_3C^t\,(S'_\beta + S'_\gamma) - 3T^2 S'_\beta S'_\gamma\,(1 - q_{\beta\gamma})\,{}_2C^t\,. \quad (21) $$

6.1.4. *Both slow channels delayed*

This measures triple chance coincidences produced by a double coincidence and two independent selected pulses:

$$ D''' = 3T^2\,({}_2C^r + {}_2C^t) S'_\beta S'_\gamma\,. \quad (22) $$

6.1.5. *One fast channel and both slow channels delayed*

This is like the preceding case, except that ${}_2C^t = 0$, hence

$$ D'''' = 3T^2\,{}_2C^r\,S'_\beta S'_\gamma\,. \quad (23) $$

Therefore, from eqs. (9), (10), (22), and (23):

$$ {}_3C'''_r = (1 - p_\beta)\,(1 - p_\gamma)\,D'''' \quad (24) $$

$$ D''' - D'''' = 3T^2\,{}_2C^t\,S'_\beta S'_\gamma \quad (25) $$

$$ {}_3C'''_t = (D''' - D'''')\,(1 - q_\beta - q_\gamma - q_{\beta\gamma})\,. \quad (26) $$

6.2. DETAILED CALCULATION OF CORRECTIONS

From eq. (11), the true triple coincidence rate is given by

$$ {}_3C^t = {}_3C - {}_3C' - {}_3C''_r - {}_3C'''_r - {}_3C''_t - {}_3C'''_t $$
$$ = {}_3C - D - {}_3C''_t - {}_3C'''_t\,. \quad (27) $$

In general, the difficulty of determining all chance coincidence corrections lies mostly in the determination of ${}_3C''_t$ and ${}_3C'''_t$, since D can be found by a single delayed coincidence measurement. The best method to be used will differ from case to case, it will depend on the relative magnitudes of the terms and on the approximations that may be made. If, e.g. third order terms can be neglected, then we have

$$ {}_3C^t \cong {}_3C - D - 2T\,{}_2C^t\,\{\,q_\beta S'_\gamma + q_\gamma S'_\beta\,\}\,. \quad (28) $$

If, in this case, ${}_2C^t$, S'_β, S'_γ are measured together with ${}_3C$ during the main measurement, one needs only D, T, q , q to determine the chance coincidence corrections.

In the following, we consider two extreme general approaches at obtaining the corrections. In the first, one measures τ, T, q_β, q_γ, q_γ and calculates all corrections from equations (4), (7), (8), (9), and (10). In the second, one measures all possible delayed coincidences and calculates the chance rates from these.

6.2.1. *Determination of the resolving times τ and T and of q_β, q_γ, q_γ*

By inserting a delay into a fast channel, one measures

$$ D = {}_3C' + {}_3C''_r + {}_3C'''_r $$
$$ = 2\tau S'_\beta S'_\gamma\,\{\,1 + 2T\,[(S_\beta - S'_\beta) + $$
$$ + (S_\gamma - S'_\gamma)] + 3T^2\,(S_\beta - S'_\beta)\,(S_\gamma - S'_\gamma)\,\}\,. \quad (29) $$

If T and the single counting rates are known, τ can be determined from (29). In principle, τ could also be determined from double coincidences alone; this, however, presupposes a τ independent of pulse height. T can be determined from a coincidence measurement with delays in a fast and in a slow channel (eqs. 17, 18), or, with better accuracy, by feeding, say, the β pulse into both fast channels and one slow channel, and delaying the slow γ channel. Use of a double pulser or, simply, of an oscilloscope may be more convenient. If the resolving time is not the same for any two input channels, all equations containing T would have to be generalized accordingly.

For the determination of q^*_β and q^*_γ consider, e.g., q^*_β. If neither the narrow-window ($q^*_\beta \approx 0$) nor the wide-window ($q^*_\beta \approx 1$) approximation can be used, this requires the measurement of ${}_3C_\beta$ (the triple coincidence rate accepting all pulses in the γ channel). Then we have

$$ q^*_\beta = {}_3C^t{}_\beta / {}_2C^t \quad (30) $$

where ${}_3C^t{}_\beta$ is ${}_3C_\beta$ corrected for chance coincidences:

$$ {}_3C^t{}_\beta = {}_3C_\beta - 2\tau S'_\beta S_\gamma - 2T\,{}_2C^t\,(1 - q^*_\beta)\,S'_\beta $$
$$ - 2T\,{}_2C^r\,(1 - p_\beta)\,S'_\beta\,. \quad (31) $$

Substitution of (31) into (30) yields

$$ q^*_\beta = \frac{{}_3C_\beta - (1 - 2T\,S'_\beta)\,{}_2C^t\,(S'_\beta/S_\beta) - 2T\,S'_\beta\,{}_2C}{(1 - 2T\,S'_\beta)\,{}_2C^t} \quad (32) $$

where ${}_2C^{\mathrm{r}}$ and ${}_2C^{\mathrm{t}}$ are given by eqs. (1) and (2). A similar equation holds for $q^*{}_\gamma$.

The separate determination of q_β, q_γ, and $q_{\beta\gamma}$ from $q^*{}_\beta$ and $q^*{}_\gamma$ can be done by successive approximations. Assuming first $q_\beta = q^*{}_\beta$ and $q_\gamma = q^*{}_\gamma$, one calculates an approximate true rate ${}_3C^{\mathrm{t}}$ from eq. (27), obtains an approximate value for $q_{\beta\gamma}$ from eq. (6), and uses this to find better values for q_β, q_γ from eqs. (5), etc.

6.2.2. *Chance coincidence correction by measuring delayed coincidences*

By substituting (25) into (21), one obtains

$$ {}_3C''_{\mathrm{t}} + {}_3C'''_{\mathrm{t}} = (D'_\beta - D''_\beta) + (D'_\gamma - D''_\gamma) - - 2T\,{}_3C^{\mathrm{t}}\,(S'_\beta + S'_\gamma) - (D''' - D'''')\,(1 - q_{\beta\gamma})\,. \tag{33} $$

Using eq. (27), this yields

$$ {}_3C^{\mathrm{t}} = \frac{{}_3C^{\mathrm{t}} - D - (D'_\gamma - D''_\gamma) - (D'_\beta - D''_\beta) + (D''' - D'''')\,(1 - q_{\beta\gamma})}{1 - 2T\,(S'_\beta + S'_\gamma)}\,. \tag{34} $$

Unfortunately, eq. (34) still contains $q_{\beta\gamma}$ and T, but only in terms that should normally be small.

Acknowledgements

The author would like to thank Prof. E. Bleuler and Mr. P. Alexander for several useful discussions.

NUCLEAR INSTRUMENTS AND METHODS 9 (1960) 137–140; NORTH-HOLLAND PUBLISHING CO.

PHASE- AND VERTICAL STABILITY OF MICROTRONS

É. KISDI-KOSZÓ and L. TURI

Central Research Institute for Physics, Budapest

Received 18 August 1960

The phase- and vertical stability of a 8 orbit, 2 MeV microtron are investigated and it is found that owing to the poor phase stability only 7% of the current intensity remains available for acceleration. The vertical drift causes further losses amounting to 90% of the current intensity. The actual output of the apparatus is 0.4% of the electron current fed into the first orbit. A simple method is proposed for improving the phase stability.

In microtrons built up to now[1]) usually a rather high drop in current intensity is observed after completion of the first orbit. In order to reduce this loss in intensity measurements were made on the 2 MeV microtron built in the Central Research Institute for Physics and operated in the mode $a = 1$, $b = 3$, to determine the fraction of electrons available for resonant acceleration due to phase stability after completion of the first orbit. At the same time the losses resulting from vertical drift were also studied. Since in microtrons, so in our apparatus too, the electrons to be accelerated are obtained by cold emission, the phase stability of electron sources with periodically varying intensity was also investigated.

The phase angles at which the electrons leave the resonant cavity and the energies gained by them in each transit[2]) were computed from orbit to orbit for electrons emitted at various times in order to determine the range of phase angles and energies within which electrons are being accelerated. In our computations the transit time τ caused by the finite width d of the accelerating gap was also taken into account. For the first orbit the variations of the transit time τ and of the energy E_{out}, respectively, at which the electrons leave the cavity are shown in terms of the starting time t_s of the electrons in fig. 1. It is due to the finite transit time that it is not the electron emitted when the field strength is at its peak which gains the maximum energy from the accelerating field but an electron emitted much earlier ($\omega t_s = 50°$ where ω is the accelerating field frequency).

For the further orbits we may calculate with good approximation the electrons to have the velocity of light. Eventually it was found that for 280 kV accelerating peak voltages and for $\omega d/c = 0.4133$ the electrons emitted in the range of phase angles $29° \leqq \omega t_s \leqq 64°$ are accelerated. Thus the phase stable region we wanted to determine comprises the electrons emitted with phase angles near to that of the electron gaining the maximum energy ($\omega t_s = 50°$).

Our next task is to determine the time dependence of electron current intensity produced by cold emission. According to the Fowler-Nordheim formula the total current obtained from a metal surface by cold emission is given by

$$I = A\varepsilon^2 \, \mathrm{e}^{-B/\varepsilon}$$

where ε is the field strength on the metal surface. A and B are constants which have been determined theoretically.

Since in our case the field strength ε varies periodically in time, therefore

$$I = I_0 \sin^2 \omega t \, \mathrm{e}^{-\beta/\sin \omega t} ,$$

[1]) P. A. Redhead, H. Le Caine and W. J. Henderson, Canad. Journ. Res. **28A** (1950) 73; C. Henderson, F. F. Heymann and R. E. Jennings, Proc. Roy. Soc. B **66** (1953) 654; H. F. Kaiser, Journ. Franklin Inst. **257** (1954) 107; A. Carrelli and F. Porreca, Nuovo Cim. **6** (1957) 729; D. Aitken and R. E. Jennings, Nature **181** (1958) 1726.

[2]) É. Kisdi-Koszó, Acta Phys. Hung. **4** (1955) 377.

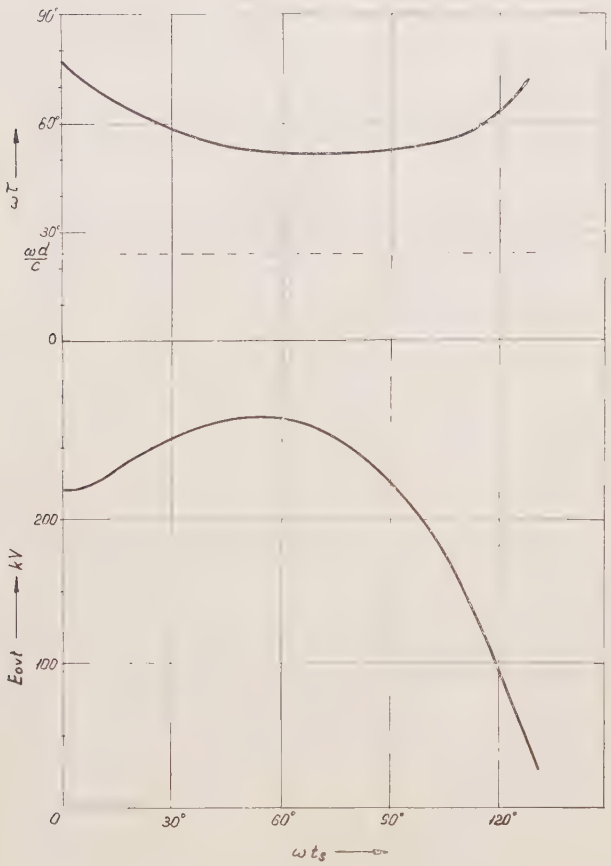

Fig. 1. Transit time τ and energy gain E_{out} in terms of the starting time t_s of electrons for 280 kV accelerating peak voltage with $\omega d/c = 0.4133$.

The vertical drift of the electrons was studied from photographs taken of the electron beam. Since radially the electrons are refocused by the homogeneous magnetic field to the gap of the cavity resonator, we are only interested in the loss due to the vertical drift normal to the plane of the orbit. In evaluating the photographs it was found that only 10% of the current is returned into the cavity. Thus it is seen that due

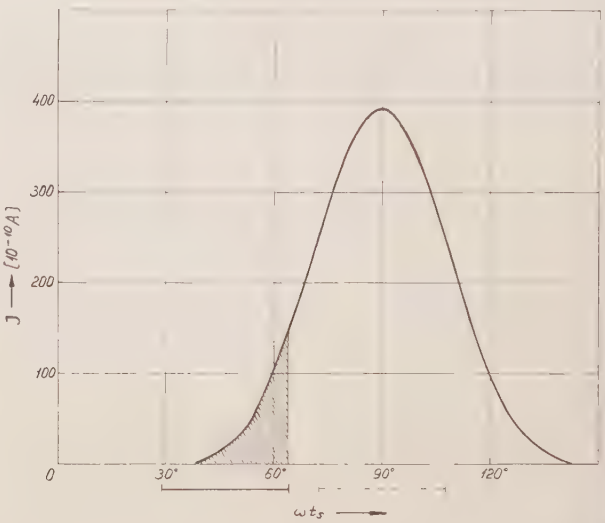

Fig. 2. The time dependence of electron current intensity obtained by cold emission for periodically varying field strength with $I_0 = 4.27 \times 10^{-5}$ A and $\beta = 7$.

where ω is the magnetron frequency. The constants I_0 and β were determined from the energy spectrum of the electrons emerging from the cavity as[3])

$$I_0 = 4.27 \times 10^{-5} A\,, \quad \beta = 7\,.$$

Within a microwave period the electron current intensity obtained by field emission varies as shown by the curve in fig. 2.

The dashed area in the figure represents the phase stable region defined above. It is seen that a serious loss in intensity (one order of magnitude) is caused by the fact that the phase stable region does not lie in the vicinity of maximum field strength. This is the reason that only 7% of the current intensity of the first orbit is left over for further acceleration.

[3]) É. Kisdi-Koszó and L. Turi, Acta Phys. Hung. to be published.

to the lack of vertical stability the current intensity obtainable from microtrons is reduced in the same measure as in consequence of insufficient phase stability.

Summarizing the effects reducing the intensity, it is seen that on the whole 0.7% of the first orbit current intensity remains available for acceleration. This value is in good agreement with the measured value of 0.4%[2]). The accelerated current intensity could be increased by applying a higher accelerating field. Then a shift of the phase stable region towards higher current intensities and a strong increase in the current obtained by cold emission are to be expected. By doubling the amplitude of the field strength the intensity can be increased by a factor of 130.

For a given microwave output the current intensity obtainable from the microtron could be

increased by an additional cavity resonator serving as injector[4]) (fig. 3). By synchronizing the phases of the injector (cavity 2) and the accelerator (cavity 1) it can be achieved that electrons emitted with a phase angle lying in the vicinity of maximum field strength arrive to the accelerating cavity with a suitable phase angle. Now, it is possible by phase focusing to keep 70% instead of 7% of the electrons available for further acceleration. In this way cold emission could become an ideal pulsed electron source delivering electrons with suitable phase angles at the frequency period of the magnetron.

To avoid the problem of magnetron synchro-

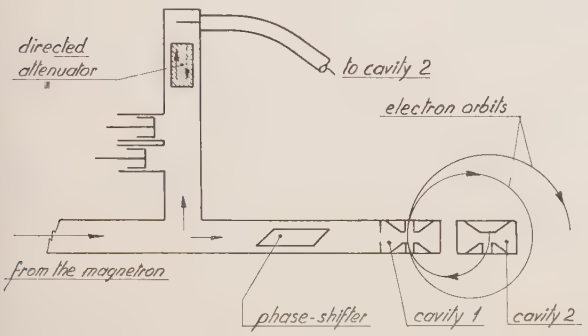

Fig. 3. Use of "injector" in a microtron. For exciting cavity 2 the microwave output dissipated other wise in the stabilizing load of the magnetron could be utilized.

nization it would be convenient to feed the injector and the accelerator from the same magnetron. For this purpose that part of the microwave output could be utilized which otherwise is dissipated in the stabilizing load of the magnetron. Replacing the resistive load by a directed attenuator (ferrit attenuator) the output used hitherto for stabilizing will be fed almost completely into the injector whilst the microwaves reflected from the latter are absorbed by the attenuator so that this assembly of directed attenuator + cavity affects the magnetron in the same way as a matched load.

For other cyclotron type accelerators vertical focusing is usually achieved by a suitable magnetic field (decreasing field with increasing radius). With microtrons, however, this method cannot be applied because the electron orbits are circles passing through the same point in the accelerator gap. For the vertical focusing either an electric or a magnetic field could be used if the microtron were built with a divided magnet where the field free section of the orbit would be sufficiently long to permit adequate focusing. Placing the cavity resonator into a field free section it is also possible to use an electron gun. The distance between the pole pieces of the

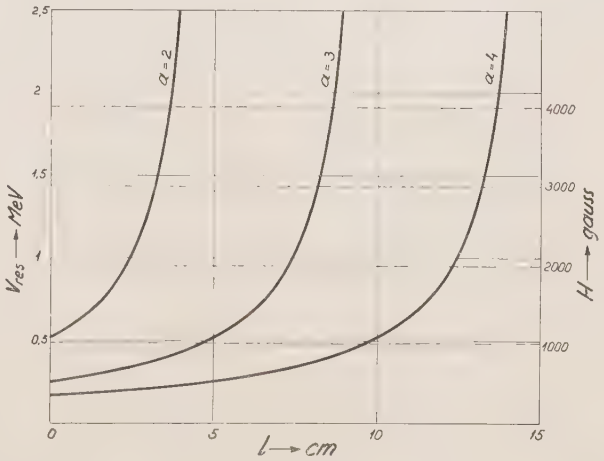

Fig. 4. V_r, H and l in a microtron with divided magnet with various parameters a for $\nu = 3000$ Mc/s and $b = 1$.

magnet may be chosen to be quite small so that the stray field is also kept rather low. A further advantage of using a divided magnet is that in this case the accelerating voltage and the magnetic field are not restricted by the so-called electron mass limitation, since the resonance conditions are modified by the length of the field free section. In a microtron using a magnet of two sections for electrons travelling with the velocity of light, we have

$$eV_r = mc^2 \frac{b}{a - b - \frac{2l\nu}{c}},$$

$$H = 2\pi\nu \frac{mc}{e} \frac{1}{a - b - \frac{2l\nu}{c}},$$

where V_r is the resonance value of the accelerating voltage

[4]) Chr. Schmelzer, Z. Naturforsch. **7a** (1952) 808 was the first to suggest the application of an injecting cavity resonator.

mc^2 is the rest mass energy of the electron
$a > b$ are positive integers
$2l$ is the length of the field free section
ν is the accelerating field frequency
H is the value of the required magnetic field strength.

In fig. 4 the values of magnetic field and accelerating voltage with various parameters a are plotted in terms of the distance between the two magnets for $\nu = 3000$ Mc/s and $b = 1$.

For microtrons with divided magnet the design presents some problems since the related values V_r, H and l for electrons emitted with velocities less than light can be determined only by numerical calculations[5]). Similarly, numerical calculations are needed for the study of the effect of field free sections on the phase focusing.

[5]) L. Turi, Reports of the Central Research Inst. f. Phys. **7** (1959) 111.

NUCLEAR INSTRUMENTS AND METHODS 9 (1960) 141–144; NORTH-HOLLAND PUBLISHING CO.

ON THE USE OF BREMSSTRAHLUNG FOR THE DETERMINATION OF TRITIUM IN AQUEOUS AND ORGANIC SYSTEMS

T. WESTERMARK, L. DEVELL and N. A. GHANEM†

Division of Physical Chemistry, The Royal Institute of Technology, Stockholm 70, Sweden

Received 10 September 1960

The bremsstrahlung method for the determination of beta radioactivity without gamma radiation is extended to the case of tritium. Using cells made from light materials, excellent results and rough agreement with theoretical estimates were obtained for water containing millicurie amounts of tritium. Applications to self-diffusion studies on water and labelling experiments are briefly described.

1. Introduction

The use of bremsstrahlung for the quantitative determination of beta radioactive substances without gamma emission is a well-known procedure[1]). However, the method does not seem to have been extended to the beta emitter of lowest energy, viz. tritium, although its bremsstrahlung has been used for various applied purposes such as concentration measurements[2]). We have found the method quite feasible and very practical for stronger samples, of the order of millicuries and upwards. Results are reported for aqueous systems as well as organic systems.

2. Theoretical Notes

It is well known that beta particles produce electromagnetic radiation (somewhat less energetic than their own energy) in matter, partly as continuous bremsstrahlung and partly as characteristic X-rays. If we consider the case of tritium (half-life 12.26 years[3]), maximum beta energy 18 keV[4]), average beta energy 5.7 keV) present in pure water, we can neglect the characteristic X-rays because in this case the hardest X-rays will be those of oxygen and they will be almost completely self-absorbed or absorbed in the walls of the container or detector window in the experiments to be described (and similarly in other possible designs).

† On leave from The National Research Centre, El-Dokki Cairo, U.A.R.

Theoretically the case of tritium is simplified because the energy of the beta particles is very small in relation to m_0c^2. The electron energy loss due to bremsstrahlung production according to Bethe-Heitler's theory in such a case reduces to[5])

$$-\frac{\mathrm{d}E}{\mathrm{d}x} = NE_0\phi_{\mathrm{rad}} \ \text{MeV/cm} \qquad (1)$$

where $\phi_{\mathrm{rad}} = \frac{1}{3}\,\bar{\phi}$ and $\bar{\phi} = (Z^2 + Z)\ 5.80 \times 10^{-28}$ cm^2 in this case. $E_0 = E_\beta + m_0c^2$ or 0.517 MeV (on an average). N = atoms/cm^3.

For notations, see Heitler[5]).

Integrating (1) and using mass per unit area instead of length, we obtain the electromagnetic energy per beta-ray (E_0 can be regarded as a constant):

$$E_\gamma = N_A E_0 \frac{(Z^2 + Z)}{A} 5.80 \times 10^{-28} \cdot R \ \text{MeV/beta-ray} \qquad (2)$$

where $N_A = 6.02 \times 10^{23}$, A = the atomic weight and R = the true range of the beta-ray in g/cm^2. For the usual case of a multi-component system, the term $(Z^2 + Z)/A$ will be replaced by $\sum_{i=1}^{n} x_i\,(Z^2{}_i + Z_i)/A_i$, where x_i is the weight-fraction of the atomic species in question.

[1]) W. J. Whitehouse and J. L. Putman, Radioactive isotopes (Clarendon Press, Oxford, 1953).

[2]) M. M. Kannuna and J. F. Cameron, J. Appl. Rad. Isotopes **2** (1957) 76.

[3]) W. M. Jones, Phys. Rev. **100** (1955) 124.

[4]) J. F. Cameron, J. R. Rhodes and P. F. Berry, AERE-R 3086 (1959).

[5]) W. Heitler, The quantum theory of radiation (3rd ed.) (Clarendon Press, Oxford, 1954) p. 251–255.

Inserting the average beta energy for tritium and assuming[6]) its true range to be 0.06×10^{-3} g/cm^2, we get an order of 2.5×10^{-4} keV for E_γ per beta particle in water.

Thus it is seen that, in a medium with very large dimensions compared with the beta energy but very small in comparison with the half-value thickness for bremsstrahlung absorption, the bremsstrahlung energy can be expected to be a fraction of the order of 4.5×10^{-5} of the beta energy for water and vary as $\Sigma\, x(Z^2 + Z)/A$ with the medium. The intensity relations might be assumed roughly to be about the same.

The bremsstrahlung has a continuous distribution which has been studied only very recently[4]). By means of the spectral data, it is possible to design a cell for an optimized detection of tritium bremsquanta from water. The design has to include the selection of a low atomic number wall of small thickness. The data given by Cameron[4]) *et al.* have been very useful for this work. From the above theoretical notes, it can be shown that the production of bremsstrahlung in water and in an organic solvent (say benzene) differs only by a few percent and that some gain in relation to the solvent is got by dissolving heavy-atom inorganic salts in water or heavy halogen compounds (or other heavy-atom additive) in the organic solvent. In these cases, characteristic K X-rays are expected (cf. Cameron's case of Ti or Zr targets) but not higher in Z than what corresponds to the maximum beta energy. Hence some optimum (with Z) is to be expected. On the other hand, self-absorption will be expected to counteract this intensity increase resulting from the higher mean atomic number.

3. Experimental

The experimental arrangement is explained by means of fig. 1 and its text. The design of the cell was made according to the above considerations.

Perspex has been used as wall material for aqueous systems and the window was made from 18 mg/cm^2 polyester sheet (Du Pont's "Mylar").

[6]) A. T. Nelms, Nat. Bur. Stand. Circular 577 (1956) p. 26 and 28.

The latter was found to absorb about 30% of the incident radiation. The detector chosen was an argon-filled Geiger counter, actually of the same

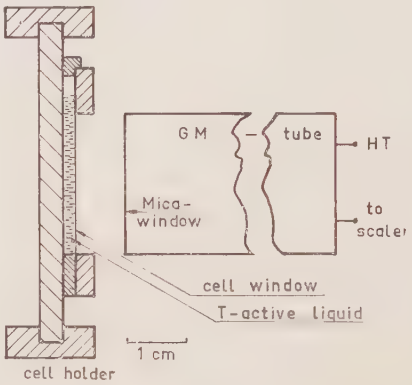

Fig. 1. Scheme of T-measurement on active liquids by bremsstrahlung. Cell for water was made from perspex with 18 mg/cm^2 polyester window, volume 1.2 ml. For organic liquids, a similar cell of teflon, (window also of teflon) was used; GM-tube: Mullard Mx118, filled with argon and halogen.

type as the one used by Kannuna and Cameron for sulphur determinations[2]). The argon K-electron absorption matches the bremsstrahlung distribution reasonably well and so the detection efficiency should be rather high. A scintillation detector with good electronic properties might be a future improvement. The detector was connected to a conventional scaler and an appropriate point on the plateau and discriminator level were found.

4. Results for Pure Water

Tritiated water, procured from AERE at Harwell, was diluted by known factors. The sample was standardized against a standard tritium water sample (from New England Nuclear Corporation) by the liquid scintillation method. This work was performed for us by the Isotope Techniques Laboratory using the Ekco liquid scintillation unit. (Model N-612).

The bremsstrahlung counting rate as a function of tritium concentration is shown in fig. 2. As expected, a straight line was obtained. The deviation from linearity was found to be nearly the same as the statistical errors of counting.

The addition of 0.2 ml extra tritium water on top of the standard 1.2 ml did not change the

counting-rate. The reason is apparently that the wall effectively stops all bremsstrahlung from the top layer. Thus the activity measurement is

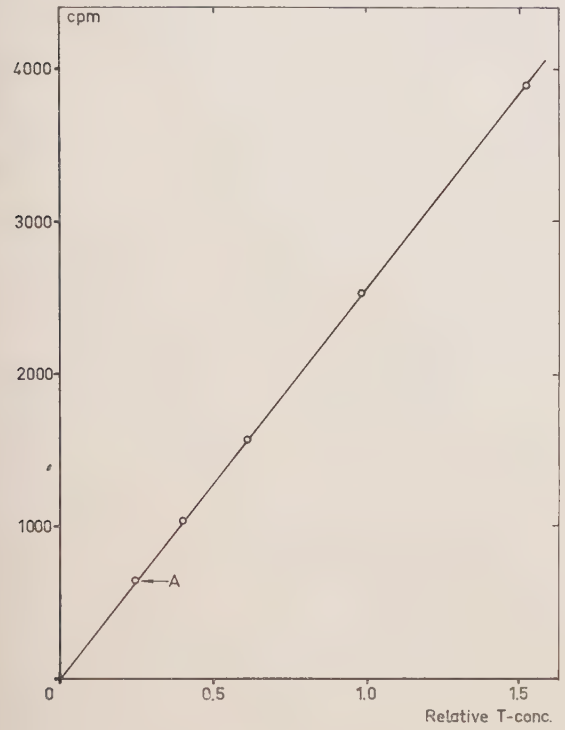

Fig. 2. Counting-rate of T bremsstrahlung measured by apparatus in fig. 1. Counting time 60 min for each point. Background 65 cpm when the apparatus was shielded with 10 mm lead (lined with 2 mm Al). The point A was absolutely standardized (cf. text) and has a T-concentration of 3.8 mc/ml (± 15%).

confined to an active volume limited by the window area and thus corresponds to the true concentration. The solid angle of the cell in relation to the counter was found by a hard beta ray standard source (UX_2) to be 10%. By using the theoretical estimate, the detection efficiency was found to be 7%.

5. Water Solutions

From (2) it is evident that larger bremsstrahlung yields would be expected if the effective average of $(Z^2 + Z)/A$ for the medium increases but self-absorption reduces the effect.

We have not investigated this effect systematically but have noticed that the addition of lead nitrate steadily decreases the bremsstrahlung counting rate with increasing concentration.

6. Organic Systems

A similar cell to that of fig. 1 was constructed using teflon and the window was also made from teflon (thickness 0.25 mm). It works very satisfactorily and the counting rates were found to be very similar to those for water for the same tritium concentrations.

7. Applications to Diffusion Studies, Labelling Experiments and T Content in Steel Electrodes

7.1. DIFFUSION STUDIES

The method has already been applied to the selfdiffusion of water by one of us (L.D.). Preliminary data show that the method will provide a good complement to other possible methods of tritium analysis and because of its simplicity and accuracy it might even be the best one. The relatively high concentration of tritium which is necessary for the detection of the bremsstrahlung is of no disadvantage in the diffusion measurements. As shown by the first set of experiments, the heat generated by the beta radiation does not give rise to any convection in the diffusion cell. The accuracy of the method is sufficient for the diffusion measurements. During one day, the standard deviation of the average was not larger than 0.1%. A special point in this application is that it is sufficient with quotients between two liquid activities obtained after diffusion has proceeded for some time, and so no standardization at all is necessary.

7.2. TRITIUM LABELLING EXPERIMENTS

The bremsstrahlung method for tritium determinations in organic compounds has turned out to be very practical in connection with the microwave labelling project[7]). This method yields normally specific activities of the order of hundreds of millicuries per gram. The total amount of matter is only 10–50 mg and so total T-activities of, say, 1–50 mc are got. The

[7]) T. Westermark, H. Lindroth and B. Enander, J. Appl. Rad. Isotopes **7**, (1960) 331; N. Ghanem and T. Westermark, J. Am. Chem. Soc. **82** (1960) 4432; N. Ghanem and T. Westermark, Paper presented to the IAEA-conference on "The Use of Radioisotopes in the Physical Sciences and Industry", Copenhagen 1960.

substances may be solid or liquid. The direct and non-destructive measurement of bremsstrahlung is very useful because it gives in a few minutes a sufficiently good indication concerning the result of the labelling experiment. The total T-activity fixed in the sample is quickly found after standardization with a known sample and by appropriate selfabsorption corrections. The result of the various purification steps is then readily followed by counting the purified samples with the same geometry. As an example, the first labelling experiment on carboxy-methyl-cellulose showed a specific activity of 350 mc/g directly (when enclosed in a bag of 7 mg/cm^2 polyester sheet). When left in contact with air overnight, the activity went down to 80 mc/g. The material was digested in boiling water, cooled and an excess of methanol added. The liquids were distilled off under reduced pressure. The activity of the dry material was then 14 mc/g. This example thus yields rough information concerning adsorptively fixed tritium and tritium exchangeable with water.

7.3. STEEL ELECTRODES

Bremsstrahlung counting solved our problem of measuring the amount of tritium fixed to the steel electrodes of the DC- and 50 Hz AC-glow discharge tritium labelling experiments[7]). After treatment, the electrodes were removed and counted. Standardization against a titanium disk of known T content (from the Wesix Company, Calif., USA) yielded amounts of about 0.5 mc (after correction for the atomic number difference and assuming the tritium depth distribution to be similar).

Acknowledgements

The authors wish to thank Professor O. Lamm for his encouragement and the excellent working conditions placed at our disposal. We are further indebted to Mr. H. Lindroth and Miss R. Persson for introductory laboratory work. Miss M. Ågeland has assisted with most of the experimental data presented here. Thanks are also due to Mr. H. Forsberg of the Isotope Techniques Laboratory for the absolute standardization.

NUCLEAR INSTRUMENTS AND METHODS 9 (1960) 145–148; NORTH-HOLLAND PUBLISHING CO.

A NOTE ON THE BACKGROUND IN NaI SCINTILLATION COUNTERS†

S. RABOY and C. C. TRAUL

Argonne National Laboratory, Argonne, Illinois

Received 29 August 1960

The residual background in sodium iodide (thallium activated) crystals has been studied with the scintillation spectrometer with an anticoincidence annulus. The characteristic response of this system to gamma rays is used to identify background peaks as coming from gamma rays and not-charged particles. There are contributions from the natural radioactivity of K^{40}, the Th^{232} series, and the U^{238} series. By controlled experiments it was concluded that the decays from K^{40} and the U^{238} series originate in the room surroundings and that the activity from the Th^{232} series originates in the immediate vicinity of the sodium iodide crystal, such as the materials of the package. The results are consistent with the assumption of no radioactive contaminant within the crystal itself.

1. Introduction

The use of an anticoincidence annulus of NaI(Tl) with a NaI(Tl) scintillation counter[1]) permits the energies and areas of photopeaks to be determined with good precision. Since the multiple processes characteristic of scintillation counters have been largely eliminated, the degree of precision depends largely upon the counting statistics[2]). Care must be taken however to determine and to remove the effects of the backgrounds from radioactivity in the crystal and its environment. The purpose of this article is to describe the background observed at this laboratory. The energies of the lines are given and an attempt is made to identify the radioactive sources.

2. Discussion

The background was observed in the apparatus described in ref.[1]). Briefly, the pulses from a NaI(Tl) crystal 2.4 inches in diameter and 6 inches long are analyzed by a 256-channel pulse sorter[3]) if there is no pulse in a NaI(Tl) scintillation counter which surrounds the first crystal. The anticoincidence annulus is a cylinder 8 inches in diameter and 12 inches long with a hole 2.5 inches in diameter on the axis. Pulses from the anticoincidence annulus are detected by six 6292 photomultiplier whose anodes are connected in parallel.

If a gamma ray is scattered by the center crystal into the annulus and if the scattered gamma ray loses more than about 30 keV in the annulus, the pulse is discarded electronically. In this way ambiguities from the multiple processes

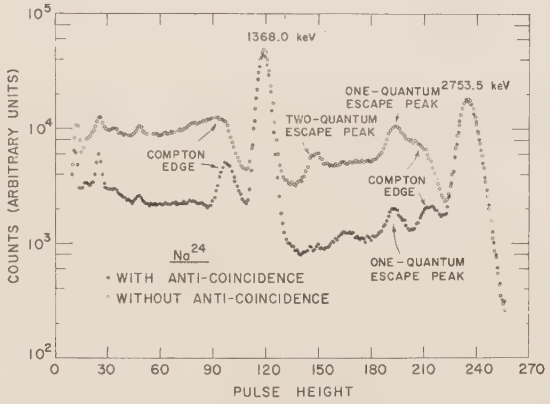

Fig. 1. The gamma-ray spectrum from Na^{24} with and without the anticoincidence annulus. The spectra have been normalized at the 2.75-MeV peak and the ordinate is approximately the actual number of counts.

† Work performed under the auspices of the U.S. Atomic Energy Commission.

[1]) C. C. Trail and Sol Raboy, Rev. Sci. Instr. 30 (1959) 425.

[2]) A procedure to use a digital computer, to determine the height, width, and position (with errors) of full-energy peaks of gamma rays will be published soon by R. Julke, J. Monahan, S. Raboy and C. C. Trail.

[3]) R. W. Schuman and J. P. McMahon, Rev. Sci. Instr. 27 (1956) 675.

in the crystal are suppressed. For comparison, fig. 1 shows the response of this apparatus to the 2.75- and 1.37-MeV gamma rays from Na^{24} with and without the anticoincidence annulus. Fig. 1 shows that the anticoincidence annulus reduces

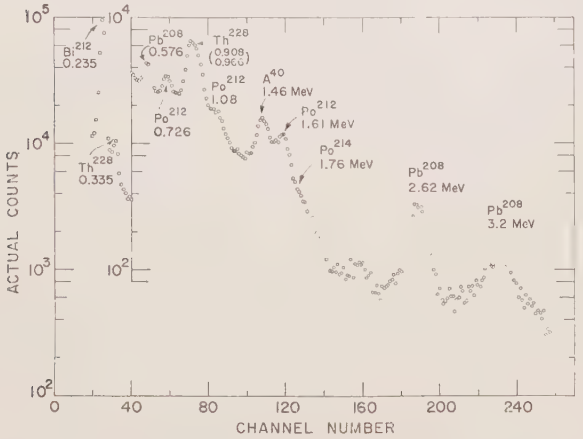

Fig. 2. The background spectrum in the spectrometer with the anticoincidence annulus functioning and 2 inches of lead surrounding the crystals, photomultipliers, and preamplifiers. The data were obtained in about 23 hours.

the spectrum from Compton scattering of the 2.75-MeV gamma ray by about a factor of four. The spectrum obtained with the anticoincidence annulus shows a Compton edge which results from back-scattered radiation escaping through the entrance aperture. A one-quantum escape peak is evident at pulse height 195 but no two-quantum escape peak is present in this apparatus. A peak at pulse height 165 is presumably from a radioactive contaminant in the source. Fig. 2 shows the background observed when the anticoincidence apparatus is surrounded with 2 inches of lead. The crystals, their photomultipliers, and the preamplifiers were inside the lead shield. The energy scale has been determined with the 898.4- and 1835.5 keV lines of Y^{88} on the assumption that the apparatus has a linear energy response[4]). This assumption has been found to be good to a few percent over the range used.

Fig. 3 shows the background spectrum obtained when the lead was removed from the apparatus. We note first that a prominent line, which we attribute to the decay of K^{40} to A^{40}, appears at 1.4 MeV. The intensity of the line

with the 2-inch lead shield is $7.5 \pm 1.0\%$ of the intensity without the shield. The intensities were determined by the method of Covell[5]). The uncertainties associated with the intensities are statistical only and do not include any estimate

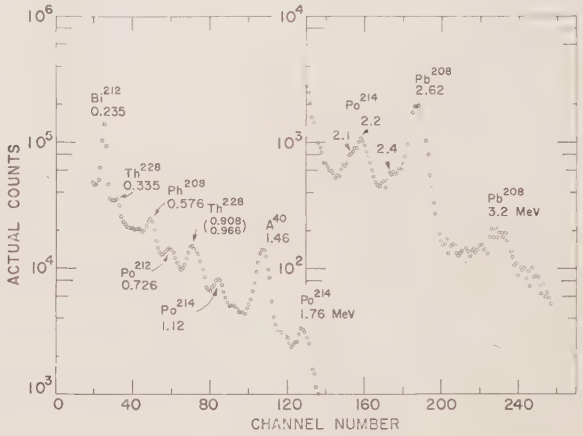

Fig. 3. The background spectrum obtained as in fig. 2 but with no lead around the spectrometer. These data were collected in about 26 hours.

of the experimental errors. Since the calculated transmission[6]) of 2 inches of lead for a 1.4-MeV gamma ray is 5.5%, we see that most of the K^{40} is outside the lead shield.

The gamma ray at 2.6 MeV is the well-known line from the β-decay of Tl^{208} to Pb^{208} in the thorium decay series. In this case the calculated transmission of the shield is 8% while the ratio of intensities is $20 \pm 2\%$. We conclude that some thorium is contained in the packaging, photomultiplier, associated circuitry, and shielding rather than in the outer crystal or center crystal.

The NaI(Tl) crystals are excluded from consideration as sources of the thorium decay chain because of the characteristics of the full-energy peaks of the 2.6-MeV gamma ray. The 2.62-MeV gamma ray follows a β particle with a maximum energy of about 1.3 MeV. If this occurred in the center crystal and the 2.62-MeV gamma ray underwent a full-energy interaction we would,

[4]) J. Monahan, S. Raboy and C. C. Trail, to be published.

[5]) D. F. Covell, U.S. Naval Radiological Defense Laboratory Report TR-288.

[6]) Gladys White Grodstein, National Bureau of Standards Report 583 (1957).

see a β spectrum 2.6 MeV higher. If the decay occurred in the outer annulus, the β event would actuate the anticoincident circuit and a pulse caused in the center crystal by the 2.62-MeV gamma ray would not be analyzed.

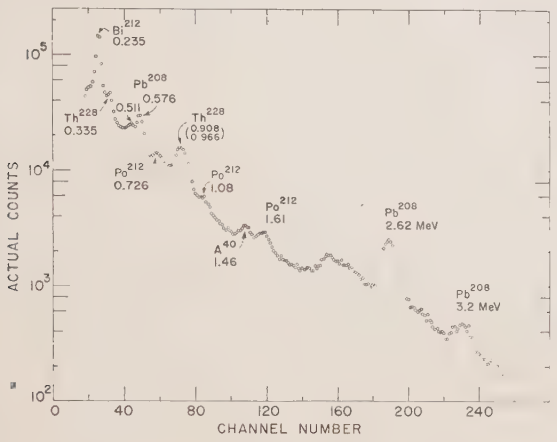

Fig. 4. The background spectra in the crystal surrounded with 2 inches of lead but with no anticoincidence gating. The running time was about 26 hours.

The most intense branching of the Tl^{208} decay is to the 3.2-MeV level of Pb^{208} which emits a 580-keV gamma ray in coincidence with the 2.6-MeV radiation. The peak at 576 keV is presumably this cascade gamma ray. The intensity is reduced by the 2 inches of lead to $20 \pm 1\%$ of the intensity with no lead. The calculated transmission for 576 keV is 0.1% and we thus have additional evidence for the existence of thorium in the counter system. The ratio of intensities, with and without the lead, of the peak at 3.2 MeV is 0.9 ± 0.2 and thus is associated with thorium in the crystal and package. It appears this peak comes from a summing of the 0.580-keV and 2.6-MeV lines by the center crystal, a process for which the geometric arrangement is extremely favorable. If it were a crossover, we should see an increase in intensity corresponding to the increase of the intensity of the 2.6-MeV gamma ray when the lead is removed. This sum peak at 3.2 MeV has been observed by other investigators[7]).

There has been some conjecture that the peak at 3.2 MeV is due to α particles from the thorium in the crystal. Fig. 4 shows the spectrum of the background obtained with the counter shielded and no anticoincidence gating of the analyzer. Comparison of the shapes of the spectrum of a high-energy gamma ray with and without anticoincidence in fig. 4 with the corresponding shapes in fig. 1 suggests that the 3.2-MeV line has the characteristics of gamma radiation.

In fig. 4 we note the appearance of a peak corresponding to a gamma ray of about 510 keV. This peak is missing in fig. 2 (anticoincidence annulus functioning). We attribute this gamma ray to a branch of the Tl^{208} decay, which occurs 33% of the time and leads to a 511-583-2620 keV cascade. The detection of the peak of the 511-keV gamma ray when the anticoincidence gate is removed and then the absence of the peak when the anticoincidence gate is working indicates that the Tl^{208} decays (Th decay chain) occur in the regions very close to the crystals such as the reflector or Al can. For the 511-keV gamma ray to appear in the spectrum, both the center crystal and the annulus must miss detecting the 583 keV or 2620 keV gamma rays. This is improbable for a geometrical situation which has the Tl^{208} source very close to the crystal. On the other hand, the branch which feeds the cascade 583--2620 keV can lead to a peak corresponding to the 583-keV gamma ray. The 2620 keV may escape detection by the anticoincidence ring. When the anticoincident circuit is disconnected we see the peak at 510 keV since scintillations produced in the annulus by the coincident gamma rays have no influence on the analysis of pulses from the center crystal. The 1.08-MeV line in fig. 2 may result from the 511-keV and 576-keV sum peak or may be due to a transition in Po^{212} which Emery and Kane[8]) report as a weak doublet of energy 1074 keV and 1078 keV in the decay of radiothorium.

The peak at 726 keV is assigned to a 727-keV transition from the first excited state in Po^{212} and the 1.61-MeV gamma ray is identified as the

[7]) P. R. Bell, R. C. Davis, G. G. Kelley and J. E. Francis, privately circulated report.

[8]) G. T. Emery and W. R. Kane, Phys. Rev. **118** (1960) 755.

1.62-MeV line in Po^{212}, also reported by Emery and Kane[8]).

Another intense line at 238 keV has been observed in Bi^{212} and we identify the line at 235 keV as this transition and the peak at 335 keV may result partly from a 300-keV line[8]) in Bi^{212}, but is more likely due to a 335-keV transition in Th^{228} which is discussed below.

In fig. 2 there is a slight hint of a line at about 1.7 MeV which is much stronger in fig. 3, the background with no lead around the apparatus. Here we see the line of Po^{214} (RaC in the uranium-radium decay chain) at 2.4, 2.2, 2.1, and 1.1 MeV as well as the line at 1.76 MeV. These lines have been studied by Mladjenović and Hedgran[9]), who also report weaker lines at 609 keV and 768 keV which are partly masked by the gamma rays from the thorium decay chain. These sources are presumed to be external to the apparatus and possibly are contained in the masonry of the building. A line at 352 keV has been reported[10]) in Bi^{214} which is part of this decay series. This appears as a broadening of the 335 keV line in Th^{228}.

A peculiar line, composed of at least two gamma rays, is evident around 900 keV. A level reported[11]) in Th^{228} at 966 keV is fed 35% of the time by β decay of Ac^{228}. This state decays to the ground state and to the first excited state at 58 keV with about a 3 to 5 branching ratio. These 908-keV and 966-keV gamma rays are the most intense gamma rays in the decay, apart from the 58-keV gamma ray. A line about one-fourth as intense as the doublet results from the transition from the 396-keV level to the 58-keV level. This transition in Th^{228} emits the 335-keV line mentioned above.

Emery and Kane[8]) studied the decay of Th^{228} and did not observe the lines at 335 keV, 908 keV, and 966 keV. This gives additional evidence for associating these lines with the decay of Ac^{228} to Th^{228} in the decay chain of Th^{232}.

We acknowledge the valuable assistance of Joseph Peregrin who helped maintain the apparatus during the experiment.

[9]) Milorad Mladjenović and Arne Hedgran, Arkiv för Fysik **8** (1954) 49.

[10]) D. E. Muller, H. C. Hoyt, D. J. Klein and J. W. M. DuMond, Phys. Rev. **88** (1952) 775.

[11]) S. Bjornholm, O. Nathan, O. B. Nielsen and R. K. Sheline, Nucl. Phys. **4** (1957) 313.

NUCLEAR INSTRUMENTS AND METHODS 9 (1960) 149–153; NORTH-HOLLAND PUBLISHING CO.

METHOD OF EVALUATING DELAYED COINCIDENCE EXPERIMENTS

R. S. WEAVER and R. E. BELL

Radiation Laboratory, McGill University, Montreal

Received 25 July 1960

Frequently in delayed coincidence work a resolution curve is measured with good accuracy, but no exactly comparable prompt resolution curve is available. The centroid-shift method of evaluating the lifetime τ cannot be applied because the zero of time (centroid of the prompt curve) is not known. If τ is close to the instrumental limit, it cannot be measured from the logarithmic slope of the measured resolution curve. We then require an objective measure of the asymmetry of the measured curve, calculable without reference to any other curve. Such a quantity is the third moment of the measured curve about its own centroid. We show that the normalized third moment is equal to $(2\tau^3 + \varepsilon)$, where ε is the normalized third moment of the prompt curve, usually small and frequently negligible. Thus τ can be evaluated with at most only rough knowledge of the prompt curve. The McGill IBM 650 computer has been programmed to perform the arithmetical work, which is otherwise laborious. An application to an actual example is shown. Estimates are given of the accuracy to be expected from the method.

1. Introduction

In measuring short lifetimes by the delayed coincidence method, the usual procedure is to measure the time resolution curve for the radiation in question (the "delayed" curve), and a curve of the time resolution of the apparatus for a source of radiation of very short lifetime (the "prompt" curve). Ideally the prompt curve should be measured with a source identical in all respects to the delayed source, except for the lifetime. Such a source is almost never available. The position of the centroid of the prompt curve defines the zero of time for the experiment. Unfortunately this centroid position is sensitive to the detailed properties of the prompt source, and is also subject to instrumental drifts. These effects may cause large errors in evaluating the lifetime by the centroid-shift method of Bay[1]) or the area analysis method of Newton[2]), if the lifetime being measured is close to the instrumental limit. Birk, Goldring and Wolfson[3]) have recently introduced a method of analysis making detailed use of the moments of the prompt and delayed resolution curves. Their method thus depends on accurate knowledge of the prompt curve, and in their experiments they adopt a fast cycling procedure to minimize drifts.

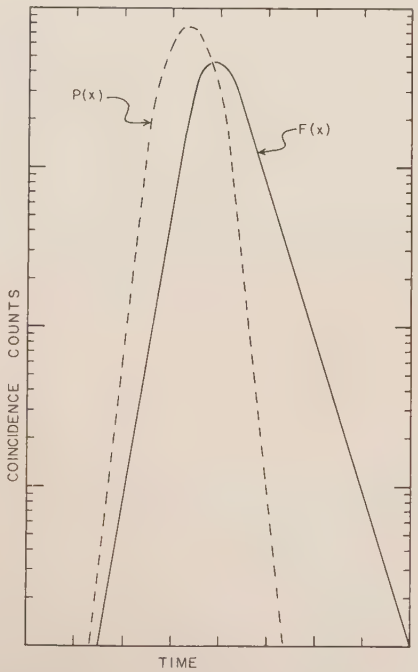

Fig. 1. Normalized prompt and delayed coincidence curves. The prompt curve is drawn with a broken line because we assume that it has not been observed accurately.

[1]) Z. Bay, Phys. Rev. **77** (1950) 419.
[2]) T. D. Newton, Phys. Rev. **78** (1950) 490.
[3]) M. Birk, G. Goldring and Y. Wolfson, Phys. Rev. **116** (1959) 730.

2. Derivation of Moment Relations

We now show that it is possible to evaluate the required lifetime from the shape of the delayed curve with only rough knowledge of the shape of the prompt curve. The relative positions of the centroids of the two curves do not enter the analysis.

In fig. 1, $P(x)$ is the unobserved true prompt curve and $F(x)$ is the measured delayed curve, both normalized to unit area and plotted on a logarithmic scale as a function of x, the delay time. The true zero of time coincides with the centroid of the unobserved prompt curve $P(x)$, and on this scale the centroid of $F(x)$ lies at $+\tau$, where τ is the mean life to be evaluated. Bay[1]) has shown that the following relation holds among the moments of the two curves:

$$M_r(F) = \sum_{k=0}^{r} \frac{r!}{k!\,(r-k)!}\, M_{r-k}(P)\, M_k(\omega) \qquad (1)$$

where $M_r(F)$ is the rth moment of $F(x)$,

$$M_r(F) = \int_{-\infty}^{\infty} x^r\, F(x)\, \mathrm{d}x \qquad (2)$$

and $\omega(x) = [\tau^{-1} \exp(-x/\tau)]$ is the radioactive decay law for the radiation of mean life τ. We have at once by integration $M_n(\omega) = n!\tau^n$; in particular

$$\begin{aligned} M_1(\omega) &= \tau \\ M_2(\omega) &= 2\tau^2 \\ M_3(\omega) &= 6\tau^3\,, \end{aligned} \qquad (3)$$

and by definition of the zero of time,

$$M_1(P) = 0\,. \qquad (4)$$

We also define $M_2(P) = \sigma^2$ (this does not imply that $P(x)$ is a Gaussian), and $M_3(P) = \varepsilon$. Now writing out Bay's relation (1) for $r = 1, 2$ and 3, we have

$$M_1(F) = \tau \qquad (5)$$

$$M_2(F) = \sigma^2 + 2\tau^2 \qquad (6)$$

$$M_3(F) = 3\sigma^2\tau + 6\tau^3 + \varepsilon\,. \qquad (7)$$

These are the first three moments of the delayed curve about the zero of time, i.e. about the (unknown) centroid of the prompt curve.

Now let us take moments about the (calculable) centroid of the delayed curve. We denote such moments by the letter N rather than the previous M. Since the centroid of $F(x)$ lies at $+\tau$, we now have

$$N_r(F) = \int_{-\infty}^{\infty} (x-\tau)^r\, F(x)\, \mathrm{d}x\,. \qquad (8)$$

Expanding (8) for the cases $r = 1, 2, 3$, and substituting known values, we get

$$N_1(F) = 0 \quad \text{(definition of centroid of } F\text{)} \qquad (9)$$

$$N_2(F) = \sigma^2 + \tau^2 \qquad (10)$$

$$N_3(F) = 2\tau^3 + \varepsilon\,. \qquad (11)$$

Thus the procedure is to calculate the centroid of the observed delayed curve $F(x)$, and adopt it as the origin of x, ensuring that (9) is obeyed. Then upon computing $N_3(F)$ from the experimental data, we have

$$\tau = \left\{ \frac{N_3(F) - \varepsilon}{2} \right\}^{\frac{1}{3}}. \qquad (12)$$

Here ε, the third moment of the prompt curve $P(x)$ about its own centroid, is usually small and frequently negligible, so that for many cases it is sufficient to write

$$\tau = \left\{ \frac{N_3(F)}{2} \right\}^{\frac{1}{3}}. \qquad (13)$$

In any case, rough knowledge of $P(x)$ will give a value of ε ($\equiv M_3(P)$) sufficiently accurate to make a correction. Even if ε is as large as $\frac{1}{3}$ of $N_3(F)$, the error in τ caused by ignoring it altogether is only about 10 %.

3. Sample Computations

The experimental data usually consist of total counts in a number of time channels, recorded in the multichannel analyzer that forms the output of a time-to-amplitude converter. The arithmetical operations are simple, but laborious if performed by hand. The McGill IBM 650 computer has been programmed to do the calculations. The output data consists of the total area of the curve, and the normalized values of the first three moments.

As an example, we use the data from the measurement of the half life of the 1507 keV excited state of Gd^{156}, published by Bell and Jørgensen[4]) (fig. 2). In this case the half-life was

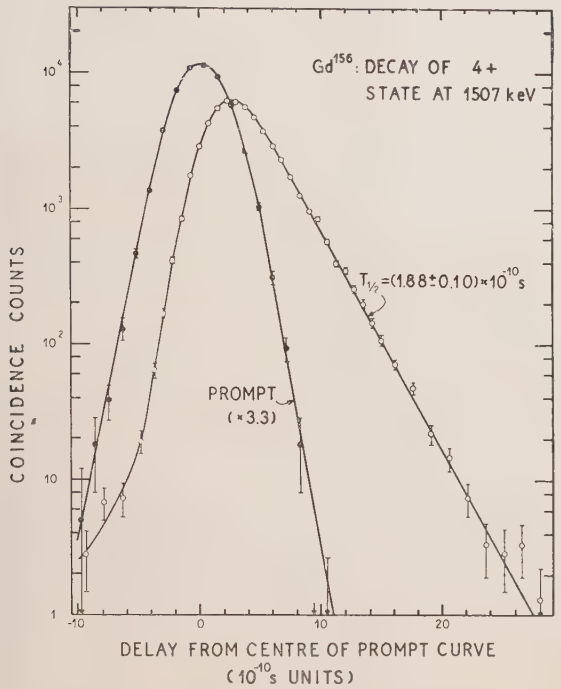

Fig. 2. A delayed resolution curve measured by Bell and Jørgensen[4]), with an approximate prompt curve for comparison, used in sample calculations by the third moment method.

read from the slope of the exponential decay of the delayed curve, and was given as $(1.88 \pm 0.10) \times 10^{-10}$ s. The assigned error of about 5% was mainly due to causes other than statistical. The prompt curve in the diagram is an example of the case discussed above, representing the approximate shape, but not the exact position, of the true prompt curve. The half-life of this state is short enough to permit a useful application of the moment procedure, and long enough to provide independent means of determination of the half life. A computer calculation of the third moment of the delayed curve yielded a result equivalent to a half-life of 1.88×10^{-10} s, the exact agreement with the published value being fortuitous. The calculated third moment of the prompt curve was 0.12% of that of the delayed curve, so that the error caused by neglecting it in calculating τ was only 0.04%. This implies that the rough practical limit mentioned above ($\varepsilon = \frac{1}{3} N_3(F)$) would have been reached if the computed third moment of the delayed curve had been about 300 times smaller, i.e. if the half life had been about 3×10^{-11} s.

As the computer lends itself to fast calculations of such quantities as moments, various rearrangements of the actual experimental data were tried. For example, the leading edge of the delayed coincidence curve has a slight tail at low values of time, due to instrumental resolution difficulties; at low values of counts on both leading and trailing edges the curve has poor statistics. The curve can be smoothed out, and new values of counts in a channel read from this smoothed curve. Using these "smoothed" values, a value of τ was obtained differing by less than 0.1% from the value obtained with the original figures. In another test, successively more and more values at the extremes of the curve were eliminated, and the value of τ obtained was found to be quite insensitive. For example, the curve for Gd^{156} (fig. 2) has values extending over more than 4 decades. If all values more than 3 decades below the peak are neglected, the value of τ obtained is only 4% lower than the "correct" value. Thus even a rough extrapolation of the 3-decade curve to correct for this neglect will give an error much less than 4%. The second moment of the prompt curve, as computed from the delayed curve, was 5.76 units; the second moment, as found directly from the approximate prompt curve itself, was 5.43 units.

4. Errors

The statistical errors that one should assign to these values of σ and τ could have been computed by having the machine carry the standard deviations of the individual points through the calculation. However, in order to give the error in closed form, we now assume that the prompt curve is a Gaussian of standard deviation σ. (The result is not sensitive to this assumption.) In that case it is easily shown (see Appendix) that

[4]) R. E. Bell and M. H. Jørgensen, Nucl. Phys. **12** (1959) 413.

the fractional standard deviation in the computed value of the lifetime is

$$\frac{\Delta\tau}{\tau} = \frac{1}{\sqrt{A}}\left(\frac{5}{12}\right)^{\frac{1}{2}}\left[\left(\frac{\sigma}{\tau}\right)^6 + 3\left(\frac{\sigma}{\tau}\right)^4 + 9\left(\frac{\sigma}{\tau}\right)^2 + \frac{53}{3}\right]^{\frac{1}{2}}$$

where A is the total of all the counts in the delayed curve. Applied to our present example, this estimate gives a standard deviation in τ of 1.3%. In an experiment like this, a systematic error of about 3% is assigned to cover instrument calibration and linearity; the statistical error in this case is therefore negligible. In our example, if the half life became smaller, the fractional standard deviation would rise, reaching 20% for a half life of $\approx 3 \times 10^{-11}$ sec.

5. Concluding Remarks

Another use of this third-moment technique would be in the "self-comparison" method of Bell, Graham and Petch[5]). The two delayed curves obtained would have a difference between their third moments of $4\tau^3$, while the third moment of the prompt curve would contribute nothing, to first order; hence the lower limit of measurement of the half life could be somewhat decreased.

Throughout this paper we have assumed that the delayed curve corresponds to a single exponential decay, in particular that chance coincidences have been subtracted and that no prompt events are occurring in the delayed curve. The neglected presence of either kind of event will cause errors, as it does in the centroid-shift case. A moment analysis can be made to take account of either type of event, as shown by Birk *et al.*[3]) for the centroid-shift case, but the work is laborious and dependent on the exact circumstances of the measurement.

One of us (R.S.W.) expresses his thanks to the National Research Council of Canada for a Studentship held during the course of this work.

[5]) R. E. Bell, R. L. Graham, and H. E. Petch, Can. J. Phys. **30** (1952) 35.

Appendix

CALCULATION OF FRACTIONAL STANDARD DEVIATION

To calculate the standard deviation in our computed τ, we assume that the number of counts, $F(x)\,dx$, in a time channel of width dx has a standard deviation $[F(x)\,dx]^{\frac{1}{2}}$. This error contributes an error in the third moment of amount $(x-\tau)^3\,[F(x)\,dx]^{\frac{1}{2}}$. Combining the various channel contributions quadratically and replacing the sum over channels by an integral, we get

$$\Delta(N_3) = \left[\int_{-\infty}^{\infty}(x-\tau)^6\,F(x)\,dx\right]^{\frac{1}{2}}\left[\int_{-\infty}^{\infty}F(x)\,dx\right]^{-1},$$

the second factor, for normalization, being just A, the total number of counts in the curve. Expanding this expression and making use of eq. (1) and eq. (3), we get

$$\Delta(N_3) = \frac{1}{\sqrt{A}}\left[M_6(P) + 15\tau^2\,M_4(P) + 40\tau^3\,M_3(P) + 135\tau^4\,M_2(P) + 264\tau^5\,M_1(P) + 265\tau^6\right]^{\frac{1}{2}}.$$

If P has been observed, the moments given here may be computed. In order to give a definite form for the error, however, we now assume that P is a Gaussian with standard deviation σ; i.e. $M_2(P) = \sigma^2$, $M_4(P) = 3\sigma^4$, $M_6(P) = 15\sigma^6$, and all odd moments are zero. We then get

$$\Delta(N_3) = \frac{1}{\sqrt{A}}\left[15\sigma^6 + 45\tau^2\sigma^4 + 135\tau^4\sigma^2 + 265\tau^6\right]^{\frac{1}{2}}.$$

This is the total error in $2\tau^3$: hence the fractional statistical error can be expressed as

$$\frac{\Delta\tau}{\tau} = \frac{1}{\sqrt{A}}\left(\frac{5}{12}\right)^{\frac{1}{2}}\left[\left(\frac{\sigma}{\tau}\right)^6 + 3\left(\frac{\sigma}{\tau}\right)^4 + 9\left(\frac{\sigma}{\tau}\right)^2 + \frac{53}{3}\right]^{\frac{1}{2}}.$$

In fig. 3 is plotted a curve of $(\Delta\tau/\tau)\sqrt{A}$ vs the ratio of σ/τ, and also the ratio of $W_{\frac{1}{2}}/T_{\frac{1}{2}}$ where $W_{\frac{1}{2}}$ is the full width at half maximum of the prompt curve and $T_{\frac{1}{2}}$ is the half life being measured. If $A = 10\,000$ counts, then the fractional error is read directly as percent.

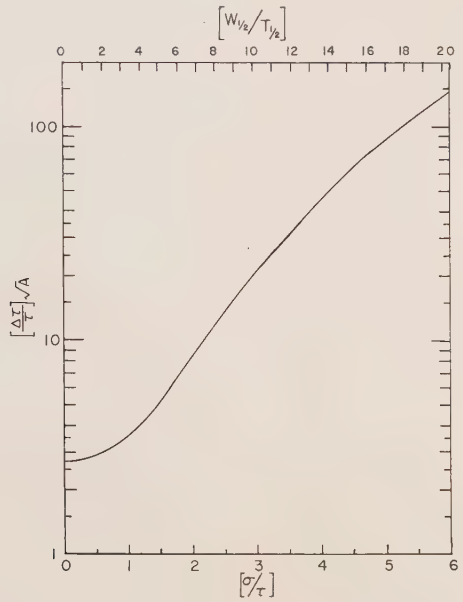

Fig. 3. Fractional standard deviation in τ plotted as a function of σ/τ (lower abscissa) or $W_{\frac{1}{2}}/T_{\frac{1}{2}}$ (upper abscissa). A is the total number of counts in the observed resolution curve.

NUCLEAR INSTRUMENTS AND METHODS 9 (1960) 154–164; NORTH-HOLLAND PUBLISHING CO.

SECTOR-TYPE DOUBLE-FOCUSING BETA-RAY SPECTROMETER

M. SAKAI, H. IKEGAMI and T. YAMAZAKI

Institute for Nuclear Study, University of Tokyo, Japan

Received 22 July 1960

A new type of magnetic beta-ray spectrometer especially suitable for electron-gamma and electron-electron directional correlation experiment was constructed. It is a version of an ordinary sector-type double-focusing spectrometer which accepts a large solid angle. Since the spectrometer was so designed that the wall of the vacuum chamber serves as the return circuit of magnetic flux, a scintillation counter or another spectrometer can be put in the space entirely free from magnetic field. Several examples for conversion spectrum, electron-gamma coincidence spectrum and pattern of electron-gamma directional correlation are presented.

1. Introduction

In the last decade the experiments on gamma-gamma directional correlation experiments were performed extensively and the spin values of the excited levels in many nuclei were definitely determined by this means. However, as is well known[1]), if we use conversion electrons in one channel or in both channels instead of gamma radiations, we could determine not only the spin value of an excited level but also its parity[2]). Moreover we have a possibility of determining the strength parameter ρ in E0 transition[3]) in special cases. And, of course, if we detect beta radiations, we can measure the pattern of beta-gamma directional correlation which gives us an important information on the nuclear matrix elements in beta transition[4]).

Because of this great advantage obtained by detecting electrons, many instruments suitable for this purpose have been devised since the pioneering instrument worked by Deutsch[5]). Recently, Gerholm and Pettersson[6]) described a new instrument for electron-gamma directional correlation experiment, adopting a medium-thick magnetic lens spectrometer for electron selector.

We started, five years ago, the development of a magnetic beta-ray spectrometer especially suitable not only for electron-gamma directional correlation experiments but also for electron-electron directional correlation experiment. This is a version of an ordinary sector-type double-focusing spectrometer[7]) which has been widely used for charged-particle analyser in nuclear reactions[8]). However, the most important feature of this instrument, different from that of the ordinary one, lies in the fact that it accepts a large solid angle. It is an essential need for the purpose of nuclear spectroscopy. In this case, a rather large fringing field which might be produced outside the magnet was considered as a large difficulty for getting good focusing properties. But, as a matter of fact, this effect was found to be not so serious as we shall see in the section 2.

[1]) F. Gimmi, E. Heer and P. Scherrer, Helv. Phys. Acta **29** (1956) 147.

[2]) M. E. Rose, L. C. Biedenharn and G. B. Arfken, Phys. Rev. **85** (1952) 5.

[3]) E. L. Church and J. Weneser, Phys. Rev. **103** (1956) 1035;
E. L. Church, M. E. Rose and J. Weneser, Phys. Rev. **109** (1958) 1299.

[4]) M. Morita and M. Yamada, Progr. Theor. Phys. **8** (1952) 449.
M. Morita and M. Yamada, Progr. Theor. Phys. **10** (1953) 111;
T. Kotani and M. Ross, Phys. Rev. **113** (1959) 622.

[5]) D. T. Stevenson and M. Deutsch, Phys. Rev. **83** (1951) 1202.

[6]) T. R. Gerholm and B-C. Petterson, Nucl. Instr. and Meth. **6** (1959) 107.

[7]) D. L. Judd, Rev. Sci. Instr. **21** (1950) 213.

[8]) C. Snyder, C. Lauritsen, W. Fowler and S. Rubin, Phys. Rev. **74** (1948) 1564;
C. Snyder, S. Rubin, W. Fowler and C. Lauritsen, Rev. Sci. Instr. **21** (1950) 852;
C. Mileiikowsky, Ark. f. Fysik **7**, No. 3 (1953) 33;
S. Rubin and D. C. Sachs, Rev. Sci. Instr. **26** (1955) 1029.

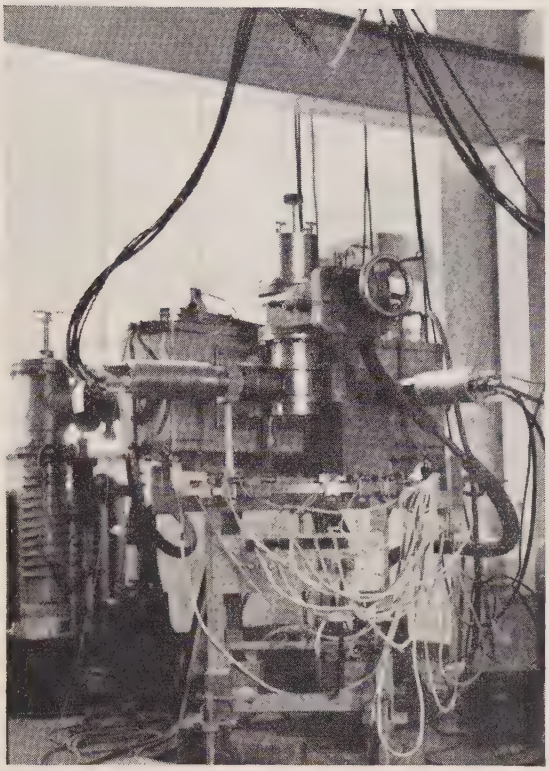

Fig. 1. Picture of INS III magnetic beta-ray spectrometer. Main body, beam channel and turn table are shown.

First two small models with $\rho = 9$ cm were constructed and their performance and an application for special problem were already published elsewhere[9,10]). And also, an experiment of conversion-electron and gamma-ray directional correlation with this model was worked out with good success[11]).

In the present article, we describe a new magnetic beta-ray spectrometer with $\rho = 18$ cm, which we call INS III beta-ray spectrometer. In this instrument, the vacuum tank serves as the return circuit of magnetic flux. By this improvement the magnetic field does not leak outside the magnet and we can avoid the magnetic-field interference between a fixed spectrometer and a movable scintillation counter or another movable spectrometer. Another merit of this instrument is that we can use electron beam in pencil form and hence we can define the resolution angle better than in the case of a lens-type spectrometer.

2. Instrument

The spectrometer consists of three parts, i.e. main body, beam channel and turn table. A picture of the whole instrument is shown in fig. 1.

2.1. MAIN BODY

It is a large semicircular vacuum chamber which contains pole tips and a pair of coils. The magnetic flux produced by these coils closes the

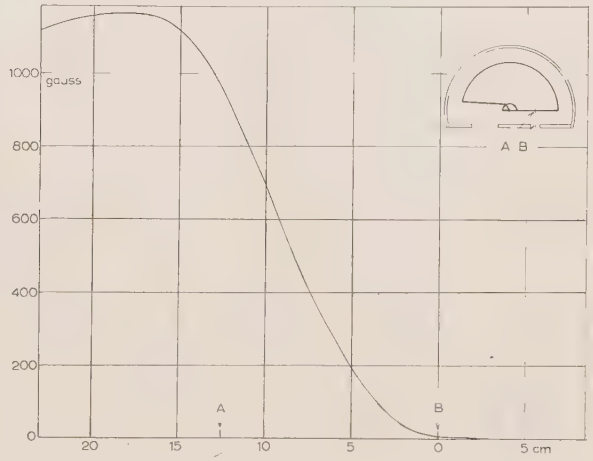

Fig. 2a

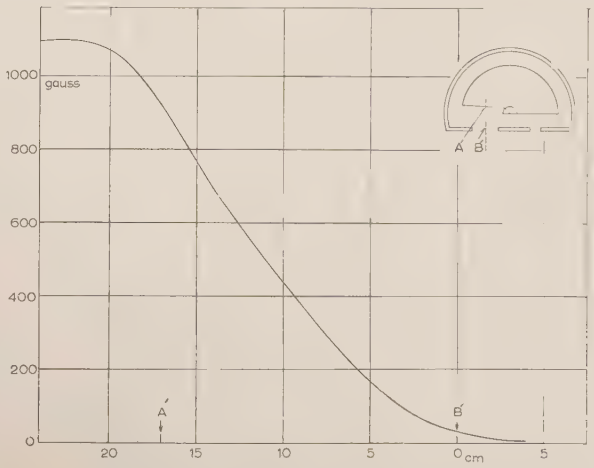

Fig. 2b. Field distribution in the vicinity of pole boundary. The direction of measurement is indicated in the inset.

[9]) M. Sakai and H. Ikegami, J. Phys. Soc. Japan **13** (1958) 1076.

[10]) T. Yamazaki, H. Ikegami and M. Sakai, J. Phys. Soc. Japan **13** (1958) 1080;

[11]) H. Ikegami, Phys. Rev. **120** (1960) No. 6 (to be published);
H. Ikegami, T. Yamazaki and M. Sakai (Paper in preparation).

magnetic circuit via the iron wall of vacuum chamber. Therefore the leakage of magnetic flux outside of the vacuum chamber is extremely small as shown in fig. 2a and 2b. Thus, we can place a scintillation counter or another spectrometer near this spectrometer without mutual

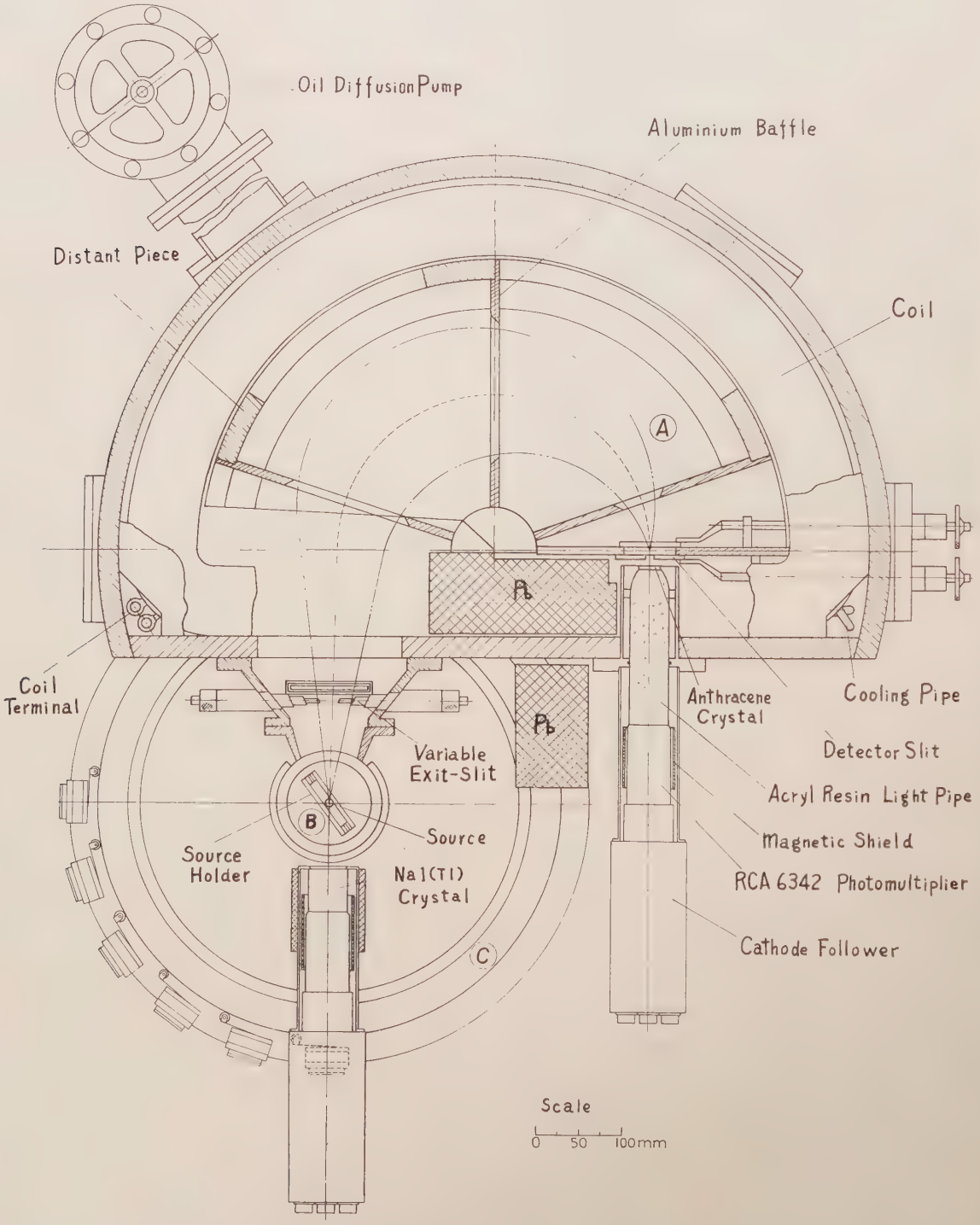

Fig. 3a. Top view.

magnetic interaction. The arrangement of coils and pole pieces in the vacuum tank can be seen in fig. 3a, b and c. The diameter of vacuum tank is 92.2 cm and that of pole piece 68.0 cm and the mean radius of curvature of electron trajectory in the spectrometer is 18 cm (henceforward to

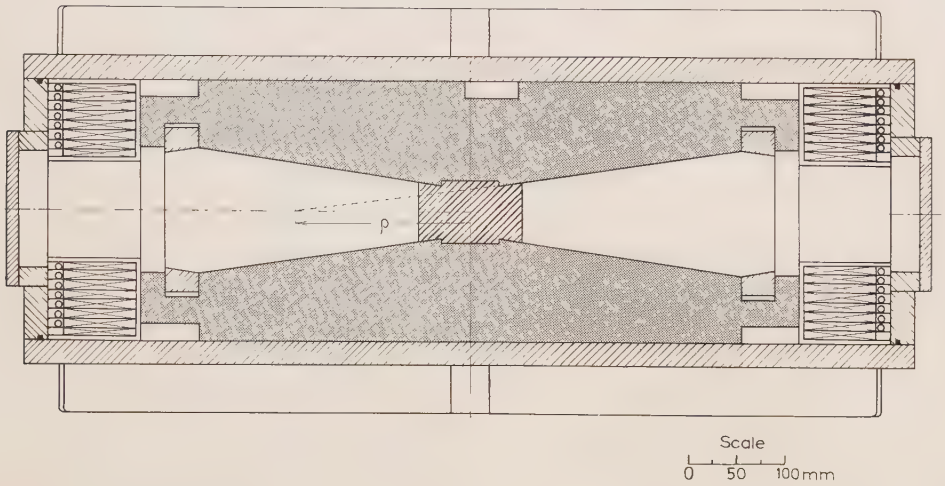

Fig. 3b. Side view-1.

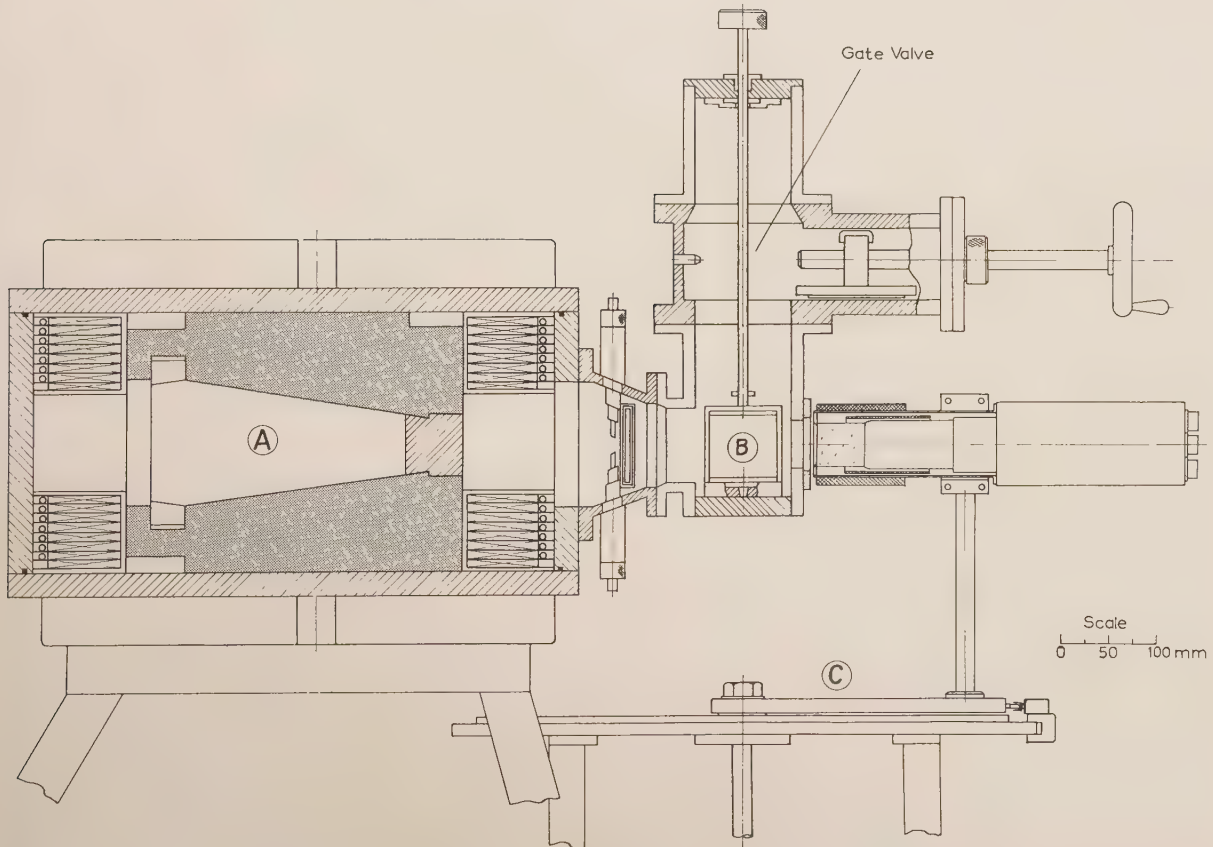

Fig. 3c. Side view-2. Schematical presentation of INS III spectrometer. A: Main body B: Beam channel C: Turn table. The scintillation counters for electron and gamma radiation are also included.

be called reference radius) and the pole gap at the reference radius is 11.5 cm. A part of trajectory is inside the beam channel, at the end of

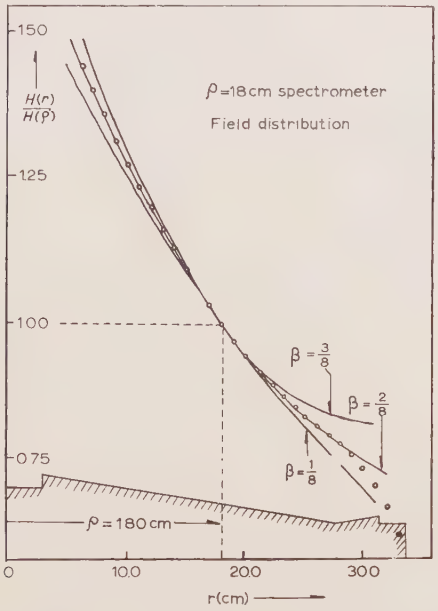

Fig. 4. Field distribution in the spectrometer. The theoretical curves for ($\alpha = \frac{1}{2}$, $\beta = \frac{1}{8}$), ($\alpha = \frac{1}{2}$, $\beta = \frac{1}{4}$) and ($\alpha = \frac{1}{2}$, $\beta = \frac{3}{8}$) are also presented.

which a source is placed. The deflection angle of 180° was chosen and a pair of pole tips can be obtained by cutting an iron disk machined by lathe. All parts of spectrometer were made of soft iron with carbon content less than 0.06% and the total weight of iron was about 800 kg†. Each coil consists of 400 turns of 1 mm × 6 mm copper strip insulated by 1 mil mylar layer. These coils were excited by 110 V, 2 kW Amplidyne Generator, coupled with an ordinary stabilizer equiped by 400 cycle Brown Chopper††. The current stability within 0.1% at 1A and within 0.01% at 10A was obtained. The linearity of the magnetic field is quite satisfactory and the field can be produced up to 1050 gauss at 10A.

The magnetic field parameters[12]) α and β were chosen to be $\frac{1}{2}$ and $\frac{1}{4}$. Then, the inhomogeneous magnetic field in the median plan has the following character;

$$B(r) = B(\rho)\left\{1 - \tfrac{1}{2}\frac{(r-\rho)}{\rho} + \tfrac{1}{4}\frac{(r-\rho)^2}{\rho^2} + \cdots\right\}; \quad (1)$$

where ρ is the reference radius of electron trajectory in the magnetic field. This field distribution can be easily obtained by cone type pole tips[13]), of which the extension of surface intersects on the median plane at ρ as shown in fig. 3b. The adjustable shim at the periphery of pole tips was empirically adjusted for keeping the suitable field distribution in the outer part of the magnet. The field distribution actually measured was shown in fig. 4. This figure shows that the required field shape can be achieved in a region wider than a reference radius.

In order to make the deflection angle, equal to π, we have to apply the correction for the fringing field. It was done by cutting the pole boundary as shown in fig. 3a. The amount of the correction was estimated under the assumption that the effective pole boundary lies 0.6 pole gap outside the actual pole edge[14]).

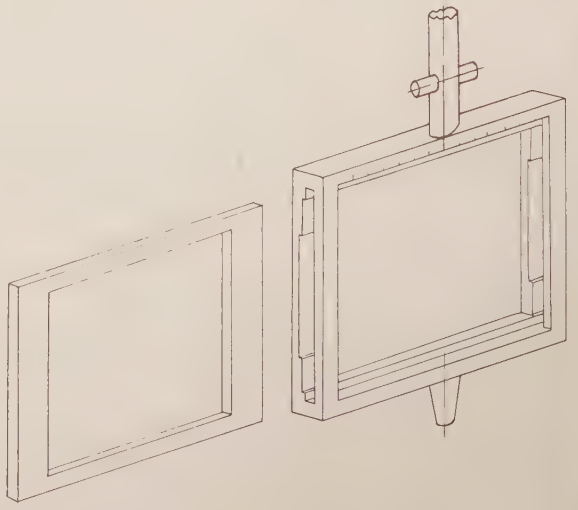

Fig. 5 Source holder.

† The magnet was constructed in Sumitomo Metal Industry, Osaka, Japan.

†† The electronics part and other accessaries were manufactured by Japan Electron Optics Laboratory Co., LTD. Tokyo, Japan.

[12]) K. Siegbahn and N. Svartholm, Nature, Lond. **157** (1946) 872.

[13]) E. Arbman and N. Svartholm, Ark. f. Fysik **10**, No. 1 (1955).

[14]) N. D. Coggeshall, J. Appl. Phys. **18** (1947) 855.

2.2. BEAM CHANNEL

This is a rectangular channel attached to the outside of the vacuum chamber and the source chamber was placed at the end of this channel. The electrons coming from the source pass through this channel and enter into the magnetic field. The source chamber is provided with a gate valve through which we can put a source in the chamber without breaking the vacuum in the main body. The plan was shown in fig. 3c. In order to avoid the scattering of electrons near the source, a source is mounted in a large aluminium frame which goes into a holder frame. The holder frame has a conical boss at its base which fits into a center hole of the source chamber, fixing automatically the position of the source. The position of the source relative to the frame can be easily adjusted by sliding the aluminium frame in the holder frame (see fig. 5).

2.3. TURN TABLE

It is a simple turn table with 60 cm diameter. Since the coincidence counting rate in electron-gamma and in electron-electron directional correlation experiment is, in general, very small, an automated recording system is indispensable. Although this kind of system is now quite common, we believe that it is worth while to describe briefly our system, because of its simpleness. The block diagram is shown in fig. 6 to facilitate the understanding of its performance. The essential point is to make use of a delayed contact contained in Ametron printer† which simplifies all the problems. Adjustment of relative position of micro-switch to contact point of moving arm is somewhat delicate but can be easily mastered. Thus, we can put any number of micro switches at any position, being able to set any number of measuring points at any angle.

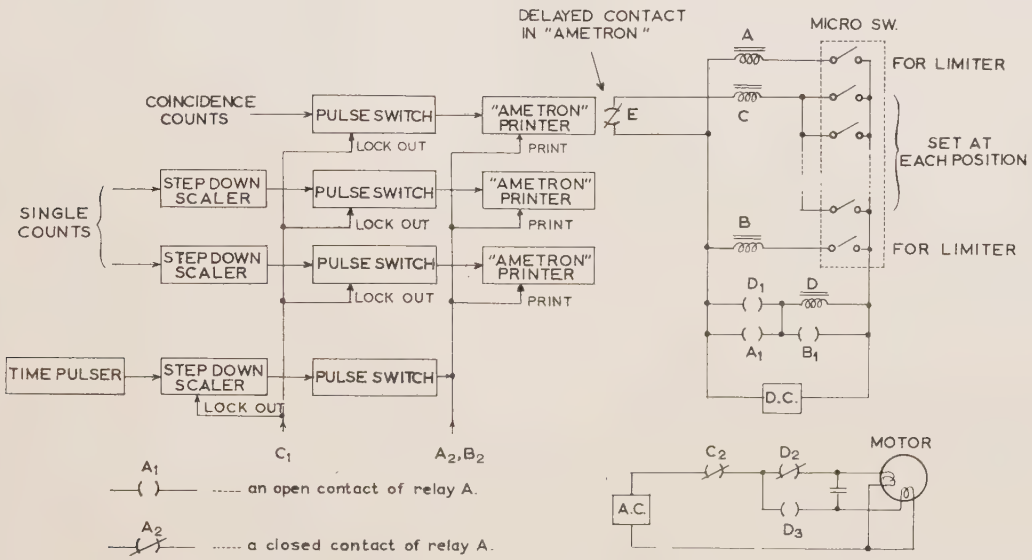

Fig. 6. Block diagram of the automated measuring system for directional correlation experiment. A, B, C and D are DC power relays. The action of this apparatus is as follows. At first let a movable counter stay at a position. Relay C being excited, driving motor stops. Each signal from electronics circuits is fed to each printer. After a definite time interval, a signal from the time programmer triggers the printing mechanism. At the same time delayed contact relay E in Ametron printer being excited for a few seconds, relay C is broken, the motor moves and counts-signals are locked out. When the counter reaches the next position, relay C is excited again and the motor stops. This action is repeated again, and in case the counter passes the end position, direction of motion is alternated by the micro switches for limiter.

3. Focusing Properties

The first order theory of images in this type of spectrometer was investigated by Judd[7]). In the

† It was purchased from Streeter-Amet Company, Grayslake, Illinois. U.S.A.

following discussion the distance is measured in unit of reference radius. The focusing condition can be described by the generalized Barber's law as follows:

$$\varphi' + \varphi + \varphi'' = \pi \tag{2}$$

where $\varphi = \Phi/\sqrt{2}$, $\varphi' = \tan^{-1} T'/\sqrt{2}$ and $\varphi'' = \tan^{-1} T''/\sqrt{2}$ and Φ, T' and T'' are the deflection angle, the distance between the entrance pole boundary and the source and the distance between the exit pole boundary and the image, respectively. (see fig. 7a and 7b). Introducing our conditions of $\Phi = 180°$ and $T'' = 0$, the source distance is given by

$$T' = 1.86\,. \tag{3}$$

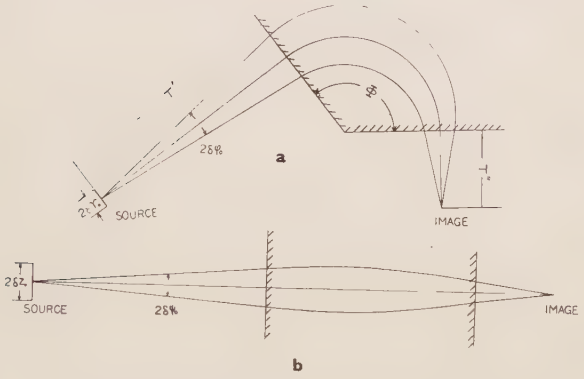

Fig. 7a. Radial focusing. 7b. Vertical focusing.

The magnification is written in the equation:

$$M = \cos\varphi - \tan\varphi'' \sin\varphi\,. \tag{4}$$

In the present case we have

$$M = -0.607\,. \tag{5}$$

The solid angle Ω is given by

$$\Omega/A = (T'^2 + 2)^{-1} \tag{6}$$

where A is the available cross-sectional area for the electron beam.
Since A is about $\frac{1}{2}$ in our case, we obtain

$$\Omega \approx 0.1 \qquad \text{(steradian)}\,. \tag{7}$$

From the second order theory[15]), the formula of the electron trajectory for a point source and the base resolution W_0 are given by:

$$\begin{aligned} r - 1 = {} & (1.86\cos\varphi + 1.41\sin\varphi)\,\delta\varphi_0 \\ & - (0.242\cos\varphi - 0.875\sin\varphi - 0.242\cos 2\varphi \\ & - 0.875\sin 2\varphi)\,\delta\varphi_0{}^2 \\ & + (1.48\cos\varphi + 0.875\sin\varphi - 1.36 \\ & - 0.119\cos 2\varphi - 0.437\sin 2\varphi)\,\delta\psi_0{}^2 \end{aligned} \tag{8}$$

$$\begin{aligned} z = {} & (1.86\cos\varphi + 1.41\sin\varphi)\,\delta\psi_0 \\ & - (0.475\cos\varphi + 0.875\sin\varphi - 0.475\cos 2\varphi \\ & - 0.873\sin 2\varphi)\,\delta\varphi_0\,\delta\psi_0 \end{aligned} \tag{9}$$

$$\begin{aligned} W_0 = {} & 0.38\,\delta r_0 + 0.133\,\delta z_0{}^2 + 0.021\,\delta\varphi_0{}^2 \\ & + 0.35\delta\psi_0{}^2 + 1.12\,\delta z_0\,\delta\psi_0 \end{aligned} \tag{10}$$

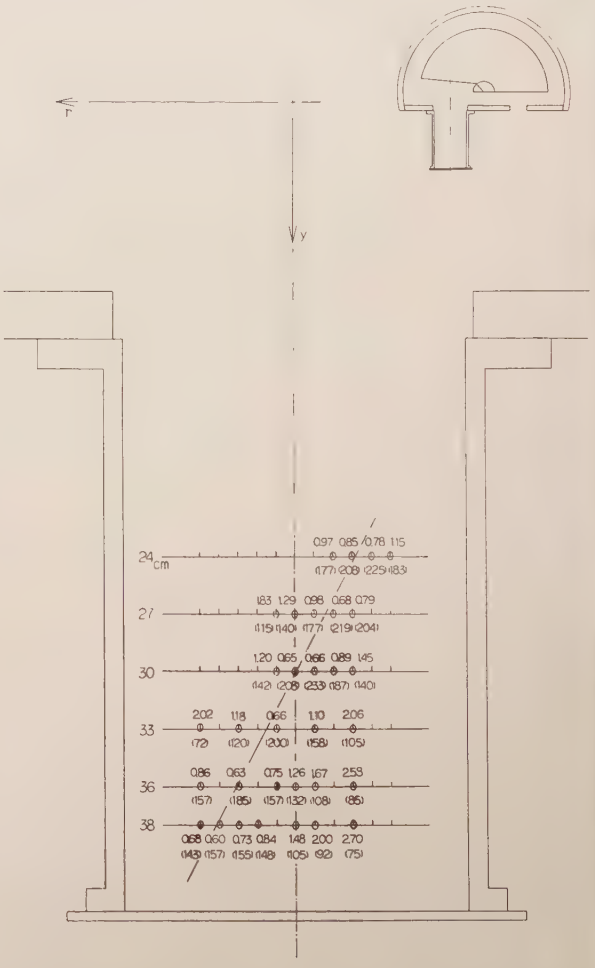

Fig. 8. Map of the focusing character at the source side. The measured resolution (%) at each point is presented in the figure. The peak value (relative solid angle) is also shown in parentheses.

[15]) E. S. Rosenblum, Rev. Sci. Instr. **21** (1950) 213; H. Ikegami, Rev. Sci. Instr. **29** (1958) 943.

where δr_0, δz_0, $\delta \varphi_0$, and $\delta \psi_0$ are schematically presented in fig. 7. The optimum conditions in magnetic spectrometers were studied in the recent article[16]) and those in this spectrometer were written in function of base resolution as follows:

$$\delta r_0 = 5.26\, W_0/5\,, \tag{11}$$

$$\delta z_0 = 1.44\, (W_0/5)^{\frac{1}{2}}\,, \tag{12}$$

$$\delta \varphi_0 = 6.99\, (W_0/5)^{\frac{1}{2}}\,, \tag{13}$$

$$\delta \psi_0 = 0.89\, (W_0/5)^{\frac{1}{2}}\,, \tag{14}$$

and

$$L = 59.9\, (W_0/5)^{\frac{5}{2}}. \tag{15}$$

The meanings of the above equations should be referred to ref.[16])

4. Performance

The focusing conditions were first studied by exchanging the source and image positions. A Geiger-counter was mounted in a sliding system, by which it can be moved in both of r and y directions. By putting a Cs^{137} source at the normal detector position, the height and the full-width at half-maximum of the conversion line were measured at each position. Fig. 8 shows a map of the focusing character. The focal line can be clearly noticed and the rather wide part on this line has a nearly equal focusing character which gives us a possibility of using this instrument as a spectrograph[17]). And T' was found to be 1.62 being consistent with the theoretical value of eq. (3). It proves that the method of correcting the fringing field by cutting pole boundary is feasible.

So far as the solid angle Ω is concerned, the relation of Ω versus W_0 can be deduced by eqs. (11), (12), (13), (14), and (15):

$$\Omega/W_0 = 1.57\,. \tag{16}$$

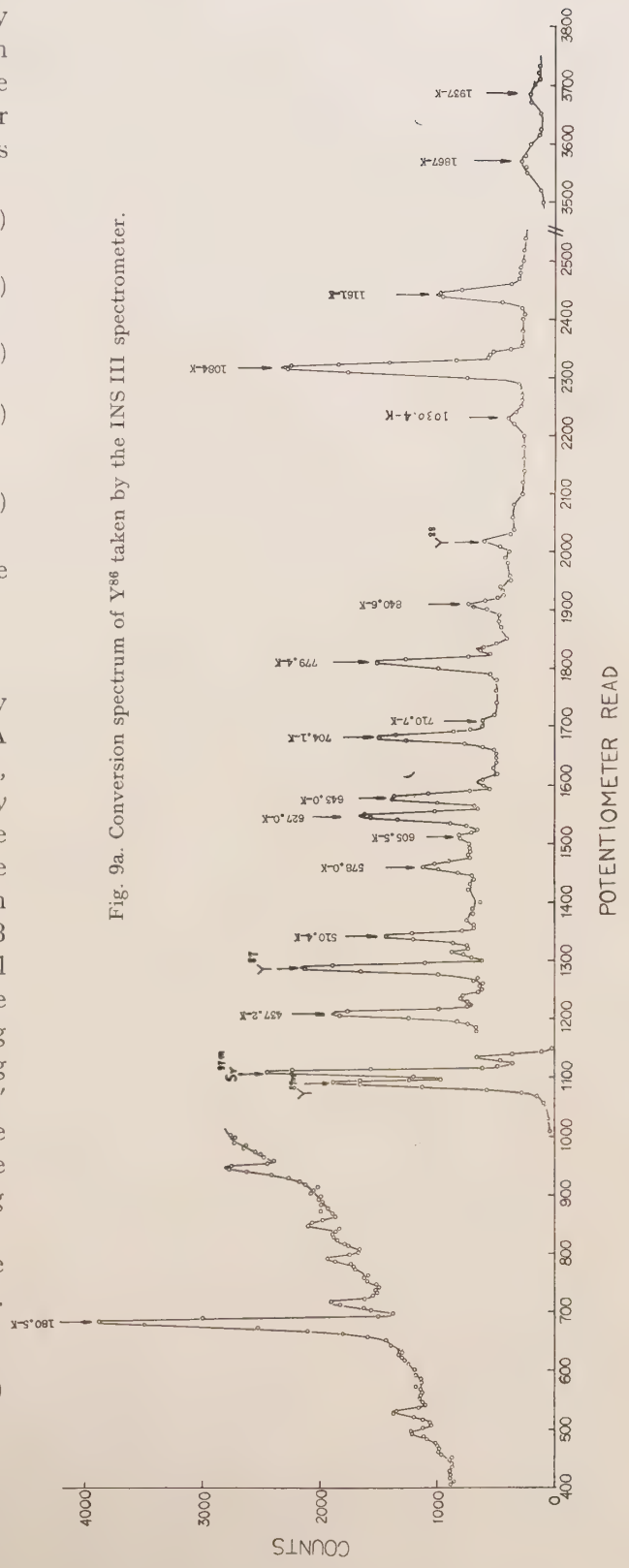

Fig. 9a. Conversion spectrum of Y^{86} taken by the INS III spectrometer.

[16]) M. Sakai, Nucl. Instr. and Meth. **8** (1960) 61.
[17]) C. Mileiikowsky, Ark. f. Fysik **10**, No. 1 (1955).

This value is a good figure if we consider that $\pi\sqrt{2}$ type spectrometer has this ratio of 1.52[16]). Although the actual experimental conditions are far from the optimum conditions, we present an example. In case of the source 20 mm long and 2.5 mm wide and of the detector slit 3 mm wide, we found the resolution at half maximum to be 0.6% and the effective solid angle to be 0.3%.

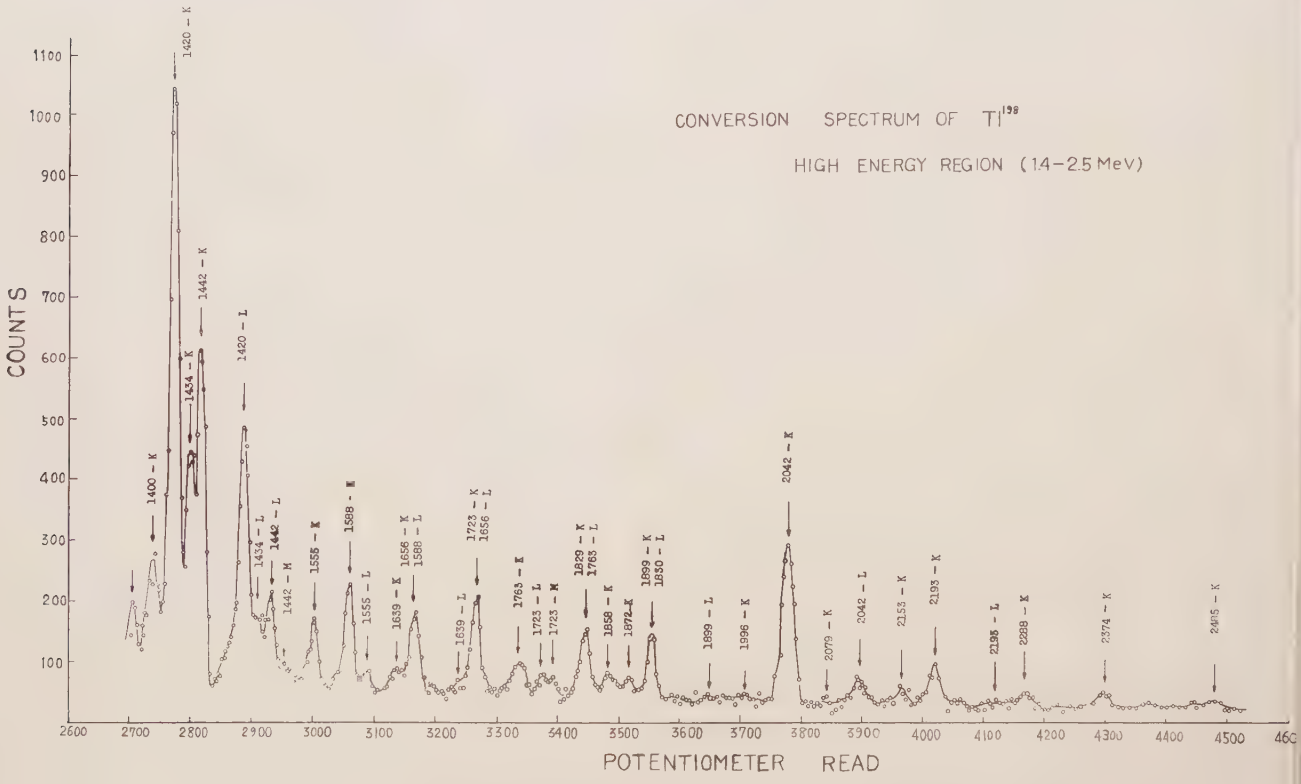

Fig. 9b. Conversion spectrum of Tl^{198} taken by the INS III spectrometer.

5. Several Examples of the Application to the Study of Nuclear Spectroscopy†

5.1. CONVERSION SPECTRUM

For examples, we present several conversion spectra taken by this spectrometer in fig. 9a and 9b. The radioactive sources were Y^{86} and Tl^{198} which were produced by the nuclear reactions of $Sr^{86}(p,n)Y^{86}$ and $Au^{197}(\alpha,3n)Tl^{198}$ in INS cyclotron[18]). We have found a number of new conversion lines in these nuclei and the decay of each peak was also followed.

† Full papers will be published elsewhere.

5.2. ELECTRON-GAMMA COINCIDENCE SPECTRUM

In the coincidence experiment the electron detector consisted of an anthracene crystal coupled with an RCA 6342 photomultiplier via 20 cm long Acryl-resin light pipe, in order to put the photomultiplier outside of the vacuum tank (see fig. 3a). The resolution at half-maximum was 25% for the electrons of energy 500 keV. Two typical coincidence spectra are shown in figs. 10a and 10b. In the inset of each figure, main decay schemes of these spectra are also presented.

5.3. ELECTRON-GAMMA DIRECTIONAL CORRELATION

Since the coincidence count in this type of experiment is very small, the entirely automated measuring system for directional correlation was fully used. The simple experimental patterns obtained by our system are presented in figs. 11a

[18]) S. Kikuchi *et al.*, J. Phys. Soc. Japan **15** (1960) 41.

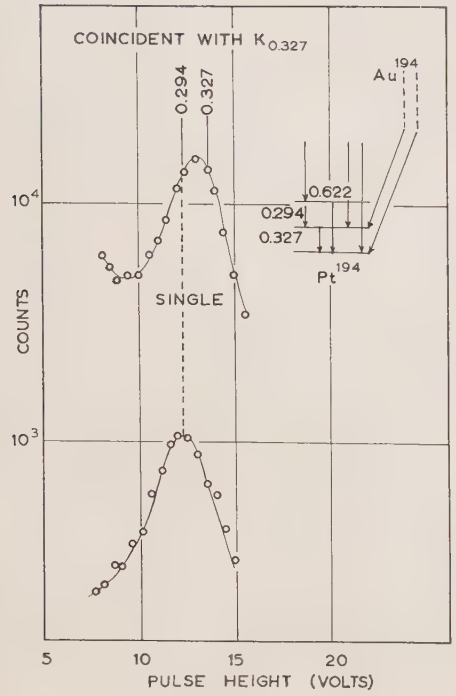

Fig. 10a

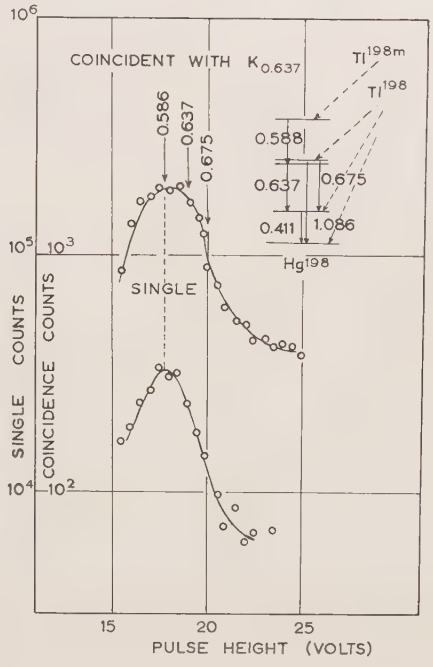

Fig. 10b

Coincidence spectra in Pt^{194} and Hg^{198}. The decay schemes involved in these spectra are presented in the inset of each spectrum.

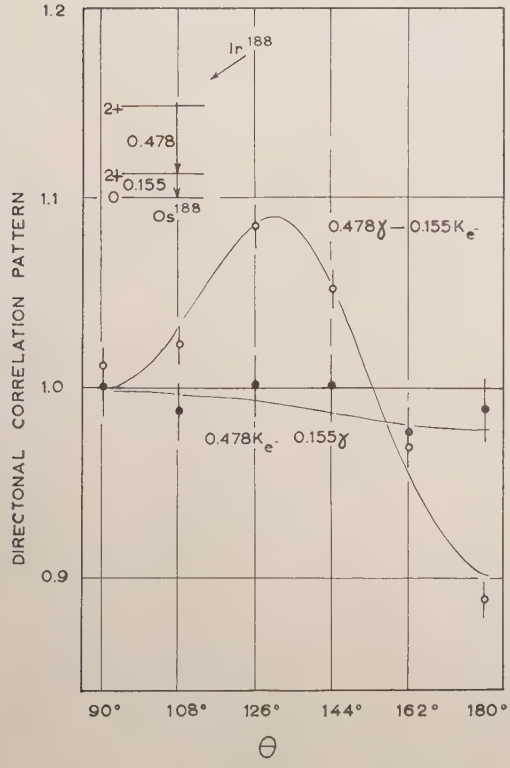

Fig. 11a

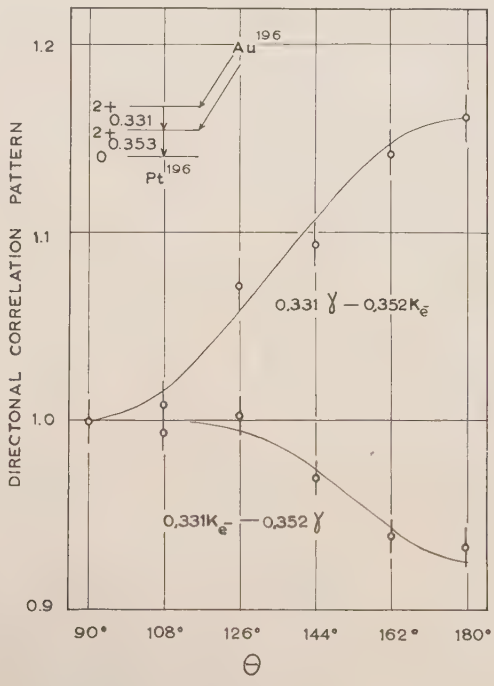

Fig. 11b

Directional correlation patterns in Os^{188} and Pt^{196}. Instrumental corrections are not performed.

and 11b. The main purpose of our experiment on the nuclei in platinum region was to determine the strength parameter ρ of E0 transition from the second 2+ level to the first 2+ level.

6. Concluding Remarks

We can enumerate the merits of this instrument as follows.

a. The vacuum tank can be constructed by soft iron. The pole pieces can be obtained from a machined iron disk. These facts are attractive from the economical point of view.

b. The leakage flux is negligible outside the spectrometer and the source distance is large. Therefore, we can turn without the magnetic interaction either a gamma scintillation counter or another beta spectrometer around the source from 90° to 180°.

c. The electron beam can be used in pencil form. It is very convenient for the directional correlation experiment.

d. It has a rather good relation of solid angle versus resolution.

e. By putting a system of accelerating electrodes in the straight section, we have a possibility of measuring very low energy conversion electrons.

f. The twin setting[10]), as we have proved this possibility, is very useful for getting rid of the scattering effect. Such a large versatility can be achieved by this instrument, that we believe that this type of instrument may be used widely, not only for nuclear spectroscopy, but also for directional correlation experiments in nuclear reactions.

We are indebted to Prof. S. Kikuchi for his encouragement and appreciation for this work.

NUCLEAR INSTRUMENTS AND METHODS 9 (1960) 165–171; NORTH-HOLLAND PUBLISHING CO.

ON THE MECHANISM OF MULTIPLE DISCHARGES IN HALOGEN-QUENCHED G.M. COUNTERS

O. J. ORIENT

Central Food Research Institute, Dept. of Radiology, Budapest

Received 20 July 1960

Multiple discharges taking place during the excitation section in counting tubes filled with neon gas to 200 mm Hg and bromine to 0.5 mm Hg pressure have been investigated. The amplitude and the distribution in time of multiple discharges have been examined with an oscillo-synchroscope. Multiple discharges occur after dead time, their amplitudes being always smaller than the main pulse. Their number diminishes and their amplitude increases with time. In the excitation section multiple discharges were separated with a threshold discriminator. Performances examined with this method show no excitation section. This confirms the observation that excitation section is due to multiple discharges of amplitudes smaller than the main discharge.

For the distribution in time of multiple discharges the evaluation of the measurements has resulted in an exponential relationship. The value obtained for the constant term making part of the exponent has been found to be identical with the decay constant of metastable neon atoms. This confirms the assumption that multiple discharges are originated by ultra-violet photons resulting from the decay of metastable neon atoms produced around the filament in the main discharge. By using the exponential time distribution of multiple discharges as obtained in measurements the probability of multiple discharges originating from metastable disintegration has been calculated.

1. Introduction

Multiple discharges produced in halogen-quenched counting tubes have been examined by La Croisette and Yarwood[1]). With neon-bromine counting tubes it has been found that starting from the initial voltage, a small addition of argon (0.5 mm Hg pressure) causes the apparation of multiple discharges to shift in the direction of higher overtension. According to conclusions drawn from experimental results multiple discharges originated from the disintegration of metastable neon atoms produced in the discharge around the filament are kept back by argon addition. The same authors have also published experimental results concerning neon-bromine counting tubes filled up to low bromine pressures (lower than 0.07 mm Hg). According to their data in this case, during the period of the discharges supplied by the counting tube, following the dead time an oscillation may be observed. In a later paper[2]) La Croisette has pointed out that the oscillation experienced with neon-bromine counting tubes filled with low pressure bromine (0.05 mm Hg) may be eliminated by small argon addition. This result also seems to confirm the hypothesis that spurious counting is due to the decomposition of metastable neon atoms originating around the filament. The same deduction is confirmed by Egan's publication[3]).

Van Zoonen and Prast[4]) have examined oscilloscope displays of discharges taking place in argon-bromine counters of low bromine pressure (0.05 mm Hg). Oscillograms have proved that in the phase following the dead time of discharges, like with neon-bromine counters, also here oscillation is produced.

Starting from data found in literature we have investigated into the mechanism of multiple discharges with neon-bromine counters, at a suitably higher bromine pressure where no oscillation comes about any longer.

[1]) D. H. Le Croisette and J. Yarwood, J. Sci. Instr. **28** (1951) 255.

[2]) D. H. Le Croisette, Rev. Sci. Instr. **25** (1954) 1023.

[3]) W. G. Egan, Rev. Sci. Instr. **26** (1956) 891.

[4]) D. Van Zoonen and G. Prast, Jr., Appl. Sci. Res. B **3** (1953) 1.

2. The Making and Filling of Tubes

a. The counting tubes prepared for measurements were placed in bulbs made of rasotherm glass. The anode filament was a tungsten wire, 0.1 mm thick, with a sensitive length of 80 mm. The cathode sleeve was made of molybdenium, its diameter measured 15 mm. Before assembling all parts of the counting tubes were degreased and cleaned carefully.

b. The operation of the deaerating and filling device was similar to that described in the paper of La Croisette and Yarwood[1]). Bromine was freed from air before filling as described in the above mentioned paper. The tubes were filled with spectroscopically pure neon gas. Twelve tubes were soldered to the pump at the same time. After freeing from air and careful baking out, the tubes cooled down to room temperature were filled with bromine vapour of near-atmospheric pressure. After a "soaking" for several days, the tubes were exhaused filled up again with fresh bromine to 0.5 mm Hg pressure and after that with spectroscopically pure neon gas to 200 mm Hg pressure. The characteristics of the tubes obtained with this procedure showed no change, whatever, not even after a storage or an operation of several months.

3. Measuring Apparatus

Counting tubes to be measured were operated from a continuously regulated stabilized power supply. The loading resistance of the counting tube was 1 MΩ. The pulses produced by the tube were fed through a 1000 pF capacity condenser to the oscillo-synchroscope on the one hand, and to a three-decade scaler graduated 1 to 1000 via a preamplifier and threshold discriminator on the other. The gain of the preamplifier could be regulated continuously from 0 to 50. The threshold voltage of the discriminator could be adjusted continuously between 5 and 75 V, discrimination uncertainty was less than 5 mV. The dead time of the whole equipment was under 5 μsec. The sweep speed of the oscillo-synchroscope could be adjusted continuously between wide limits.

The equipment has permitted the amplitude selection of counting-tube pulses and the measurement of operation characteristics. The shape of the pulses could be observed and/or photographed individually.

In addition, with the method described in the paper of Fenton and Fuller[5]) we have measured the charge brought about in the counter by a pulse, as follows: A condenser of 2 μF capacity was connected in series with the counting tube and the voltage generated on it measured with an electrostatic instrument. The condenser was charged by the pulses of the counting tube. The number of pulses required to charge the condenser to 1 V was established. The total amount of charge produced is given by the product of the condenser capacity and of the voltage generated on it. This divided by the number of pulses gives the amount of charge generated by one pulse. This measurement method finds application when the pulses of the counting tube are of the same amplitude.

4. Measurements

Operating characteristics of counter filled to 0.5 mm Hg bromine and 200 mm Hg neon gas pressure have been measured. The characteristic curve of a tube filled to such pressure is shown in fig. 1.

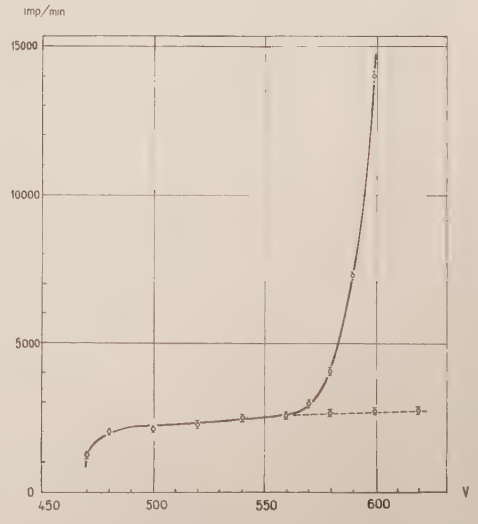

Fig. 1.

[5]) A. G. Fenton and E. W. Fuller, Proc. Phys. Soc. A 62 (1949) 32.

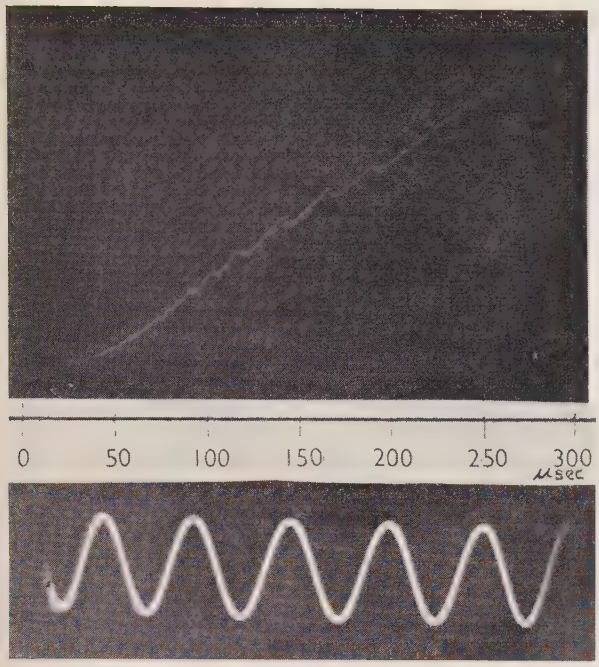

Fig. 2.

The full curve in the figure has been obtained with a gain of 50 and 5 V discrimination voltage. At this measurement the plateau was followed by a relatively steep rising exitation section.

At various section of the operation characteristics we have examined the images of the discharges with the oscillo-synchroscope at low velocities. In the region of the plateau the discharges formed a unique section and no multiple discharge was observed. At the edge of the plateau, with a voltage exceeding 560 V the main (primary) discharge was followed by a number of discharges of considerably lower amplitudes. The oscillogram shows clearly that their number increases significantly with the increase of voltage. Fig. 2 shows the image of a discharge taking place at 620 V. The lower trace shows the calibrating sinusoidal wave. (Calibrating frequency was 20 kc/s.) The main discharge is followed by numerous multiple discharges of smaller amplitudes. The number of multiple discharges decreases and their amplitudes increase with time. We measured dead time with Stever's method[6]). The dead time once fixed it could be proved that multiple discharges take place at any voltage after dead time. At the discharge shown in the figure dead time was found to be 45 μsec.

We have measured the characteristics of the counter also by separating smaller amplitude multiple discharges in the excitation section electronically with a discriminator. In this case the plateau region of the characteristics was in agreement with the measurement results obtained without the use of the discriminator. On the contrary, at voltages higher than 560 V, after the cut-off of multiple pulses no significant increase in pulse count could be observed, the plateau continued and no rise in the curve was produced. This result of measurement is represented in fig. 1, dotted line. This also supports the conclusion which may be drawn from the discharge displays that excitation is produced by pulses smaller than the primary pulse, appearing in increasing numbers with the increase of voltage. With alcohol-argon counters Wiser and Krumbein[7]) have observed multiple discharges smaller than the main pulse. In an earlier paper[8]) the author of the present article has reported of similar discharges to those examined, here observed in the excitation section of alcohol-argon gas filled counters, when examining their multiple discharges with an oscilloscope.

With the method just described the charge produced by one discharge in tubes filled to 0.5 mm Hg bromine and 200 mm Hg neon gas pressure have been measured as a function of the voltage applied to the counter. This method lends itself to measurements only up to 560 V, i.e. until the appearing of multiple pulses of varying magnitudes. In the excitation section a supplementary measurement is needed.

In order to find out the quantity of charge existing in the breakdown range at the formation of the primary discharge, the author has executed the following measurement, described in his paper mentioned above[8]) : A condenser connected

[6]) G. H. Stever, Phys. Rev. **59** (1941) 765.

[7]) H. L. Wiser and A. D. Krumbein, Phys. Rev. **98** (1955) 303.

[8]) O. J. Orient, Nucl. Instr. and Meth. **6** (1960) 309.

in series with the counter will be charged to a voltage corresponding to the total charge supplied by both primary and multiple discharges. The number of the main discharges may be measured by separating multiple discharges by means of a discriminator. From the oscillogram the ratio of areas of main and multiple discharges may be determined by planimetry. The overall charge divided by the number of primary discharges gives the charge produced by the main discharge. The ratio of the areas must also be taken into account in computation.

This method has also permitted the determination in the excitation period of the charge furnished during the main discharge, by the ion cloud formed around the filament. Fig. 3 represents the measurement result showing the relationship between the charge produced in one main discharge and the operating voltage.

According to the measurement result in the excitation period the charge produced by one discharge increases considerably with the increase of voltage. Van Zoonen and Prast in their communication[4]) mentioned above, report on similar results obtained with argon-bromine

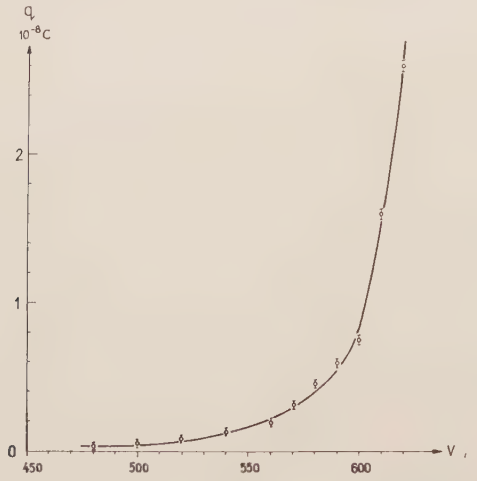

Fig. 3.

counters as to the relationship between charge and operating voltage.

Our measurements were carried out with the same counter. Similar results were obtained also with the rest of the tubes manufactured at the same occasion, as well as with counters produced at various times.

5. The Examination of Multiple Discharges

In the course of our investigation several hundreds of oscillo-synchrograms on multiple discharge have been evaluated. The qualitative estimation of every oscillo-synchrogram has proved that all multiple discharges take place after dead time, all of them are smaller than the main pulse, their number decreases and their amplitude increases with time.

We assume that multiple discharges are originated by the decay of metastable neon atoms produced in the surrounding of filament. This seems to be confirmed by the fact that multiple discharges appear in the recovery period following dead time i.e. they are the result of a process taking place in the gas space. On the other hand, as regards multiple discharges observed in the excitation section of alcohol-argon gas mixture filled counters[7,8]) and oscillations produced at low bromine pressure with halogen-quenched counters[1,2]) it has been assumed in literature that they originate in the decay of metastable inert-gas atoms.

The distribution in time of multiple discharges produced by metastable atoms decay may be determined. According to Kruithof[9]) in the avalanche formed around the filament the number of produced ions and metastable atoms is nearly equal. Atoms produced around the filament being ionized only once the number of ions produced around the filament may be found out by dividing the charge q generated in a single main discharge by the elementary charge ε. Following from the above the number of metastable atoms produced may be determined as

$$m_0 = \frac{q}{\varepsilon}. \tag{1}$$

The decay of metastable atoms is described by an exponential law:

$$m = m_0 \, e^{-\beta t} \tag{2}$$

[9]) A. A. Kruithof, Physica **7** (1950) 519.

where m is the number of metastable atoms left after a lapse of time t from the instant of production, and β is the decay constant of metastable atoms.

According to Phelps and Molnár[10]) the following relationship between decay constant and neon gas pressure holds true in this case:

$$\beta = Ap \tag{3}$$

where A is the constant equal to

$$50 \frac{1}{\text{sec mm Hg}},$$

and p is the neon gas pressure in terms of mm Hg. By substituting eqs. (1) and (3) into (2) we obtain:

$$m = \frac{q}{\varepsilon} e^{-Apt} .$$

If we divide the period of the discharge following dead time into equal intervals of time ($t = t_{i+1} - t_i$, where $i = 1, 2, 3 \ldots i \ldots n$), the number of metastable decays may be calculated for each interval. The number of decays occurring in the ith interval, m_i is the following:

$$m_i = \frac{q}{\varepsilon \Delta t} \int_{t_i}^{t_{i+1}} e^{-Apt} \, dt$$

$$= \frac{q}{\varepsilon \Delta t} \frac{1}{Ap} \left[e^{-Apt_i} - e^{-Apt_{i+1}} \right] .$$

The result is the difference of two exponential expressions. This may be written as an exponential function, namely:

$$m_i = \frac{q}{\varepsilon} e^{-Apt_i^*} . \tag{5}$$

Thus:

$$t_i^* = t_i - \frac{1}{Ap} \ln \frac{1 - e^{-Ap\Delta t}}{Ap\Delta t} . \tag{6}$$

In our case the expression

$$- \frac{1}{Ap} \ln \frac{1 - e^{-Ap\Delta t}}{Ap\Delta t}$$

gives the same value for every interval since Δt is constant.

Photons originating from the decay of metastable neon atoms produced in the surrounding of the anode filament may result in additional discharges. Let the probability of the decay of a metastable atom resulting in a new discharge be w. Then the number of multiple pulses falling within one interval, n_i, may be obtained by multiplying eq. (5) by w:

$$n_i = \frac{q}{\varepsilon} w \, e^{-Apt_i} . \tag{7}$$

The oscillograms of multiple discharges demonstrate that even the largest multiple discharge produces only charges lower by several orders of magnitude than main discharge. From this follows that in any multiple discharge the number of metastable atoms produced is smaller by several orders of magnitude. Therefore, the possibility that any of the multiple discharges may originate a further discharge may be neglected.

According to the above the distribution in time of multiple discharges may be described by an exponential relationship provided we assume that they are called forth by photons originating from the decay of metastable neon atoms.

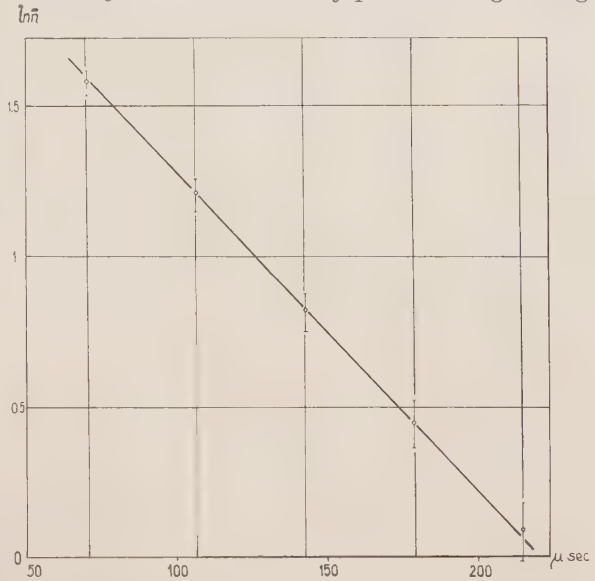

Fig. 4.

The distribution in time of multiple discharges may also be determined experimentally. To this end 100 oscillograms have been evaluated. All of them were taken with the same counter which

[10]) A. V. Phelps and J. P. Molnár, Phys. Rev. **89** (1953) 1202.

Table 1

	Time interval (μsec)	$n_{(1)}$	$n_{(2)}$	$n_{(3)}$	$n_{(4)}$	$n_{(5)}$	...	$n_{(96)}$	$n_{(97)}$	$n_{(98)}$	$n_{(99)}$	$n_{(100)}$	Σn	$\bar{n}$	σ	$\ln(\bar{n} \pm \sigma)$
1	52–88	5	4	4	5	4		5	5	5	5	4	485	4.85	0.220	$1.58\ ^{+0.04}_{-0.05}$
2	88–124	3	3	3	4	3		3	3	4	4	3	334	3.34	0.183	$1.21\ ^{+0.05}_{-0.06}$
3	124–160	2	2	2	2	3		2	2	2	3	2	228	2.28	0.151	$0.826\ ^{+0.054}_{-0.069}$
4	160–196	1	1	2	1	2		2	2	2	1	2	157	1.57	0.125	$0.451\ ^{+0.076}_{-0.082}$
5	196–232	1	1	1	2	1		1	1	1	1	1	110	1.10	0.105	$0.096\ ^{+0.089}_{-0.103}$

was used for the preceding measurements. Operating voltage was set to 620 V. Fig. 2 referred to above shows such an oscillogram with the calibrating sinusoid. In the range of multiple discharge the time axis has been divided into five equal intervals. The corresponding values are given in table 1. We have counted the number of multiple discharges on each oscillogram, and listed some of the values in table 1.

We have formed the average numbers of pulses occurring in the intervals, the mean square deviation in the averaging and the natural logarithms of and errors in the averages. These values are equally given in table 1.

We have represented the logarithms and the errors in the multiple discharges counted in the intervals by entering them at the values corresponding to the half of each interval of time.

Allowing also for errors, a fairly good approximation of a straight line has resulted. This demonstrates that measurements give an exponential relationship for the distribution in time of multiple discharges.

The directional tangent of the straight line was found to be $1.06 \times 10^4 \pm 0.1 \times 10^4$. This is in fairly good agreement with the decay constant given in literature for metastable neon atoms. Namely, according to measurement executed by Phelps and Molnár[10]) with 200 mm Hg neon gas pressure the decay contant may be computed from eq. (3) as 1×10^4.

The logarithms of the numbers of discharges measured have been charted at the middle points of the time intervals. This affected our work with an error whose magnitude may be computed from eq. (6). The variance was but 0.4 μsec for each interval. This result in a negligible small difference and, besides, it does not influence the value of the decay constant anyhow, only causes the time axis to shift.

With β, $q(620\ \mathrm{V})$ and the average numbers of discharges belonging to the several intervals to be known the values w for each interval may be computed from eqs. (6) and (7). The values w belonging to each of the five intervals and their averages are listed in table 2.

Table 2

w_1	w_2	w_3	w_4	w_5	$\bar{w}$
6.32×10^{-9}	6.45×10^{-9}	6.38×10^{-9}	6.43×10^{-9}	6.72×10^{-9}	6.47×10^{-9}

Values β and w when measured with tubes manufactured at various times, have given a variance of maximum 10 per cent.

By comparing the values w thus obtained with

the data published in literature[8,11]) in connection with alcohol-argon filled counters, we have found that with bromine-quenched tubes these values are lower by several orders of magnitude. This may be explained by the electro-negative behaviour of bromine vapour; namely, bromine intercepts part of the electrons produced by photons originating from the metastable decay before they could reach the surroundings of the anode filament and start a new avalanche.

[11]) E. Huster and E. Ziegler, Zeits. f. Phys. **146** (1956) 281.

NUCLEAR INSTRUMENTS AND METHODS 9 (1960) 172–174; NORTH-HOLLAND PUBLISHING CO.

SMALL SCATTERING CHAMBER FOR LARGE ANGULAR REGION

H. R. E. TJIN A DJIE, F. J. DE HEER and L. A. CH. KOERTS

Instituut voor Kernphysisch Onderzoek, Amsterdam

Received 10 September 1960

A description is given of a small vacuum chamber for scattering of charged particles on nuclei at low and intermediate energies (< 30 MeV). The chamber has an angular range of 0° to 160° and can be used without foils in front of the counters.

In charged particle scattering experiments it is often helpful to have a small scattering chamber available, the counters of which are easily accessible. This reduces the time necessary for changes during the experiment as well as the cost of construction. In order to obtain freedom to observe at an abitrary scattering angle, one has to work with a window foil around the chamber[1]) or with a rubber packing that holds the vacuum during rotation[2]). The first method introduces considerable energy loss in the case of low energy particles. In the second method it is necessary to give up the possibility of observation in a certain region of scattering angles. It is possible to reduce this limitation in a simple way:

We have constructed a scattering chamber (diam. 24 cm) for the study of scattered particles at every angle between 0° and 160° without the use of entrance or exit foils (fig. 1). The chamber consists of two parts, a lower fixed part and an upper rotating part, which carries the detector counter. In order to maintain the vacuum during the rotation, the upper part supported by a ball bearing, rotates over the circumference of a rubber O-ring. Ballbearing and O-ring are embedded in the upper edge of the lower part of the chamber.

This lower part of the chamber carries two entries A and B for the particle beam (produced by a cyclotron), which has a fixed direction. If the beam enters through A, the detector counter which is looking through hole D can observe the particles coming from target T at angles from 20° up to 160° with the beam. These limits in angle are determined by the radius of the chamber and the space necessary for the O-ring and ball bearing construction. The chamber is supported by a frame and can be tilted around an axis, perpendicular to the plane of drawing and passing through the scattering center. By tilting the chamber over 20° around this axis, the beam of particles enters through B with the result that the detector counter at D now covers the angles from 0° up to 140°.

In the case where A is used as a beam entry it is possible to determine absolute cross-sections by connecting a Faraday cup at C and integrating the current. At the same time a fixed monitor counter at M observes particles coming from T at an angle of 20° with the incoming beam. In the case where B is the beam entry the monitor counter is connected to C and counts again particles scattered over 20°. A relative variation of cross-section with angle can be obtained in this way in both positions of the chamber. Determination of the absolute cross-section for some angles larger than 20° in the case where A is beam entry fixes the absolute scale of the angular distribution of the cross-section for the whole region of angles from 0° up to 160°.

There is another counter port in the lower part of the chamber, looking in a direction under 20°

[1]) M. K. Brussel, N. M. Hintz and J. H. Williams, Ann. Progr. Rep. Univ. of Minn. Lin. Accelerator Lab. (March 1957).

[2]) K. Ahnlund, Ark. f. Fys. 10 (1956) 373.

with TC and the plane of drawing. This hole can be used for energy control.

The chamber was aligned with respect to the cyclotron beam by adjusting the frame. The beam dimensions inside the chamber are determined by a rigid collimating system that slides into A or B. Counter slit systems of various lengths and diameters can be connected to the counter ports D and M. The scintillation counter at D is supported separately in order to avoid strain on the slit system. In the case of gas scattering a rectangular slit is used at S1'. It is necessary then, that the slit direction is perpendicular to the plane of scattering. This is realized by rotating the slit around the axis DT when the angle of observation is changed†.

The target holder T can be rotated either independently or coupled with the upper half of the chamber. In the latter case T rotates with half the angular speed of the chamber, so that for elastic scattering the energy spread in the target is minimized. Three targets can be mounted on targetholder T and used successively without breaking the vacuum.

In the bottom of the chamber two holes were made for gas filling and vacuum control. During

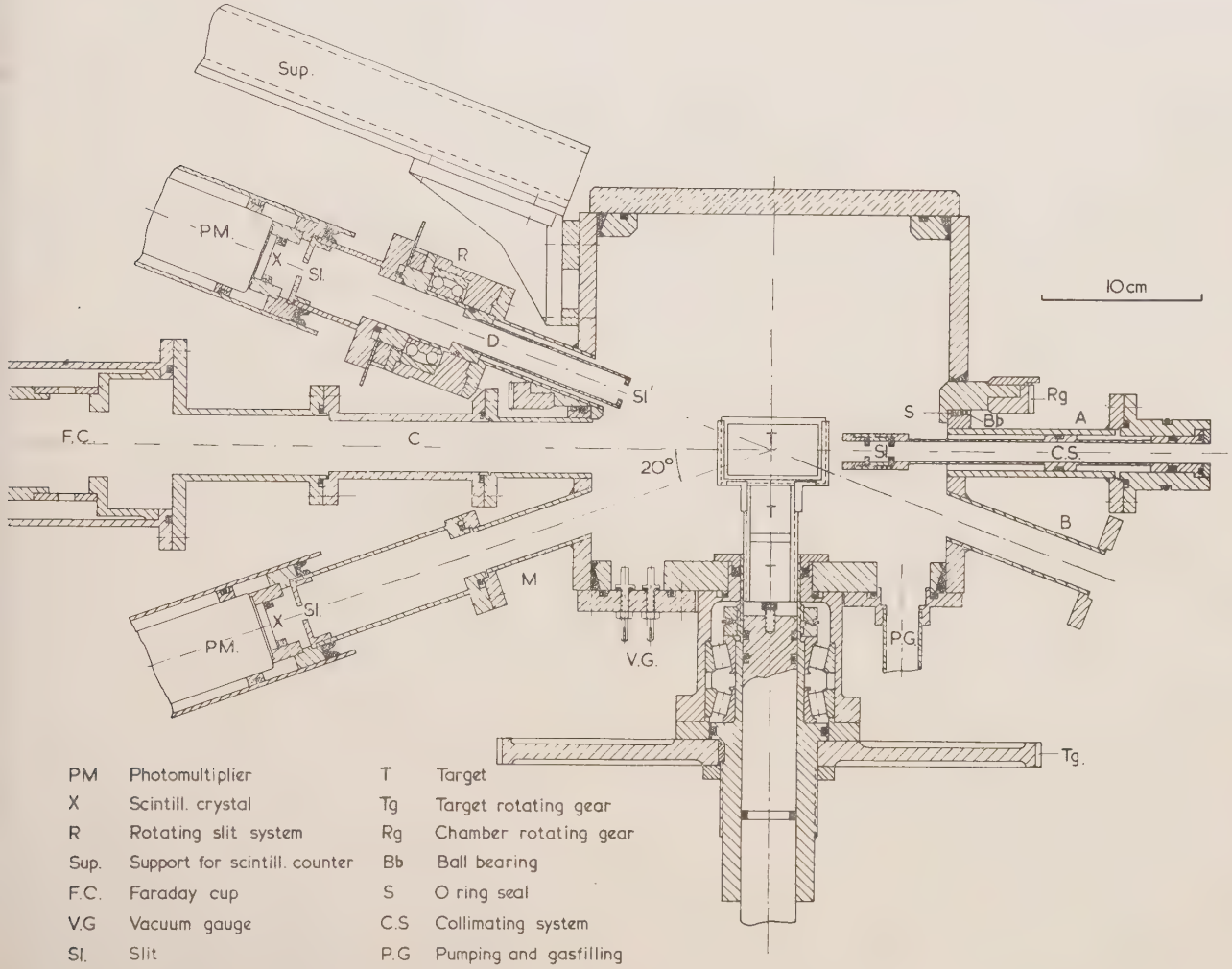

PM	Photomultiplier	T	Target
X	Scintill. crystal	Tg	Target rotating gear
R	Rotating slit system	Rg	Chamber rotating gear
Sup.	Support for scintill. counter	Bb	Ball bearing
F.C.	Faraday cup	S	O ring seal
V.G	Vacuum gauge	C.S	Collimating system
Sl.	Slit	P.G	Pumping and gasfilling

Fig. 1. Vertical section of the scattering chamber.

† This idea was worked out by K. W. Brockman and W. T. H. van Oers.

the experiment the chamber is connected with the cyclotron vacuum system through the entrance collimator. The change from the horizontal to the tilted position of the chamber does not take more than 20 minutes.

Acknowledgements

The authors wish to thank Prof. Dr. P. C. Gugelot for his encouragement and interest in the development, Mr. H. J. M. Akkerman and Mr. J. Ladru for advice and help in the construction.

This development was performed as part of the program of the Foundation for Fundamental Research of Matter (F.O.M.) with the financial support of the Organization for Pure Research (Z.W.O.).

NUCLEAR INSTRUMENTS AND METHODS 9 (1960) 175–180; NORTH-HOLLAND PUBLISHING CO.

A METHOD FOR THE MEASUREMENT OF GAMMA-RAY SPECTRA IN OMNIDIRECTIONAL GAMMA-RAY FIELDS

L. C. THOMPSON

University of Georgia, Athens, Georgia

Received 19 August 1960

A method is presented for analyzing pulse-height distributions from a scintillation detector exposed to an omnidirectional gamma-ray field through a collimator opening in a lead shield. The method is a combination of analytical and experimental procedures and provides corrections for collimator penetration and scattering effects.

1. Introduction

The need sometimes arises to measure continuous gamma-ray spectra in omnidirectional gamma-ray fields. In such cases it is very often desirable to measure the absolute gamma-ray spectrum as a function of direction at a given point in space. The absolute spectrum should be given as number of gamma rays/MeV sec cm^2 sr versus gamma-ray energy. The simpliest way of making such spectral measurements is by measuring the pulse-height distribution from a scintillation detector within a lead shield. A collimator opening in the shield allows the detector to accept radiation only from a given solid angle of space. The analysis and reduction of such a spectrum involves a number of problems not encountered in the analysis of scintillation detector pulse-height distributions from point sources. The most important additional factors are the scatter and energy degradation of gamma rays by the collimator walls and the direct penetration of gamma-rays through the collimator edges. These connections are not at all trivial in most cases. This paper presents a method for making these corrections and reducing such spectra.

The basic theory of the gamma-ray collimator has been developed by Mather[1]). Mather, however, assumes a non-energy sensitive totally absorbing detector, and he does not take into account the energy degradation of a gamma ray after scattering. His calculations are not directly applicable to scintillation spectrometer pulse-height distributions without further work. This paper shows how Mather's collimator calculations can be extended by experimental measurements and how the results can be incorporated into a method for analyzing pulse-height distributions from a scintillation detector exposed to an omnidirectional gamma-ray field through a collimator opening in a lead shield.

[1]) Robert L. Mather, J. Appl. Phys. 28 (1957) 1200.

2. Data Needed and Conditions Assumed for Reducing the Spectra

The type of gamma-ray collimator considered in this study is shown in fig. 1 and will be designated as a straight cylindrical gamma-ray collimator. The comparison of this collimator to an ideal non-scattering and totally absorbing collimator is simplified if certain terms are defined:

(a) Geometrical aperture—the radiation aperture in the absence of penetration and scattering effects.

(b) Penetration aperture—the increase in size of the aperture due to penetration of radiation without scatter through the collimator edges.

(c) Scattering aperture—the increase in size of the aperture due to radiation scattering from the surfaces of the collimator. The energy of some of these photons will be considerably reduced whereas others will have lost very little energy.

These apertures are generally expressed in cm^2

and depend upon the energy of the gamma ray, the length and diameter of the collimator, the material of which the collimating shield is made, and the source-collimator geometry. They are particularly suitable for determining the amount

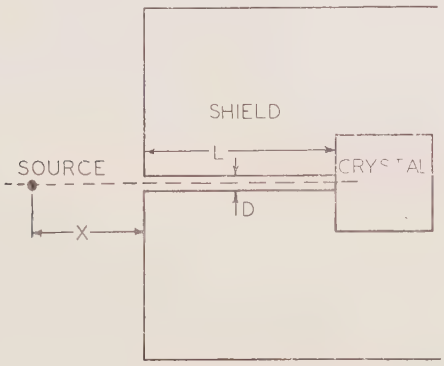

Fig. 1. Diagram of a straight cylindrical gamma-ray collimator. L = length of collimator. D = diameter of collimator. X = distance of source from end of collimator.

of radiation passing through the collimator from a point source either on or off the collimator centerline.

If the collimator is in an isotropic gamma-ray field, it is necessary to perform an integration over solid angle to obtain the amount of radiation passing through the collimator. Let $N(E)$ be the number of gamma rays/MeV cm² sr sec incident on the collimator. Let $G(\theta)$ be the geometrical aperture for unidirectional radiation that makes an angle θ with the collimator centerline. The number of gamma rays/sec passing through the geometrical aperture is given by

$$\int_0^\infty N(E)\,\mathrm{d}E \int_0^\pi G(\theta)\,2\pi \sin\theta\,\mathrm{d}\theta\,.$$

The integral

$$\int_0^\pi G(\theta)\,2\pi \sin\theta\,\mathrm{d}\theta$$

will be designated in this paper as the "integrated geometrical aperture". The "integrated penetration aperture" and the "integrated scattering aperture" are similarly defined. They depend, however, on the gamma-ray energy whereas the integrated geometrical aperture does not. The units of the integrated apertures are sr cm².

The analysis of scintillation spectra taken by a detector within a collimator is considerably simplified if the following conditions are satisfied:

1. The diameter of the crystal is to be much larger than the diameter of the collimator. This is to justify the assumption that all gamma rays passing through the collimator enter the crystal close to the collimator centerline.

2. The length of the collimator is to be much greater than its diameter. This is to justify the assumption that the direct path length in the crystal of all gamma rays entering the crystal through the geometrical or penetration apertures is approximately the same.

3. The length of the collimator is to be such that the number of gamma rays that penetrate the entire length is much less than the number that enter through the geometrical aperture.

4. The omnidirectional gamma-ray field being studied must be approximately isotropic over the effective "solid angle of acceptance" of the collimator. This can usually be accomplished by decreasing the effective "solid angle of acceptance" of the collimator through increasing the length and/or decreasing the diameter of the collimator.

If these conditions are satisfied, the following information must be available for the collimator and scintillator being used in order to analyze spectra properly:

1. The magnitude of the integrated geometrical aperture. Mather[1]) finds the integrated geometrical aperture to be

$$\frac{\pi^2 D^4}{16L^2} \text{ if } L \gg D\,.$$

2. The ratio $P(E)$ of the integrated penetration aperture to the integrated geometrical aperture as a function of gamma-ray energy. Mather[1]) finds that the ratio $P(E)$ can be expressed as a function of μL where μ is the linear absorption coefficient of the collimator material for the gamma rays. This ratio is plotted in fig. 9 of ref.[1]).

3. The ratio $S(E)$ of that part of the integrated scattering aperture in which the gamma rays suffer very little energy degradation to the integrated geometrical aperture as a function of

gamma-ray energy. The numerator in $S(E)$ includes only those collimator scattered gamma rays that would still lie under the photopeak of the original gamma ray if totally obsorbed in the crystal. Mather[1]) gives an approximate method for calculating the integrated scattering aperture. Tomnovec and Mather[2]) utilize a method for modifying the integrated scattering aperture to include only those scattered gamma rays that would still lie under the photopeak of the original gamma ray if totally absorbed in the crystal. The ratio $S(E)$ may thus be obtained utilizing these methods. For collimators of greatest interest, the ratio $S(E)$ is fortunately rather small. (See Section 4.4.)

4. Two sets of monoenergetic gamma-ray response functions as a function of gamma-ray energy. One set is for a point source on collimator centerline, and the other is for an isotropic gamma-ray field. A method for obtaining these response functions will be discussed in Section 4.1.

5. In an isotropic gamma-ray field, the ratio $R(E)$ of the number of photons of energy E outside the collimator that finally interact with the crystal to the number of photons of energy E outside the collimator that finally interact with the crystal after having suffered very little or no energy degradation in the collimator. "Very little energy degradation" is here defined as including only those collimator scattered gamma rays that would still lie under the photopeak of the original gamma ray if totally absorbed in the crystal. This ratio must be known as a function of gamma-ray energy. This ratio is, of course, always larger than one. A method for determining $R(E)$ is given in Section 4.3.

3. Method for Reducing the Spectra

A method for analyzing pulse-height distributions from a scintillation detector exposed to an omnidirectional gamma-ray field through a collimator opening in a lead shield may be developed analogous to the iteration or "stripping" process for analyzing continuous pulse-height distributions from point sources. If the information listed in Section 2 is known for the particular collimator being used and if the requirements listed in Section 2 are satisfied, then the continuous pulse-height distributions may be analyzed as follows.

The pulse-height distribution is assumed to be plotted as number of pulses/MeV sec versus pulse height in MeV. This distribution is first divided into a number of energy bins. Probably the most satisfactory method is to construct the bin widths to be proportional to the spectrometer resolution. Those pulses lying in the very highest energy bin will be due to the total absorption of gamma rays of that energy in the crystal. From a knowledge of the response function of the detector in an isotropic gamma-ray field of this energy, the contribution of gamma rays in this energy bin to the entire pulse-height distribution can be found. The number of gamma rays in this energy range that finally interact with the crytal is divided by $R(E)$ to obtain the number of gamma rays in this energy range outside the collimator that pass through the collimator with very little or no energy degradation and interact with the crystal. This number is next divided by the efficiency of the crystal for detecting gamma rays of this energy, the effective opening of the collimator for gamma rays of this energy which is given by

$$\frac{\pi^2 D^4}{16 L^2}\,[1 + P(E) + S(E)]\,,$$

and the width of the energy interval. One point expressed as number of gamma rays/MeV sec cm^2 sr is thus obtained at the midpoint of the highest energy bin on the analyzed spectrum. The contribution that gamma rays in this energy range make to the pulses in all lower bins is subtracted off, and the process is then repeated for the next to highest energy bin. By repetition, a completely analyzed spectrum is finally obtained.

The method of matrix inversion as applied to the analysis of continuous NaI pulse-height distributions from the point sources has been discussed by many authors and several response

[2]) F. M. Tomnovec and R. L. Mather, J. Appl. Phys. 28 (1957) 1208.

matrices have been published[3–8]). A response matrix could likewise be constructed for an omnidirectional gamma-ray field and would be suitable for a particular type collimator and scintillation detector.

4. Experimental Measurements

4.1. RESPONSE FUNCTIONS IN AN ISOTROPIC GAMMA-RAY FIELD

Response functions from a point gamma-ray source taken as a function of distance off collimator centerline may be utilized to obtain the response function in an isotropic gamma-ray field. Let $f(E,Y)$ be the absolute response function observed in the crystal, where Y is the distance of the source off collimator centerline, and E is the pulse height. The functions $f(E,Y)$ are measured as a function of increasing Y until the spectrum obtained with the collimator plugged is the same as that obtained with the collimator unplugged. Then the response function from an isotropic gamma-ray field of this energy is given by

$$F(E) = \int_0^{y_{\max}} f(E, y)\, 2\pi y \, \mathrm{d}y \,. \qquad (1)$$

This method has been used to obtain response functions due to isotropic gamma-ray fields of 0.412 MeV and 2.62 MeV for the collimator-crystal geometry shown in fig. 1. For both gamma-ray energies, a 3 in. diameter by 3 in. long Harshaw mounted NaI(Tl) crystal was used. The collimating shield was made of lead, and the diameter of the bore was 0.50 in. For the 0.412 MeV gamma ray from Au-198, $L = 3.94$ in. and $X = 12.22$ in. For the 2.62 MeV gamma ray from Tl-208, $L = 8.5$ in. and $X = 18.00$ in.

Eq. (1) was integrated numerically. Fig. 2 compares the isotropic field response function to the point source on collimator centerline response functions for the 0.412 MeV gamma ray. The areas of the photopeak of the two gamma rays have been normalized. Fig. 3 is a similar plot for the 2.62 MeV gamma ray.

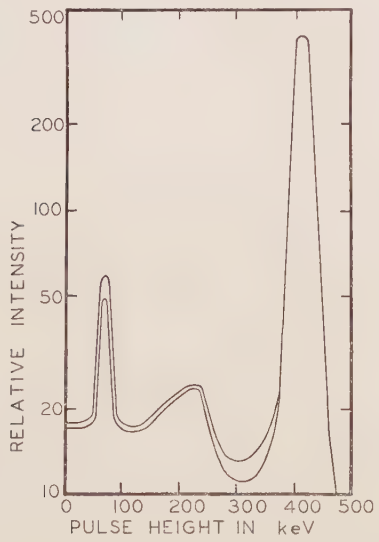

Fig. 2. Comparison of the isotropic field response function (upper curve) to the point source on collimator centerline response function (lower curve) for the 412 keV gamma ray from Au-198. The detector was a 3 in. diameter by 3 in. long NaI (Tl) crystal. $L = 3.94$ in. $D = 0.50$ in. The photopeak areas of the two curves have been normalized.

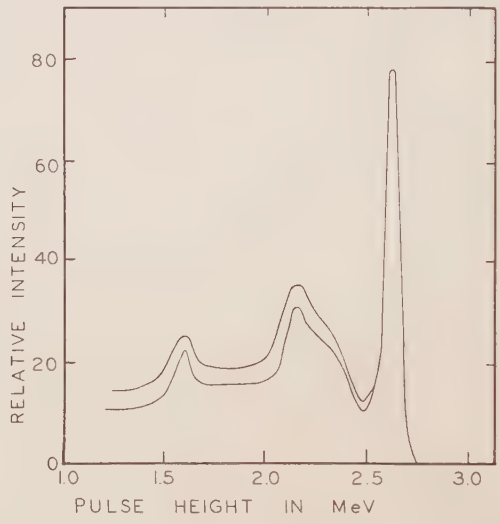

Fig. 3. Comparison of the isotropic field response function (upper curve) to the point source on collimator centerline response function (lower curve) for the 2.62 MeV gamma rays from Tl-208. The detector was a 3 in. diameter by 3 in. long NaI (Tl) crystal. $L = 8.50$ in. $D = 0.50$ in. The photopeak areas of the two curves have been normalized.

[3]) J. W. Motz, Phys. Rev. **100** (1955) 1560.
[4]) N. Starfelt and H. W. Koch, Phys. Rev. **102** (1956) 1598.
[5]) J. H. Hubbell, Rev. Sci. Instr. **29** (1958) 65.
[6]) W. R. Dixon and J. H. Aitken, Can. J. Phys. **36** (1958) 1624.
[7]) J. Kockum and N. Starfelt, Nuc. Instr. and Methods **4** (1959) 171.
[8]) H. M. Childers, Rev. Sci. Instr. **30** (1959) 810.

4.2. RESPONSE FUNCTIONS FROM POINT SOURCES ON COLLIMATOR CENTERLINE

It is obvious that the pulses lying between the upper and lower curves in both figs. 2 and 3 are due to the interaction with the crystal of energy degraded gamma rays. The question remains as to just what part of the lower curves in fig. 2 and 3 are due to the interaction of energy degraded gamma rays with the crystal. This problem may be checked experimentally in the following manner. As a point source of gamma rays is moved along collimator centerline away from the collimator, the ratio between the solid angle subtended by the collimator walls at the source and the solid angle subtended by the bare crystal at the source decreases. Therefore the response functions taken at larger source-collimator distances should contain a smaller fraction of energy degraded gamma rays.

Sets of response functions of this type were run for the 0.412 MeV gamma ray from Au-198, the 1.112 MeV gamma ray from Zn-65, and the 2.62 MeV gamma ray from Tl-208. Response functions were run for the following values of X and L using a lead shield having a collimating hole 0.50 in. in diameter:

Gamma-ray energy (MeV)	L (in.)	X (in.)
0.412	4	0.25, 1,2,3,4,6,8,10
1.112	6	0.25, 1,2,3,4,6,8,10
2.62	8	1,2,4,8,12,18,24,36

For the 0.412 MeV gamma ray, the response functions were practically the same for all values of X. For the 1.112 MeV gamma ray, the response functions were approximately the same for all values of X greater than 4 in. At smaller distances the photofraction did decrease by as much as 5%. For the 2.62 MeV gamma ray, the response functions changed very little for values of X greater than 12 in. At smaller distances, the fraction of energy degraded radiation in the spectrum did increase considerably more than it did at 1.112 MeV.

An additional set of response functions were measured involving the 2.62 MeV gamma ray. The length of the collimator was set at 14 in., and the source was placed 12 in. from the end of the collimator on collimator centerline. With the source fixed in place, response functions were taken as the collimator length was reduced from 14 in. to 8 in. No change whatsoever in the response functions was observed.

Two conclusions may be drawn from these experiments:

1. In the gamma-ray energy range below 3 MeV, very little energy degraded gamma rays enter the crystal for this type of collimator if the source is at least 12 in. from the end of the collimator and on the collimator centerline.

2. Scatter by the collimator is much more important at 2.62 MeV than it is at 0.412 MeV. This is to be expected from the change in the relative importance of the photoelectric effect, Compton scattering, and pair production in lead as a function of photon energy[9,11]) and also from the change in the angular distribution of Compton-scattered photons as a functions of photon energy[10]).

4.3. DETERMINATION OF THE FACTOR $R(E)$

The factor $R(E)$ may be found as follows. The areas under the photopeaks of the two types of response functions (point source on centerline and isotropic field) are first normalized as was done in figs. 2 and 3.

The response function from a point source at a large distance from the end of the collimator and on collimator centerline is due essentially to the interaction of non-energy degraded gamma rays with the crystal and represents that part of the isotropic field response function which is due to gamma rays which have suffered either no energy degradation in the collimator or less than the amount consistent with the definition of $R(E)$. $R(E)$ is therefore the ratio of the area under the isotropic field response function to the area under the point source on collimator centerline

[9]) G. R. White, National Bureau of Standards Report 1003 (1952).

[10]) Ann T. Nelms, N.B.S. Circular 542, August 28, 1953.

[11]) C. M. Davisson and R. D. Evans, Rev. Modern Phys. 24 (1952) 79.

response function if the areas under their photopeaks are normalized.

4.4. THE ACCURACY OF THE SUM $P(E) + S(E)$

Mather's method[1]) for calculating $P(E)$ appears to be quite valid. Tomnovec and Mather's method[2]) for calculating $S(E)$ does contain some significant approximations, but $S(E)$ should be most accurate for gamma rays that lose little energy after scattering off the collimator walls.

Tomnovec and Mather[2]) checked the validity of the sum $P(E) + S(E)$ experimentally at 1.112 and 1.59 MeV for a collimator 0.5 in. in diameter through 8 in. of lead. Another experimental check on the accuracy of the sum $P(E) + S(E)$ at 2.62 MeV may be made using the data acquired for fig. 3. The results were as follows:

Gamma-ray energy (MeV)	$P(E) + S(E)$ Theory	$P(E) + S(E)$ Experiment	Investigator
1.112	0.46	0.39	Tomnovec and Mather[2])
1.59	0.65	0.60	Tomnovec and Mather[2])
2.62	0.73	0.75	This paper

The agreement between theory and experiment is actually quite good. As a matter of fact, quite a bit of variation in the theoretical values result if the absorption coefficients of Davisson and Evans[11]) are used instead of those of White[9]). It should also be noted for the collimators used in the above experiments, $S(E)$ lies between 0.03 and 0.05 for gamma energies between 0.5 and 2.0 MeV with $P(E)$ the dominant term except at very low energies[2]).

5. Conclusions

This method for analyzing spectra taken in omnidirectional gamma-ray fields should be quite satisfactory provided monoenergetic gamma sources of sufficient intensity are available to allow one to measure isotropic field response functions. Below 3.00 MeV, this should present no problems. At higher energies, it may be necessary to resort to particle accelerators for the required monoenergetic gamma rays. If these gamma sources should prove to be of low intensity, it might be necessary to develop some method for extrapolating from the response function measured on collimator centerline to the isotropic field response function at the higher gamma-ray energies.

NUCLEAR INSTRUMENTS AND METHODS 9 (1960) 181–194; NORTH-HOLLAND PUBLISHING CO.

THE RAPID RECOGNITION OF A SIGNIFICANT INCREASE IN THE RATE OF ARRIVAL OF PULSES OCCURRING AT RANDOM

C. H. VINCENT

United Kingdom Atomic Energy Authority, A.W.R.E., Aldermaston, Berks

Received 5 August 1960

There is a fundamental lower limit to the time in which it is possible to recognise an excursion in the mean rate of pulses occurring at random and to distinguish it reliably from a chance fluctuation. This lower limit is found and is evaluated numerically for the case of an exponential excursion. It is possible to build relatively simple electronic equipment which will give indication of such an excursion in little more than the absolute minimum time over a wide range of conditions of initial pulse rate and of excursion period. An example of such a circuit is described and is shown to be capable of responding in less than one period of the excursion or in less than the time to count 200 pulses at the initial rate, whichever is the greater. This circuit will give false indication only on extremely rare voltage fluctuations exceeding 10 standard deviations, which are of negligible probability per year. It is suggested that the method described may be of use to give rapid warning of excursions in reactors and critical assemblies. In any case, the theoretical optimum found constitutes a standard of reference by which equipment for such warning may be judged.

1. Introduction

For the safe operation of nuclear reactors and critical assemblies, it is necessary to have automatic equipment which will detect and remedy the existence of a supercritical state which is causing an excessively rapid increase of power level and neutron flux. This problem may be divided into two aspects, the recognition of the excessively supercritical state from the nature of the signals received from a detector in the assembly concerned, and the action taken to remedy the situation. This paper is concerned only with the first aspect, that is, with the production of a suitable warning signal which is to be passed on to the protection equipment to indicate that an undesirable state exists and to initiate the remedial action. Moreover, it deals particularly with the special problems that arise at low power and flux levels, due to the fact that the outputs of the detectors used at such levels consist of sequences of pulses corresponding to the detection of individual neutrons.

From the safety point of view, it is necessary that the increasing rate of pulse arrival which indicates the supercritical condition should be recognised as quickly as possible. On the other hand, it will cause great inconvenience if the recognition equipment responds to an effect which is purely a random fluctuation and does not really indicate a significant increase in the mean pulse rate. It takes time to check the equipment and start up again after an unnecessary shut-down. Taken separately, the requirements of attaining a high speed of response or of recognising only increases of genuine significance are not difficult to meet. However, the combination of maximum speed of response with maximum freedom from spurious alarms is one requiring careful thought and it is not clear that present conventional reactor instruments, such as reactor period meters, achieve the optimum performance possible in this respect.

In the present paper, an attempt is made to re-examine this problem from a fundamental point of view. We consider a channel which carries pulses occurring at random. That is, there is a certain probability $\rho\delta t$ that a pulse will occur in a short time interval δt. We consider firstly the inherent statistical limitations that exist in the most rapid recognition of the fact that ρ has started to increase at a certain time and secondly the design of suitable electronic

equipment to detect such an increase in practice with a performance not far short of the theoretically possible optimum. We are particularly concerned with determining conditions under which it is possible to detect an excursion in a

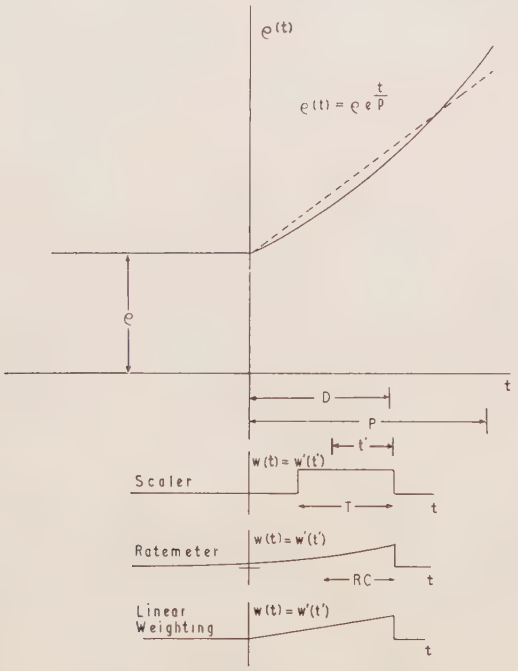

Fig. 1.
This shows an exponential excursion together with some of the weighting functions which might be used in detecting it.

time interval from its commencement less than one period of that excursion, as this was specified as a desirable performance for the recognition equipment. While this is a quite arbitrary specification, it is a reasonable one, and it has the advantage that the higher the degree of supercriticality (and therefore the more urgent the operation of the safety equipment) the less the time spent on recognition.

In general terms, it may be said that the equipment required must contain some form of ratemeter, together with means for detecting a significant increase in its reading. The conventional reactor period meter, which records the rate of increase of the output of a logarithmic ratemeter, is only one example of what is possible. One might use a scaler or register arranged to show at any time the number of pulses which have arrived in the preceding T seconds, together with an appropriate device for detecting an increase. Alternatively, one might use an ordinary diode pump circuit to add a fixed charge to a storage condenser for each pulse received, together with a leakage resistor, in the fashion of an ordinary linear ratemeter. Both these examples are special cases of a more general method in which each pulse adds to the total reading a quantity $w'(t')$, where t' is the time that has elapsed since the pulse occurred and $w'(t')$ is a weighting function. In the scaler case, $w'(t') = 1$, for $t' < T$, and $w'(t') = 0$, for $t' > T$ (see fig. 1).

In the ratemeter case,

$$w'(t') = e^{-\frac{t'}{RC}}$$

where RC is the time-constant of the condenser and resistor. It is to be expected that some weighting functions will be more satisfactory than others and it is of obvious importance to determine whether there is an optimum weighting function.

2. General Theory

Consider an excursion in which there is a constant mean rate of pulse arrival $\rho(0)$ until a time given by $t = 0$. It will be convenient to write ρ for $\rho(0)$. For $t > 0$ let

$$\rho(t) = \rho[1 + f(t)] .$$

If detection of the excursion occurs at a time $t = D$, the increase in the output reading at that time is given by

$$\int_0^D \rho w'(t')f(t)\mathrm{d}t = \int_0^D \rho w'(D - t)f(t)\mathrm{d}t .$$

Now the significance of this is determined by its ratio to the standard deviation of the reading at the steady rate ρ. This standard deviation is given by

$$\sqrt{\int_0^\infty \rho[w'(t')]^2 \, \mathrm{d}t'} .$$

The value of D is determined by the requirement that the significance ratio

$$r = \frac{\int_0^D \rho w'(D - t)f(t) \, \mathrm{d}t}{\sqrt{\int_0^\infty \rho[w'(t')]^2 \, \mathrm{d}t'}} \qquad (1)$$

should reach a specified minimum value K. Let us investigate the maximum value of this ratio, for any given value of D, as the weighting function is varied.

For any given value of D, we may write

$$\int_0^D \rho w'(t')f(t)\,\mathrm{d}t = \int_0^D \rho w'(D-t)f(t)\,\mathrm{d}t$$

$$= \int_0^D \rho w(t)f(t)\,\mathrm{d}t \qquad \text{say}.$$

It is obvious that $w(t)$ should be 0 for $t < 0$ (that is $t' > D$) since any weighting given to pulses occurring before the excursion starts would only increase the standard deviation without affecting the registered increase and would therefore decrease the significance factor of the latter. We may therefore write for the standard deviation

$$\sqrt{\int_0^\infty \rho[w'(t')]^2\,\mathrm{d}t'} = \sqrt{\int_0^D \rho[w'(t')]^2\,\mathrm{d}t'}$$

$$= \sqrt{\int_0^D \rho[w(t)]^2\,\mathrm{d}t}\,.$$

We then require to find the form of $w(t)$ which will give the maximum value of r for any given ρ, D and $f(t)$, where

$$\frac{r^2}{\rho} = \frac{\left[\int_0^D w(t)f(t)\,\mathrm{d}t\right]^2}{\int_0^D [w(t)]^2\,\mathrm{d}t}\,. \tag{2}$$

Any function $w(t)$ from $t = 0$ to $t = D$ can be put in the form

$$w(t) = Af(t) + \delta(t)$$

where A is constant and $\delta(t)$ is such that

$$\int_0^D f(t)\delta(t)\,\mathrm{d}t = 0$$

by taking

$$A = \frac{\int_0^D f(t)w(t)\,\mathrm{d}t}{\int_0^D [f(t)]^2\,\mathrm{d}t}\,.$$

Substituting for $w(t)$ in the expression for r^2/ρ in equation (2), we obtain

$$\frac{r^2}{\rho} = \frac{\left[\int_0^D f(t)\{Af(t) + \delta(t)\}\,\mathrm{d}t\right]^2}{\int_0^D [Af(t) + \delta(t)]^2\,\mathrm{d}t}$$

$$= \frac{A^2\left[\int_0^D \{f(t)\}^2\,\mathrm{d}t\right]^2}{A^2\int_0^D \{f(t)\}^2\,\mathrm{d}t + \int_0^D \{\delta(t)\}^2\,\mathrm{d}t}\,. \tag{3}$$

Since $\{\delta(t)\}^2$ is always positive, it follows that its integral must be a minimum and that the above expression must be a maximum when $\delta(t) \equiv 0$. That is, the required weighting function is one which is proportional to $f(t)$ at any time from $t = 0$ to $t = D$.

We then have, for this optimum weighting function

$$\frac{r^2}{\rho} = \int_0^D \{f(t)\}^2\,\mathrm{d}t\,. \tag{4}$$

This shows that for any given value of ρ and for any given excursion, as specified by the function $f(t)$, the maximum ratio r obtainable by varying the weighting function $w'(t')$ for a given value of D is an increasing function of D. At the minimum time D for a significant increase, therefore, equation (4) becomes

$$\frac{K^2}{\rho} = \int_0^D \{f(t)\}^2\,\mathrm{d}t\,. \tag{5}$$

The problem still remains, of course, of ensuring that the optimum weighting function, or one close to it, is applied in any particular case. Nevertheless, the above equation serves as a very useful basis of comparison, as an absolute optimum with which the performance of any actual equipment may be compared. Moreover, since equation (3) contains only a second order term in $\delta(t)$, the fitting of the weighting function to $f(t)$ does not need to be very exact in order to obtain a close approach to the optimum performance. For example, if we take $\frac{3}{2}t$ as a quite crude approximation to $f(t) = \mathrm{e}^t - 1$ from $t = 0$ to $t = 1$ (see fig. 1), the reduction in the ratio for r^2/ρ from the optimum is only about 1%.

Since $f(t)$ is normally a rising function of t, in the cases of interest, it is to be expected that a falling function $w'(t')$ of t' will be best, in general. (It will be remembered that $w'(t') = w'(D - t) = w(t)$, as given above.) The duration of the weighting function waveform $w'(t')$ may be matched to the requirement for optimum performance on each excursion that comes by using a multiplicity of circuits with different weighting function durations and taking the response of the fastest of these. The exact form of the weighting function $w'(t')$ for optimum performance can only be specified when the exact form of the excursion to be detected is known as well, that is, when $f(t)$ is given. Fortunately, as we have seen above, the exact matching of the two waveforms is not a critical requirement. The precise form of $w'(t')$ will normally be determined by the choice of a simple and convenient arrangement to produce it, rather than by an attempt to match precisely the expected form of the excursions. We shall consider exact exponentially rising excursions in all the examples taken in this paper, in order to give $f(t)$ a specific form and enable the expected performance to be calculated. However, the circuits proposed may be expected to respond similarly for any other form of rising rate in the excursion.

3. Application to an Exponential Excursion

In the case of an exponential excursion, we have, for $t > 0$.

$$\rho(t) = \rho e^{t/P}$$

where P is the "period" of the excursion, and

$$f(t) = (e^{t/P} - 1) .$$

We therefore have

$$\frac{K^2}{\rho} = \int_0^D (e^{t/P} - 1)^2 \, dt$$

$$= \tfrac{1}{2} P [(e^{D/P} - 2)^2 - 1] + D$$

or

$$\frac{K^2}{\rho P} = \tfrac{1}{2} (e^{D/P} - 2)^2 - \frac{1}{2} + \frac{D}{P}$$

or

$$\frac{K^2}{M} = \tfrac{1}{2} (e^X - 2)^2 - \tfrac{1}{2} + X \qquad (6)$$

where $M = \rho P$ is the mean number of pulses which would occur in one excursion period at the initial steady rate, and $X = D/P$. The absolute value of the time-scale is of no theoretical importance in this problem and the last form of the equation has the advantage of being independent of it. In fig. 2 we have plotted X against M/K^2, which is a more convenient form in practice. It will be seen that a large increase in M/K^2 is needed to produce a small decrease in X.

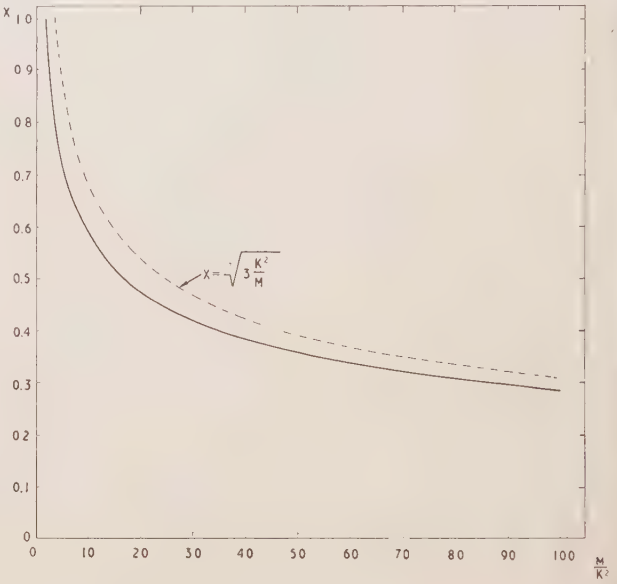

Fig. 2. Graph showing the absolute minimum value of X for an exponential excursion as a function of M/K^2.

The best fit weighting curve for $X \ll 1$ (for $M \gg K^2$) is a straight line through the origin, being the beginning of an exponential rise. In this case, we have either from equation (6) or directly the approximate answer

$$\frac{K^2}{M} = \frac{X^3}{3}$$

i.e.

$$X = 1.4422 \left(\frac{K^2}{M}\right)^{\frac{1}{3}}. \qquad (7)$$

This curve is shown (dotted) for comparison in figure 2 and it will be seen to fit the optimum curve quite well down to fairly low values of M/K^2.

The best fit weighting function for $X \gg 1$

($M \ll K^2$) is an exponential one, $e^{t/T}$, where $T = P$, in this case. We then have, approximately,

$$\frac{K^2}{\rho} = \int_0^D (e^{t/P})^2 \, dt$$

$$= \tfrac{1}{2} P \, e^{2D/P}$$

i.e.

$$X = -\tfrac{1}{2} \log_e \left(\frac{1}{2} \frac{M}{K^2}\right). \qquad (8)$$

4. Theory of the Diode Pump Circuit

Let us now consider the theory of an ordinary diode pump (linear ratemeter) circuit, as shown in fig. 3A and see how its performance compares

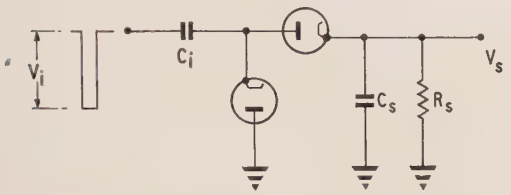

Fig. 3A. The diode pump ratemeter circuit.

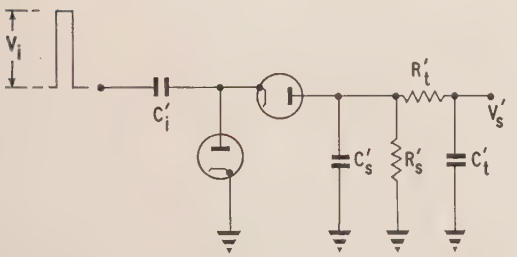

Fig. 3B. The counterbalancing diode pump ratemeter circuit.

with the theoretical optimum. Let C_s be the storage capacity of the diode pump circuit, C_i the charging capacity and R_s the leakage resistance. Let the input pulse amplitude be V_i. The discharge time-constant of the storage condenser is then

$$T = R_s C_s .$$

The mean voltage on the storage condenser with a given input pulse rate ρ, neglecting any reduction in the charge per pulse as this voltage rises, is

$$V_s = R_s V_i C_i \rho . \qquad (9)$$

We can regard this as the storage of N input charges where

$$N = \frac{C_s V_s}{C_i V_i}$$

$$= \rho T . \qquad (10)$$

The problem of calculating the fluctuation of voltage or charge superimposed on these values is essentially the same as the well-known problem of calculating the noise generated by a shot-noise diode connected in parallel with a resistor and condenser. It gives as answer a root mean square fluctuation of $\sqrt{N/2}$ charges or $\sqrt{\frac{1}{2}N}$ $V_i C_i / C_s$ volts. We assume here that the input pulse duration and dead-time are short enough to be neglected in comparison with the mean time-interval between the pulses.

In the case of an excursion, we may consider the fluctuations discussed above as superimposed on a smoothly varying current $V_i C_i \rho(t)$ into the storage condenser. We are now concerned with the response of the circuit when $\rho(t)$ suddenly starts to increase from its constant value ρ. Let us assume that the increase is an exponential one with period P, starting at a time $t = 0$. The response of the circuit can be obtained by ordinary circuit theory, which gives

$$\frac{V_s(t)}{V_s(0)} = \frac{T}{P+T} e^{-t/T} + \frac{P}{P+T} e^{t/P} . \qquad (11)$$

For a specified value of K, this will represent a significant increase on the mean value before the excursion at a minimum delay D if

$$\frac{T}{P+T} e^{-D/T} + \frac{P}{P+T} e^{D/P} = 1 + \frac{K\sqrt{\rho T/2}}{\rho T} . \qquad (12)$$

(This result may also be deduced directly from equation (1).)

The function of D on the left-hand side of this equation is a monotonic increasing one having the value of 1 at $D = 0$, and ∞ at $D = \infty$. There is therefore always a solution for D and this solution is unique.

If we put $X = D/P$ and $B = T/P$, we obtain

$$\frac{B}{B+1} e^{-X/B} + \frac{1}{B+1} e^{X} = 1 + \frac{1}{\sqrt{2B}} \sqrt{\frac{K^2}{M}} . \qquad (13)$$

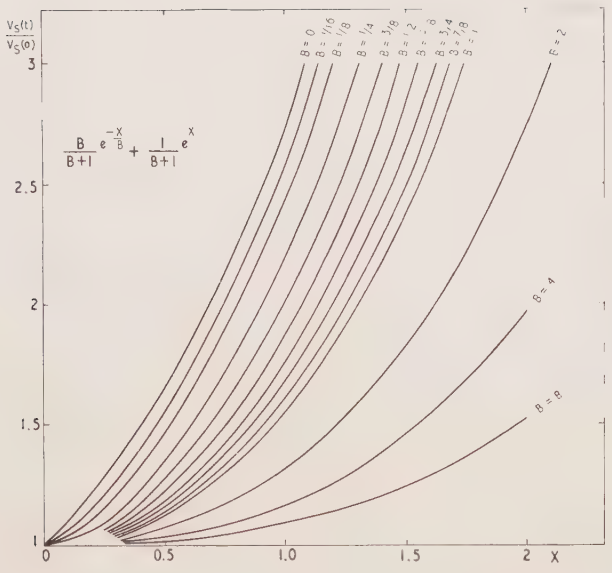

Fig. 4. The response of a diode pump ratemeter circuit to an exponentially rising input.

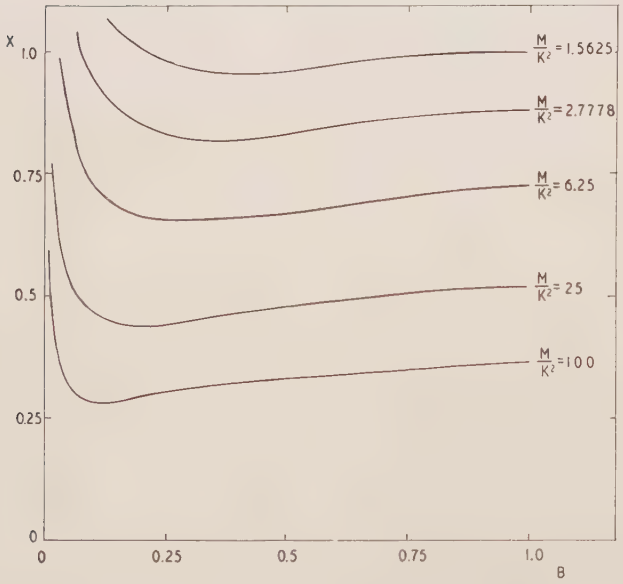

Fig. 5. Determination of the optimum time-constant for a ratemeter circuit with exact bias.

We require to find the value of B which gives the minimum value of X for each value of M/K^2 and to plot this minimum value of X against M/K^2. An approximate graphical derivation of this function is shown in figs. 4 and 5. In fig. 4, the different curves give the left-hand side of the equation (13) as a function of X for various values of B, as labelled. The curves of fig. 5 are obtained from the interceptions, for a fixed value of M/K^2 in each case, of these curves with the abscissae representing the corresponding values of the right-hand side of the equation. The minimum value of X for each value of M/K^2 is clearly shown and it will be seen that the value of B is not very critical at the minima, which are broad. Fig. 6 shows the minimum value of X plotted against M/K^2. The values for this curve were computed numerically. (The value of B at the minimum is also shown and this will be seen to be slightly less than $\frac{1}{2}X$.) The optimum curve from our previous case (fig. 2) could not be shown for comparison, as the two curves are so close as to render this impracticable. The ratemeter curve lies only at most one per cent higher than the absolute minimum curve, over the range shown.

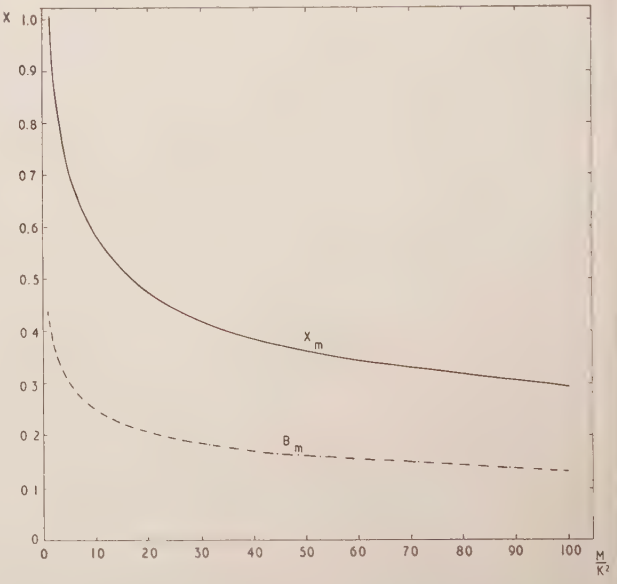

Fig. 6. The minimum value of X for the ratemeter circuit with exact bias plotted as a function of M/K^2. The value of B at which this occurs is also shown.

5. Method of Application

We have now shown that it is theoretically possible to detect an excursion of period P in a time D from its commencement, which may be less than P, provided that

1. The theoretical minimum necessary input

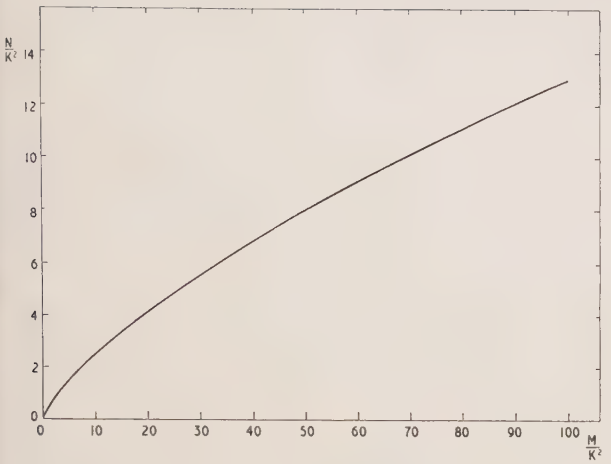

Fig. 7. The relationship between N/K^2 and M/K^2 in the exact bias ratemeter circuit at the optimum condition.

pulse rate is available, to make M/K^2 sufficiently large.

2. The pulses are applied to a diode pump circuit of the type described, having a suitable time-constant, preferably the optimum time-constant corresponding to the optimum value of B in fig. 5.

3. Means are provided to detect a significant increase in the voltage across the storage condenser above its steady value.

Since the value of the time-constant is not very critical at the optimum (see fig. 5), it should be possible to meet the time-constant requirement by having a sequence of pump circuits, fed with the same input pulses and having their time-constants spaced by a suitably small ratio.

Two parameters, say P and M, are needed to describe any given excursion fully, as regards the input signal received by the equipment. Since two parameters are required to describe the input signal, the arrangement of detection circuits must possess two corresponding variables, if it is to respond suitably to all possible inputs (over a range determined by the requirements of the particular task). One of these variables is provided by the choice of the time-constant T, from the range of values provided by the sequence of circuits, to obtain the optimum T for the given P and M. The other variable must be provided by the ability of each circuit to operate satisfactory over a range of input rates or storage condenser voltages. We may express this by saying that each circuit must be able to operate over a range of values of ρT (that is, of N). It should be noted that the optimum value of T is an explicit, mathematically determinable function of P and M, once a value has been specified for K, since the optimum value of B is found from equation (13) as a function of M/K^2, and $T = BP$.

At the optimum condition, we have that

$$B = F\left(\frac{M}{K^2}\right)$$

where F is the function given in fig. 6. It follows that

$$\begin{aligned} N &= MB \\ &= MF\left(\frac{M}{K^2}\right) \\ &= K^2 \frac{M}{K^2} F\left(\frac{M}{K^2}\right) \\ &= K^2 F'\left(\frac{M}{K^2}\right) \qquad \text{say,} \end{aligned}$$

i.e.

$$\frac{N}{K^2} = F'\left(\frac{M}{K^2}\right).$$

We may therefore plot N/K^2 against M/K^2, as shown in fig. 7. It can be seen in fig. 6 that a large increase in M/K^2 is needed to produce a small decrease in X. The corresponding increase in N/K^2, while less, as shown in fig. 7, is also large.

6. Choice of K

K must be chosen so as to make accidental or false alarms so rare as to be negligible. That is, such alarms should only occur through random voltage fluctuations on an average of once in months or years, at most. Table 1 shows how the probability $P(K)$ that a given value of K will be exceeded at any given instant falls off in accordance with a Gaussian distribution, which may be expected when a reasonably large number of pulses is involved, as is the case under all the conditions which will be of interest to us in

practice. If τ is a minimum time for which the chosen value of K must be exceeded to operate the indicating device and ρ_F is the mean rate of false alarms, we have

$$\rho_F \tau < P(K) .$$

That is

$$\rho_F < \frac{P(K)}{\tau} .$$

This inequality follows since all time intervals with output levels above K which operate the indicator must exceed τ in their duration. Moreover, any other time intervals with output levels above K which do not operate the indicator increase the inequality. τ may be made negligibly small in comparison with the detection time D, in practice.

TABLE I
Probability of a positive deviation exceeding K standard deviations for a Gaussian distribution

K	$P(K)$
1.6	0.5×10^{-1}
3.3	0.5×10^{-3}
4.9	0.5×10^{-6}
6.5	0.5×10^{-10}
8.0	0.6×10^{-15}
10.0	0.8×10^{-23}

If one takes $K = 10$, which is of the right order and should be quite adequate for the shortest reasonable value for τ, $K^2 = 100$ and this enables figs. 6 and 7 to be read directly in terms of M and N.

In practice, it is only possible to make any given circuit operate satisfactory over a finite range of values of ρ or of N. This is mainly because of difficulties arising in the circuit used to indicate a significant increase in voltage. However, it is relatively easy to arrange for a simple circuit to provide a nearly constant value of K over a range of 10 to 1 or more in ρ, with higher values outside that range. We shall now describe such a circuit and investigate its performance.

7. Description of the Proposed Indication Circuit

If a positive voltage from a diode pump circuit of the type shown in fig. 3A is balanced against a negative voltage from a similar circuit of opposite polarity (receiving the same input pulses, reversed in sign, see fig. 3B), the mean voltages will be equal if the values of $R_s C_i V_i$ are the same. If the negative circuit has a suitably longer time-constant, which may be obtained either by means of a larger storage capacity C'_s or by means of a following integrating circuit, as shown, the difference voltage becomes an indication of the variation of the positive output from its mean value. This difference voltage may be applied to a discriminator and at any given steady input pulse rate this discriminator may be biassed to operate if the variation is a positive one of significant value. The storage condenser voltage of a diode pump circuit may be specified conveniently, as we have already seen, by N, the equivalent number of input charges. Unfortunately, from the aspect of simplicity, the discriminator bias required to show a significant variation from a steady mean value of N is $K\sqrt{N/2}$ and it is not possible to provide a really simple circuit which will give this accurately over a wide range of values of N. However, if we increase the relative contribution in the balancing device of the output voltage of the long time-constant circuit, a variable bias proportional to N is obtained, in effect. If this bias is combined with a fixed negative bias, also, the minimum increase in N which will operate the discriminator is then given by

$$\Delta N = \alpha + \beta N$$

where α and β are constants depending on the fixed bias and on the variable bias adjustment, respectively. Such a linear relationship can be made to approximate roughly to the parabola (for constant K)

$$\Delta N = K\sqrt{\frac{N}{2}}$$

over a range of 10 to 1 or more in values of N. In fig. 8, for example, taking

$$K = \Delta N \sqrt{\frac{2}{N}}$$

it is found that K lies between 10 and 11.8 from $N = 100$ to $N = 1000$. In this figure, we have taken the tangent at $N = 312.5$.

$$\Delta N = 62.5 + 0.2N$$

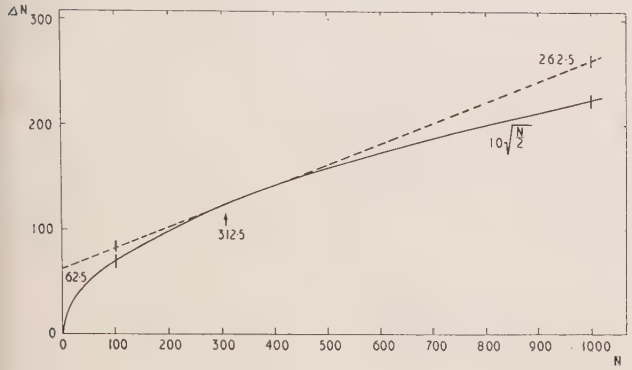

Fig. 8. Approximation to a part of a parabola by a straight line.

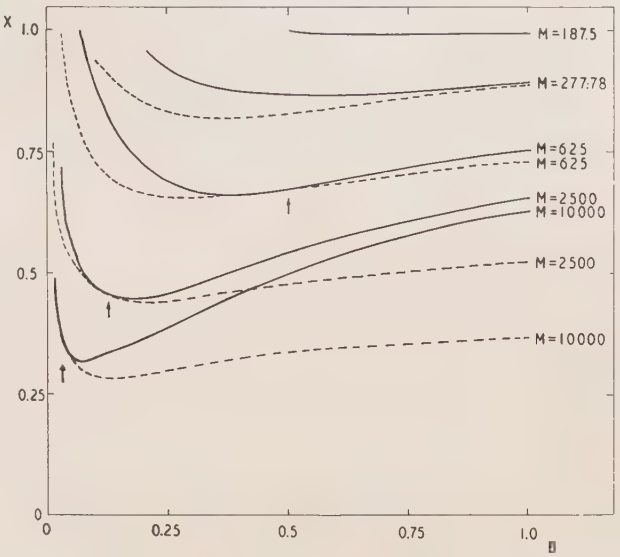

Fig. 9. Determination of the optimum time-constant for a ratemeter circuit with linear bias.

as the straight line approximation to the parabola.

$$\Delta N = 10\sqrt{\frac{N}{2}}.$$

8. Analysis of the Action of the Indication Circuit

It now remains to investigate how the performance of such a circuit would vary from the theoretical optimum for a fixed value of K. This may be done quite simply from fig. 4, again. It is only necessary to substitute for equation (13)

$$\frac{B}{B+1}\,e^{-X/B} + \frac{1}{B+1}\,e^{X} = 1 + \frac{\alpha}{N} + \beta$$

$$= 1 + \beta + \frac{\alpha}{BM}. \qquad (14)$$

Fig. 9, which corresponds to fig. 5 in the previous case, may then be drawn immediately, for any given values of α and β. The values taken here are $\alpha = 62.5$ and $\beta = 0.2$. The corresponding curves for a fixed K of 10, derived from fig. 5, are shown by dotted lines, for comparison. The curves for the linear bias approximation case show broad minima only slightly higher than those for the exact square root law case (dotted lines). From the position of the tangent in fig. 8 at $N = 312.5$, it is to be expected that each pair of curves will agree at a value of B to make $N = 312.5$. This is indicated by a small vertical arrow under each point of osculation.

Fig. 10, which corresponds to fig. 6 in the previous case, shows the minimum value of X as a function of M. The values for this curve were

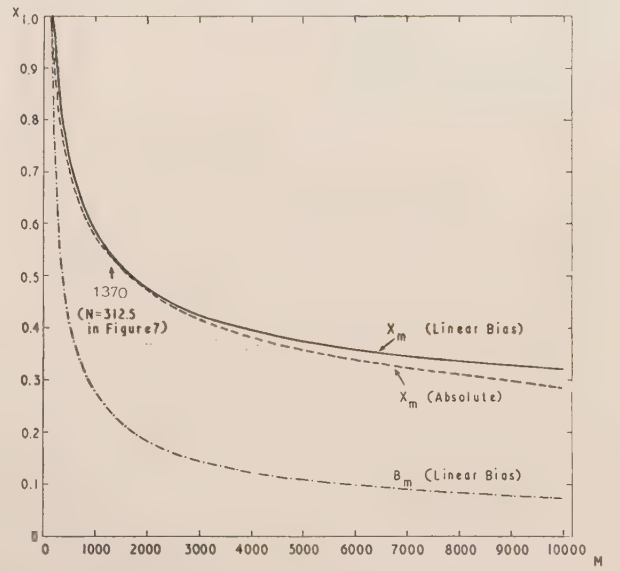

Fig. 10. Graph showing the minimum value of X for the linear bias case as a function of M.

computed numerically. The dotted line shows, for comparison, the absolute optimum function for $K = 10$. (The value of B at the minimum in

the linear bias case is also shown.) It will be seen that over a wide range of values of M, from about 200 to 10000, the minimum value of X obtainable with the linear approximation bias is of the same order as that obtainable with the exact

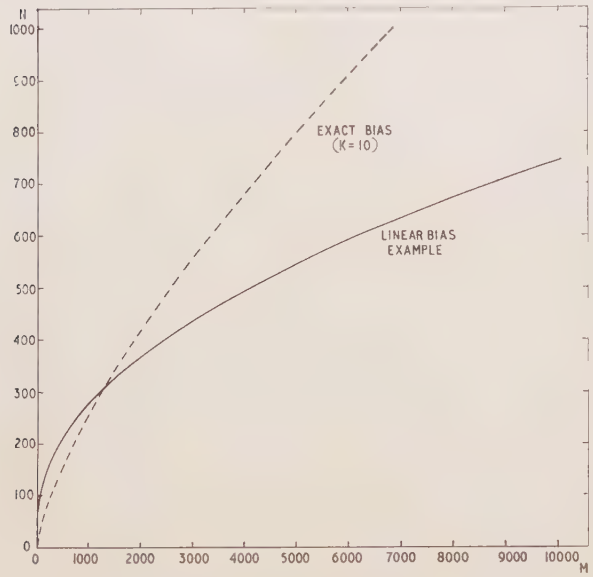

Fig. 11. The relationship between N and M in the linear bias ratemeter circuit described, at the optimum condition.

square root law bias for $K = 10$ and is little above the absolute optimum value. The values for the whole of this range lie under 1.5 $(K^2/M)^{\frac{1}{3}}$, which is slightly greater than the approximation (for large M/K^2) in the optimum case. Moreover, since the minima in the linear approximation case are still reasonably broad, there need not be a great further increase because B is only selected from a set of discrete values in practice. (These correspond to the time-constants T of the sequence of circuits used and the nearest value may be somewhat off the optimum, depending on how closely the values of T are spaced.)

The optimum value of N in this case is a function of M only (for given α and β, that is). Fig. 11 shows this relationship for the values of α and β already stated. The dotted curve is obtained by putting $K = 10$ in the relationship given in fig. 7, for the previous case, and it will be seen that the values of N for the higher values of M are distinctly lower in the linear bias example.

9. High and Low Values of M

The calculated performance shown in fig. 10 is very satisfactory, but for completeness it is also necessary to determine limits for the performance outside the range shown, that is, for $M < 200$ and for $M > 10000$. The following two rules are useful in this connection.

RULE 1

The value of X at its minimum always decreases for an increase in M.

RULE 2

The value of ρD at the minimum always decreases for a decrease in M.

These rules may be proved as follows.

Proof of Rule 1

Consider two circuits A and B exposed to excursions with the same period P, the value of ρ and therefore of $M = \rho P$ being higher in the case B. Let the time-constant T_A of circuit A be chosen to give optimum conditions and let the time-constant T_B of circuit B be chosen so that

$$\rho_B T_B = N = \rho_A T_A .$$

Then, since $\rho_B > \rho_A$, we have $T_B < T_A$. It follows from reference to equation (11) and fig. 4 that the voltage rise in circuit B must be faster than the voltage rise in circuit A. Since the values of N and therefore the bias conditions are the same in the two cases, it follows that $D_B < D_A$. Since P is the same in both cases, this shows that $X_B < X_A$. Now the optimum response for the excursion applied to B must be faster still (or, at worst, the same). We have therefore shown that the optimum value of X for a given value of M is always a decreasing function of M, as would be expected.

Proof of Rule 2

Consider two circuits A and B exposed to excursions with the same initial mean rate ρ, the value of P and therefore of M being lower in case B. Let the time-constant T_A be chosen to give optimum conditions and let the time-constant T_B be the same. Simply from the fact that the

input to circuit B will be greater at all relevant times, because of the shorter period of the excursion applied to it, it follows that the voltage rise in that circuit must be the faster. Since the values of N and therefore the bias conditions are the same for the two circuits, we have that $D_B < D_A$. Since $\rho_B = \rho_A$, this gives $\rho_B D_B < \rho_A D_A$. Moreover, the optimum response to the excursion applied to circuit B must be faster still (or, at worst, the same). We have therefore shown that the optimum value of ρD for a given value of M is an increasing function of M.

APPLICATION OF THESE RULES

Both these rules apply to the ratemeter type of circuit with any biassing arrangement in which the bias is some specified function of N. They therefore apply for both the exact square root law bias case and the linear approximation case. Referring to the latter case, and to fig. 10, we see that for all $M > 10000$ we have $X < 0.32$. From fig. 11, this corresponds to $N > 744$ at optimum. Also, for all $M < 200$ ($N < 147$ at optimum), since

$$\rho D \equiv X\rho P \equiv XM$$

$$\rho D < 0.964 \times 200 .$$

That is,

$$\rho D = XM < 193 .$$

This tells us that for $M < 200$, X lies under a hyperbolic curve passing through the point $M = 200$, $X = 0.964$ in fig. 10. It also tells us that D is then less than the time required to count 193 pulses at the initial rate. In using this inequality, we effectively set a lower limit ($N = 147$) to the number of pulses which are involved and therefore to the degree of departure from an Gaussian distribution which may be expected. We may now summarise the results for the particular linear approximation bias which we have taken for $K = 10$ as follows (table 2). Note also that for $M << \alpha$ we have $X \to \log_e \alpha/M$. That is, the first 63 pulses, approximately, in the excursion then give warning at optimum.

10. Effect of Random Fluctuations on Time of Response

The random fluctuations which will be superimposed on any actual rising input to a diode pump circuit will inevitably affect the time that the voltage output takes to reach the triggering level, and may either increase or decrease this time. Such fluctuations will usually affect the effective triggering level by about 1 part in K and the delay D correspondingly (for example, $\pm 10\%$ for $K = 10$). This variation is, of course, inherent in the nature of the signal being received. It means, in effect, that owing to the random fluctuation, the increase in the input pulse rate from the detector has not precisely followed the general increase in flux level. No possible modification to the circuit following the detector could alter this. The variation is quite a small one and should not normally be so great as to be of much importance in the practical application of the circuit to the detection of

TABLE 2
Performance of the ratemeter type of circuit with the particular linear bias approximation chosen

Condition (M)	Performance (D)	Performance (X)
$M < 200$	$D < \frac{200}{\rho}$	$X < \frac{200}{M}$
$200 < M < 10000$	$D < 1.5 \left(\frac{100}{M}\right)^{\frac{1}{3}} P$	$X < 1.5 \left(\frac{100}{M}\right)^{\frac{1}{3}}$
$M > 10000$	$D < 0.32P$	$X < 0.32$

excursions. For experimental tests of the theory of operation of the circuit, it may be necessary to take the mean of a number of readings under each set of conditions, in order to reduce errors due to this variation.

11. Practical Considerations

11.1 CIRCUIT ARRANGEMENTS

The necessary input pulses for the diode pump circuits may be obtained from a flip-flop, which is triggered by the original pulses from the neutron detector. This flip-flop determines the amplitude and duration of the pulses and should have a sufficiently small deadtime, probably of the order of a few microseconds, to ensure that the loss of pulses from this cause is not too serious, even at the highest pulse rates involved. Equal pulses of opposite sign may be obtained from an invertor stage and both trains of pulses may be fed to the diode pump circuits from low impedance outputs.

The positive and negative diode pump circuits of each pair may be identical, apart from polarity, if the necessary time-constant for the negative-output circuit is obtained by means of an integrating circuit, as shown in fig. 3B. Moreover, the pairs of circuits need only differ from each other in the values of the leakage resistor R_s used. In this case, the charge and voltage increments per pulse are the same for all the circuits. The biassing arrangements can then be the same for every pair of circuits and any pair of circuits performs exactly the same as any other pair, in theory, provided that the initial input pulse rate considered is varied in inverse proportion to the time-constant of the circuit and the time-scale of the excursion considered is varied in direct proportion to it. That is to say, the successive pairs of circuits differ only in their time-scale.

11.2. SPACING OF TIME-CONSTANTS

The circuit that responds first will normally be the one having the time-constant T which gives with the initial count-rate ρ the value of $N = \rho T$ which is nearest to the optimum for the value of M in the excursion concerned (see fig. 11). This is the same as taking the time-constant T that corresponds to the value of B nearest to the minimum in the appropriate curve of fig. 9. Since the minima of the curves in this latter figure are fairly broad, it is not necessary to have very closely spaced values of T to ensure that the nearest actual delay is reasonably close to the minimum delay. For example, one might take spacings by a factor of $\sqrt{10}$. If one applies this to the curve for $M = 2500$ in fig. 9, one finds that in the worst case X would be increased to about 0.475 from its minimum value of 0.446, an increase of 6.5%, which would not be too serious.

11.3. BALANCING CIRCUIT TIME-CONSTANT

The time-constant used in the balancing circuit should be chosen to have a value intermediate between the maximum excursion period to be detected by this method and and the minimum period required in controlled changes of power level. For example, if these were 10 s and 100 s, respectively, this time-constant might be 30 s. There would be some decrease in the speed of response for the slowest undesired excursions, due to partial following by the balancing circuit. There would also be some decrease in the margin of protection against false alarms due to random variations, for the fastest controlled changes in power level, due to incomplete following of the mean level by the balancing circuit. However, neither of these effects would be too serious, provided that there was a reasonable margin between the maximum period requiring recognition for alarm purposes and the minimum desired period of controlled variations.

One would normally use a fairly high resistance in the integrating circuit, to obtain the desired time-constant without using an unduly large capacitor. For example, one might use 30 MΩ for R_t' and 1 μF for C_t'. To give a typical range of T from 10 ms to 10 s, with C_s at 1 μF also, one would require values of R_s (7 values at $\sqrt{10}$ spacing) ranging from 10 kΩ to 10 MΩ. It is clear that the loading effect of the integrating circuit would be negligible on all these circuits except possibly one or two at the highest time-constant end, where it might cause a small

modification of performance. The circuit used for adding the positive and negative output voltages and the bias voltage must be suitable for the relatively high output impedance of the integrating circuit, if this is used.

11.4. EFFECT OF SATURATION

The circuits which we have proposed are basically simple ones and their performance is correspondingly amenable to calculation. It is necessary to bear in mind that as the output voltage V_s of a diode pump circuit increases the increments of voltage per pulse decrease in proportion to $V_i - V_s$. So far, no consideration has been given to this effect. To achieve a performance close to that given in table 2, it is necessary that this effect should not be too serious at the maximum value of $N + \Delta N$ concerned, which is 955 at $M = 10000$. From the definition of N given in equation (10), we have

$$\frac{V_s}{V_i} = N \frac{C_i}{C_s}.$$

If the value of C_i is 100 pF and the value of C_s is 1 μF, this makes V_s less than 10% of V_i at $N = 955$. This would not cause a serious departure from the performance stated in table 2. It would be possible to reduce the change in the voltage increment even further by the use of a somewhat more complicated pumping circuit specially designed for this purpose.

11.5. RANGE OF OUTPUT VOLTAGES

It is not desirable to use too small a value of C_i, as this capacitor then acts as a capacity voltage divider with the diode pump circuit stray input capacity and the effective input pulse voltage is reduced accordingly. This effective pulse voltage determines the saturation output voltage, which equals it. We have seen above that the range of values of N of interest in the particular example taken is about $N = 150$ to 750. If C_i and C_s have the values of 100 pF and 1 μF, respectively, as suggested above, and $V_i = 200$ V, this gives a working range of V_s of 3 V to 15 V, and a corresponding range of bias voltages of 1.85 V to 4.25 V, which is quite suitable for the sensitive discriminators now available, even allowing for some attenuation in the adding circuit. It does not follow that it would be necessary to use a separate discriminator for each pair of diode pump circuits, as it might be possible to connect the outputs from several such pairs to a common discriminator via suitable diodes.

11.6. CONDITIONS AT EXTREMES OF THE RANGE FOR EACH CIRCUIT

Since the speed of performance specified in table 2 is to be obtained from circuits functioning with values of N between 150 and 750, in every case, our main concern with values of N outside that range is that they should not give rise to any false alarms. For the lower values of N, it is clear from fig. 8 that the value of K for this circuit increases very rapidly as N decreases, so that the probability of a false alarm arising at the lower values of N is negligible, even although one may not be able to assume the Gaussian distribution, which was taken for higher values of N, when $N < 150$.

For the highest values, $N > 750$, since the effect of saturation is always to reduce the voltage increments and therefore the output voltage below the values specified in our theory and since K increases also as N increases, the chances of false alarms in this region are even less than in the working region and therefore negligible. Provision must be made, of course, for other less sensitive devices to come into operation or for other detectors at points of lower neutron density to be brought into use, when the operating flux level required is beyond the range of the shortest time-constant circuits (which saturate at the highest input rates). This is normal practice. At higher input rates, there is no longer any fundamental difficulty in obtaining rapid recognition of short period excursions.

11.7. RELIABILITY

The type of circuit described has the advantage that if the diode pump circuit which should give the first warning of a particular excursion

has failed, its duty will be taken over by a neighbouring one requiring only a slightly longer time to act. Moreover, the whole assembly should be sufficiently simple to be built into a moderately sized unit and used in duplicate or triplicate as might be required by the safety policy for the reactor concerned.

11.8. PRELIMINARY EXPERIMENTAL RESULTS

It is not intended to describe experimental work in any detail in this paper. However, it may be stated that circuits of the type described were built and tested against an electronic pulse generator which was capable of giving randomly timed pulses at a steady mean pulse rate and also of producing exponential excursions in pulse rate on demand. Precautions were taken to isolate the discriminator from mains-borne or other electrical disturbances which might trigger it spuriously. Results have been obtained in satisfactory accordance with the theory and have confirmed that the circuits can respond in a fraction of an excursion period.

12. Conclusions

There are no fundamental electronic difficulties in closely approaching the limit of what is statistically possible in the rapid recognition of excursions in the mean rate of pulses occurring at random, at least over a wide range of potentially useful conditions. In view of this and of the demand which now exists for the very rapid detection of excursions in reactors and critical assemblies, in order to ensure the utmost safety, it seems desirable that the performance of equipment used at present for this purpose should be evaluated in terms of the optimum described above. Equipment based on the method described above might then be considered useful to supplement or replace present types of equipment in some cases.

A difficulty which might arise in some cases would be the existence of any significant local changes in the neutron flux at the detector in the reactor which were not caused by excursions in the total reactor power. Such changes might be caused, for example, by thermal effects due to irregular flow of a coolant being circulated by pumps. The electronic equipment would obviously indicate any significant increase in neutron flux, whatever the cause. Nevertheless, although some difficulties might have to be overcome in its application, the method described appears to be sufficiently promising to warrant further investigation.

Acknowledgements

The author wishes to thank Mr. F. J. Birkin, of this establishment, who carried out all the more laborious numerical work with a digital computer, and Messrs. R. J. Lamden and W. G. Gore, also of this establishment, who have carried out preliminary experimental work on equipment designed in accordance with the above principles.

NUCLEAR INSTRUMENTS AND METHODS 9 (1960) 195–198; NORTH-HOLLAND PUBLISHING CO.

ON RESOLUTION AND LUMINOSITY OF A NEUTRON DIFFRACTION SPECTROMETER FOR SINGLE CRYSTAL ANALYSIS

G. CAGLIOTI, A. PAOLETTI, and F. P. RICCI

Comitato Nazionale per le Ricerche Nucleari, Divisione Studi e Ricerche, Roma, Italy

Received 5 August 1960

In this paper some criteria for the choice of the collimators for a crystal spectrometer for neutron diffraction are established in order to achieve a good compromise between luminosity and resolution.

General expressions for the full width at half maximum and for the luminosity of the diffraction peaks are developed for single crystal samples.

1. Introduction

Owing to the increasing interest in single crystal neutron diffraction work, it seemed useful to establish some criteria for the choice of suitable collimators for a crystal spectrometer to be used with single crystal samples, in order to obtain a good compromise between luminosity and resolution.

In a previous paper[1]) we have already discussed the case of a *powder* sample. In this paper we extend the treatment to the case of a *single crystal* sample.

2. Derivation of the Full Width at Half Maximum and of the Luminosity of the Diffraction Peaks; Single Crystal Sample

We shall use the same formalism as in ref.[1]). A list of symbols will be found at the end of this paper.

Furthermore, we shall assume that both the monochromating crystal and the single crystal sample are actually made of mosaic blocks oriented in a gaussian distribution. The full widths at half maximum are indicated with β_1 and β_2 respectively.

We shall again make the approximation that the i-th collimator reduces the intensity of the incident neutron beam by a gaussian factor in the arguments $2(\ln 2)^{\frac{1}{2}}\,\phi_1/\alpha_1$, $2(\ln 2)^{\frac{1}{2}}\,\phi_2/\alpha_2$ and $2(\ln 2)^{\frac{1}{2}}\,(\rho - \phi_3/\alpha_3)$. But since the size of single crystal samples is usually much smaller than the size of powder samples, we must point out that the above gaussian approximation seems to be not so good, in the present case, when the width of the single crystal sample is smaller than the horizontal width of any Soller element.

As in ref.[1]) we will neglect the effect of the vertical angular divergence and of the total reflection by the walls of the Soller elements†.

Let θ_0 be the Bragg angle for a central ray ($\phi_1 = 0$; $\eta_1 = 0$) and let θ be the Bragg angle for any individual ray. A neutron of wavelength in the range $(\lambda, \lambda + \mathrm{d}\lambda)$ will be associated to a value of $\theta - \theta_0$ in the range $(\delta, \delta + \mathrm{d}\delta)$. Such a neutron will follow the path indicated in fig. 1 defined by the following equations:

$$\phi_1 = 2\delta - \phi_2 \tag{1}$$

$$\eta_1 = \phi_2 - \delta \tag{2}$$

$$\eta_2 = a\delta - \Phi_2 - \tfrac{1}{2}\rho \tag{3}$$

$$\phi_3 = 2a\delta - \phi_2 \tag{4}$$

$$a = \frac{(\mathrm{d}\lambda/\mathrm{d}\theta)\ \text{monochromating crystal}}{(\mathrm{d}\lambda/\mathrm{d}\theta)\ \text{sample}} = \frac{d\cos\theta}{d_{\mathrm{B}}\cos\theta_{\mathrm{B0}}}. \tag{5}$$

The probability $I(\rho)\mathrm{d}\rho$ for the neutron we considered reaching the BF_3 detector whose axis

[1]) G. Caglioti, A. Paoletti and F. P. Ricci, Nucl. Instr. 3 (1958) 223.

†) For the effect of the total reflection see P. Szabò, Nucl. Instr. and Meth. 6 (1960) 183.

makes an angle in the range $(\rho, \rho + d\rho)$ with the direction $2\theta_{B_0}$ is given by

$$I(\rho)\, d\rho = H\, d\rho \int_{-\infty}^{+\infty} d\phi_2 \int_{-\infty}^{+\infty} d\delta \exp - \left[\left(\frac{\phi_1}{\alpha'_1}\right)^2 + \left(\frac{\eta_1}{\beta'_1}\right)^2 + \left(\frac{\phi_2}{\alpha'_2}\right)^2 + \left(\frac{\eta_2}{\beta'_2}\right)^2 + \left(\frac{\rho - \phi_3}{\alpha'_3}\right)^2\right] \tag{6}$$

where H is a constant, $\alpha'_i = \alpha_i/2(\ln 2)^{\frac{1}{2}}$ and $\beta'_j = \beta_j/2(\ln 2)^{\frac{1}{2}}$; $(i = 1, 2, 3)$; $(j = 1, 2)$.

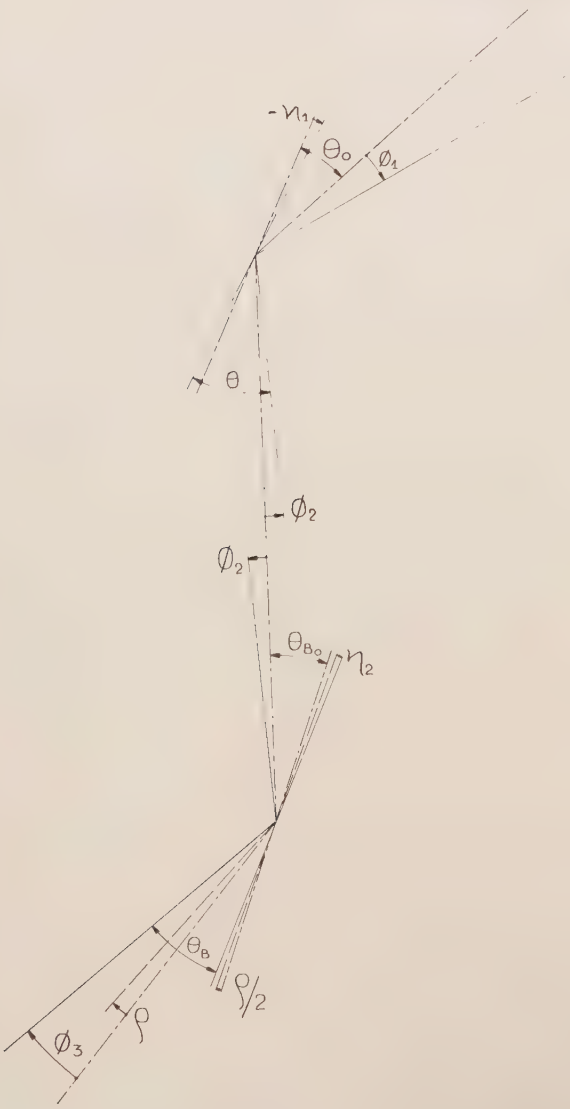

Fig. 1. — · — · — Path of a central ray ($\phi_1 = 0$, $\eta_1 = 0$). ———— Path of any individual ray, with the sample crystal rotated of an angle $\varrho/2$.

Taking into account equations (1)–(4) we obtain from (6) after long but elementary algebra:

$$I(\rho)\, d\rho = H\, d\rho \frac{\pi\alpha_1\alpha_2\alpha_3\beta_1\beta_2}{A_{\frac{1}{2}}} \exp - \frac{(4 \ln 2)\, \rho^2}{A_{\frac{1}{2}}^2} \tag{7}$$

where the full width at half maximum of the diffraction peak is:

$$A_{\frac{1}{2}} = \left\{ \frac{\alpha_3^2\beta_2^2(4\beta_1^2 + \alpha_1^2 + \alpha_2^2) + \alpha_2^2(4\beta_1^2 + \alpha_1^2)(\beta_2^2 + \alpha_3^2) - 2a\alpha_2^2(\alpha_1^2 + 2\beta_1^2)(\alpha_3^2 + 2\beta_2^2) + (4\beta_2^2 + \alpha_3^2)(\beta_1^2 + \frac{1}{4}\alpha_1^2 + \frac{1}{4}\alpha_2^2) + \frac{1}{4}\alpha_2^2(4\beta_1^2 + \alpha_1^2)}{a^2[(\alpha_1^2\alpha_2^2 + \alpha_1^2\beta_1^2 + \alpha_2^2\beta_1^2)(\alpha_3^2 + 4\beta_2^2) + \alpha_1^2\alpha_2^2\beta_1^2]} \right\}^{\frac{1}{2}} \cdot \tag{8}$$

By integration of (7) with respect to ρ we obtain for the luminosity (expressed in arbitrary unit)

$$L = \frac{\alpha_1\alpha_2\alpha_3\beta_1\beta_2}{[(4\beta_2^2 + \alpha_3^2)(\beta_1^2 + \frac{1}{4}\alpha_1^2 + \frac{1}{4}\alpha_2^2) + \frac{1}{4}\alpha_2^2(4\beta_1^2 + \alpha_1^2)]^{\frac{1}{2}}} \cdot \tag{9}$$

In table 1 we report a short selection of $A_{\frac{1}{2}}$ and L values obtained from (8) and (9) for several cases of practical interest.

3. Conclusions

With reference to equations (8) and (9), and to their analogous (11) and (12) of reference[1]), we may state that, in the case of a single crystal sample:

1. The luminosity is not any more a symmetrical function of α_1 and α_2. It may still be considered practically symmetrical if α_1^2, (and α_2^2) are smaller than $4\beta_2^2 + \alpha_3^2$ (cf. the selections $(\beta_1, \beta_2, \alpha_1, \alpha_2, \alpha_3) = (20, 3, 10, 20, 30)$ and $(20, 3, 20, 10, 30)$ in table 1) and/or if α_1 (and α_2) are larger than $2\beta_1$. Furthermore, the luminosity is roughly dependent in a linear way on α_3 when $\alpha_3 \ll 2\beta_2$ [cf. (20, 60, 30, 30, 30), (20, 60, 30, 30, 60) and (20, 60, 30, 30, 120)) and very slowly dependent on α_3 when $\alpha_3 > 2\beta_2$ (cf. (20, 15, 20, 20, 60) and (20, 15, 20, 20, 120)].

As far as the luminosity is concerned it seems therefore convenient to choose $\alpha_3 > 2\beta_2$.

2. The function $A_{\frac{1}{2}}^2$ is a sum of three quantities: the first, which is independent on a, gives the largest contribution to $A_{\frac{1}{2}}^2$ for small values

TABLE 1
Selection of full widths at half maximum and luminosities computed according to (8) and (9).

β_1 (min. arc)	β_2 (min. arc)	α_1 (min. arc)	α_2 (min. arc)	α_3 (min. arc)	$A_{\frac{1}{2}}(a \to 0)$ (min. arc)	$A_{\frac{1}{2}}(a = 1.5)$ (min. arc)	$A_{\frac{1}{2}}(a = 3)$ (min. arc)	$L \times 10^{-2}$
20	3	10	10	10	14	15	31	1.9
		10	20	30	31	16	35	4.4
		10	20	60	35	17	36	5.0
		20	10	30	19	27	56	4.9
		20	10	60	20	27	56	5.1
		20	20	30	31	28	60	8.2
		20	20	60	35	28	61	9.3
		30	20	10	19	36	76	6.1
20	15	10	10	10	13.9	18.0	36	4.3
		10	20	30	33	26	45	17
		10	20	60	41	31	46	23
		20	10	30	25	34	61	18
		20	10	60	32	38	62	23
		20	20	30	33	35	68	32
		20	20	60	41	38	68	42
		20	20	120	47	40	68	47
		20	30	60	50	38	73	56
		30	20	10	20	40	87	19
		30	20	60	42	45	87	58
		30	20	120	46	46	87	63
		30	30	30	39	43	94	56
		30	30	60	51	45	94	77
		30	30	120	57	46	95	88
		30	60	30	48	44	105	72
		30	60	60	66	46	108	107
		30	60	120	77	46	110	128
		60	20	10	21	56	115	26
		60	60	20	41	63	147	58
		60	60	30	51	63	152	110
		60	60	60	73	63	162	169
		60	60	120	89	64	171	209
20	60	30	30	30	39	52	109	88
		30	30	60	61	68	115	162
		30	30	120	93	93	129	259
		30	60	30	48	59	135	129
		30	60	60	69	72	138	238
		30	60	120	102	94	147	382
		60	20	10	22	59	127	32
		60	60	20	48	84	202	150
		60	60	30	54	86	203	209
		60	60	60	75	94	203	390
		60	60	120	108	109	206	628

of a. The third term, which is important in broadening the diffraction peaks for large values of a, is a practically symmetrical increasing function of α_1 and α_2, so that it seems convenient to use values of α_1 and α_2 approximately equal. Furthermore, since $A_{\frac{1}{2}}{}^2$ is practically independent of α_3 for any a as long as $\alpha_3 \gg 2\beta_2$, it is convenient to fix $\alpha_3 > 2\beta_2$. On the other hand, because of the interest of keeping $A_{\frac{1}{2}}$ small when a increases, it is suitable to have α_1 and α_2 smaller than α_3 [cf. (20, 15, 30, 30, 120) and (20, 15, 60, 60, 20)].

The variety of possible experimental situations is so large that it is difficult to make a

general and complete discussion of equations (8) and (9). We only like to add that, in order to obtain a good resolution in the range of interest, the value $a = d \cos\theta / d_B \cos\theta_B$ should lay in the neighborhood of the one which minimizes $A_{\frac{1}{2}}$, i.e.

$$(a) A_{\frac{1}{2}} = \text{minimum}$$

$$= \frac{\alpha_2^2 (\alpha_1^2 + 2\beta_1^2)(\alpha_3^2 + 2\beta_2^2)}{(\alpha_1^2\alpha_2^2 + \alpha_1^2\beta_1^2 + \alpha_2^2\beta_1^2)(\alpha_3^2 + 4\beta_2^2) + \alpha_1^2\alpha_2^2\beta_1^2} \quad (10)$$

In other words[2]) it is convenient to use a value of $d \cos\theta$ for which the a value is as close as possible to (10).

Symbols

α_i $(i = 1,2,3)$ horizontal angular divergence of the i-th collimator, i.e. ratio of the width s_i to the length l_i of its Soller elements.

β_j $(j = 1,2)$ full width at half maximum of the gaussian distribution of the projections of the normal to the reflecting planes of any mosaic block of the crystal upon a horizontal plane. $j = 1,2$ refers to the monochromator and sample respectively.

η_j $(j = 1,2)$ angular displacement from the average of the projection of the normal to the reflecting planes of any block upon a horizontal plane. The sign of η_j is chosen so the Bragg angle would be increased when η_j is positive.

ρ angle between the axis of the BF_3 detector and the direction $2\theta_{B_0}$ for which the diffracted intensity has a maximum.

ϕ_1, ϕ_2, $\rho - \phi_3$ angles made by the projection on a horizontal plane of any individual ray with centerline of the i-th collimator $(i = 1,2,3)$.

[2]) See also B.T.M. Willis, AERE Rep. 3104/Oct. 1959.

NUCLEAR INSTRUMENTS AND METHODS 9 (1960) 199–211; NORTH-HOLLAND PUBLISHING CO.

A HIGH TEMPERATURE SPUTTERING ION SOURCE FOR A LABORATORY ISOTOPE SEPARATOR†

W. L. RAUTENBACH

Nuclear Physics Division, National Physical Research Laboratory, Council for Scientific and Industrial Research, Pretoria, South Africa

Received 17 August 1960

The general principles governing the operation of a high temperature sputtering ion source are discussed and a technical description of the ion source is given. Special attention has been given to discharge characteristics, ion currents in the sputtered metals, realisation of selfsputtering, efficiency in sputtered material and the average time spent by sputtered atoms on the walls of the discharge chamber. Possible uses for this type of ion source are discussed briefly.

1. Introduction

One of the main problems encountered in electromagnetic isotope separation is to find suitable ion sources for solid charge material. Several types of ion sources are described in the literature, e.g. gas discharge ion sources with heated discharge chambers and ovens[1]), surface ionization ion sources[2]) and a sputtering ion source for metals of very low vapour pressure[3]).

For the work planned with the isotope separator at Pretoria[4]) a special ion source is required and for this reason a "high temperature sputtering ion source" has been developed. It employs a gas discharge in a discharge chamber maintained at high temperature to avoid condensation of metallic charge material[1]). The charge material is vaporised by cathode sputtering[3]) from a cooled electrode.

In this paper the isotope separator is considered as an analysing instrument used to evaluate the performance of the ion source. Information about the isotope separator is given elsewhere[4,5]).

2. General Considerations

Consider a discharge chamber which is vapour tight except for the outlet of area B_0. A cooled sputtering electrode of the metal to be sputtered, with total area B, is introduced into the discharge chamber and bombarded by ions from the discharge. The sputtered atoms are prevented from condensing permanently on the walls of the discharge chamber by maintaining it at a sufficiently high temperature T. A vapour of n_s sputtered atoms per cc is thereby formed in the discharge chamber and the atoms of this vapour are ionized by the discharge.

Under equilibrium conditions sputtered atoms are lost from the vapour by escaping as neutrals and ions through the outlet of the ion source and by recondensing on the cooled sputtering electrode. If the rate of evaporation from the sputtering electrode is sufficiently low and assuming that the condensation coefficient of metal on its own substrate is ≈ 1[6]), the following balance equation is obtained for the sputtered material:

$$\frac{SJ}{e} = n_s \left[\frac{kT}{2\pi M_s}\right]^{\frac{1}{2}} B + n_s \left[\frac{kT}{2\pi M_s}\right]^{\frac{1}{2}} B_0 + \frac{I_s}{e}, \quad (1)$$

† This paper describes part of the work submitted in partial fulfilment of the requirement for the degree of Doctor of Science at the Potchefstroom University for C.H.E., Potchefstroom, South Africa.

[1]) See for instance: K. O. Nielsen, Nucl. Instr. **1** (1957) 289.

[2]) See for instance: R. H. Dawton in "Electromagnetically Enriched Isotopes and Mass Spectrometry", edited by M. L. Smith, (Butterworths Scientific Publications, London, 1956); Chapter 5.

[3]) J. Druaux and R. Bernas in [2]), Chapter 4.

[4]) W. E. Frahn, W. L. Rautenbach and L. E. Wåhlin, Nucl. Instr. and Meth. **7** (1960) 253.

[5]) W. L. Rautenbach, thesis, Potchefstroom (1959).

[6]) G. Wessel, Zeitschrift für Physik **130** (1951) 539.

where S is the sputtering efficiency in atoms per incident ion,

J the ion current to the sputtering electrode,

e the charge of an ion,

M_s the mass of a sputtered atom,

I_s the ion current of the sputtered material through the outlet and

k Boltzmann's constant.

$$P_s = \frac{[2\pi M_s kT]^{\frac{1}{2}}}{e} Sj \,. \tag{6}$$

At a constant temperature of $T = 773°K$ and an atomic wieght of 100 for the sputtered material

$$P_s \approx 5 \times 10^{-5} \times Sj \text{ mm Hg} \,, \tag{7}$$

where j is given in mA/cm². Thus P_s depends only on the sputtering efficiency and the density of the sputtering ion current.

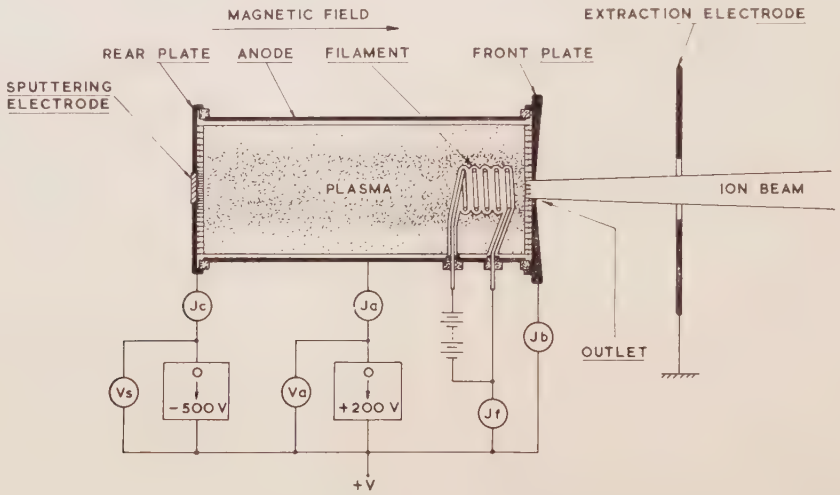

Fig. 1. Diagram of the discharge chamber.

The efficiency η_s of the ion source for the sputtered material is given by:

$$\eta_s = \frac{(I_s/e)}{I_s/e + n_s \left[\frac{kT}{2\pi M_s}\right]^{\frac{1}{2}} B_0} \times 100\% \,. \tag{2}$$

For the best gas discharge ion sources $\eta \leqslant 20\%$[7]), which implies that:

$$n_s \left[\frac{kT}{2\pi M_s}\right]^{\frac{1}{2}} B_0 >> \frac{I_s}{e} \,. \tag{3}$$

Combination of eq. (3) and (1) yields:

$$n_s = \left[\frac{2\pi M_s}{kT}\right]^{\frac{1}{2}} \frac{B}{B + B_0} \frac{Sj}{e} \,, \tag{4}$$

where $j = J/B$ is the average density of the ion current on the sputtering electrode.

If $B >> B_0$

$$n_s = \left[\frac{2\pi M_s}{kT}\right]^{\frac{1}{2}} \frac{Sj}{e} \,. \tag{5}$$

The partial pressure P_s in sputtered material is therefore given by:

Sputtering efficiencies of ~ 1 can be obtained for a number of metals at ion energies in the region of a few hundred electron volts[8]). Ion current densities of ~ 1 mA/cm² can be obtained by immersing the sputtering electrode as a negative probe into the plasma of the discharge. At $S = 1$ and $j = 1$ we obtain from eq. (7)

$$P_s \approx 5 \times 10^{-5} \text{ mm Hg} \,. \tag{8}$$

Stable discharge conditions can only be obtained if the pressure in the discharge chamber is higher than a minimum value P_{min}[9]). If

[7]) See for instance J. Koch in "Electromagnetic Isotope Separators and Applications of Electromagnetically Enriched Isotopes", edited by J. Koch, (North Holland Publishing Company, Amsterdam, 1958), Chapter 4.

[8]) G. K. Wehner, Phys. Rev. **108** (1957) 35.

[9]) D. Bohm in "The Characteristics of Electrical Discharges in Magnetic Fields", edited by A. Guthrie and R. K. Wakerling (McGraw-Hill, New York, 1949), Chapter 4.

$P_s < P_{min}$ after the discharge has been started by introducing a carrier gas, a partial pressure P_g must be maintained in the carrier gas so that

$$P_s + P_g \geq P_{min} . \quad (9)$$

The relative yield in sputtered material, R_s, is defined by:

$$R_s = \frac{I_s}{I_g} \propto \frac{P_s}{P_g} \quad (10)$$

where I_g is the ion current in ions of the carrier gas through the outlet of the ion source. For a high relative yield, P_{min} should be as low as possible, which is also the requirement for high efficiency[10]). Furthermore the partial pressure in the sputtered material should be high implying large values of S and j, i.e. a high negative voltage on the sputtering electrode[11]) and a plasma of high density in the discharge chamber.

The "Finkelstein" discharge[12]) is best suited to our requirements. It has a low minimum pressure[10]), well known discharge characteristics[10]) and is used extensively on laboratory isotope separators[1,13,14,15]). In the sputtering ion source the filament is placed near to the outlet of the discharge chamber (fig. 1). At pressures above P_{min} a plasma is formed by the primary electrons which oscillate between the the front and rear plates due to the collimating effect of the axial magnetic field. The plasma is at a potential of a few tens of volts negative with respect to the anode[16]) and ion currents will flow across space charge sheats to the filament as well as to the front and rear plates. The ions arriving at the rear plate will have an energy corresponding to the potential difference between plasma and rear plate. The rear plate acts as a negative plane probe with respect to the plasma. Increasing the negative potential of this plate will therefore increase the thickness of the space charge sheath while the ion current to this plate will remain constant and reflection of primary electrons will take place as usual. Due to the collimating effect of the magnetic field the plasma is expected to have a maximum density in the vicinity of the axis of the discharge chamber. This will lead to a high ion current density j to the central region of the rear plate which is replaced by the metal to be sputtered.

Therefore, apart from the introduction of sputtered atoms into the discharge region the sputtering voltage should not affect the discharge conditions of the ion source, which should be similar to those obtained for the conventional ion source with the filament at the rear of the chamber[10]).

3. Technical Description of the Ion Source

In order to achieve high efficiency a vapour tight discharge chamber 110 mm in length is used[10]). It is thermally insulated from the ion source housing by mounting it as a unit on three thin stainless steel rods (fig. 2), and is surrounded by magnet coil in a brass container supplying a maximum magnetic field of 500 gauss.

The discharge chamber (fig. 3), with stainless steel anode and front and rear plates, is maintained at high temperature by means of a filament of 0.5 mm tungsten wire mounted near to the outlet and a 1.0 mm molybdenum heating element around the rear of the anode. The ends of the filament are clamped in 1.0 mm molybdenum wires[1]) fixed to stainless steel blocks. These blocks rest only on the circumferance of the pyrophyllite insulator in order to shield the upper surface of the insulator from tungsten evaporated from the filament. In this way good insulation between filament and anode is insured. Heat shields between the discharge and the front and rear plates, as well as one around the anode serve to increase the temperature of the discharge region. Heat dissipated by the filament, anode heater and magnet is removed by circulating paraffin oil through cooling jackets.

Gas is introduced into the discharge chamber

[10]) O. Almén and K. O. Nielsen, Nucl. Instr. **1** (1957) 302.
[11]) G. K. Wehner in "Advances in Electronics and Electron Physics", Vol. 7 (Academic Press, New York, 1955), p. 265–271.
[12]) A. T. Finkelstein, Rev. Sci. Instr. **11** (1940) 94.
[13]) J. O. Burgman and G. Andersson, Nucl. Instr. **3** (1958) 33.
[14]) O. Almén, G. Bruce and A. Lundén, Nucl. Instr. **2** (1958) 249.
[15]) T. Alväger and J. Uhler, Arkiv för Fysik **13** (1958) 145.
[16]) J. Kistemaker and J. Snieder, Physica **19** (1953) 950.

through a stainless steel tube insulated from the rear plate. The metal to be sputtered is melted into a depression in a copper sputtering electrode. The surface of the metal is turned in a lathe to obtain a smooth flat surface. This surface lies in the same plane as the rear heat shield and is separated from it by a gap of 0.25 mm for thermal insulation. A stainless steel cone centres the sputtering electrode and forms a long path for heat conduction from the rear plate to the sputtering electrode. The sputtering electrode is cooled by connecting it to a paraffin cooled copper rod by means of a copper heat conductor. Its temperature can be changed by

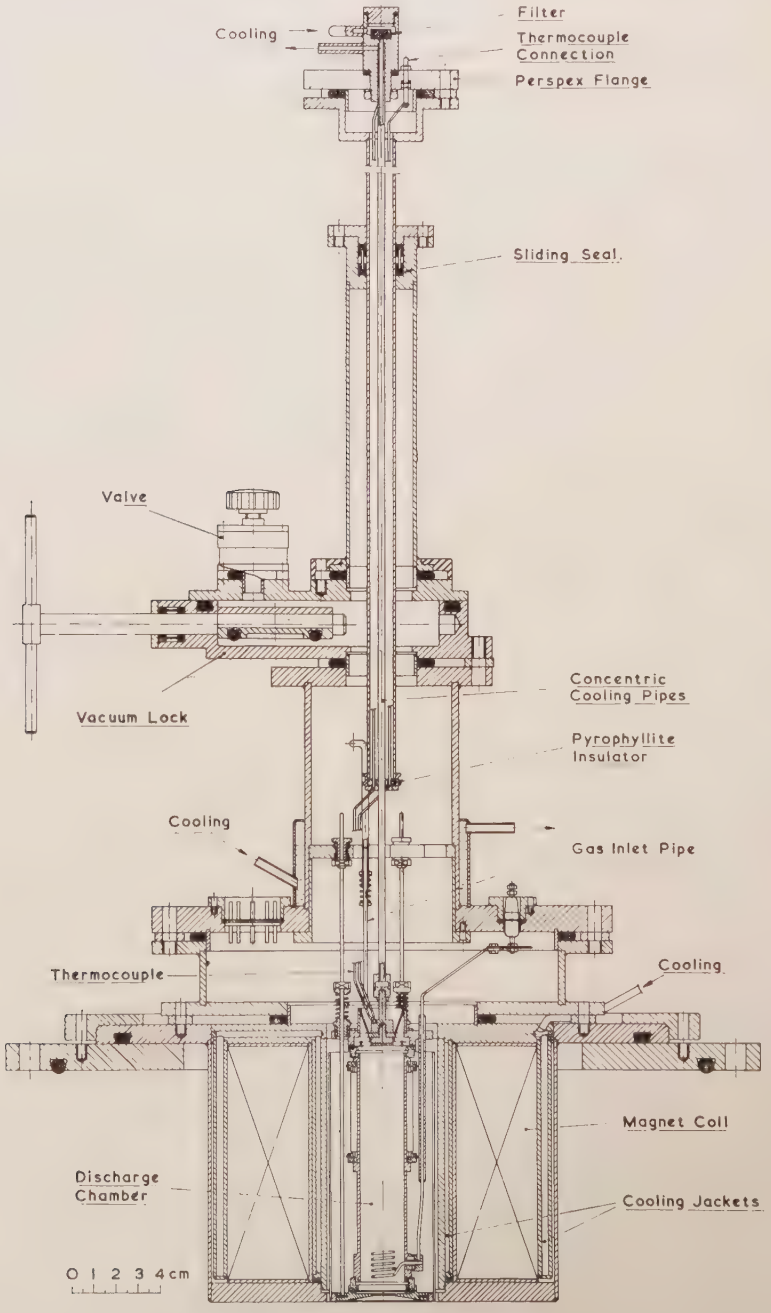

Fig. 2. The ion source housing with the discharge chamber in position.

altering the cross section and length of the heat conductor. A thermocouple, connected to the end of the heat conductor, gives an indication of the temperature of the metal to be sputtered. By using a vacuum lock the sputtering electrode can be withdrawn and interchanged without breaking the main vacuum.

4. Operating Conditions

4.1. COMPARISON WITH CONVENTIONAL ION SOURCE

When this ion source is operated as a gas ion source the considerations advanced in Section 2 show that its characteristics should be similar to that of the conventional ion source. To test this

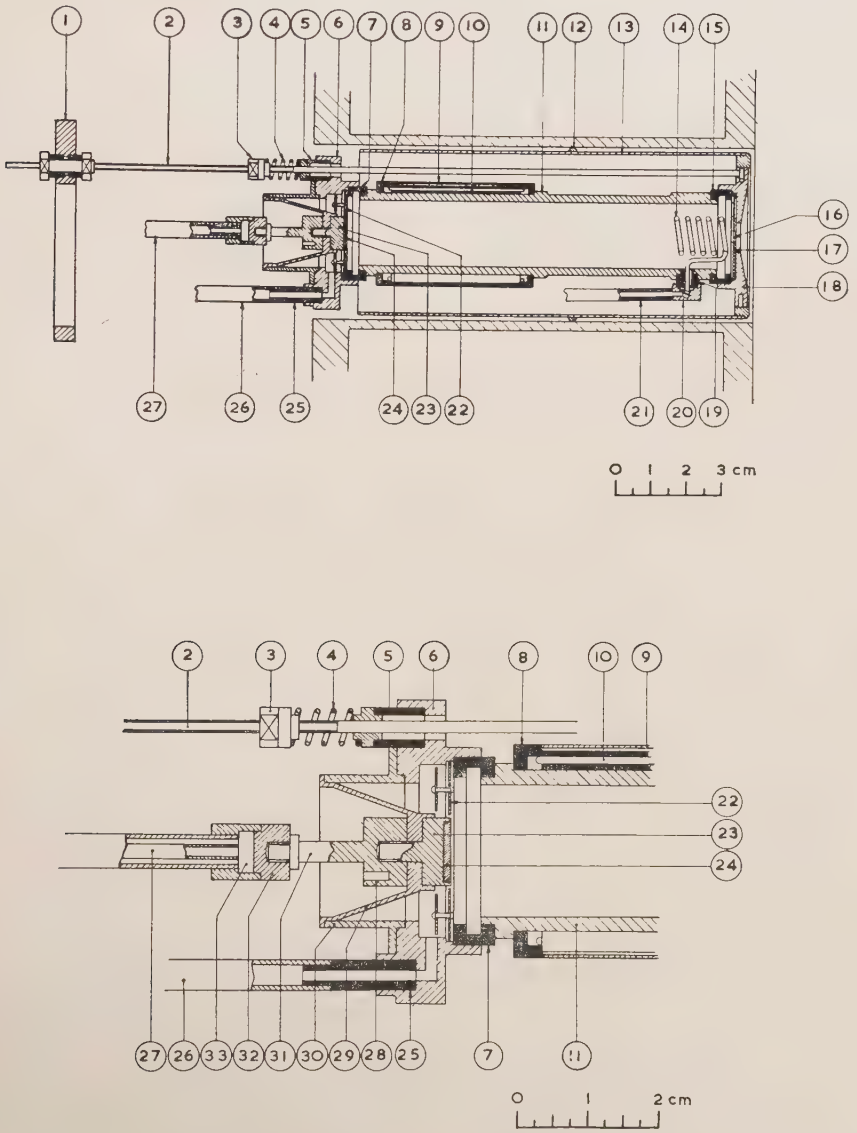

Fig. 3. Discharge chamber: (1) Mounting ring, (2) Mounting rods, (3) Nut, (4) Compression spring, (5) Insulator, (6) Rear plate, (7) Insulating ring, (8) Insulating ring for mounting anode heater, (9) Heat shield, (10) Anode heating element, (11) Anode, (12) Centring lugs, (13) Heat shield, (14) Filament, (15) Insulator, (16) Outlet, 3.5 mm in diameter (17) Front heat shield, (18) Front plate, (19) Filament insulator, (20) Filament connecting block, (21) Filament lead, (22) Rear heat shield, (23) Sputtering electrode, (24) Metal to be sputtered, (25) Gas inlet insulator, (26) Gas inlet pipe, (27) Concentric cooling pipes, (28) Hole for thermocouple, (29) Centring cone for sputtering electrode, (30) Centring cylinder, (31) Heat conductor, (32) Cooled copper block, (33) Cooling cavity.

a stainless steel sputtering electrode is used in order to have a negligible pressure in sputtered material.

Fig. 4 gives the resolving power "RP" for krypton as a function of pressure in the discharge chamber at constant acceleration voltage and extracted ion current. Changing the sputtering voltage from 0 to — 500 volts does not affect the RP.

An experimental setup[5]) is employed to measure the currents to the different electrodes of the discharge chamber at constant acceleration voltage and extracted ion current. The dependence of these parameters on krypton

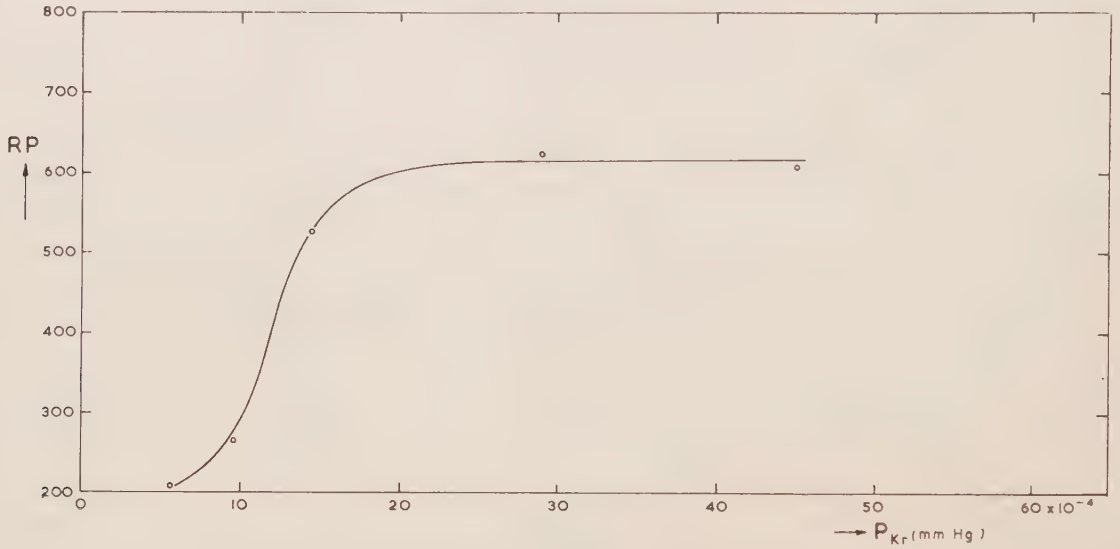

Fig. 4. Resolving power, RP, for krypton as a function of the pressure.

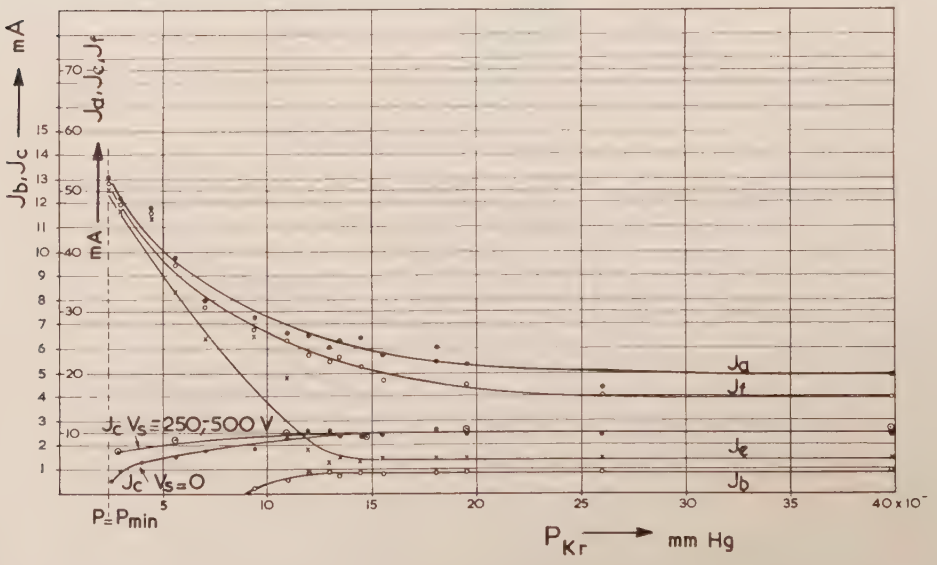

Fig. 5. Discharge characteristics for the ion source as a function of the krypton pressure at a constant extracted ion current of 60 μA, an acceleration voltage of 30 kV and an acceleration distance of 30 mm. (The magnetic field is 350 gauss, anode voltage 150 volts, J_c is the current to the rear plate at sputtering voltages of $V_s = 0$, — 250 and — 500 volts, J_b the current to the front plate, J_e the electron emission current from the filament, J_f the total current to the filament and J_a the anode current.)

pressure is given in fig. 5. Changing the sputtering voltage does not affect the discharge conditions with the exception of the total ion current to the rear heat shield and sputtering electrode external plasma surface with the minimum corresponding to the transition region[5]). Similar results are obtained for a conventional ion source.

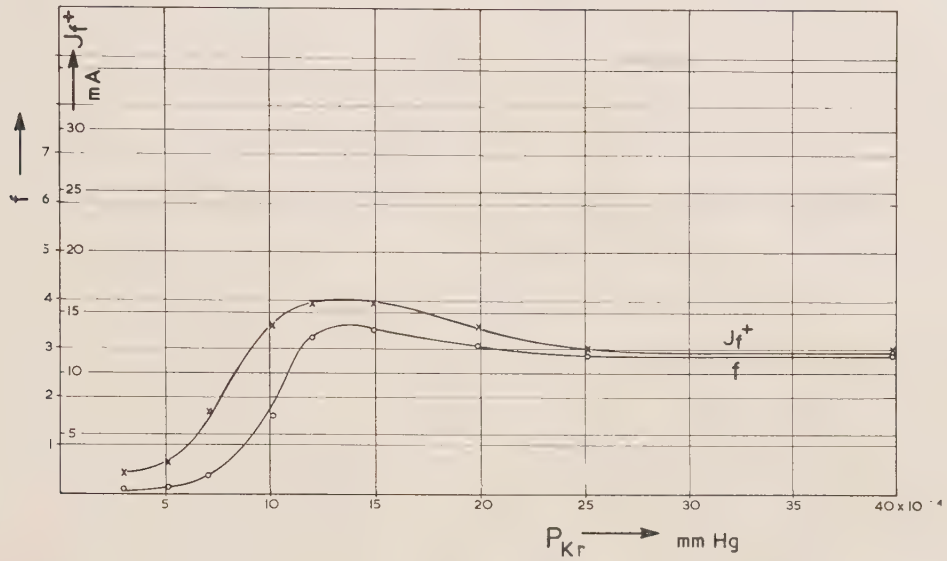

Fig. 6. The average number of ionizations per primary electron, f, and the ion current to the filament, J^+_f, as functions of the krypton pressure.

at low operating pressure. In fig. 6 the average number of ions produced per primary electron, $f = (J_a - J_e)/J_e$, and the ion current to the filament, $J^+_f = J_f - J_e$, are given as functions of the krypton pressure.

The ion sources have similar characteristics in the high pressure region where the discharge characteristics are independent of the pressure. In the low pressure region the conventional discharge chamber gives a constant "RP" up to P_{min} and no maximum in f or J^+_f is found. The differences between the ion sources are probably due to "hash", i.e. instabilities in the discharge at low pressure due to the proximity of the filament to the outlet.

Fig. 7 shows the dependence of the resolving power RP on the extracted ion current when the ion source is operated in the high pressure region of the discharge. The acceleration voltage is 40 kV and the distance between outlet and extraction electrode vary between 20 and 150 mm. The first maximum in RP for each curve occurs at an internal plasma surface and the second at

4.2. OPERATION AS A HIGH TEMPERATURE SPUTTERING ION SOURCE

4.2.1. *General Conditions of Operation*

The temperature at the centre of the anode is 750° C at 500 watts dissipated by filament and anode heater. The temperatures of the front and rear heat shields are expected to be in the vicinity of 600° C. Thus, in order to obtain high relative yield (see Sec. 2) only metals with vapour pressures in excess of 1×10^{-4} mm. Hg at 600° C are sputtered.

Sputtering electrodes of 10 mm diameter are used because measurements indicate that 75 % of the ion current to the rear of the discharge chamber is incident of such an electrode. This ensures a high value of j. The outlet diameter is 3.5 mm so that $B \gg B_0$.

Sputtering electrodes of bismuth, lead, antimony, cadmium, zinc and selenium have been prepared. Due to the vapour pressures and melting points of these elements a heat conductor which maintains the sputtering electrode at $\sim$ 130° C is used.

Heavy incident ions yield higher values of S than light ions[11]) and xenon is therefore used as carrier gas.

Under usual sputtering conditions the total ion current to the rear heat shield and sputtering electrode vary between 1 and 10 mA and the

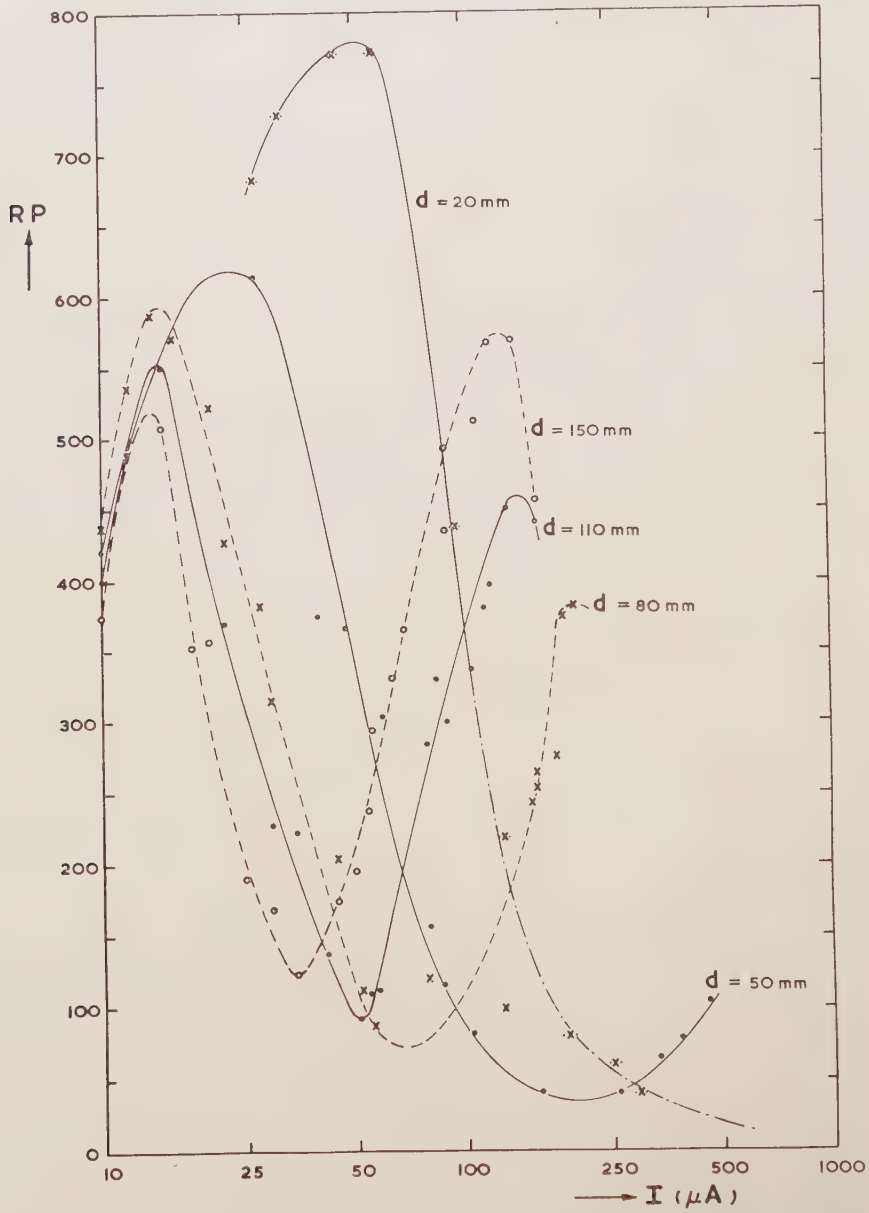

Fig. 7. The resolving power, RP, as a function of the extracted krypton ion current.

Ion currents in all the abovementioned elements with the exception of selenium are obtained under sputtering conditions. No loss in weight of a Se sputtering electrode is observed after sputtering for an hour and it appears that Se cannot be sputtered[17]).

amount of material removed from a sputtering electrode per hour lies between 1 and 10 mg while the ion currents in sputtered material are 1 to 100 μA at the collector of the isotope

[17]) E. Blechsmidt, Annalen der Physik **81** (1926) 999.
[18]) L. E. Wåhlin, Nucl. Instr. and Meth. **7** (1960) 269.

separator. At a maximum sputtering voltage of — 500 volts the relative yield is usually larger than one.

Fig. 8 shows the mass spectrum of lead determined at the collector of the isotope separator[18]). The resolving power under sputtering conditions is similar to that obtained in sec. 4.1.

After sputtering for a few minutes the Pb, Cd and Zn sputtering electrodes emerge with peculiar black surface layers while the Bi surface appears light grey and the Sb surface remains

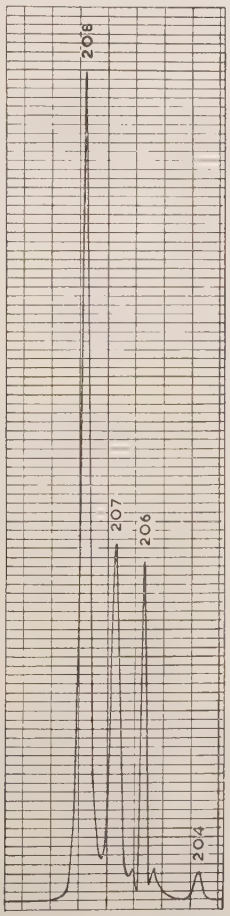

Fig. 8.
The mass spectrum of lead employing xenon as the carrier gas.

bright. The black surface layers appear grey when viewed at small angles. These layers are not caused by impurities in the Xe because similar results are obtained if Pb is sputtered under Cd or selfsputtered (see sec. 4.2.3). When a Pb electrode is maintained at a temperature near to its melting point the sputtering electrode emerges with bright patches and a larger amount of lead is removed by sputtering. The probable explanation of these effects is that submicroscopic cones, which inhibit sputtering, are formed under the combined action of sputtering and recondensation[11,17,19]).

4.2.2. *Yield and Relative Yield in Sputtered Material*

The yield is defined as the extracted ion current of the sputtered material, I_s, whereas the relative yield R_s is defined by eq. (10). In order to obtain optimum operating conditions for the ion source it is necessary to determine the dependence of yield and relative yield on the xenon pressure P_{Xe} and on the sputtering voltage V_s.

In fig. 9 the yields in Cd^+ and Xe^+ ions are shown versus P_{Xe} for different sputtering voltages at constant extracted ion current. These results have been obtained at high resolving power, i.e. at the high pressure region of the discharge. The ion currents in Cd^+ and Xe^+ ions are measured on a collector at the exit of the magnetic field[5]). These results are used to obtain the relative yield in Cd^+ as a function of sputtering voltage at constant P_{Xe} (fig. 10), as well as the dependence of relative yield on P_{Xe} at constant sputtering voltage (fig. 11).

It follows from figs. 9, 10 and 11 that both the yield and the relative yield for Cd^+ ions increase with increasing sputtering voltage and decreasing xenon pressure. This tendency is expected theoretically: An extension of eq. (10) yields

$$R_{Cd} \propto \frac{\sigma_{Cd}}{\sigma_{Xe}} \frac{n_{Cd}}{n_{Xe}} \qquad (11)$$

where σ_{Xe} and σ_{Cd} are the effective ionization cross sections for xenon and cadmium atoms respectively. At constant anode voltage σ_{Cd}/σ_{Xe} will be constant and at constant temperature $P_{Xe} \propto n_{Xe}$. According to eq. (5) $n_{Cd} \propto Sj$ and equation (11) is transformed into

$$R_{Cd} \propto \frac{Sj}{P_{Xe}}. \qquad (12)$$

[19]) A. Guentherschulze and W. Tolmien, Zeitschrift für Physik **119** (1942) 685.

The Xe and Cd ions will have nearly the same space charge effects in the ion beam owing to the slight difference in mass. Changing the relative yield will, therefore, not effect the form of the beam or that of the plasma emitting surface at constant extracted ion current[20]). Thus, according to the results of fig. 5 the total ion current to the rear of the discharge chamber will remain constant. If "j" is taken as constant in eq. (12) and the distribution of ion current to the rear heat shield and sputtering electrode is assumed to remain constant, we get

$$R_{Cd} \propto \frac{S}{P_{Xe}}. \tag{13}$$

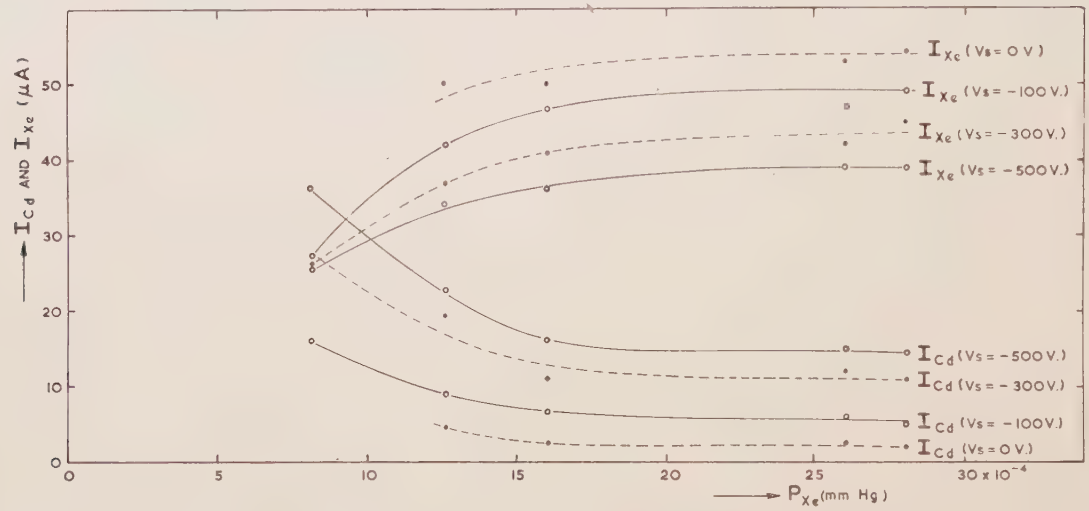

Fig. 9. The ion currents in Cd^+ and Xe^+ ions as functions of xenon pressure at different values of the sputtering voltage V_s.

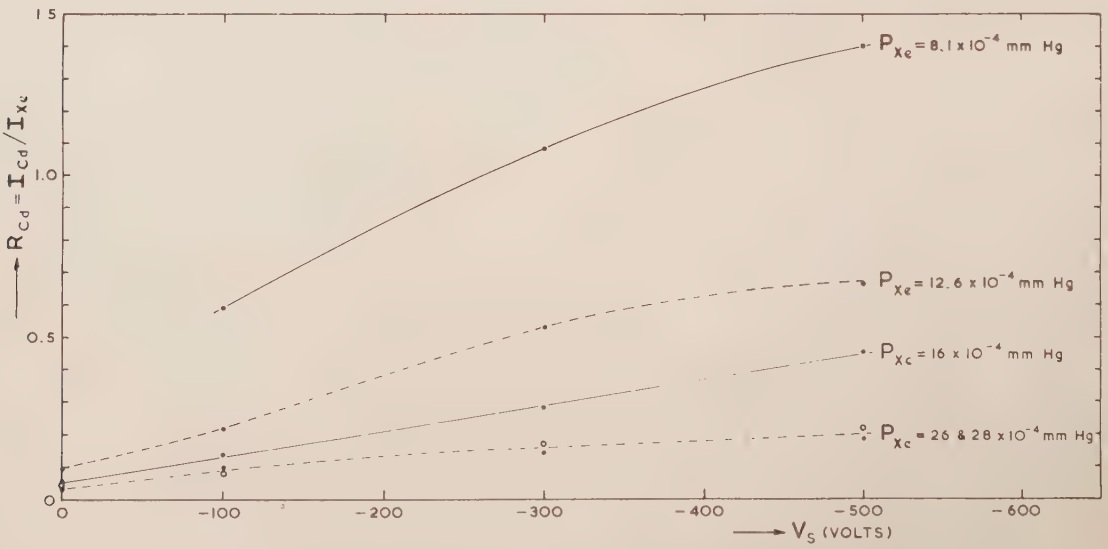

Fig. 10. The relative yield, R_{Cd}, for cadmium as a function of sputtering voltages V_s.

The sputtering efficiency S is nearly proportional to the sputtering voltage V_s[11]), and therefore

$$R_{Cd} \propto \frac{V_s}{P_{Xe}}. \tag{14}$$

[20]) See [10]), eq. (2).

Equation (14) is in good agreement with fig. 10. The agreement with fig. 11 is not as good, probably because of the fact that the effect of contamination in the xenon on the sputtering efficiency[11]), will change with changing xenon pressure.

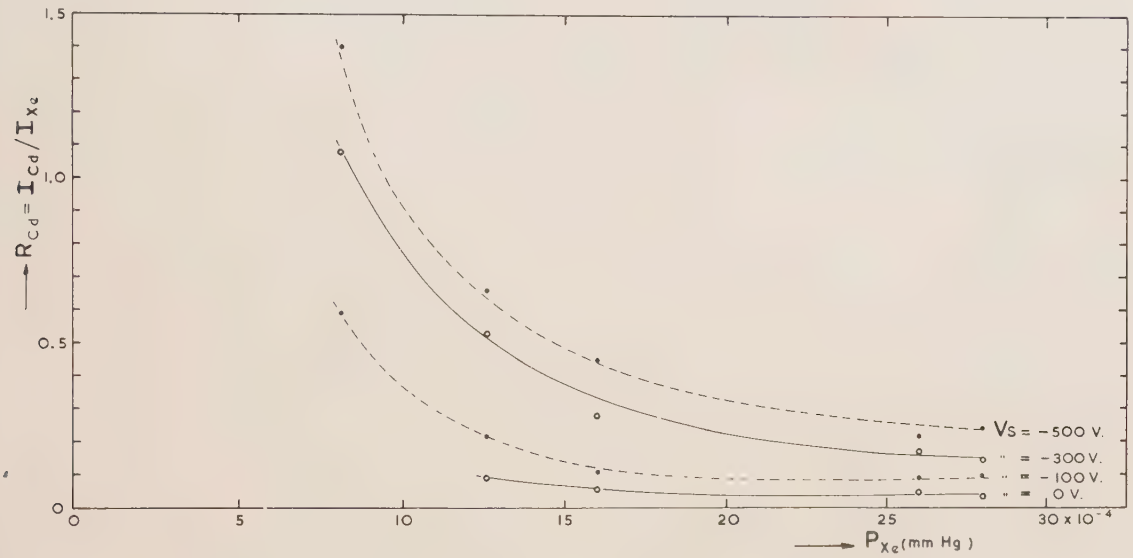

Fig. 11. The relative yield, R_{Cd}, as a function of xenon pressure.

A tentative conclusion can be drawn from fig. 10. The different curves differ only in gradient due to the different values of P_{Xe}. At high relative yield the sputtering electrode will be bombarded mainly by Cd^+ ions while at low relative yield the Xe^+ ions will predominate. In the case where cadmium is sputtered by Cd^+ ions the sputtering efficiency S in eq. (1) should be replaced by $(S_{Cd-Cd} - \beta)$, where S_{Cd-Cd} gives the number of atoms removed per incident cadmium ion and β is the probability that an incident ion may condense on its own substrate. The similarity of the curves in fig. 10 shows that

$$S_{Xe-Cd} \approx (S_{Cd-Cd} - \beta) , \qquad (15)$$

where S_{Xe-Cd} is the sputtering efficiency for cadmium by xenon ions. Because of the slight mass difference between Cd and Xe ions one expects $S_{Xe-Cd} \approx S_{Cd-Cd}$ with the result that β must be small. This will be the case if the incident ion is reflected as a neutral after colliding with the surface of the sputtering electrode.

The previous result is of general importance for if $\beta \approx 1$, then sputtering of a metal by its own ions will cause a loss in sputtered material from the discharge if the sputtering efficiency is below 1. This will cause a drop in the relative yield at low xenon pressure instead of the observed rise (fig. 11).

4.2.3. *Selfsputtering*

According to eq. (7) the partial pressure in sputtered material is given by

$$P_s \propto Sj . \qquad (16)$$

If this pressure is higher than the minimum pressure P_{min} the discharge will not be extinguished if the pressure in the carrier gas is reduced to zero provided the sputtering rate of the metal by its own ions is sufficient to maintain P_s above P_{min}. Usually P_s will lie in the low pressure region of the discharge. The following argument shows that the discharge will automatically change into the high pressure region when selfsputtering occurs. According to fig. 6 a slight increase in the pressure in the discharge chamber will cause f to rise, thereby increasing the rate of ion production fJ_e (fJ_e is the primary electron current). This in turn will increase j, thereby giving rise to a still higher value of P_s according to eq. (16). This will continue until the high pressure region is reached where the discharge conditions are independent of pressure. The

same argument shows that the discharge will go out if P_s has been originally reduced.

In order to operate the discharge in the high pressure region

$$P_s \geqslant P_k \text{ and } S_{M-M}\, j \geqslant \text{constant}\,, \qquad (17)$$

where P_k is the threshold pressure for operation in the high pressure region and S_{M-M} is the self-sputtering efficiency.

When transition to the high pressure region occurs it is accompanied by an increase in the extracted ion current due to the increase in the ion production rate.

Selfsputtering has been obtained for bismuth and lead. If the sputtering voltage is kept at — 500 volts and the xenon pressure reduced while the filament emission is increased to maintain a constant extracted ion current a point is reached where the anode current and extracted ion current rise suddenly. Once this condition has been obtained the xenon pressure can be reduced to zero without influencing the discharge. Under this condition the extracted ion current is too large to be focussed by the isotope separator due to space charge effects, but the ion current can be reduced by decreasing the filament emission. In the case of lead the discharge goes out at an extracted ion current below 300 μA, which is still too high, but for bismuth ion currents $\sim$ 100 μA can be obtained. For selfsputtering of bismuth only mass lines due to Bi^+ and Bi^{++} ($\sim$12%) are present on the collector. Good resolving power is obtained in this case.

According to eq. (17) the discharge will go out if S_{M-M} is reduced by reducing the sputtering voltage. This is found to be true for lead as well as for bismuth.

Under normal conditions of operation self-sputtering cannot be achieved for cadmium, antimony and zinc but it should in principle be possible if S and j can be increased sufficiently.

4.2.4. *Efficiency for Sputtered Material*

The efficiency is defined as the percentage of sputtered atoms arriving as singly charged ions at the collector of the isotope separator. The ion currents are measured by a collector at the exit of the magnetic field and the loss in weight of the sputtering electrode is determined. The results are given below:

Element	Carrier gas	Efficiency (%)
Pb	Xe	4.1
Cd	Xe	1.7
Bi	Xe	3.5
Bi	Selfsputtered	4.3

The efficiencies obtained are satisfactory, considering that the ion source is operated in the high pressure region and that some sputtered material is lost through the gap between sputtering electrode and rear heat shield.

4.2.5. *The Average Time Spent by a Sputtered Atom in the Discharge Chamber*

The production rate of sputtered atoms can be changed abruptly by changing the sputtering voltage. This is accompanied by a change in sputtered ion current from one equilibrium value to another. The time, τ, taken for the sputtered ion current to change by 90% gives an indication of the average time spent by sputtered atoms on the walls of the discharge chamber between condensation and re-evaporation. "τ" is determined experimentally by registering the ion current in sputtered material as a function of time at the collector of the isotope separator after changing the sputtering voltage suddenly. The mass spectrum is kept in position during the

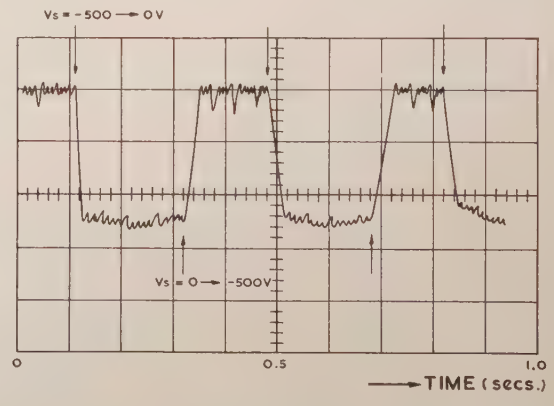

Fig. 12. Oscilloscope trace showing the change in Cd^+ ion current when the sputtering voltage is alternated between 0 and — 500 volts.

measurement by means of pin stabilisation[18]). If the transition occurs in a short time interval a triggered oscilloscope is used. For longer intervals a chart recorder is used. Fig. 12 is a photograph of the oscilloscope screen showing how the Cd^+ ion current changes when the sputtering voltage alternates between 0 and — 500 volts. (The sputtering voltage takes less than 10 milliseconds to change.) The results for different metals are given below:

Element	τ
Cd	0.025 sec
Cd	0.16 sec†
Zn	0.4 sec
Pb	22 sec
Bi	22 sec
Sb	20 min

† For this result, the discharge chamber was heated only by the filament, and it was therefore obtained at a lower temperature than the other results.

The second result for cadmium shows, as expected, that a lower temperature of the discharge chamber is accompanied by a longer time τ[21]).

The general tendency is for elements with higher vapour pressure to have shorter times τ with the exception of Sb which has nearly the same vapour pressure as Pb and Bi but a value of τ nearly 60 times as large. A possible explanation is that Sb tends to evaporate as Sb_2[22]), in fact Sb_2^+ ions are found.

5. Concluding Remarks

This type of ion source has excellent possibilities for the separation of short-lived radio-active isotopes produced on the surface of the cooled sputtering electrode by an external cyclotron beam. A fairly high beam current can be tolerated because the sputtering electrode is directly cooled. This is a definite advantage compared to the high temperature type of ion source where the charge material must be maintained within narrow temperature limits[1]). The surface layers of highest specific activity are continuously removed from the sputtering electrode and ionized in the gas discharge. Under continuous operation an equilibrium amount of short half-life activity builds up at the collector of the isotope separator which can be used as an isotope-pure source for a beta spectrometer connected directly to the isotope separator[4,23]).

The ion source can also be used in conjunction with the isotope separator to study sputtering phenomena especially where sputtering of a metal by its own ions takes place.

The range of elements handled by this ion source can be extended by increasing the temperature of the discharge chamber and by developing a method for the preparation of sputtering electrodes of the alkaline and alkaline earth groups of metals. These metals form intermetallic compounds with copper when melted and do not adhere to steel sputtering electrodes. The best way of preparing sputtering electrodes appears to be the evaporation of the metal into the discharge chamber with the sputtering electrode in position. Condensation will take place on the cooled sputtering electrode forming an oxide free surface for sputtering.

The useful life of the ion source is $\sim$ 10 hours. Operation is usually terminated by a short circuit across the insulation ring between rear plate and anode caused by the formation of a conducting layer. Better shielding of this ring should improve the operation of the ion source.

Acknowledgements

I would like to thank Prof. Dr. W. E. Frahn for his interest in this project and for many stimulating discussions. I am also indebted to Prof. Dr. P. H. Stoker, who despite his many responsibilities, found time to discuss problems. The helpful suggestions of Mr. L. E. Wåhlin are appreciated as well as the co-operation of the technical personnel of this laboratory. My thanks are also due to Mr. G. O'Grady and the workshop personnel for their skilful work.

[21]) L. B. Loeb, "Kinetic Theory of Gases", 2nd edition (McGraw-Hill, New York, 1934), p. 325–348.

[22]) See [11]), p. 258.

[23]) J. Koch in "Electromagnetically Enriched Isotopes and Mass Spectrometry", edited by M. L. Smith. (Butterworths Scientific Publications, London, 1956), Chapter 25.

NUCLEAR INSTRUMENTS AND METHODS 9 (1960) 212–220; NORTH-HOLLAND PUBLISHING CO.

DE LA DECOMPOSITION DES INTENSITES SPECTRALES EN COURBES DE GAUSS

L. G. PREUSS† et J. P. ESCARFAIL

Ecole Polytechnique Fédérale, Zürich

Reçu le 23 Août 1960

The increasing precision of measuring methods such as nuclear spectrography calls for a fast and sensitive method of decomposition into Gaussian curves, particularly if a suspected smaller maximum is smoothed out by a neighbouring band. The resulting asymmetrical intensity curve is then often considered as the sum of two curves described by formula (1) and having a common half-width h. A simple graphical method is proposed which allows one to check whether such a decomposition is significant to a given degree of accuracy. It also gives accurate values for the parameters D_1, D_2, ν_1, ν_2 and h with comparative ease. It follows that—even in the general case—an automatic recording of the logarithmic derivative on which this method is based will allow a more critical insight of any such intensity curve known to better than 1 %, by making full use of the available precision. This in turn strongly suggests the use of a computer coupled to the spectrograph for that purpose.

1. Introduction

La précision constamment croissante des mesures spectrographiques, tant des spectres β et γ que celles de la corrélation $\gamma - \gamma$ ou encore les mesures de spectres d'absorption de sels métalliques en chimie, pour ne citer que celles-là, ne permet plus à l'observateur de tirer le meilleur parti possible des information contenues dans un spectre tel que celui de la figure 1 sans de laborieux calculs. La complexité même de ceux-ci risque d'ailleurs de masquer la distinction entre les erreurs de mesure et celles dues à l'appareil mathématique employé. C'est pourquoi, chaque fois que l'on peut supposer le spectre composé d'une superposition de courbes de Gauss de la forme:

$$y_i = D_i \, e^{-\left(\frac{\nu-\nu_i}{h_i}\right)^2} \qquad (1)$$

il paraît indiqué de le compléter par sa dérivée logarithmique. Celle-ci pourra avec avantage être enrégistrée directement par une machine analogique de conception similaire à celle donnant la dérivée du pH dans certains appareils de titration automatique. La dérivation sera appliquée ici au logarithme de la grandeur mesurée, ce qui n'offre guère de difficultés. Dans la cas simple de bandes nettement séparées, la dérivée sera pratiquement représentée par une suite de droites de pentes $-2/h_i^2$ coupant l'axe des ν en ν_i. Nous allons examiner le cas – assez fréquent – de courbes en cloche plus ou moins déformées dont on a lieu de supposer qu'elles sont dues à la superposition de deux courbes de la forme (1) et d'égales demi-largeurs:

$$y = D_1 \, e^{-\left(\frac{\nu-\nu_1}{h}\right)^2} + D_2 \, e^{-\left(\frac{\nu-\nu_2}{h}\right)^2}. \qquad (2)$$

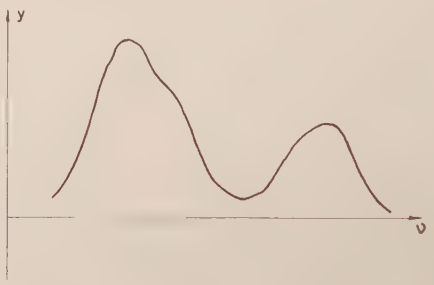

Fig. 1.

Vainhstein *et al.*†† indiquent une méthode pour décomposer une bande dans ces conditions. Celle-ci nous a paru cependant d'un intérêt restreint: en effet toute pseudo-courbe en cloche peut être ainsi décomposée en deux courbes de Gauss. Il manque tout critère permettant de dire si une bande est formée de deux, plusieurs, ou

† Institut für techn. Physik an der ETH.

†† E. E. Vainhstein et I. I. Antipova-Karatäva, Russian Journal of Inorganic Chemistry 4 (1959) 355.

même aucune courbe de Gauss. Nous avons donc cherché une méthode analytique qui permette non seulement de retrouver rapidement les paramètres D_1, D_2, ν_1, ν_2 et h mais encore – ce qui est également important – de vérifier quantitativement si l'hypothèse de composition (2) est justifiée, et ce sans recourir au calcul et à la sommation des courbes composantes obtenues. De plus la méthode proposée utilise tous les points de la courbe expérimentale, ce qui permet une plus grande précision et se prête particulièrement bien à l'utilisation d'une machine analogique couplée à demeure au spectrographe. Enfin la dérivée logarithmique ainsi enrégistrée donne une image générale de l'allure de la courbe: dans le cas de mesures de grande précision (supérieure à 1% p.ex.) elle met en relief les caractéristiques de la bande examinée, même si celle-ci n'est pas composée de la superposition de deux courbes de Gauss de même demi-largeur.

2. Analyse d'une Courbe Composée

Considérons la courbe de la formule (2), courbe formée par la somme de deux courbes en cloche de même demi-largeur h et de maxima D_1 respectivement D_2 aux points d'abscisses ν_1 et ν_2. Nous remplacerons ces quatre dernier paramètres par les nouvelles grandeurs:

$$d = \frac{\ln D_1 + \ln D_2}{2}, \qquad d_0 = \frac{\ln D_1 - \ln D_2}{2}$$

$$\nu_0 = \frac{\nu_1 + \nu_2}{2}, \qquad \bar{\nu}_0 = \frac{\nu_2 - \nu_1}{2}$$

et introduisons comme nouvelle variable:

$$\bar{\nu} = \nu - \nu_0 .$$

Dans ces conditions l'on vérifie facilement que l'équation (2) peut s'écrire:

$$y = e^{\left(-\frac{\bar{\nu}^2 + \bar{\nu}_0^2}{h^2} + d\right)} \left[e^{\left(2\frac{\bar{\nu}\bar{\nu}_0}{h^2} - d_0\right)} + e^{-\left(2\frac{\bar{\nu}\bar{\nu}_0}{h^2} - d_0\right)} \right] \quad (2')$$

ou:

$$y = e^{-\frac{\bar{\nu}^2 + \bar{\nu}_0^2}{h^2} + d} \cdot 2 \operatorname{ch}\left(2\frac{\bar{\nu}\bar{\nu}_0}{h^2} - d_0\right)$$

dont la dérivée logarithmique devient:

$$Y' = \frac{dy}{d\bar{\nu}} \frac{d\bar{\nu}}{d\nu} \frac{1}{y} = -\frac{2\bar{\nu}}{h^2} + \frac{2\bar{\nu}_0}{h^2} \cdot \operatorname{th}\left(2\frac{\bar{\nu}\bar{\nu}_0}{h^2} - d_0\right). \quad (3)$$

Cette dernière est donc la somme d'une droite de pente $-2/h^2$ et d'une tangente hyperbolique. Elle est symétrique par rapport au point C de coordonnées $\bar{\nu}_c$, Y'_c:

$$\bar{\nu}_c = d_0 \frac{h^2}{2\bar{\nu}_0}, \qquad Y_c' = -\frac{d_0}{\bar{\nu}_0} = -\frac{2\bar{\nu}_c}{h^2}$$

que nous appellerons son centre. En effet l'expression

$$Y' - Y'_c = -\frac{2(\bar{\nu} - \bar{\nu}_c)}{h^2} + \frac{2\bar{\nu}_0}{h^2} \operatorname{th}\frac{2\bar{\nu}_0}{h^2}(\bar{\nu} - \nu_c) \quad (3')$$

est bien une fonction impaire de $(\bar{\nu} - \bar{\nu}_c)$.

La courbe Y' admet évidemment comme asymptotes les droites:

$$(m_1): \quad Y' = -\frac{2}{h^2}(\bar{\nu} + |\bar{\nu}_0|) \text{ pour } \bar{\nu} \to -\infty \quad (4)$$

$$(m_2): \quad Y' = -\frac{2}{h^2}(\bar{\nu} - |\bar{\nu}_0|) \text{ pour } \bar{\nu} \to +\infty . \quad (5)$$

Nous désignerons encore par (m) leur médiane:

$$(m): \quad Y' = -\frac{2}{h^2}\bar{\nu} \quad (6)$$

par (t) la tangente à Y' en son centre C qui est également point d'inflexion:

$$(t): \quad Y' = -\frac{2}{h^2}\bar{\nu} + \left(\frac{2\bar{\nu}_0}{h^2}\right)^2 (\bar{\nu} - \bar{\nu}_c) \quad (7)$$

et par (z) et (x) les parallèles aux axes par le point C:

$$(z) \qquad \bar{\nu} = \bar{\nu}_c$$

$$(x): \quad Y' = Y'_c . \quad (8)$$

Il nous est maintenant possible de définir les points et grandeurs caractéristiques suivants:

A_1, A_2 et A sont les points de rencontre de l'axe des ν avec les asymptotes (m_1) (m_2) et leur médiane (m).

D'après (4) et (5) leurs abscisses sont:

$$\bar{\nu}(A_1) = -|\bar{\nu}_0| \qquad \bar{\nu}(A_2) = +|\bar{\nu}_0| \qquad \bar{\nu}(A) = 0$$

ou encore:

$$\nu(A_1) = \nu_1 \qquad \nu(A_2) = \nu_2 \qquad \nu(A) = \nu_0 \text{ si } \nu_2 \geq \nu_1$$

et:

$$\nu(A_1) = \nu_2 \qquad \nu(A_2) = \nu_1 \qquad \nu(A) = \nu_0 \text{ si } \nu_1 \geq \nu_2 .$$

B_1 et B_2 désignent les intersections de la droite (z) avec (m_1) et (m_2). D'après (4), (5) et (8) il vient:

$$Y'(B_2) - Y'(C) = Y'(C) - Y'(B_1) = \frac{2}{h^2} \mid \bar{v}_0 \mid$$

soit:

$$(B_1C) = (CB_2) - \frac{2}{h^2} \mid \bar{v}_0 \mid \geqslant 0 .$$

C_1 et C_2 seront les intersections de la tangente (t) avec les asymptotes. En tenant compte de (4), (5) et (7) on obtient:

$$v_c - v(C_1) = v(C_2) - v_c = \frac{h^2}{2 \mid \bar{v}_0 \mid} .$$

La surface des triangles CB_1C_1 et CB_2C_2 sera donc égale à:

$$\tfrac{1}{2}(B_1C) \{ v_c - v(C_1) \} = \tfrac{1}{2}(CB_2) \{ v(C_2) - v_c \} = \tfrac{1}{2} . \quad (9)$$

Cette relation qui doit obligatoirement être vérifiée constitute un moyen de contrôle extrèmement efficace.

Considérons à présent le rectangle dont l'un des côtés est B_1B_2 et dont l'autre côté passe par le point A. Sa surface, que nous considérerons arbitrairement avoir le signe de $\bar{v}_c$, sera:

$$(B_1B_2) \cdot \bar{v}_c = \operatorname{sign} \bar{v}_0 \cdot 2d_0 . \quad (10)$$

Nous sommes maintenant en mesure de déterminer à partir de la représentation graphique de sa dérivée logarithmique tous les éléments des courbes de Gauss dont est composée la courbe à analyser (fig. 6):

a. La pente des asymptotes est égale à $-2/h^2$.

b. Les abscisses des intersections de l'axe des v avec les asymptotes sont celles des maxima des courbes cherchées.

c. Le rapport des hauteurs des maxima est donné par (10):

$$\ln \frac{D_1}{D_2} = 2d_0 = \operatorname{sign} \bar{v}_0 \cdot (B_1B_2)\, \bar{v}_c . \quad (10')$$

$\bar{v}_c$ est de même signe que $\{(D_1 - D_2 \cdot \operatorname{sign} \bar{v}_0\}$. Par rapport au milieu des abscisses des sommets des courbes composantes, le centre C de la dérivée logarithmique se trouve donc toujours du côté du plus petit sommet.

Si nous appelons y_0 la valeur de y pour $v = v_0$ l'équation (2') entraîne:

$$D_1 + D_2 = y_0 \, e^{\left(\frac{\bar{v}_0}{h}\right)^2}$$

et, avec (10'), il vient finalement:

$$D_1 = y_0 \frac{e^{\left(\frac{\bar{v}_0}{h}\right)^2}}{1 + e^{-2d_0}} \quad (11)$$

$$D_2 = y_0 \frac{e^{\left(\frac{\bar{v}_0}{h}\right)^2}}{1 + e^{2d_0}} \quad (11')$$

ce qui complète la détermination des paramètres des courbes cherchées.

3. Considérations Pratiques et Contrôle

La courbe Y' peut être obtenue suivant les cas:

1. Soit à partir de la tangente à une courbe continue prise par exemple directement sur la bande d'un appareil enrégistreur.

2. Soit, si la courbe est donnée point par point, par une méthode des différences plus ou moins poussée:

$$Y'_0 = \frac{y_1 - y_{-1}}{v_1 - v_{-1}} \frac{2}{y_1 + y_{-1}} \quad (12)$$

ou mieux:

$$Y'_0 = \frac{y_{-2} - 8y_{-1} + 8y_1 - y_2}{12 \cdot \Delta v} \frac{1}{y_0} . \quad (13)$$

3. Soit encore en utilisant la relation:

$$Y'_0 = \frac{\ln y_1 - \ln y_{-1}}{v_1 - v_{-1}} . \quad (14)$$

4. Soit enfin par une machine analogique donnant directement la dérivée logarithmique à partir du spectre.

L'évaluation de l'erreur commise sur Y' pour une erreur donnée δy sur la mesure de y dépendra évidemment de la méthode de calcul employée. Si l'on utilise la formule (14) par exemple, les y_i étant pris à des intervalles équidistants Δv, l'erreur sur Y' devient:

$$\delta Y' = \frac{2}{\Delta v} \frac{\delta y}{y} \quad (\text{en admettant: } \delta v \equiv 0) .$$

Si toutefois la détermination de Y' à partir des valeurs expérimentales est faite avec suffisamment de soin pour pouvoir négliger les erreurs dues à la dérivation devant les erreurs de mesure – ce qui est toujours possible dans le cas d'une calculatrice couplée au spectrographe – on aboutit à l'importante constatation suivante:

Si $\overline{Y}'$ désigne la dérivée logarithimique obtenue expérimentalement et si elle est considérée issue d'une superposition de deux courbes de Gauss, alors elle doit pouvoir – à l'erreur $\delta\overline{Y}'$ près – être assimilée à une courbe théorique Y' du type défini par l'équation (2):

$$\overline{Y}' = Y' + \delta\overline{Y}' .$$

Or tant que l'erreur de mesure δy de la courbe initiale est petite devant y, l'intégrale sur l'erreur absolue de la dérivée logarithmique sera:

$$\int_{\nu(P)}^{\nu(Q)} \delta\overline{Y}' \, d\nu = \Big[\ln (y + \delta y) - \ln y\Big]_{\nu(P)}^{\nu(Q)} =$$

$$= \left(\frac{\delta y}{y}\right)_{\nu(Q)} - \left(\frac{\delta y}{y}\right)_{\nu(P)} .$$

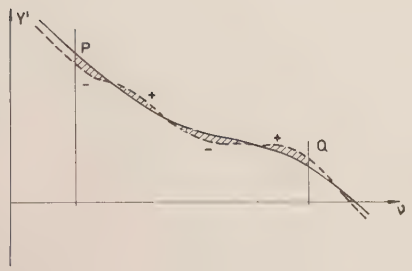

——— Y' . . .. $\overline{Y}'$

Fig. 2.

C'est-à-dire que, la surface comprise entre $\overline{Y}'$ et la courbe théorique choisie Y' étant considérée comme de signe différent des deux côtés de cette dernière, $\overline{Y}'$ devra osciller autour de Y' de telle sorte que la portion de surface comprise entre ces courbes et limitée par deux abscisses quelconques $\nu(P)$ et $\nu(Q)$ reste inférieure à la somme des erreurs relatives maxima sur les mesures de $y(P)$ et de $y(Q)$ (fig. 2). Cette condition restrictive rend ainsi le choix de $Y'(\nu)$ pratiquement univoque particulièrement si outre $\overline{Y}'$ l'on tient compte de sa symétrique obtenue par retournement d'un papier calque; dans le cas où ce choix est possible, il est inutile de contrôler l'exactitude de la décomposition en reconstituant la courbe d'origine à l'aide des paramètres trouvés. Dans le cas contraire, la décomposition en deux courbes de Gauss (1) de même demi-largeur n'est pas licite dans le cadre de l'approximation demandée.

4. Application

Pour analyser une courbe spectrométrique $y = y(\nu)$ et déterminer les courbes de Gauss qui la composent, on procède de la manière suivante:

1. On calcule la dérivée logarithmique $Y' = Y'(\nu)$ d'après l'un des procédés mentionnés plus haut.

2. On trace la courbe $Y' = Y'(\nu)$. Celle-ci doit être *continue*.

3. On cherche les asymptotes et le centre de la courbe Y'. On doit ici distinguer 3 cas

a. Y' possède deux branches non symétriques ou deux branches "inversées" (fig. 3a, 3b)

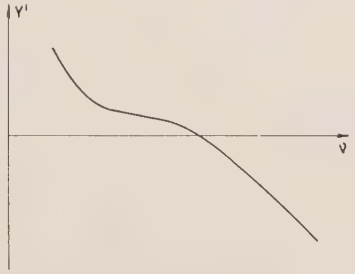

Fig. 3a.

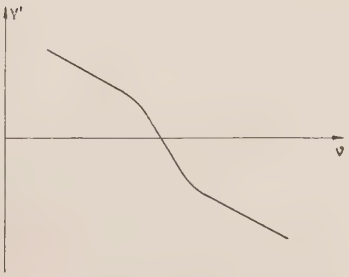

Fig. 3b.

La courbe y n'est pas composée de deux courbes de Gauss de même demi-largeur. Dans le second cas y peut être une courbe de Lorentz.

Toute partie droite sur la courbe Y' correspond à une partie de courbe de Gauss pour y.

b. Y' possède deux branches symétriques.

La courbe y est formée de deux courbes de

Fig. 3c.

Gauss dont les hauteurs sont de même ordre de grandeur.

On cherche d'abord le centre C de la courbe Y': pour cela on dessine la courbe sur du papier calque, on la retourne sur le dessin original et on cherche le point qui revient sur lui-même:

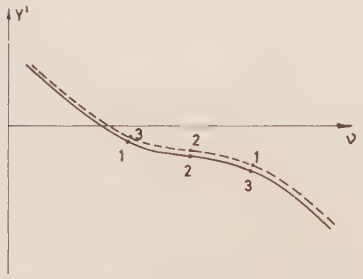

Fig. 4a.

On trace la tangente d'inflexion (t) et l'axe (z) passant par C. On trace les asymptotes (m_1) et (m_2) qui coupent (z) en B_1 et B_2, et (t) en C_1 et C_2. On place ces asymptotes de manière à ce que:

$$\{ \nu(C_1) - \nu_c \}\,(CB_1) = \{ \nu(C_2) - \nu_c \}\,(CB_2) = 1 .$$

On trace la médiane (m):

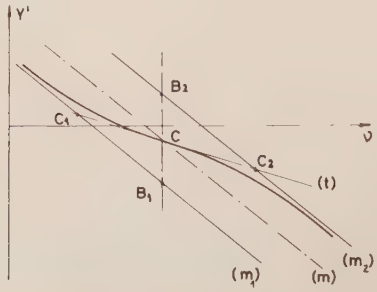

Fig. 4b.

c. Y' ne possède qu'une seule branche:

La courbe y est formée d'une courbe de Gauss principale, à laquelle s'ajoute une courbe de Gauss de dimension très inférieure.

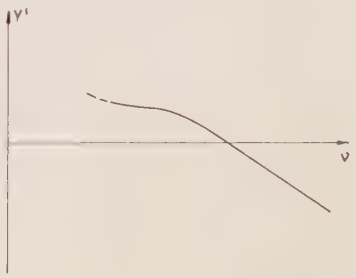

Fig. 3d.

On trace d'abord l'asymptote de la branche connue: (m_2) par exemple, et la tangente (t) passant par les points situées sur la partie la moins inclinée de la courbe. Soit C_2 leur point de rencontre.

On trace l'axe (z) coupant (m_2) en B_2 et (t) en C. On place celui-ci de manière à ce que:

$$\{ \nu(C_2) - \nu_c \}\,(CB_2) = 1 .$$

On trace l'autre asymptote (m_1) symétrique par rapport à C et la médiane (m).

4. On doit maintenant contrôler si la tangente hyperbolique définie par ses asymptotes et son centre est bien identique à la courbe Y'. Si Y' est régulière, un contrôle sur 8 points est suffisant.

On a:

$$\begin{aligned} \text{th } 0.5 &= 0.46 \\ \text{th } 1 &= 0.76 \\ \text{th } 1.5 &- 0.90 \\ \text{th } 2 &= 0.96 . \end{aligned}$$

On porte donc sur un graphique particulier en ordonnée $CB_1 = CB_2$ avec les mêmes unités que sur la représentation de Y' et en abscisse les valeurs précédentes (fig. 5):

Les ordonnées obtenues pour Y' à l'aide de ce graphique sont alors reportées sur le dessin à partir de la médiane (m), de part et d'autre de C et à des abscisses:

$$\bar{\nu} = \pm 0.5\,g\,; \quad \pm 1\,g\,; \quad \pm 1.5\,g\,; \quad \pm 2\,g$$

avec

$$g = \bar{\nu}(C_2) - \bar{\nu}_c .$$

Si les points obtenus se trouvent "à l'intérieur" de la courbe expérimentale, il faut écarter un peu les asymptotes et déplacer légèrement le centre et la tangente (t) pour conserver la relation (9) et calculer de nouveaux points. Dans le cas contraire il faut resserrer un peu les asymptotes.

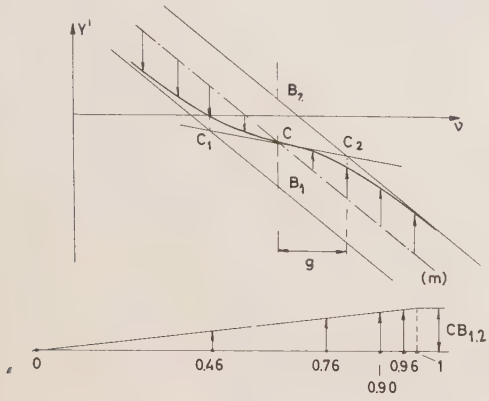

Fig. 5.

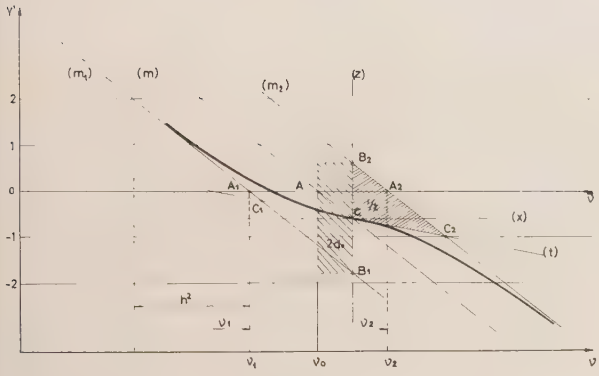

Fig. 6.

Enfin si les points sont dans le domaine d'erreur de la courbe Y', la tangente hyperbolique coincidence avec Y' et la courbe expérimentale y avec la courbe composée des deux courbes de Gauss ainsi déterminées. Il est inutile de recomposer ces courbes pour effectuer la vérification sur y.

5. Les asymptotes ainsi déterminées (m_1) et (m_2) coupent l'axe des ν aux points A_1 et A_2 d'abscisses ν_1 et ν_2; la médiane (m) le coupe au point A d'abscisse ν_0.

On évalue sur le graphique d_0 à l'aide de (10') (le signe de $\bar{\nu}_0$ dépendant uniquement de la répartition arbitraire des indices 1 et 2). L'exposant du numérateur de (11) et (11') découle de la relation facilement vérifiable suivante:

$$\left(\frac{\bar{\nu}_0}{h}\right)^2 = \tfrac{1}{8}\,(A_1A_2)\,(B_1B_2)\,. \qquad (15)$$

Les courbes composantes sont alors totalement définies: $\nu(A_1)$ et $\nu(A_2)$ sont les fréquences des maxima; leurs hauteurs sont données par (11) (11') et (15), la demi-largeur commune h par:

$$h = \sqrt{2\,\frac{(A_1A_2)}{(B_1B_2)}}\,.$$

Remarque: On peut aussi songer à profiter du fait que (3') – considéré comme équation en $(Y' - Y'_c)$ et $(\bar{\nu} - \bar{\nu}_c)$ – ne dépend que de deux paramètres pour graver cette famille de courbes ainsi que leurs asymptotes sur quelques feuilles de plexiglas qui simplifieront notablement la recherche des paramètres inconnus.

Remerciements

Les auteurs souhaitent remercier Monsieur W. Schneider pour son aide active ainsi que l'examen du manuscrit; l'un d'entre nous, L.G.P., tient plus particulièrement a exprimer sa reconnaissance envers Monsieur le Professeur E. Baumann, Directeur de la Section de Recherches Industrielles pour son encouragement et l'autorisation de publication.

Exemples

Nous avons calculé 4 exemples: les courbes ont été normées sur h et la dérivée logarithmique calculée à l'aide de la formule (12). Comme premier exemple nous avons choisi une courbe de Gauss pure, pour étudier la précision de la méthode sur h.

Dans le deuxième exemple nous avons composé deux courbes de Gauss de même hauteur et très écartées.

Dans le troisième exemple nous avons choisi un rapport des hauteurs et un écartement moyens pour les courbes composantes, la courbe la plus grande étant située à gauche.

Dans le quatrième exemple, nous avons ajouté à la première courbe une courbe nettement plus petite et assez rapprochée. La grande courbe était située à droite.

Nous n'indiquerons que dans le premier cas le détail des calculs de la dérivée logarithmique.

EXEMPLE NO. 1:

On obtient bien une droite pour Y' mais dont la pente diffère légèrement de la pente théorique:

$$h = 1.02 \qquad (h_{\text{théorique}} = 1) .$$

Cela vient de la formule (12) qui ne suffit plus pour les extrémités de la courbe. En pratique une erreur de 2% reste sensiblement inférieure aux erreurs d'expérience qui sont assez grandes dans les extrémités des courbes de Gauss.

Le tableau suivant donne le calcul de Y', calculée suivant la formule (12)

v	y_0	$y_1 - y_{-1}$	$y_1 + y_{-1}$	Y'_0	v
0.0	1.000				
		— 0.039	1.961	— 0.19	0.1
0.2	0.961				
		— 0.109	1.813	— 0.60	0.3
0.4	0.852				
		— 0.154	1.550	— 0.99	0.5
0.6	0.698				
		— 0.171	1.225	— 1.40	0.7
0.8	0.527				
		— 0.159	0.895	— 1.78	0.9
1.0	0.368				
		— 0.131	0.605	— 2.17	1.1
1.2	0.237				
		— 0.096	0.378	— 2.54	1.3
1.4	0.141				
		— 0.0637	0.2183	— 2.92	1.5
1.6	0.0773				
		— 0.0381	0.1165	— 3.27	1.7
1.8	0.0392				
		— 0.0209	0.0575	— 3.63	1.9
2.0	0.0183				

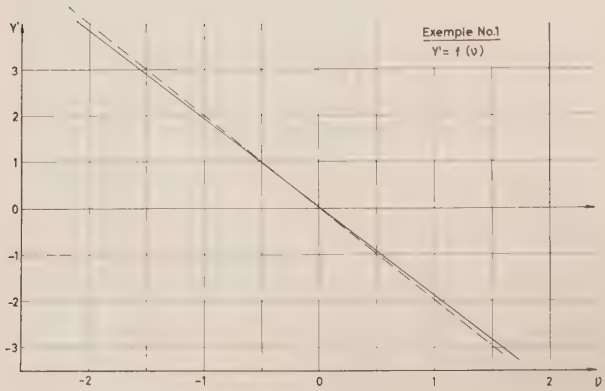

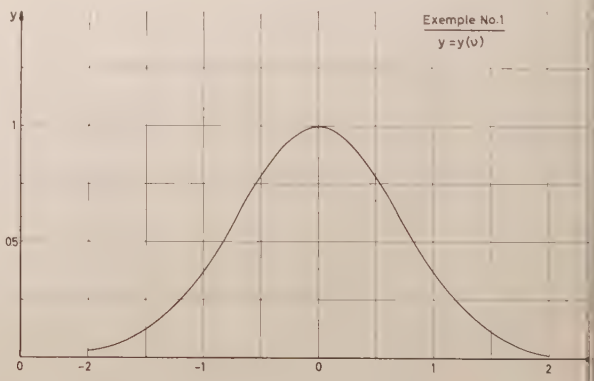

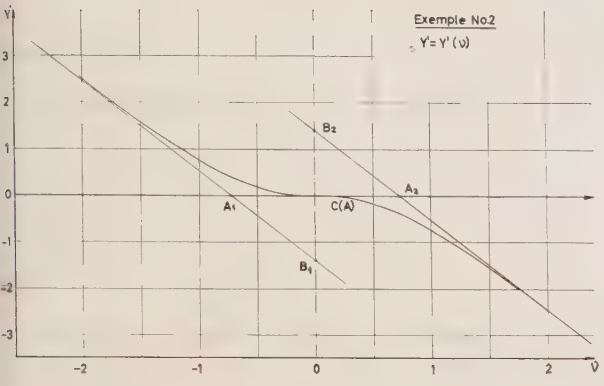

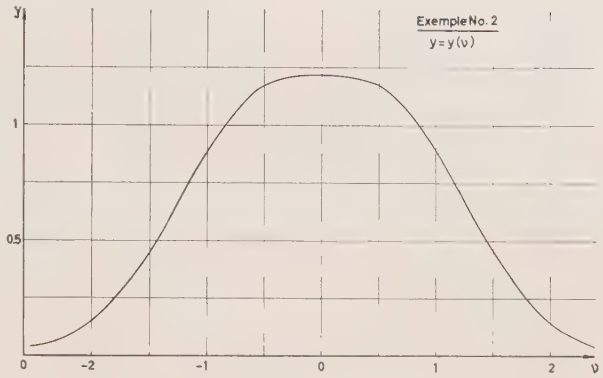

EXEMPLE NO. 2:

	Valeurs mesurées	Valeurs théoriques
h	1.02	1.00
v_1	— 0.72	— 0.70
v_2	+ 0.72	+ 0.70
D_1	1.01	1.00
D_2	1.01	1.00

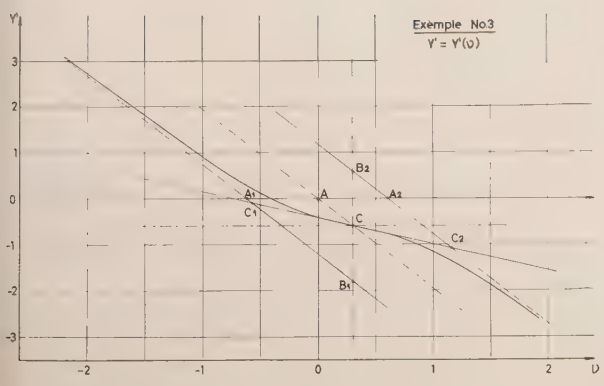

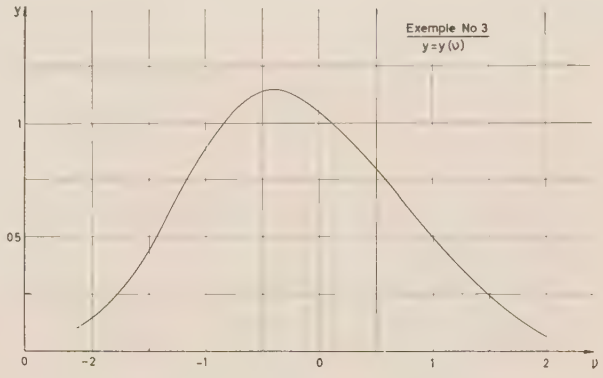

EXEMPLE NO. 3:

	Valeurs mesurées	Valeurs théoriques
h	1.01	1.00
v_1	— 0.62	— 0.60
v_2	+ 0.60	+ 0.60
D_2	1.02	1.00
D_2	0.48	0.50

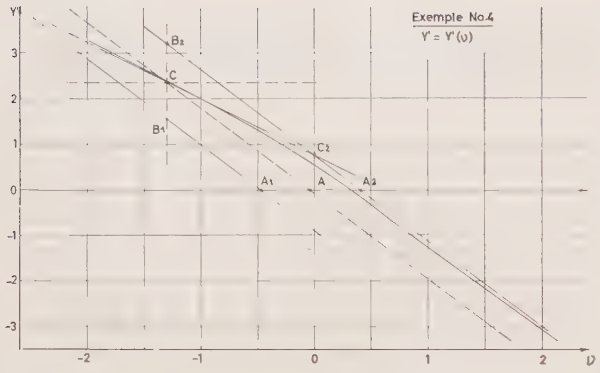

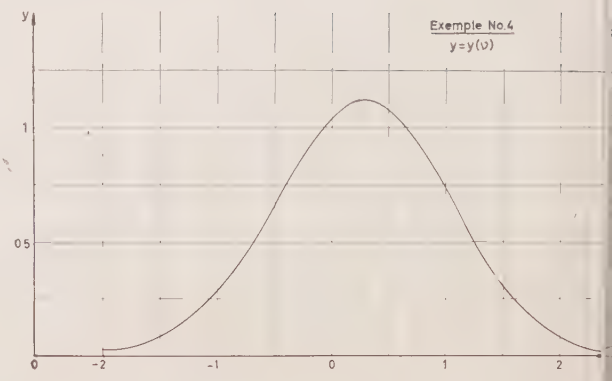

EXEMPLE NO. 4:

	Valeurs mesurées	Valeurs théoriques
h	1.03	1.00
ν_1	— 0.46	— 0.40
ν_2	+ 0.40	+ 0.40
D_1	0.14	0.20
D_2	1.05	1.00

La première courbe de Gauss est assez mal définie, mais c'est parce qu'elle est très petite par rapport à l'autre.

NUCLEAR INSTRUMENTS AND METHODS 9 (1960) 221–225; NORTH-HOLLAND PUBLISHING CO.

A PRECISION CLOCK FOR MEASURING TIME INTERVALS†

R. W. FINDLEY, R. A. REITER and T. A. ROMANOWSKI

Carnegie Institute of Technology, Pittsburgh, Pennsylvania

Received 8 August 1960

A precision electronic clock which uses 10 Mc pulses to measure time intervals is described. The linearity and the average channel width of the system were determined by measuring time intervals between randomly distributed pulses. In these tests about 250 000 counts per channel were accumulated showing that the system was linear. The slope of the random distribution of pulses was $0.000\,02 \pm 0.0003$ per channel. It was also found, to an accuracy of 0.016%, that the channel width of the time scale was equal to the period of the 10 Mc oscillator. This system is suitable for time interval measurements in a region from 0–15 μsec with an 0.1 μsec resolution.

1. Introduction

A precision electronic time interval measuring system was developed for use in a series of experiments involving mu meson decays[1,2,3]) and it is felt that this apparatus could also be used in time of flight measurements. The system was used to measure time intervals up to 15 μsec with a resolution of 0.1 μsec.

A time interval is measured by scaling cycles of a 10 Mc oscillator during that interval, then a count is stored in one of 200 channels in the memory of a pulse height analyzer. The channel number corresponds to the number of scaled cycles of the 10 Mc oscillator. In such a way a record is accumulated of the time distribution of pulses.

The design of the system is flexible and it can be readily adopted to measure times, in terms of frequencies, ranging from 2–10 Mc. Preliminary tests also showed that it would be possible to use higher frequencies up to 30 Mc with a faster scaler substituted in the system.

2. The System

The block diagram of the system is shown in fig. 1. It is desired to measure a time interval between two pulses called start and stop. These pulses generate a fast gate[4]) whose width corresponds to the time interval between them. Then the gate and a 10 Mc continuous wave train from a precision oscillator are fed to a coincidence circuit. The output of that circuit,

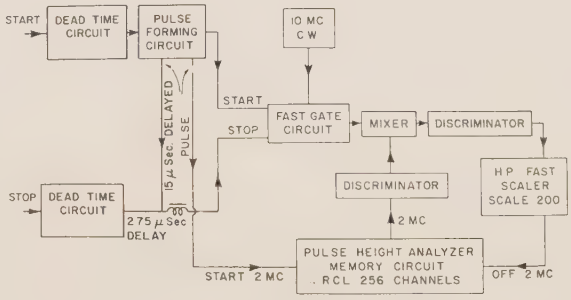

Fig. 1.

which is a wave train containing some number of 10 Mc cycles related to the measured time interval, is stored in a fast scaler. The scaler, with a scale of 200, is then complemented by a 2 Mc wave train originating from the memory circuit of a pulse height analyzer. The process of complementing addresses a channel of the memory, corresponding to the number of 2 Mc pulses necessary to overflow the fast scaler, and the

† This work was partially supported by the U.S. Atomic Energy Commission.

[1]) R. A. Reiter, T. A. Romanowski, R. B. Sutton and B. G. Chidley, Phys. Rev. Letters 5 (1960) 22.

[2]) W. J. Bertram, Jr., R. A. Reiter, T. A. Romanowski, R. B. Sutton, to be published in Phys. Rev. Letters.

[3]) W. J. Bertram, Jr., R. A. Reiter, T. A. Romanowski, R. B. Sutton, to be published in Nuovo Cimento.

[4]) Z. Bay and N. T. Grisamore, IRE Translations on Electronic Computers EC-5 (1956) 121.

measurement is stored in that channel. Therefore the measured time in terms of 10 Mc cycles is equal to 200-N where N is the channel number in which the event is stored. In such a way times are measured with 0.1 μsec resolution using a pulse height analyzer capable only of 0.5 μsec resolution.

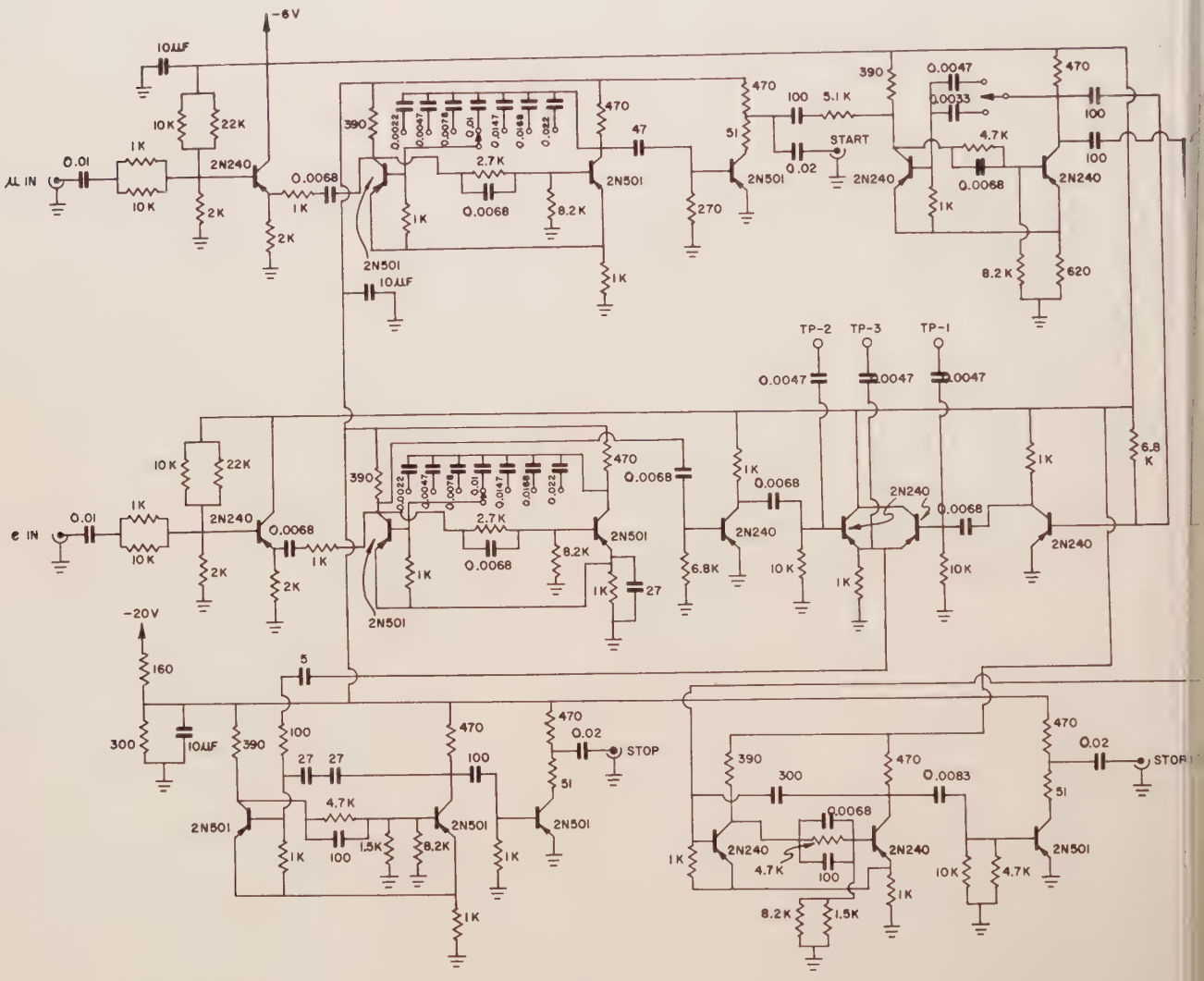

Fig. 2.

The dead time circuits in the system were provided to insure that the pulse height analyzer had a sufficient time to store an event. The stop pulse should be delayed with respect to the start pulse by at least 0.2 μsec. Such a delay shifts the "zero" time of the apparatus allowing the fast gate to reach the full amplitude. Otherwise the data accumulated in the first two channels is not reliable. In the experiment, an arbitrary delay[5]) of 2.75 μsec was used.

The pulse forming circuit generates two pulses delayed by 15 μsec or 20 μsec with respect to the start pulse. One pulse is used to turn off the fast gate in case there is no stop pulse and the other pulse starts the 2 Mc wave train from the pulse height analyzer in order to complement the fast scaler.

In this system 10 Mc pulses were obtained from a Tektronix type 180 Time-Mark Generator.

[5]) Advance Electronics Delay Model 652.

There is no phase correlation between the fast gate and the 10 Mc pulses. Therefore the output wave train from the coincidence circuit contained one or two pulses whose amplitudes could balanced perfectly, and therefore there is a range of pulse heights triggering the scale from one state only. To remove this "odd-even" effect it was necessary to shape the 10 Mc and 2 Mc input

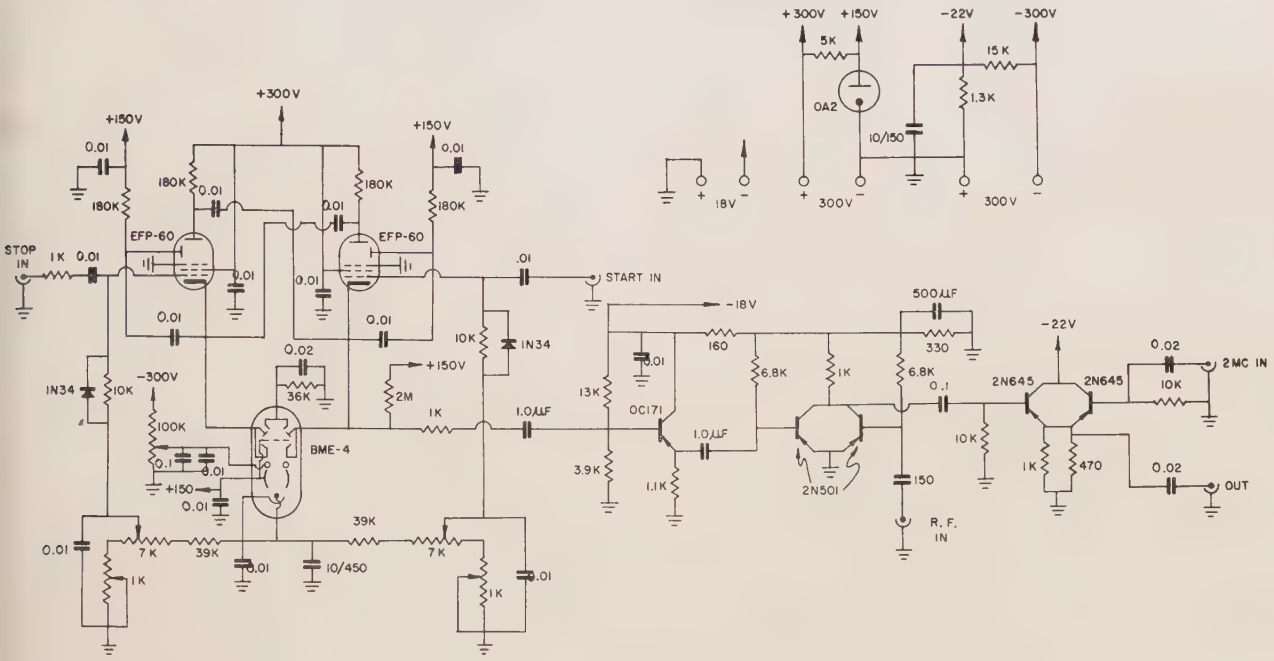

Fig. 3.

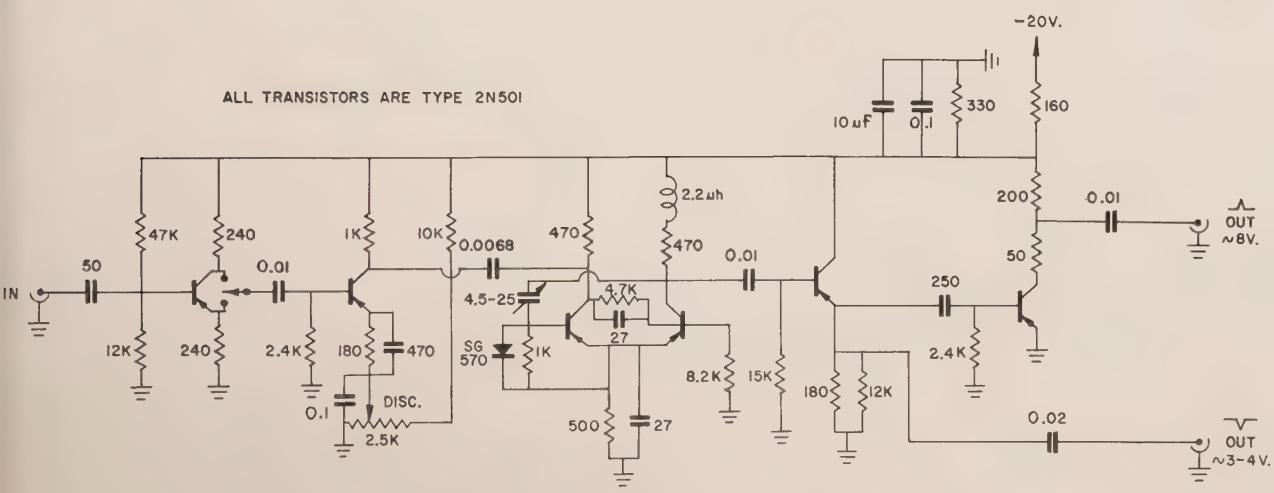

Fig. 4.

range from zero to maximum. The Hewlett-Packard scaler which scaled this train showed a preference for stopping on either an even or odd number of counts. This is caused by the first binary scale in the circuit, which can not be to the fast scaler by means of a fast discriminator.

The mixer circuit provides a proper impedance match between the coincidence circuit, the pulse height analyzer and the Hewlett-Packard scaler. It was necessary for the operation

of the mixer to shape the 2 Mc wave train from the pulse height analyzer.

3. Fast Gate Circuit

The fast gate circuit is shown in fig. 3. The EFP-60 and the BME-4[6]) comprise the fast flip-flop circuit generating the positive gate pulse about 1 V high. The gate is fed to an input of a double coincidence circuit made up of 2N501 transistors. The other input is fed with a continuous 10 Mc wave train with the amplitude of 5 volts peak to peak. The negative 8 volt output from the coincidence circuit goes to a 2N645 transistor mixer which also passes shaped 2 Mc 8 V negative pulses. The fast gate, the coincidence circuit and the mixer are constructed on the same chassis.

4. Fast Discriminator and Scaler

A fast discriminator is shown in fig. 4. The input to this circuit can be either negative or positive with amplitudes between 2–8 volts. Positive and negative outputs are available.

The Hewlett-Packard scaler Model 520A was converted to a scale of 200 by adding another binary stage similar to the last binary in that scale.

5. Pulse Height Analyzer

The memory of the RCL Model 20611 256 channel pulse height analyzer was used to store the information on the time correlation between pulses. The necessary circuit modifications of the pulse height analyzer are shown in fig. 5. Component designations are as specified by the manufacturer and the parts added in the modification are identified with an X. XJ-1 provides the 2 Mc wave train while XJ-2 is the input for the pulse to stop the 2 Mc. The switch XS-1 converts the pulse height analyzer to normal operation.

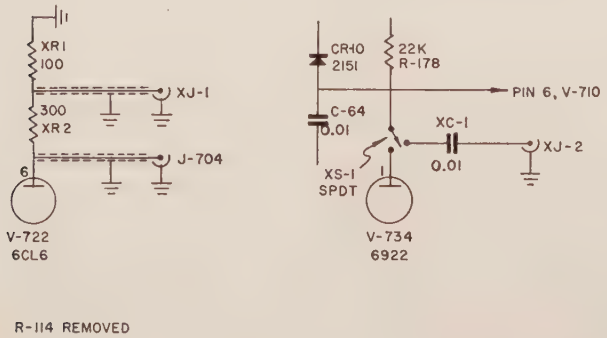

Fig. 5.

The analyzer is equipped with a read out of its memory in a form of an oscilloscope picture, a chart record and also has a digital output.

6. Linearity Checks of the Equipment

The linearity of the system was checked by feeding the start and stop inputs from randomly phased pulse generators. The pulses fed to the stop input were obtained from a Tektronix type 180 time-marker generator. The rate of these pulses was 20 kc and the pulses were derived from the same oscillator as the 10 Mc wave train. Therefore the ratio of the clock frequency to the stop rate should be 500 and is independent of the exact frequency of the oscillator. This test allowed for a linearity check and it checked the average channel width as well.

A straight line with a zero slope is expected from such a test and the average number of

Table 1

A_{sc}	A_{meas}	b(channel [1])	χ^2 †
11 908	11 909 ± 10	0.000 02 ± 0.000 3	117
20 009	20 009 ± 13	−0.000 006 ± 0.000 2	109
20 336	20 335 ± 14	−0.000 02 ± 0.000 2	117
13 099	13 119 ± 11	−0.000 02 ± 0.000 03	127
10 001	9 988 ± 9	−0.000 006 ± 0.000 03	100
22 939	22 933 ± 13	0.000 002 ± 0.000 2	91
27 069	27 068 ± 15	−0.000 04 ± 0.000 2	101
53 795	53 793 ± 23	0.000 008 ± 0.000 1	133
21 376	21 365 ± 15	−0.000 01 ± 0.000 2	128
28 436	28 453 ± 15	−0.000 01 ± 0.000 02	102
26 490	26 483 ± 15	0.000 004 ± 0.000 02	115
15 731	15 728 ± 12	−0.000 02 ± 0.000 2	112
14 893	14 904 ± 12	−0.000 03 ± 0.000 03	130
286 083	286 037 ± 47	−0.000 006 ± 0.000 05	101

† χ^2 is expected to be 113 ± 16.

[6]) BME-4 a special switching tube manufactured by the National Union Electric Corp.

pulses accumulated per channel is a product of: the number of start pulses, the channel width and the stop rate. During these tests the total number of start pulses was recorded by a scaler. The straight lines obtained from this test were analyzed by an IBM 650 Computer with a method of least squares fitting a function $A(1 + bn)$ where A is the number of counts in a channel, b is the slope of the line and n is the channel number. The origin in the analysis was taken at the center of the line and therefore the value obtained for A represented the average number of counts per channel.

Table 1 contains the results of such tests taken at approximately 12 hour intervals during an experiment. The column A_{sc} shows the expected number per channel which is equal to 1/500 of the total number of start pulses.

A_{meas}, the number of counts per channel, is obtained from the least square fit. Column b shows the slope and its error; and, finally, the column χ^2 shows goodness of fit to the data. From the table it is evident that the average channel width is equal, with an accuracy of 0.016%, to one period of the oscillator. An absolute calibration of the frequency was made and it was found to be (10.0016 ± 0.0002) Mc. The system is linear to the accuracy of about 2/10 000 per channel.

Because of the lack of phase correlation between the gate and the 10 Mc, the resolution of this apparatus for time interval measurements is equal to a channel width.

The distribution of χ^2 obtained from the analyzer of the data shows that the systematic errors, compared to the statistical errors, are small.

Acknowledgements

We are indebted to Prof. R. B. Sutton and Dr. B. G. Chidley for advice during the course of the development of this apparatus.

NUCLEAR INSTRUMENTS AND METHODS 9 (1960) 226–228; NORTH-HOLLAND PUBLISHING CO.

NUCLEAR REACTIONS FROM RECOIL PROTONS IN A REACTOR†

S. S. GLICKSTEIN and R. G. WINTER

Department of Physics, The Pennsylvania State University, University Park, Pennsylvania, U.S.A.

Received 11 August 1960

Samples of H_3BO_3, $(C_2H_4)_n$ and H_2O were exposed to the fast neutron flux next to the core of a 10^5 watt "swimming pool" reactor. The reactions $B^{11}(p,n)C^{11}$, $C^{12}(p,\gamma)N^{13}$, $C^{13}(p,n)N^{13}$, and $O^{18}(p,n)F^{18}$ were initiated by recoil protons and the positron activities of the products were observed. The yields, in atoms produced per gram of sample per second of irradiation, were 5000 for C^{11}, 800 for N^{13}, and 100 for F^{18}. The fast neutron spectrum was measured with threshold detectors, and the yields were computed. The agreement of the calculated and measured results is good.

1. Introduction

When fission neutrons slow down in a hydrogenous medium, there is produced an appreciable number of fast recoil protons. The protons are capable of initiating nuclear reactions, most commonly (p,n) reactions, in light elements. These reactions are of some interest; they can be the origin of various background activities, and can be used to produce small radioactive sources that cannot be made in a reactor by other means. We have measured the fast neutron flux near the core of The Pennsylvania State University Research Reactor, computed the recoil proton flux and resultant yield of the reactions $O^{18}(p,n)F^{18}$, $C^{13}(p,n)N^{13}$ and $B^{11}(p,n)C^{11}$ in samples of H_2O, $(C_2H_4)_n$ and H_3BO_3, and measured these yields.

2. Determination of the Fast Neutron Flux

The thresholds of the (p,n) reactions that were studied are all above 2.5 MeV. It is, therefore, sufficient to know the neutron spectrum for energies above 2.5 MeV. In this region, an adequate representation of the neutron flux is given by the function $\varphi_0 \exp(-aE_n)$, where φ_0 and a are two constants that must be obtained experimentally. We adopt the value $a =$ 0.58-MeV measured at the Oak Ridge Bulk Shielding Reactor[1]). The quantity φ_0, for a reactor power level of 10^5 watts, was determined through measurement of the activity of threshold detectors. The experimental yield was equated to the result of the numerical integration

$$\int_0^\infty \sigma(E_n)\varphi_0 \, e^{-0.58\, E_n/\mathrm{MeV}} \, dE_n ,$$

where $\sigma(E)$ is the cross section for the threshold reaction. Table 1 gives the results for the four threshold detectors that were used. The mean of the four values for φ_0 is used here. The fast neutron flux is then

$$\varphi_n(E_n) = 1.3 \times 10^{11} \, e^{-0.58\, E_n/\mathrm{MeV}} \ \text{neutrons/sec cm}^2\ \text{MeV}. \quad (1)$$

The accuracy of this result is limited by the uncertainties in the absolute normalization of $\sigma(E_n)$ given in the fourth column of table 1.

Since some of the samples extended some distance from the core, the fast neutron flux decrease with distance was determined. The results are shown in fig. 1.

3. Computation of the Proton Flux and Reaction Yields

In the energy region that is of interest here, neutron-proton scattering is isotropic in the center-of-mass system. It follows that the proba-

† Based on a thesis submitted by S. S. Glickstein in partial fulfillment of the requirements for the M.S. degree in physics at The Pennsylvania State University, and partly supported by the U.S.A. Office of Ordnance Research. A summary of some of the results is given in Bull. Am. Phys. Soc., II, 4, 287.

[1]) Selected Reference Material, United States Atomic Energy Program, Research Reactors, U.S. Government Printing Office, 1955.

Table 1
Determination of the fast proton flux

Reaction	Threshold energy (MeV)	References for $\sigma(E)$	Probable error quoted for absolute $\sigma(E_n)$	φ_0 (neutrons/sec cm^2 MeV)
$Al^{27}(n,p)Mg^{27}$	1.90	Hughes and Harvey[2])	none given	1.0×10^{11}
$Fe^{56}(n,p)Mn^{56}$	2.94	Terrell and Holm[3])	20 %	2.1×10^{11}
$Al^{27}(n,\alpha)Na^{24}$	3.27	Grundl, Henkel and Perkins[4])	10 %	1.1×10^{11}
$Si^{28}(n,p)Al^{28}$	4.01	Marion, Brugger and Chapman[5])	50 %	0.9×10^{11}

bility of a proton acquiring an energy greater than E in a collision with a neutron of energy E_n is $(E_n - E)/E_n$. The number of protons that acquire an energy greater than E per sec cm^3 is then given by

$$N(E) = \int_0^\infty n_0 \sigma_s(E_n) \varphi_n(E_n) \frac{E_n - E}{E_n} \, dE_n \qquad (2)$$

where n_0 is the number of hydrogen atoms per cm^3, and $\sigma_s(E_n)$ is the total neutron-proton scattering cross section at energy E_n. Numerical integration, with expression (1) for $\varphi_n(E_n)$, the values of $\sigma_s(E_n)$ given by Hughes and Harvey[2]) and the n_0 for water, yields the values of $N(E)$, which are approximated very closely by

$$N(E) = 1.75 \times 10^{10} \, e^{-0.93 \, E/\mathrm{MeV}} \ /\mathrm{cm^3 \, sec} \, . \qquad (3)$$

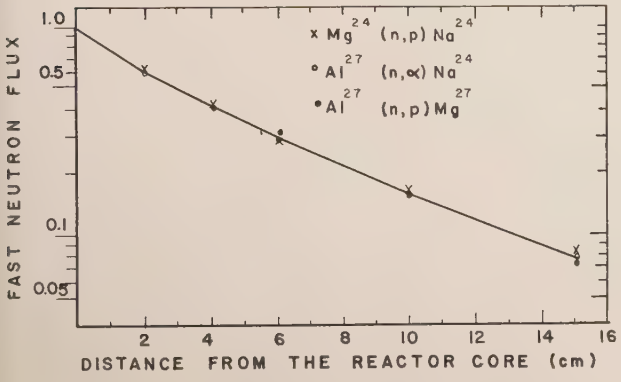

Fig. 1. Normalized fast neutron flux fall off.

Equation (3) gives the proton source density. To determine the flux density, consider a sphere of projected area dA surrounded by water that is both a source and an absorber of protons. The number of protons, with energy greater than E created in a spherical shell of thickness dR at a distance R from dA is $N(E)\, 4\pi R^2 dR$. The solid angle intercepted by dA is $dA/4\pi R^2$. The number of protons created between R and $R + dR$ with energy greater than E, headed toward dA, per area dA, is then simply $N(E)dR$. The flux density of protons at dA with energy greater than E is given, therefore, by

$$\varphi'(E) = \int_0^\infty N(E + \Delta E(R)) \, dR \, , \qquad (4)$$

where $E + \Delta E(R)$ is the energy that a proton at a distance R must have to reach dA with energy E.

The stopping power of water for protons of a few MeV energy is given by

$$-\frac{dE}{dR} = \frac{270}{E} \mathrm{MeV^2/cm} \, . \qquad (5)$$

Integration from zero to R yields

$$E + \Delta E(R) = \sqrt{E^2 + 540R \ \mathrm{MeV^2/cm}} \, . \qquad (6)$$

Substitution of equations (3) and (6) into (4) then gives $\varphi'(E)$. Differentiation of $\varphi'(E)$ with respect to E finally yields $\varphi(E)$, the flux density at the energy E:

$$\varphi(E) = 6.5 \times 10^7 \, E \, e^{-0.93 \, E/\mathrm{MeV}} \ \mathrm{protons/cm^2 \, sec \, MeV} \, . \qquad (7)$$

The center of the sample of water used for the $O^{18}(p,n)F^{18}$ reaction was 3.7 cm from the core, where the neutron flux is 0.46 times the value at the core. The yield expected is given by 0.46 times the density of O^{18} atoms times the integral

[2]) D. J. Hughes and J. A. Harvey, BNL 325, 1st ed. (1955).

[3]) J. Terrell and D. M. Holm, Phys. Rev. **109** (1958) 2031.

[4]) J. A. Grundl, R. L. Henkel and B. L. Perkins, Phys. **109** (1958) 425.

[5]) J. B. Marion, R. M. Brugger and R. A. Chapman, Phys. Rev. **101** (1956) 247.

Table 2
Summary of results

Sample	Proton flux (/sec cm² MeV)	Reaction	Source of cross section data	Predicted activity	Measured activity
H_2O	$6.5 \times 10^7 E\, e^{-0.93E}$	$O^{18}(p,n)F^{18}$	Blaser, Boehm, Marmier, Scherrer[7])	120	120
		$O^{17}(p,\gamma)F^{18}$	Dubridge, Barnes, Buck, Strain[6])	negligible	
$(C_2H_4)_n$	$7.6 \times 10^7 E\, e^{-0.93E}$	$C^{13}(p,n)N^{13}$	Blaser *et al.*[7])	650	800
		$C^{12}(p,\gamma)N^{13}$	Jarmie and Seagrave[8])	30	
H_3BO_3	$3.1 \times 10^7 E\, e^{-0.93E}$	$B^{11}(p,n)C^{11}$	Blaser *et al.*[7])	3500	5000
		$B^{10}(p,\gamma)C^{11}$	Jarmie and Seagrave[8])	negligible	

over energy of the product of the known (p,n) cross section and $\varphi(E)$.

Essentially identical computations give the yields expected for the $C^{13}(p,n)N^{13}$ reactions in $(C_2H_4)_n$ (polyethylene) and the $B^{11}(p,n)C^{11}$ reaction in H_3BO_3. The results are summarized in table 2.

Some contributions might be expected from the reactions $O^{17}(p,\gamma)F^{18}$, $C^{12}(p,\gamma)N^{13}$, and $B^{10}(p,\gamma)C^{11}$. Computations using the known (p,γ) cross sections show that this process is completely negligible in boron, and contributes about 5% in carbon, as shown in table 2. In oxygen, the experiment of Dubridge, Barnes, Buck, and Strain[6]) shows that the (p,γ) contribution is negligible.

4. Measurements of the F^{18}, N^{13}, and C^{11} Yields

Samples of H_2O, $(C_2H_4)_n$ and H_3BO_3 were exposed to the fast neutron flux next to the core of the reactor at a power level of 10^5 watts. The 0.51 MeV positron annihilation gamma rays from the 112 minute F^{18}, the 10 minute N^{13}, and the 20 minute C^{11}, were counted with a 3 × 3 inch NaI(Tl) crystal and single channel pulse-height analyzer.

The efficiency of detection was determined with a Cu^{64} positron source made of copper foil that was irradiated in a known thermal flux. After irradiation, the copper was dissolved and placed into a container of the same shape and location as that used for the H_2O, $(C_2H_4)_n$, and H_3BO_3 samples. The yields are given in table 2.

The agreement between the predicted and measured yields is gratifying. The difference is, in fact, smaller than might be expected from the uncertainties in the fast neutron flux measurements (table 1) and in the positioning of the samples.

It is a pleasure to acknowledge helpful discussion with Dr. C. H. Blanchard and Dr. D. J. Donahue, and the cooperation of Dr. R. G. Cochran and the reactor staff.

[6]) L. A. Dubridge, S. W. Barnes, J. H. Buck and C. V. Strain, Phys. Rev. **53** (1938) 447.

[7]) J. P. Blaser, F. Boehm, P. Marmier and P. Scherrer, Helv. Phys. Acta **24** (1951) 465.

[8]) N. Jarmie and J. D. Seagrave, AEC Pub. LA 2014.

NUCLEAR INSTRUMENTS AND METHODS 9 (1960) 219–232; NORTH-HOLLAND PUBLISHING CO.

PULSE SHAPE DISCRIMINATION AND ENERGY RESPONSE OF CALCIUM TUNGSTATE CRYSTALS

W. R. DIXON and J. H. AITKEN

National Research Council, Ottawa, Canada

Received 20 July 1960

The scintillation response of calcium tungstate crystals to gamma rays, protons and alpha particles has been studied. It is shown that there is a difference in shape between gamma-ray and alpha-particle pulses, and that this effect may be exploited to discriminate between particles.

1. Introduction

Although calcium tungstate was once favourably considered as a scintillator for gamma-ray detection[1,2]) it has not been widely used for that purpose, and its properties have not been thoroughly investigated. Recently we have been interested in the possibility of observing the $Ca^{40}(n,p)$ and $Ca^{40}(n,\alpha)$ reactions in calcium tungstate crystals, and in that connection have studied the response to protons, alpha particles and gamma rays. The use of calcium tungstate crystals has also been reported by Beard and Kelly[3]) in a search for the natural alpha activity of tungsten.

During our study of the scintillation response of calcium tungstate we have found that pulse-shape discrimination can be used to distinguish between alpha particles on the one hand, and protons and gamma rays on the other. This effect has not previously been reported in calcium tungstate.

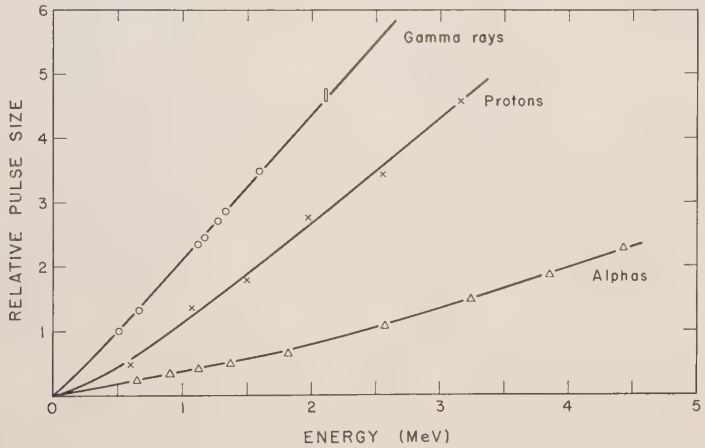

Fig. 1. Energy calibration of a calcium tungstate crystal for gamma rays, protons and alpha particles.

2. Energy Calibration and Resolution

An energy calibration of a calcium tungstate crystal for gamma rays, protons and alpha particles is shown in fig. 1. The gamma-ray sources used were Na^{22}(0.511, 1.28 MeV), Cs^{137}(0.662 MeV), Zn^{65}(1.12 MeV), Co^{60}(1.17, 1.33 MeV), and ThC″ (escape peaks at 1.60, 2.11 MeV). Protons of

[1]) R. J. Moon, Phys. Rev. **73** (1948) 1210.
[2]) R. H. Gillette, Rev. Sci. Instr. **21** (1950) 294.
[3]) G. B. Beard and W. H. Kelly, Nuclear Physics **16** (1960) 591.

known energy 3.2 MeV from the d(d,p)t reaction were used with aluminum absorbers to obtain the proton calibration. A Po^{210} source was used to supply 5.3 MeV alpha particles, and the air path varied to give lower energies. The possibility that the response to gamma-rays might differ from the response to electrons (due to a surface effect) was tested with Tl^{204} and Cs^{137} beta-sources. No evidence for such a surface effect was found.

It can be seen from fig. 1 that alpha particles give pulses only about $\frac{1}{5}$ the size from gamma rays of the same energy, and protons give pulses about $\frac{2}{3}$. The fact that alpha particles give much smaller pulses was first noted by Kallmann[4]), but seemingly denied by Garlick and Fatehally[5]). Beard and Kelly[3]) have reported that 5.3 MeV alpha particles produce approximately the same size pulses as 1.7 MeV gammas, which is in qualitative agreement with fig. 1. The relative response to alpha particles and protons in fig. 1 seems to agree with some recent results of Bass *et al.*[6]). It can also be seen from fig. 1 that the calibration curve is decidedly non-linear for alpha particles and slightly non-linear for protons and gamma-rays, particularly at low energies. These calibration curves seem to depend slightly on the particular crystal used.

For these measurements a clear crystal of dimensions approximately 3 mm × 4 mm × 12 mm was used, with a polished aluminum reflector. The crystal was suspended just above the surface of a 1″ diameter photomultiplier (Du Mont 6467) without any fluid or grease; it was located at about the centre of a hemispherical reflector of radius $\frac{1}{2}$″. The response of this crystal to a Na^{22} source is shown in fig. 2. The resolution obtainable was 11% for 3 MeV protons, 19% for 4 MeV alpha particles, and 22% for 0.662 MeV gammas. This resolution did not depend on the exact position and mounting of the crystal. However, consistently bad resolution was obtained whenever a crystal was wrapped closely in aluminum reflector and coupled closely to the face of the photomultiplier. The explanation for the relatively good resolution with the large reflector probably is simply that once light has

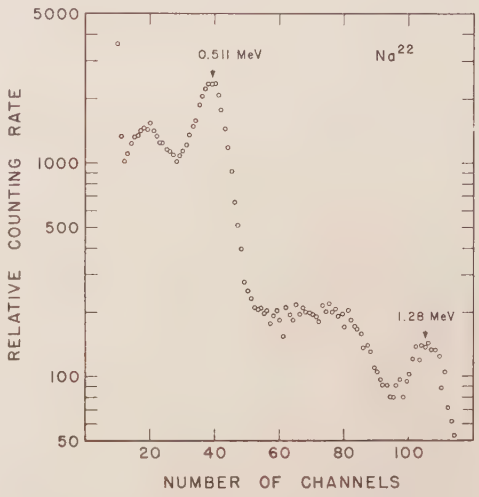

Fig. 2. Response of a calcium tungstate crystal to a Na^{22} gamma-ray source.

escaped from the crystal, it can be reflected onto the photocathode surface without having to traverse the crystal again. Difficulties with light trapping in calcium tungstate crystals because of the large index of refraction have been discussed previously by Gillette[2]).

In order to obtain the best resolution, a long time constant is needed to integrate the current from the photomultiplier, and there should be no short clipping times in the subsequent circuitry. We have used 2.2 megohms to give an integrating time of about 20μsec. Some difficulty may arise with the kicksorter if it is designed to analyze only pulses of short rise time. We have successfully used a Technical Measurement Corporation kicksorter (256 channels) to analyze these pulses.

3. Pulse-Shape Discrimination

Pulse-shape discrimination in calcium tungstate between alpha particles and gamma rays was first found by observing the ratio of pulse sizes with different clipping times in the amplifier. No significant effect was observed between protons and gamma-rays. The ratio α/γ increases

[4]) H. Kallmann, Research **2** (1949) 62.

[5]) G. F. J. Garlick and R. A. Fatehally, Phys. Rev. **75** (1949) 1446.

[6]) R. Bass, T. W. Bonner and H. P. Haenni, Bull. Amer. Phys. Soc. Series II, **5**, No. 4 (1960) 248.

with shorter clipping times, indicating a faster decay of the scintillations produced by alpha particles.

The pulse-shape effect was studied further by methods described by Litherland *et al.*[7]), Owen[8]) and Bormann *et al.*[9]). In the first method, a single channel analyzer operating on the pulses through a fast time constant ($\sim 1\ \mu$sec), was used to gate a kicksorter which was analyzing the pulses through the slow time constant ($\sim 20\ \mu$sec). Two peaks, due respectively to alpha particles and gamma rays, could be well separated, the most favourable ratio of peak positions being about 1.7. In the second method (in reality an extension of the first), the single channel analyzer was not used, the fast and slow pulses rather being stretched to have flat tops, and then applied to give horizontal and vertical deflections respectively on an oscilloscope (Tektronix 585). In addition, an intensifier pulse was generated to brighten the trace during the flat tops. The resulting sequence of dots on the oscilloscope screen was then photographed with a Polaroid camera. A set of photographs is shown in fig. 3. It clearly shows that alpha particles and gamma rays can be separated, although the statistical fluctuations, particularly in the fast pulse (horizontal), are rather large. Because of this, mono-energetic alpha-particles produce a group of dots extended more in the horizontal (fast) direction than in the vertical (slow) direction.

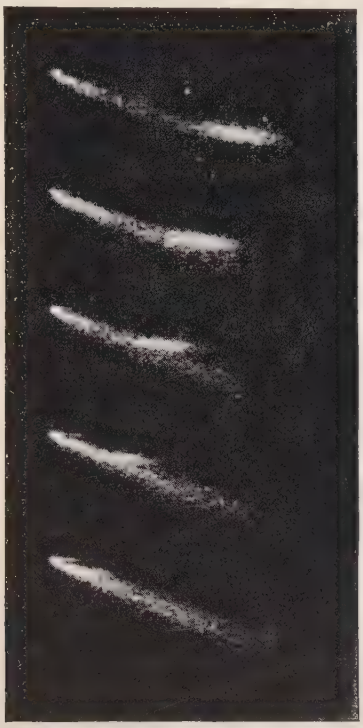

Fig. 3.

Fig. 3. Pulse-shape discrimination in calcium tungstate between alpha particles and gamma rays from a Co^{60} source, as shown by the oscilloscope dot method. The approximate alpha-particle energies are, in order, 4.3, 3.7, 3.1, 2.4 and 1.6 MeV.

Fig. 4. Pulse-shape discrimination in calcium tungstate between alpha particles and gamma rays from a Co^{60} source, by use of a difference amplifier. The approximate alpha-particle energies are (a) 3.5 MeV (b) 2.7 MeV. The solid curves are with discrimination, the dashed without.

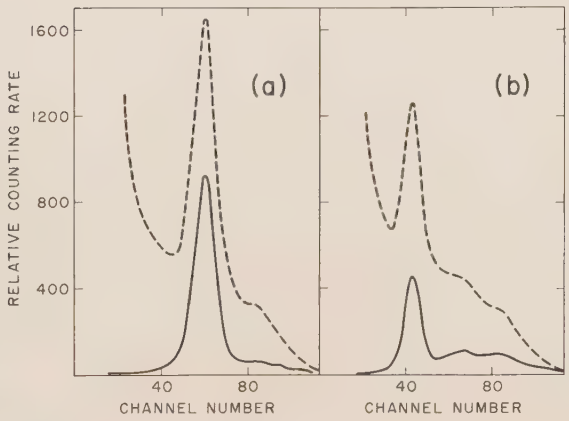

Fig. 4.

In the third method the fast pulse and the slow pulse were amplified and fed to a difference amplifier, whose output was used to gate the kicksorter analyzing the slow pulses. The difference amplifier was similar to a circuit shown by Owen[8]); it consisted of a double triode (6J6),

[7]) A. E. Litherland, E. Almqvist, R. Batchelor and H. E. Gove, Phys. Rev. Letters **2** (1959) 104.

[8]) R. B. Owen, Nucleonics **17**, No. 9 (1959) 92.

[9]) M. Bormann, G. Andersson-Lindström, H. Neuert and H. Pollehn, Zeits. f. Naturforsch. **14**a (1959) 681.

with, however, separate inputs from the two amplifiers, and with a 5 μsec delay line to delay the fast pulse. The amplitude of the slow pulse could be varied to obtain the optimum discrimination. Fig. 4 shows the spectrum of pulses due to combined source of Po^{210} alpha particles and Co^{60} gamma rays, with and without pulse-shape discrimination. Statistical fluctuations limit the separation possible; the gamma rays can be completely eliminated only by sacrificing many alpha-particle pulses as well.

No separation of proton and gamma-ray pulses was achieved by these methods.

4. Further Discussion

The scintillation process in calcium tungstate is not well understood. Gillette[2]) found that the initial decay time was 0.5 μsec, but that there were one or more subsidiary peaks of less than one-third the height of the initial pulse. Belcher[10]) refers to a phosphorescence with an exponential decay of half-life 20 μsec. Jordan and Bell[11]) observe only a long decay with time constant about 10 μsec. Cook and Mahmoud[12]) observe a phosphorescence of decay constant 15 μsec, with a primary pulse cleanly separated from subsidiary pulses. More recently Kallmann and Brucker[13]) report a decay time of 3.1 μsec for α-excitation and 3.2 μsec for β-excitation, while Beard and Kelly[3]) have apparently confirmed this result, obtaining 3.3 μsec for both kinds of excitation. It should also be mentioned that if calcium tungstate is irradiated with high intensities, a phosphorescence of the order of minutes is observed[2,14]).

Observations which we have made on the shape of the "current" pulse—taken with a load time constant of about 0.2 μsec—seem to indicate a decay time between 5 and 10 μsec. The pulse is very jagged, but it is not clear that one should interpret this as a primary pulse followed by a sequence of secondary pulses. We have checked that there were no significant number of after-pulses in the photomultiplier, and the crystal had been kept quiescent in the dark for several days, so that there should have been no significant effect from the long phosphorescence noted above. Further observations on the fully integrated pulse—taken with a load time constant of about 400 μsec—show that the time required for an alpha-particle pulse to reach $(1 - e^{-1})$ of its final amplitude is 5 μsec.

Finally we wish to remark that the time required for the pulse to reach its maximum value can be used as a parameter to distinguish between particles, provided that a suitable load time constant is chosen[9]). For example, if the load time constant is such that the time to reach the maximum is 3.5 μsec, then we have found that alpha-particle pulses reach their maximum at a time about 10 % earlier than do proton and gamma-ray pulses.

The authors are indebted to Dr. G. G. Eichholz for the loan of some calcium tungstate crystals.

[10]) E. H. Belcher, Nature **166** (1950) 742.
[11]) W. H. Jordan and P. R. Bell, Nucleonics **5**, No. 4 (1949) 30.
[12]) J. R. Cook and K. A. Mahmoud, Proc. Phys. Soc. **67** B (1954) 817.
[13]) H. Kallmann and G. J. Brucker, Phys. Rev. **108** (1957) 1122.
[14]) J. R. Cook, Proc. Phys. Soc. **71** (1958) 422.

NUCLEAR INSTRUMENTS AND METHODS 9 (1960) 233–241; NORTH-HOLLAND PUBLISHING CO.

LA STABILISATION DU CHAMP MAGNETIQUE PAR UN MASER A RESONANCE MAGNETIQUE NUCLEAIRE (I)†

P. GRIVET et H. HAHN

Laboratoire d'Electronique et de Radioélectricité de la Faculté des Sciences de l'Université de Paris; B.P. no 9, Fontenay-aux-Roses, Seine

Reçu le 18 mai 1960

We present the description of a new system for regulating the magnetic field of an electromagnet, with an accuracy significantly superior to the limit accessible with a current regulator. The essential element is a nuclear resonance maser using a liquid stream for linking the magnetic field with the frequency of a radio signal generated by the maser.

In the first part we describe the structure and the relevant properties of this peculiar form of maser. The theory is compared with the measured values obtained with the equipment which will be described in part II.

1. Introduction

Dans de nombreux domaines de la physique appliquée, il est essentiel de pouvoir disposer d'un champ magnétique très stable et d'en connaître la valeur. C'est ainsi qu'il existe déjà un très grand nombre de publications qui, toutes, proposent une série de solutions.

Les travaux, effectués par Benoit, Fric *et coll.* dans notre laboratoire et aboutissant à la réalisation d'un auto-oscillateur de type maser à résonance magnétique nucléaire (RMN)[1–6], nous ont amenés à tenter de mesurer et de stabiliser un champ magnétique à l'aide de ce nouveau dispositif. Les deux problèmes sont étroitement liés car tout appareil permettant la mesure continue du champ magnétique peut facilement s'adapter à un système stabilisateur. Notre système de régulation est donc constitué de trois parties fondamentales:

— Un maser qui effectue la conversion du champ magnétique, la grandeur à régler, en une grandeur plus facile à mesurer par les méthodes classiques de l'électronique: la fréquence d'oscillation du maser.

— Un organe comparateur qui produit la tension d'erreur pour un écart entre la valeur de la grandeur à régler et sa valeur désirée. Celle-ci est donnée par la grandeur de référence, qui est une fréquence.

— Un organe de réaction, capable de réagir sur le champ magnétique, et commandé par la tension d'erreur, de façon à réduire l'écart.

Voici, en bref, les caractéristiques essentielles de ces élements. La pulsation ω_m du maser est pratiquement asservie au champ magnétique B_0 par la relation, écrite dans le système MKSA, que nous emploierons exclusivement dans ce mémoire:

$$\omega_m \cong \gamma B_0$$

avec le rapport gyromagnétique,

$$\gamma = (267.51 \pm 0.002) \times 10^6 \frac{1}{\text{sec Ts}} \quad \text{pour } H_1^1\ ^{7}) .$$

Avec ce dispositif on peut ramener la mesure d'un champ à celle d'une fréquence. La réalisation d'un fréquencemètre HF[8]) nous a permis de

† This is an abridged text of the "3d cycle" thesis, submitted by H. Hahn, to the Faculté of Paris.

[1]) H. Benoit, CR Acad. Sci. Paris **246** (1958) 3053.
[2]) H. Benoit, Thèse, Paris, 1959.
[3]) H. Benoit et C. Fric, CR Acad. Sci. Paris **249** (1959) 537.
[4]) H. Benoit, P. Grivet et L. Guibe, CR Acad. Sci. Paris, **246** (1958) 3608.
[5]) H. Benoit, P. Grivet, L. Guibe et M. Sauzade, Jour. Phys. Rad. (novembre 1958) 905.
[6]) C. Fric, CR Acad. Sci. Paris **249** (1959) 80.
[7]) P. L. Bender et R. L. Driscoll, IRE Transactions on Instrumentation **1** no. 7 (1958) 176.
[8]) H. Hahn, CR Acad. Sci. Paris **249** (1959) 1199.

mesurer et d'enregistrer l'évolution d'un champ magnétique[9]).

La tension de sortie du fréquencemètre est proportionnelle à l'écart entre la fréquence du maser et une fréquence de référence stabilisée par un quartz; cette tension est susceptible d'être prise comme signal d'erreur dans une boucle de contreréaction, diminuant ainsi la dérive résiduelle[10]).

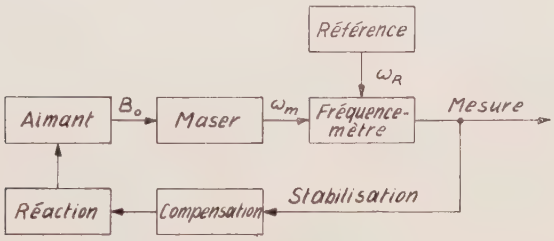

Fig. 1. Mesure et stabilisation du champ magnétique par un maser à RMN.

Le principe du fonctionnement de notre dispositif est montré par le schéma de la fig. 1. Les détails de chaque élément de la chaîne seront donnés dans les chapitres suivants.

2. La Mesure d'un Champ Magnétique par un Maser à RMN

2.1. MESURES PRELIMINAIRES

Dans nos expériences, il nous arrive souvent d'avoir à mesurer un champ avec une précision plus ou moins grande. Nous avons effectué ces mesures par la méthode classique de RMN, puisque le même dispositif peut fonctionner également en autodyne et en maser.

Pour effectuer des mesures d'après ce principe, la fréquence de l'autodyne est modulée par la BF autour d'une valeur $f_c = \omega_c/2\pi$. On cherche le signal de résonance en faisant varier l'amplitude de balayage. Lorsque le signal de résonance est bien centré sur l'écran de l'oscilloscope, ce qui est le cas pour $\omega_c = \omega_0 = \gamma B_0$, on effectue la mesure de la fréquence à l'aide d'un hétérodyne HF industriel, le balayage étant coupé.

Le signal de résonance est une courbe d'absorption, qui montre des battements (wiggles), dus au passage non-adiabatique par la résonance. Nous avons même pu constater[11]) l'effet Gooden-Gabillard[12]) car la stabilité du champ de

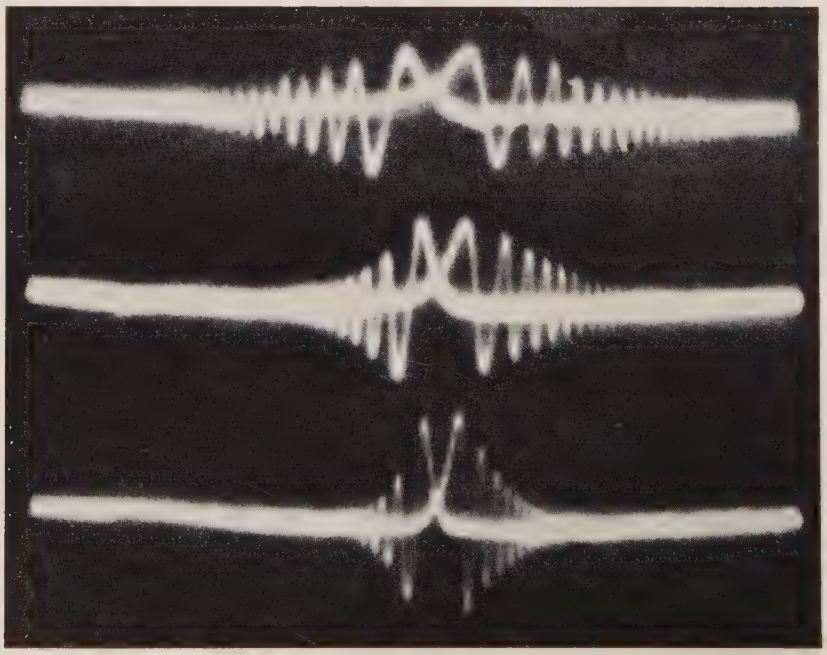

Fig. 2. Raies de résonance pour eau en mouvement; balayage triangulaire.

[9]) C. Fric et H. Hahn, CR Acad. Sci. Paris **250** (1960) 680.
[10]) H. Hahn, CR Acad. Sci. Paris **250** (1960) 2335.
[11]) C. Fric et H. Hahn, CR Acad. Sci. Paris **250** (1960) 1471.
[12]) R. Gabillard, Thèse Paris 1952; et "La résonance paramagnétique nucléaire" (Editions du CNRS, Paris, 1955) 36 et 135.

l'aimant préstabilisé était suffisante, c'est-à-dire que sa dérive restait inférieure à $10^{-5}\ B_0$/sec.

La raie de résonance dans le cas d'un balayage rapide permet la mesure directe du temps de relaxation transversale T_2, en utilisant la décroissance exponentielle du signal[12]). L'enveloppe des battements, après le passage par la résonance, est donnée par la formule:

$$a = A_0\, e^{-t/T_2}\ .$$

Nous avons trouvé pour le temps de relaxation transversale, en tenant compte de l'inhomogénéité locale du champ directeur et du mouvement du liquide, qui correspondent aux conditions du fonctionnement en maser, la valeur moyenne:

$$T_2 = 1.3 \times 10^{-3}\ \text{sec.}$$

L'écart moyen quadratique $\sqrt{\langle \delta B_0^2 \rangle}$ du champ

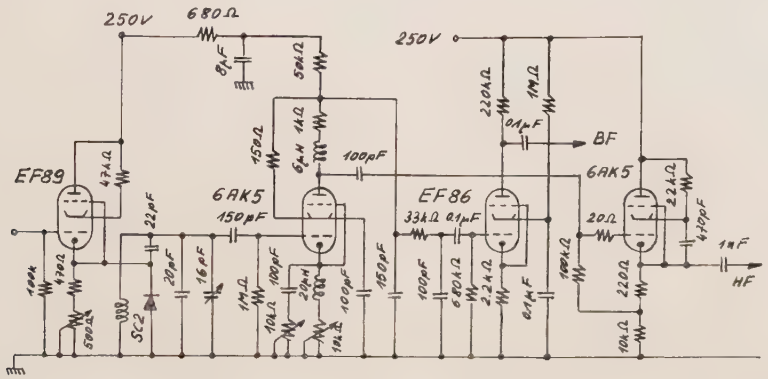

Fig. 3. Oscillateur autodyne à modulation de fréquence.

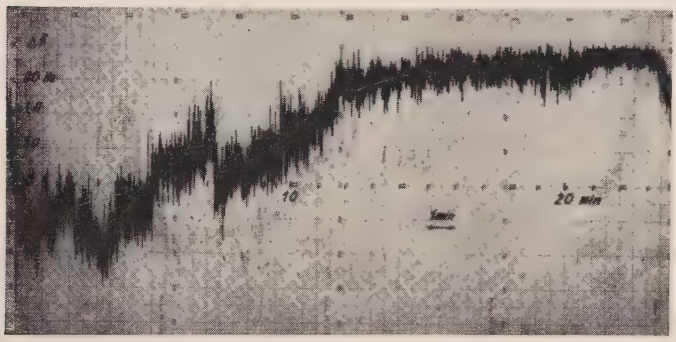

Fig. 4. Stabilité de fréquence de l'oscillateur autodyne.

Les battements† avant le passage par la résosonance et dus à la mémoire de phase ont ici disparu, puisque le liquide est en mouvement et ne séjourne pas assez longtemps dans la bobine. Nous avons utilisé les photos de la fig. 2 qui ont été prises avec un balayage triangulaire, correspondant à une fréquence de 25, 50, 100 Hz, ce qui assure un étalonnage linéaire en temps. La représentation logarithmique de l'enveloppe est une droite de pente $1/T_2$.

† Ce sont ces battements qui constituent l'effet Gooden-Gabillard.

dans l'échantillon qui correspond à cette valeur de T_2 est donné par la formule[13]):

$$\sqrt{\langle \delta B_0^2 \rangle} \cong \frac{1}{\gamma T_2} = 30 \times 10^{-7}\ \text{Ts}\ .$$

Pour obtenir le signal de résonance nous avons utilisé le dispositif de Fric[6]) où le condensateur vibrant était remplacé par une diode à capacité variable[14]). Les perturbations microphoniques

[13]) P. Grivet, Rev. Gén. Electr. (juillet 1958) 365.

[14]) D. A. Jennings et W. H. Tanttila, Rev. Sci. Instr. **30** (1959) 137.

ont ainsi pratiquement disparu. Le circuit de l'autodyne est représenté sur la fig. 3. C'est une variation des circuits employés par Hopkins[15]) et Wang[16]).

Le fréquencemètre, décrit au chapitre 3, nous a permis de mesurer la stabilité de fréquence de l'autodyne, fonctionnant en oscillateur normal. L'enregistrement de la fig. 4 nous montre qu'il y a des fluctuations à court terme de $\pm$ 10 Hz et une dérive de 100 Hz par 20 min.

2.2. DESCRIPTION QUALITATIVE DU MASER[1–6])

2.2.1. L'arrangement géométrique du maser à RMN est montré sur la Fig. 5. Dans cette méthode on utilise comme source HF l'émission stimulée des signaux de protons dans un courant d'eau dont on a retourné le sens du moment magnétique macroscopique par une excitation en passage rapide.

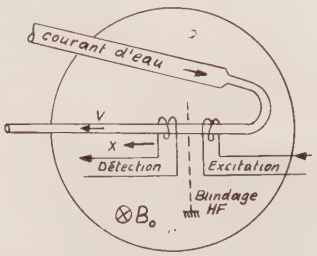

Fig. 5. Schéma de principe du maser à RMN d'après[1]).

2.2.2. Avant de passer par la bobine d'excitation l'eau séjourne dans l'entrefer de l'électroaimant pendant un temps grand devant T_1, temps de relaxation longitudinal, pour que le moment magnétique macroscopique dû au paramagnétisme nucléaire ordinaire puisse s'établir.

2.2.3. La bobine d'excitation est placé perpendiculairement au champ directeur dans une partie de l'entrefer où le champ a un gradient radial. Elle est attaquée par une tension dont la fréquence correspond à la valeur moyenne du champ directeur règnant dans la bobine; dans nos expériences elle est de 29 MHz. En parcourant la bobine, un élément de volume du liquide subit donc un balayage du champ magnétique autour de sa valeur de résonance en passage adiabatique rapide. Si les conditions ci-après sont satisfaites, son moment magnétique macroscopique sera retourné par ce passage; autrement dit, on dispose maintenant d'un courant d'eau où la température de spin des protons est négative.

La première condition garantit un passage adiabatique et s'écrit sous la forme

$$v \frac{\partial B_0}{\partial r} \ll \gamma B_1^2$$

$\partial B_0/\partial r$ = gradient radial du champ directeur

B_1 = champ magnétique de la HF

v = vitesse d'écoulement.

Il y a plusieurs conditions relatives au passage rapide, mais la plus sevère est

$$\gamma B_1 \gg \frac{1}{T_2}.$$

Les deux conditions obligent à appliquer des champs HF très forts et limitent la méthode à des substances à temps de relaxation grands. En réalité le retournement ne sera pas parfait et le moment magnétique par unité de volume après le passage sera de:

$$M_z = -FM_0$$

F = Facteur de retournement ($\simeq 0.8$)
M_0 = moment magnétique correspondant à l'équilibre thermique et donné par la formule de Brillouin[17]). Son approximation pour des températures ordinaires s'écrit:

$$M_0 = \frac{N\mu_I^2}{3kT} \frac{I+1}{I} B_0 = \chi H_0$$

χ = susceptibilité en volume statique
= $4\pi\, 3.3 \times 10^{-10}$ pour les protons dans l'eau à 18°C.

Par définition[17]) la température de spin des noyaux T_{sp} et la température du réseau de la substance T_{sub}, qui est normalement la température ambiante, sont liées par l'équation:

$$T_{sp} = \frac{M_0}{M_z} T_{sub} = -\frac{1}{F} T_{sub}.$$

[15]) N. J. Hopkins, Rev. Sci. Instr. **20** (1949) 401.
[16]) T. C. Wang, Phys. Rev. **99** (1955) 566.
[17]) G. Laukien, Handbuch der Physik **38**/1 (Springer, éd., Berlin, 1958); ou P. Grivet "La résonance paramagnétique nucléaire" (éditions du CNRS).

Après cette perturbation de l'état d'équilibre thermique, le système a tendance à le retrouver avec la constante de temps T_1. Le temps de parcours τ, que met l'élément de volume considéré pour gagner la bobine de détection, devrait être petit devant ce temps de relaxation

$$\tau \ll T_1 .$$

Les composantes du moment magnétique perpendiculaire au champ directeur, qui pourraient subsister après l'excitation, ont sûrement disparu lorsque l'eau atteint la deuxième bobine, car les inhomogénéités du champ directeur et l'écoulement d'eau concourrent à leur suppression complète.

Le champ directeur peut changer un peu sa valeur sans que le retournement cesse. C'est seulement l'endroit où se produit la résonance, qui se déplace le long de la bobine.

2.2.4. L'eau à moment magnétique retourné ou encore à température de spin négative traverse ensuite la bobine détectrice du maser. La bobine perpendiculaire au champ directeur, ici très homogène, fait partie d'un circuit oscillant à fort coefficient de surtension.

Supposons qu'il y ait dans cette bobine, parfaitement découplée de la première, un champ magnétique HF d'une fréquence f_m qui corresponde à la fréquence de précession f_0, définie par le champ directeur local. On se trouve donc dans les conditions propices à une émission stimulée[18]). La probabilité de transition en émission spontanée est négligeable pour les fréquences en question; c'est pourquoi le temps de relaxation T_2 reste le même dans les expériences d'absorption et d'émission. Les protons reviennent à l'état d'équilibre en émettant un rayonnement à la fréquence d'excitation, fournissant ainsi de l'énergie au champ HF. Si les pertes du circuit sont assez faibles, il peut donc exister une oscillation, dont l'énergie est fournie exclusivement par les protons. On a le comportement typique d'un auto-oscillateur du type maser.

La fréquence de cette oscillation est déterminée par le champ magnétique à un certain entraînement (pulling) près, dû au désaccord du circuit oscillant. La fréquence du maser suit le champ magnétique instantanément, si la dérive du champ est suffisamment petite pour que l'on puisse toujours supposer un régime stationnaire de l'oscillation. En pratique cette condition sera toujours satisfaite pour un aimant préstabilisé.

Le facteur de surtension très élevé peut être atteint en augmentant le coefficient de surtension naturel Q_i d'un circuit oscillant normal par réaction positive avec un seul tube qui travaille donc en multiplicateur de Q. Nous avons fait nos expériences avec le montage de Fric qui ne se distingue que par les détails de l'autodyne décrit au chapitre 2.1. La réaction est rendue variable pour que l'on puisse toujours rester un peu au-dessous de la limite d'accrochage parasite. Une variation de l'alimentation permet un réglage fin du coefficient de surtension artificiel Q.

2.2.5. Etant donné que le montage de l'autodyne est un récepteur très sensible, la mesure du Q se fait en recevant le signal d'un générateur dont la fréquence est accordée sur le circuit oscillant de l'autodyne. Le couplage du générateur est assez faible pour que le Q ne soit pas modifié. Pour cette mesure, l'autodyne est branché comme pour la mesure d'un champ et balayé en fréquence. On décrit alors sur l'écran de l'oscilloscope la courbe de surtension du circuit oscillant. Le balayage étant étalonné, on trouve facilement la largeur a mi-hauteur Δf_h, d'où le facteur de surtension par la formule:

$$Q = \sqrt{3}\,\frac{f_0}{\Delta f_h} .$$

Nous avons travaillé normalement avec un Q qui correspond à des valeurs

$$\Delta f_h = 28 \text{ kHz}$$
$$Q \cong 18\,500 .$$

2.3. L'ENTRAINEMENT DE LA FREQUENCE

2.3.1. Pour les calculs de ce chapitre nous envisagerons la RMN sous son aspect macroscopique, décrit par les équations de Bloch[17]):

$$T_2\dot{M}_x + M_x = \gamma T_2(M_y B_z - M_z B_y)$$

$$T_2\dot{M}_y + M_y = \gamma T_2(M_z B_x - M_x B_z)$$

$$T_1\dot{M}_z + M_z = \gamma T_1(M_x B_y - M_y B_x) + M_0$$

[18]) H. Wolf, Z. ang. Phys. (octobre 1958) 480.

valable pour

$$B_z = B_0 \gg B_x , B_y$$

avec

$$M_0 = \chi H_0$$

M_x, M_y, M_z } vecteur du moment magnétique par unité de volume = intensité d'aimantation.

Les calculs suivants dont Vladimirsky[19]) a fourni le premier principe, donnent alors l'expression de la condition d'oscillation, la plage d'accrochage, la fréquence d'oscillation, si le circuit oscillant est légèrement désaccordé. Pour ce calcul, on suppose que la bobine contient un échantillon au repos, à moment magnétique initialement retourné. Les propriétés de l'échantillon seront décrites par les équations de Bloch. Le circuit oscillant restant toujours un élément passif, le champ HF B_x est créé par des courants induits, couplés au moment magnétique. En tenant compte de ce couplage on obtient le système des équations différentielles qui représentent le mouvement du moment magnétique macroscopique:

$$T_2\dot{M}_x + M_x - \omega_0 T_2 M_y = 0$$

$$\omega_0 T_2 M_x + T_2\dot{M}_y + M_y - \gamma B_x T_2 M_z = 0$$

$$\gamma B_x T_1 M_y + T_1\dot{M}_z + M_z = M_0$$

$$Q\ddot{B}_x + \omega_0\dot{B}_x + \frac{Q}{LC} B_x + \mu_0\eta Q\ddot{M}_x = 0$$

avec

$$\omega_0 = \gamma B_0 ,$$

$$\frac{1}{LC} = (\omega_0 + \Delta\omega_c)^2 = \omega_c^2$$

Q = facteur de surtension artificiel du circuit oscillant.
η = coefficient de remplissage de la bobine.

[19]) K. V. Vladimirsky, Nucl. Instr. 1 (1957) 329.

Si les conditions initiales sont:

$$M_x = M_y = B_x = 0 , \qquad M_z = -FM_0$$

le système a alors la solution évidente:

$$M_{x0} = M_{y0} = B_{x0} = 0,$$

$$M_{z0} = M_0 - (1 + F) M_0 \, e^{-t/T_1} .$$

On étudie sa stabilité par un calcul de perturbation, c'est-à-dire que l'on s'intéresse au comportement des petites variations (δM_x, δM_y, δM_z, δB_x) de cette solution.

Après linéarisation et application de la transformation de Laplace on trouve le système de 4 équations, écrit dans le schéma suivant:

δM_x	δM_y	δB_x	δM_z	=
$1 + pT_2$	$-\omega_0 T_2$	0	0	0
$\omega_0 T_2$	$1 + pT_2$	$-\gamma T_2 M_{z0}$	0	0
$\mu_0\eta Q p^2$	0	$Qp^2 + \omega_0 p + \frac{Q}{LC}$	0	0
0	0	0	$1 + pT_1$	0

2.3.2. Par élimination de δM_y et en tenant compte du fait que le facteur $(1 + pT_1)$ ne peut pas introduire une instabilité, nous pouvons montrer que le maser à protons est régi par un système de deux équations:

— La première décrit les propriétés de l'échantillon, exposé à un champ magnétique HF,

— La deuxième donne les propriétés du circuit oscillant, excité par une variation du moment magnétique macroscopique.

L'avantage de cette représentation est de montrer directement la signification physique des différentes grandeurs, surtout celle du coefficient de surtension nucléaire Q_n. De plus, elle permet de trouver, sans peine, les formules pour les conditions d'accrochage et d'entraînement. A titre d'exemple nous donnons le système d'équations pour un seul circuit oscillant. (Tableau p. 239.)

Le coefficient de surtension nucléaire Q_n est dans nos expériences de 130000.

Il peut y avoir une oscillation sur la pulsation ω_m, qui est très proche de la pulsation de précession ω_0, si la déterminante disparaît:

$\mu_0\delta M_x$	δB_x	$=$
$a_{11} = \frac{1}{Q_n} + \left(\frac{p}{\omega_0} + \frac{\omega_0}{p}\right)$	$a_{12} = \frac{\omega_0}{p}\chi F$	0
$a_{21} = \frac{p}{\omega_0}\eta$	$a_{22} = \frac{1}{Q} + \left(\frac{p}{\omega_0} + \frac{\omega_0}{p}\frac{1}{\omega_0^2 LC}\right)$	0

avec $Q_n = \frac{1}{2}\omega_0 T_2$

$$D(p_m) = a_{11}a_{22} - a_{12}a_{21} = 0$$
$$\text{pour} \quad p_m = j\omega_m = j(\omega_0 + \Delta\omega_0) .$$

L'expression pour la condition d'accrochage est alors:

$$a_{12}a_{21} \geqslant |\, a_{11} \,|\, |\, a_{22} \,| .$$

L'entraînement est donné par la formule:

$$\measuredangle\, a_{11} + \measuredangle\, a_{22} = 0 .$$

Cela veut dire qu'un déphasage du circuit électrique doit être compensé par le "circuit nucléaire".

2.3.3. La condition d'accrochage s'exprime sous la forme:

$$-\mu_0\gamma\eta M_{z0} = \eta\chi F \geqslant \frac{1}{Q_n Q}\left\{1 + \left(\frac{Q_n Q}{Q_n + Q}\frac{2\Delta\omega_c}{\omega_0}\right)^2\right\} .$$

Des oscillations ne sont possibles que pour un moment magnétique retourné, $M_{z0} < 0$. Le facteur de surtension limite Q_1, donnant encore des oscillations pour un circuit parfaitement accordé, est de:

$$Q_1 = \frac{1}{\eta\chi F Q_n} .$$

Le facteur $F\chi$ est la susceptibilité des protons dans l'eau à la température $|\, T_{spin} \,|$.

Les valeurs numériques sont dans notre cas:

$\chi = 4\pi\, 3.3 \times 10^{-10}$ $\qquad$ $Q_n = 130\,000$

$F \cong 0.8$ $\qquad$ $Q_1 \cong 4\,000$.

$\eta \cong 0.6$

Cette valeur de la surtension limite est inférieure à la valeur de $Q = 18500$ que nous pouvons atteindre avec le multiplicateur de Q.

2.3.4. On trouve l'approximation pour l'entrainement $\Delta\omega_0$, s'il y a un désaccord du circuit oscillant $\Delta\omega_c$ par rapport à ω_0, à partir de la relation:

$$Q_n\,\Delta\omega_0 + Q(\Delta\omega_0 - \Delta\omega_c) = 0$$

d'où

$$\Delta\omega_0 = \frac{Q}{Q_n + Q}\Delta\omega_c$$

et la pulsation de l'oscillation du maser

$$\omega_m = \omega_0 + \frac{Q}{Q_n + Q}\Delta\omega_c .$$

Les valeurs numériques, déterminées à partir de l'équation précédente et vérifiées par une mesure directe, sont pour un fonctionnement normal du maser de:

$$\Delta\omega_0 = \tfrac{1}{8}\,\Delta\omega_c .$$

On pourrait réduire l'effet de l'entraînement en augmentant T_2 par un champ plus homogène. La limite pour T_2 serait alors le temps de séjour de l'eau dans la bobine[2]). Les améliorations apportées par un T_2 plus grand sont proportionnelles au carré de T_2, puisque cela permettrait aussi de diminuer le Q du circuit oscillant.

2.4 SUPPRESSION DE L'ENTRAINEMENT

Il existe une autre possibilité de réduire et même de supprimer l'effet de l'entraînement en employant deux circuits oscillants couplés. Cette méthode est analogue à celle utilisée pour les masers à ammoniac[20]). On suppose que le circuit oscillant (L_1, C_1, Q_1), seul parcouru par l'eau, est couplé par induction mutuelle (M) à un autre circuit oscillant (L_2, C_2, Q_2).

Nous avons ici à la base de l'analyse les équations de Bloch, complétées par deux autres qui décrivent le circuit électrique:

[20]) J. Bonanomi, J. Hermann, J. DePrins, P. Kartaschoff, Rev. Sci. Instr. (nov. 1957) 879.

$$Q_1\frac{M}{L_1}\ddot{B}_2 + Q_1\ddot{B}_x + \omega_0\dot{B}_x + Q_1\frac{1}{L_1C_1}B_x + \mu_0\eta Q_1\ddot{M}_x = 0$$

$$Q_2\frac{M}{L_2}\ddot{B}_x + Q_2\ddot{B}_2 + \omega_0\dot{B}_2 + Q_2\frac{1}{L_2C_2}B_2 = 0\,.$$

En appliquant la même methode que pour le circuit simple, nous retrouvons pourtant à la fin le même système d'équations. Ce n'est que le coefficient a_{22} qui a changé, car lui seul contient toutes les propriétés du circuit électrique du maser.

$$a_{22} = \frac{1}{Q_1} + \left(\frac{p}{\omega_0} + \frac{\omega_0}{p}\frac{1}{\omega_0^2L_1C_1}\right) - k^2\frac{(p/\omega_0)^2}{\frac{1}{Q_2} + \left(\frac{p}{\omega_0} + \frac{\omega_0}{p}\frac{1}{\omega_0^2L_2C_2}\right)}$$

avec le facteur de couplage:

$$k^2 = \frac{M^2}{L_1L_2}\,.$$

Dès maintenant nous admettons la simplification:

$$\omega_c^2 = \frac{1}{L_1C_1} = \frac{1}{L_2C_2}\,.$$

La condition d'accrochage, pour le cas d'un parfait accord $\omega_c = \omega_0$, est de:

$$\chi F\eta \geqslant \frac{1}{Q_nQ_1}(1 + k^2Q_1Q_2)\,.$$

Cette formule reflète le fait physique, que la puissance dissipée dans le deuxième circuit oscillant doit être également fournie par les protons de l'eau.

L'entraînement de fréquence $\Delta\omega_0$, dû à un faible désaccord $\Delta\omega_c$ des circuits oscillants, est donné en première approximation par la formule:

$$Q_n\Delta\omega_0 + Q_1\frac{1 - k^2Q_2^2}{1 + k^2Q_1Q_2}(\Delta\omega_0 - \Delta\omega_c) = 0\,.$$

Nous pouvons faire disparaître l'entraînement par un choix particulier du couplage:

$$k = \frac{1}{Q_2}\,.$$

C'est le couplage "critique" classique lorsque $Q_1 = Q_2$.

Ici, la condition d'accrochage devient:

$$\chi F\eta \geqslant \frac{1}{Q_nQ_1}\left(1 + \frac{Q_1}{Q_2}\right)$$

d'où l'intérêt d'un Q_2 très grand.

2.5. PRECISION DE LA MESURE

2.5.1. L'entraînement de fréquence est un effet important, puisqu'il représente la limite effective de la précision de la mesure d'un champ magnétique, basée sur la mesure de la fréquence d'un maser piloté par le champ. L'influence de l'entraînement s'explique plus facilement à l'aide d'une formule, identique à la précédente mais sous une autre forme, qui définit la fréquence du maser f_m comme barycentre de la fréquence de résonance du circuit oscillant f_c et de la fréquence de précession f_0 des protons affectées de leurs coefficients de surtension respectifs:

$$f_m = \frac{Q_nf_0 + Qf_c}{Q_n + Q}\,.$$

Le champ magnétique est donc lié à la fréquence d'oscillation du maser, qui est seule mesurable, par l'équation:

$$f_m = \left(1 - \frac{Q}{Q_n + Q}\right)\frac{\gamma}{2\pi}B_0 + \frac{Q}{Q_n + Q}f_c$$

avec $Q_n = \frac{1}{2}\gamma B_0T_2\,.$

Nous nous sommes bornés à des mesures relatives du champ magnétique, c'est-à-dire que nous nous sommes contentés de déterminer les petites variations par rapport à une valeur fixe.

La variation de fréquence du maser δf_m, due à une derive du champ δB_0, est donnée, en tenant compte d'une fluctuation éventuelle de la fréquence de résonance δf_c, par la formule:

$$\delta f_m = \left(1 - \frac{Q}{Q_n + Q}\right)\frac{\gamma}{2\pi}\delta B_0 + \frac{Q}{Q_n + Q}\delta f_c\,.$$

Ici on peut supposer Q_n constant.

2.5.2. Pour un circuit oscillant parfaitement stable ($\delta f_c = 0$), la variation du champ magnétique δB_0 est donnée par la formule:

$$\frac{\gamma}{2\pi}\delta B_0 = \left(1 + \frac{Q}{Q_n}\right)\delta f_m\,.$$

Et pour les conditions dans lesquelles nous travaillons:

$$\frac{\gamma}{2\pi}\delta B_0 = 1.15\,\delta f_m\,.$$

Nous voyons donc, que nous faisions une erreur de 15% en négligeant l'entraînement et en employant la formule trop simple, que nous avions signalée dans l'introduction:

$$\left(\frac{\gamma}{2\pi}\delta B_0 \cong \delta f_m\right).$$

2.5.3. En pratique la fréquence de résonance du circuit oscillant n'est pas tout à fait stable. Nous avons évalué au chapitre 2.1 la valeur de $|\delta f_c|$ par son fonctionnement en oscillateur. Il faut compter avec une fluctuation rapide de $\pm$ 10 Hz et une dérive lente de 100 Hz par 20 min. Le champ magnétique est donc donné en fonction du temps à partir d'une mesure de la fréquence du maser par la formule pratique, valable pour nos expériences:

$$\frac{\gamma}{2\pi}\delta B_0(t) = 1.15\,\delta f_m(t) \pm 1.3\text{ Hz} \pm 0.63\,\frac{t}{\text{min}}\text{ Hz}.$$

La mesure de la fréquence introduit, cependant, encore une certaine incertitude. En utilisant les résultats du chapitre suivant, on trouve finalement la formule pratique pour la mesure d'un champ magnétique à l'aide de notre dispositif:

$$\frac{\gamma}{2\pi}\delta B_0(t) = 1.15\,\delta f_m(t) \pm 1.5\text{ Hz} \pm 1\,\frac{t}{\text{min}}\text{ Hz}$$

$$\delta f_m(t) = \text{fréquence enregistrée}.$$

A titre d'exemple, nous montrons sur la fig. 6 l'enregistrement de la fréquence d'un maser pilotée par un champ magnétique stabilisé[21,9]). Nous pouvons en déduire que le champ a une stabilité sur 20 min de au moins:

$$(2.0 \pm 0.7) \times 10^{-6}.$$

qui supprime cette influence néfaste au détriment de la précision à court terme. Le fait que l'amplitude d'oscillation est très sensible à un désaccord Δf_c entre la fréquence de résonance du circuit oscillant f_c et la fréquence de précession f_0, nous permet de tenir cet écart très petit, en cherchant l'amplitude maxima par un règlage automatique ou à la main. Ce dernier procédé a l'inconvénient de nous obliger à surveiller de temps en temps (toutes les 10 minutes en pratique) l'amplitude des oscillations, et de nous faire retrouver la meilleure condition de fonctionnement pour le maser. En revanche, on peut ainsi tenir l'écart $\Delta f_c \leqslant 120$ Hz, ce qui équivaut à une incertitude sur la valeur du champ magnétique exprimée par la formule:

$$\frac{\gamma}{2\pi}\delta B_0 = 1.15\,\delta f_m \pm 15\text{ Hz}.$$

Cela correspond à une précision de $\pm 5 \times 10^{-7}$, indépendante de la durée de mesure. En tenant compte de l'incertitude introduite par la mesure de fréquence, on peut dire que nous sommes à même d'effectuer des mesures relatives d'un champ magnétique avec une précision de: $\pm 7 \times 10^{-7}$.

Conclusion

Ces premières expériences portaient sur un électro-aimant médiocre ($T_2 = 1.3$ ms) et de-

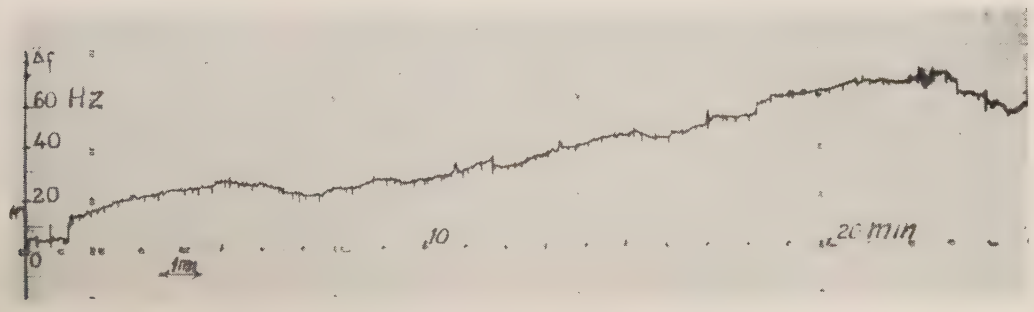

Fig. 6. Enregistrement d'un champ magnétique.

2.5.4. Pour des mesures qui s'étendent sur une longue période, l'altération du résultat due à la dérive du circuit oscillant devient inacceptable. Nous avons donc imaginé une méthode de mesure

viendraient beaucoup plus faciles avec un appareil de haute uniformité, comme ceux utilisés en spectroscopie de haute résolution, où l'on atteint facilement $T_2 = 0.1$ s. La précision du régulateur serait alors considérablement augmentée aussi.

[21]) C. Fric, CR Acad. Sci. Paris **246** (1958) 3602.

BOOK REVIEWS

WARD C. SANGREN. *Digital Computers and Nuclear Reactor Calculations*, John Wiley Sons Inc., New York. 208 pages, price $ 8.50.

Now, sixteen years after the first high speed digital computer, the Mark I, was completed, digital computers are an indispensable tool in almost every field of engineering and physical science. This very rapid development in the field of high speed calculations did not, however, allow scientists and engineers to become familiar with the use of digital computers. Only a minority of these scientists and engineers had the opportunity to learn the technique of programming or to follow lectures in numerical analysis or computer theory. On the contrary almost everybody should at least know what a digital computer "can" do and when such a powerful tool could advantageously be used. The lack of information about the use of digital computers was particularly eminent for technical people working in the nuclear reactor field.

With "Digital Computers and Nuclear Reactor Calculations", Ward C. Sangren presents a short, clear, and easily understandable introduction to the use of numerical analysis and digital computers in general and particularly to their application to high speed nuclear reactor calculations. The book is written in such a way that each of the chapters can be read independently and each of them can be well recommanded as an introduction to the special field discussed in it.

In chapter 1 the author makes first a brief survey of the history of nuclear reactors and digital computers. In the rest of this chapter he makes the reader familiar with general problems of nuclear reactors and digital computers. Chapters 2, 3 and 4 present a very nice introduction to digital computers, programming and numerical analysis. Chapter 2 deals with the structure of digital computers. Each of the basic units is discussed and up to date information about digital computers is presented. Chapter 3 introduces the reader to the technique of programming.

In chapter 4 the fundamentals of numerical analysis are discussed. Although the size of the book limits the discussion of the various methods outlined in this chapter, the author presents a very complete and interesting survey of them.

The last four chapters deal with the more important nuclear reactor calculations, e.g. fission-product poisoning, diffusion and age-diffusion calculations, solution of the transport equation, kinetics, burnout etc.. In addition, the Monte Carlo method is discussed as an example of a typical method of computer calculations (chapter 7: "Transport equation—Monte Carlo").

At the end of the book a very useful bibliography, divided according to the topics of the chapters as well as other special topics, has been added.

In conclusion, the present book can be well recommanded as an up to date introduction to the field of digital computers and nuclear reactor calculations. WERNER SCHNEIDER

WOLFGANG GRUHLE, *Elektronische Hilfsmittel des Physikers*, Springer-Verlag, Berlin, 1960. 200 Seiten mit 167 Abb., Gln. DM 29.60.

Unter "elektronischen Hilfsmitteln" versteht der Verfasser Apparate und Bausteine der Impulstechnik, wie sie vor allem in der Kernphysik allgemein angewendet werden. Das Buch soll dem Physiker eine Übersicht über die möglichen Lösungen elektronischer Probleme und damit die Unterlagen für den Entwurf und Eigenbau von Geräten geben, die für eine spezielle physikalische Aufgabenstellung erforderlich sind. Diesem Zweck entspricht die sinnvolle Gliederung des Buches in die folgenden Abschnitte: 1. Besprechung der Bauelemente, 2. Signalerzeugung, 3. Signalveränderung, 4. Signalkombination, 5. Signalregistrierung und 6. Strom- und Spannungsquellen. Im 1. Kapitel wird kurz die Wahl und Handhabung von Röhren, Halbleitern und Koaxialkabeln beschrieben. Der 2. Abschnitt befasst sich mit den verschiedenen Typen von elektronischen Schaltern und Röhrengeneratoren, dem Problem der Triggerung und den Strahlungsdetektoren. Das Kapitel über Signalveränderung ist zweckmässig unterteilt in Amplitudenveränderung, zeitliche Änderung des Impulses und Formänderung. Im 4. Kapitel werden die Methoden der Amplitudenkombination, die verschiedenen Koinzidenzverfahren, sowie die Amplituden- und Zeitinspektion behandelt. Der 5. Abschnitt beschreibt die Möglichkeiten der analogen und digitalen Registrierung. Die Vielkanalregistrierung wird nur prinzipiell erwähnt, da der Selbstbau hier kaum in Frage kommt. Abschliessend findet man im 6. Kapitel eine kurze Diskussion des Problems der Strom- und Spannungsstabilisierung.

Kennzeichnend für das Buch ist, dass es weder ein Lehrbuch der Elektronik sein will, noch fertige Schaltungen für einen bestimmten Apparat liefert. Der Verfasser setzt elementare Kenntnisse auf dem Gebiet der Elektronik voraus und verzichtet auf eine Herleitung der Formeln. Dagegen wird gezeigt, wie man an Hand der gegebenen Beziehungen eine Schaltung berechnen kann. Die einzelnen Kreise werden ausführlich in Bezug auf ihr impulstechnises Verhalten diskutiert. Stets weist der Verfasser auf die charakteristischen Schwierigkeiten einer Schaltung hin und macht Vorschläge zu ihrer Behebung. Die Schaltungen enthalten keine Wertangaben für die einzelnen Komponenten und können daher dem jeweiligen Verwendungszweck angepasst werden. Bei der Beschreibung der Kreise imponiert die klare Gliederung und die anschauliche Darstellung der Verhältnisse durch die zahlreichen Impulsdiagramme. Der Verfasser hat es verstanden, genau das Wesentliche zu sagen, was dem Bedarf des Physikers entspricht. Man läuft daher nicht Gefahr, sich "totzulesen", wie das in der Literatur über Elektronik zuweilen möglich ist. In diesem Sinne füllt das Buch eine für den Praktiker seit langem fühlbare Lücke. Mit vielen praktischen Ratschlägen zur Lösung einer elektronischen Aufgabe wendet sich das Buch auch an Studenten und Praktikanten, die mit der Planung und dem

Selbstbau elektronischer Geräte beschäftigt sind. Es sei jedoch ausdrücklich darauf hingewiesen, dass der Vefasser den Eigenbau von Geräten, die industriell angefertigt werden, nicht empfiehlt und das Buch mehr für die Fälle gedacht ist, in denen der Eigenbau unumgänglich ist. Nicht zuletzt auf Grund des ausführlichen Literaturverzeichnisses mit nicht weniger als 358 Hinweisen ist dieses Buch ein wertvoller Ratgeber für alle diejenigen, denen die Impulstechnik ein unentbehrliches Werkzeug ist.

E. MATTHIAS

J. G. LINHART: Plasma Physics (North-Holland Publ. Co., Amsterdam, 1960, xi + 278 p.).

The book begins with a derivation of the fundamental equations for a plasma, both considering the motion of single, charged particles, and using the fluid description. This is followed by a discussion of equilibrium and stability problems, oscillations, waves and transport phenomena. Relativistic cases are often included. The latter part of the book is devoted to a survey of the applications of plasma physics, mainly controlled fusion research, but also particle accelerators, space propulsion, etc. Pertaining to each chapter there are extensive reference lists. The author supports the definition of a plasma as a medium where $(n_e + n_{ions})/n_{neutrals} >> 1$, and thus ionization processes, etc. are not treated.

The author's intention has been to make a collection (for which there is a need, undoubtedly) in a textbook of material now scattered about in a number of books and original papers. In most cases there are also very thorough discussions of the problems, although they might sometimes have been given in a more stringent and concentrated form. Especially, large parts of the chapters on applications are somewhat circumlocutory. In addition, there are unfortunately a number of misprints and other trivial errors, some of which are corrected in an errata sheet.

LARS HÖGBERG

NEWS ITEMS

Preliminary Announcement

of the

1961 INTERNATIONAL CONFERENCE ON HIGH MAGNETIC FIELDS

to be held at the

MASSACHUSETTS INSTITUTE OF TECHNOLOGY

on the

1st, 2nd, 3rd of November 1961

Scope of Conference

It is the purpose of the conference to bring together scientists from a variety of research areas who are concerned with the generation and use of high magnetic fields. The areas will include primarily plasma physics, solid state physics, low temperature physics, nuclear physics, electronics. The emphasis in all papers should be on basic concepts and new techniques in the generation and experimental use of high magnetic fields. Invited papers will be aimed at reviewing the broad scope of the various specialized research programs, while contributed papers will be more specialized. Magnetic materials per se and the design of conventional magnets are not considered to be within the scope of the conference.

Conference Committee

Dr. Benjamin Lax, Massachusetts Institute of Technology, Chairman

Dr. Henry Kolm, Massachusetts Institute of Technology, Secretary

Professor Francis Bitter, Massachusetts Institute of Technology

Dr. Frederic H. Coensgen, Lawrence Radiation Lab., University of California

Dr. Wilhelm F. Gauster, Oak Ridge National Laboratory

Dr. Robert G. Mills, Princeton University.

In addition, distinguished scientists from abroad will be invited to serve on the Conference Committee.

Attendance

It is expected that approximately 250 to 300 scientists will attend.

Program

Invited and contributed papers will be presented during the three day program. Not more than two simultaneous sessions are planned.

Sponsorship

The conference will be jointly supported by the U.S. Air Force Office of Scientific Research and the Massachusetts Institute of Technology.

Publications

Complete papers presented at the conference will be published in a volume of conference proceedings as promptly as possible. The conference programs will contain abstracts of papers to be presented.

Further details will be announced. Please address inquiries to Dr. Henry H. Kolm, Magnet Laboratory, Armory Building, Massachusetts Insititute of Technology, Cambridge 39, Massachusetts.

THIRD INTERNATIONAL CONFERENCE ON ANALOG COMPUTATION

(BELGRADE, September 4–9, 1961)

The Third International Conference on Analog Computation will take place in Belgrade from September 4th to 9th, 1961. This Conference, organised by the International Association for Analog Computation and the Yugoslav National Committee for ETAN, will be divided into four sections:

1. Theoretical considerations.
2. Analog computing equipment.
3. Application of analog methods and devices.
4. Connection between analog and digital techniques.

The first section will deal with general and specific theoretical problems concerning the principles of analog computation, the characteristics of computing equipment and the solution of various problems by analog methods.

The second section is devoted to practical achievements and experiences in the design and realisation of various analog computers and computing elements.

The third section will deal with the application of analog computing devices for simulation, computation and analysis in industry, science and engineering.

The fourth section will consider the relation between analog and digital techniques, their common aspects and interferences.

Apart from the scientific programme a special entertainment programme for the participants of the Conference and their families (visits, excursions, banquets) will also be arranged.

An exhibition of analog computing equipment and components will be organised during the Conference in conjunction with the International Fair of Technical Achievements which is held every Autumn in Belgrade.

The Conference may be attended by all persons interested, either as individuals or as elected representatives of scientific institutions or companies.

Each person taking part in the Conference is entitled to read a paper which must deal with questions concerning analog computation or related branches.

All correspondence relating to the Third International Conference on Analog Computation should be addressed to

YUGOSLAV COMMITTEE FOR ETAN
Terazije 23/VII, Belgrade
Yugoslavia

Companies wishing to participate in the exhibition of analog computing equipment are requested to contact the Organising Committee of the Conference who will be pleased to provide them with full information concerning terms and conditions of participation.

For the Organising Committee
L. Radanović
Secretary

ERRATA

G. Gianelli and L. Stanchi, Nonlinear operations on pulses by means of p — n junctions. Nuclear Instruments and Methods **8** (1960) 79.

Vol. 8 (1960) p. 79 first line of the second column: add at the end of the line the words "... energy and only related to the...".

A. F. Fischmann-Arbel and Israel Bar-David, A method of linear pulse amplifier design. Nuclear Instruments and Methods **7** (1960) 153.

1. Fig. 1. $K(p) = K_0/(1 + pT_1)\ (1 + pT_2)$

$$\beta(p) = \beta_0(1 + pT_3)/(1 + pT_4).$$

2. Fig. 5. V_7 is a 6197 pentode.

3. Fig. 6. The value of the choke between the plates of V_3 and V_4 is 2×125 mHy, and not 12.5 mHy.

The equivalent of tube 6061 (V_4) is the 6AQ5.

Spotlight on Industry

This section appears each month and features various happenings of interest in the nuclear industrial world and objective information on products of the nuclear manufacturers. It is offered entirely as a service and all nuclear manufacturers are cordially invited to submit clearly objective and descriptive material on their endeavours and product developments for consideration for use in this section.

FAST PULSE GENERATOR

E-H Research Laboratories, Inc., 163 Adeline Street, Oakland 20, California, U.S.A.

This E-H Model 130, has a repetition rate of 10 cps to 1 Mc/s, a rise and fall time of less than 10 mμs, two pulse outputs with a relative pulse delay between them of 200 mμs to 50 ms. With its provisions for external drive and electronic gating, its great range in pulse widths and delays, and arbitrary cable impedance feature, the Model 130 fills a long-standing need for a versatile pulser.

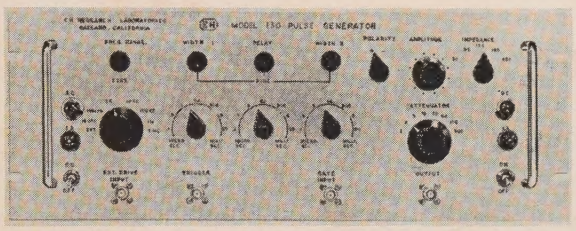

WHEELCO TRITIUM DETECTOR

Ad. Auriema, Inc. Exporters, 85 Broad Street, New York 4, N.Y., U.S.A.

Wheelco Instruments Division of the Barber-Colman Company announces a new tritium detector, to 225°C, in addition to the time-proven ionization detectors using strontium 90 and radium. Sensitivity is increased because tritium detectors have less base line noise than any other radioactive source: $\frac{1}{3}$ as noisy as strontium and $\frac{1}{30}$ as noisy as radium.

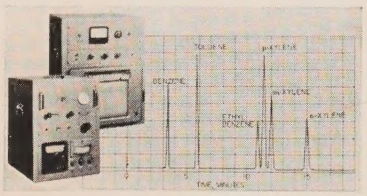

With a tritium source, the detector offers the ultimate in simplicity and can be cleaned regularly. Long life, with practically no maintenance or replacement is assured. Outstanding operating flexibility is provided because the same detector can be used for capillary or packed columns.

The chromatogram above shows complete separation of xylenes using tritium detector and 60 ft stainless steel capillary column. Temperature, 67°C; flow rate, 0.7 ml/min argon. Model 20, pictured above, is a compact, portable unit designed to use both capillary and packed columns. Also available, the Model 10, a large laboratory unit for single or dual operation.

HÖCHST REINE METALLE, HERGESTELLT IM ELEKTRONENSTRAHLSCHMELZOFEN

Degussa, Wolfgang bei Hanau (Main) Germany

Die Degussa hat in den letzten Wochen den ersten Elektronenstrahl-Schmelzofen Europas, der im Produktionsmassstab arbeitet, in Betrieb genommen.

Der Ofen unterscheidet sich im wesentlichen in der Art der Heizung von den bisher existierenden Vakumöfen. Von einer Wolframkathode werden Elektronen emittiert, die durch eine hohe Spannung von ca. 12 000 Volt beschleunigt werden. Sie erhalten dadurch Geschwindigkeiten von mehr als 60 000 km/sec und damit, trotz ihrer kleinen Masse, eine hohe kinetische Energie, die sich beim Aufschlag auf das zu behandelnde Gut in Wärme umsetzt und es zum Schmelzen bringt.

In diesem Ofen gelingt es, Metalle mit hohem Schmelzpunkt wie Wolfram, Tantal, Molybdän, Niob u. a. in einem Grade zu reinigen, wie es bisher unbekannt war. Der Prozess wird im Hochvakuum bei Drücken von 10^{-5} Torr durchgeführt und er reduziert unerwünschte Verunreinigungen zu niedrigeren Werten, als es beim Vakuum-Sintern oder Vakuum-Lichtbogen-Schmelzen möglich ist. Das Resultat sind Werkstoffeigenschaften, die bisher mit anderen Herstellungsmethoden nicht erreicht werden konnten. Sehr wahrscheinlich wird dieses Verfahren auch zur Reinigung nichtmetallischer Stoffe geeignet sein.

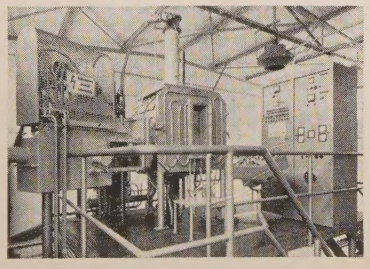

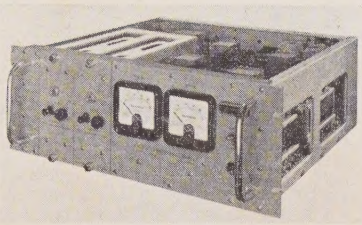

COMPUTER REFERENCE POWER SUPPLY EXCEPTIONAL STABILITY

Solartron Electronic Group Limited, Thames Ditton, Surrey

The Type AS 756.2 Computer Reference Power Supply—already known as the precision reference voltage source in Solartron "SPACE" Computers—is now generally available as an independent instrument. Two independent positive and negative outputs are provided, each capable of being loaded up to 200 milliamps.

Brief Specification

Outputs: + 100 V and — 100 V, 200 mA on each supply.

Accuracy and Stability: — 100 V better than 0.1% long term. + 100 V can be set to within 1 mV of negative supply and will remain within 5 mV.

Stabilisation Ratio: Better than 1000 to 1 on each supply.

DC Source Impedance: Less than 0.05 ohms on each supply

Ripple and Noise: Less than 15 mV pk–pk.

Size and Weight: 19″ × 17″ × 7″ hgih (48 × 43 × 18 cm) 55 lbs. (25 kg).

PUNCH TAPE SYSTEM

Nuclear Data Inc., 911 Regent Street, P.O. Box 1464, Madison Winconsin

Nuclear Data has recently announced the development and delivery of a punch tape system to work in conjunction with their ND-101 analyzer. The punch tape system consists of an ND-304 control unit, and ND-302 tape perforator and an ND-303 tape reader. This system allows you to read out on punch tape and read back into the memory with a previously punched tape. It is also possible to manually punch information with the ND-304 control unit.

RIDL MODEL 34-8, 200 CHANNEL PULSE HEIGHT ANALYZER

Radiation Instrument Development Laboratory, Inc., Northlake, Illinois

The RIDL Model 34–8 is an exceptionally versatile and reliable transistorized 200 channel pulse height analyzer. Flip a switch and it becomes a multichannel scaler (time analyzer). Flip another switch and the memory is split into two 100 channel or four 50 channel subgroups to allow for data runs in fast sequence without readout between. Use four detector systems, and the information will automatically be routed to the appropriate subgroup for each detector. Automatic subtraction of a standard reference or background does not affect the data stored in the memory. Data accumulates for a preset time followed by automatic readout to parallel or serial entry printers, tape punch or magnetic tape.

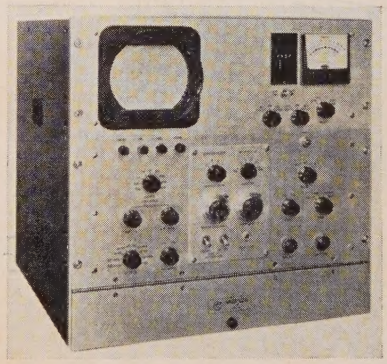

RIDL MODEL 34-12, 400 CHANNEL ANALYZER

Radiation Instrument Development Laboratory, Inc., Northlake, Illinois

The RIDL Model 34–12 Transistorized 400 Channel Analyzer is a completely new approach to multichannel analysis. Compactness, low consumption and extremely high reliability characterise the unit which also comprises multichannel scaler or time analyzer. The memory divides into four 100 channel or eight 50 channel subgroups for fast successive measurements without readout between. Four detector systems may be used with the information automatically routed to the appropriate subgroup for a preset time followed by an automatic readout of data. A standard reference spectrum or background stored in one half of the memory and then transferred to the other half will not affect the storage in the first half. This may be done continuously and automatically for successive runs.

NEW RIDL CATALOG

Radiation Instrument Development Laboratory, Inc., 61 East North Avenue, Northlake, Illinois.

The new RIDL 88 page *Catalog 61* described the radiation detecting and measuring instruments offered by this maker of quality electronic instruments. The Catalog gives general description and specifications on multichannel analyzers, spectrometers, scalers, ratemeters, pulse generators, coincidence/anti-coincidence analyzers, analog-to-digital converters, detectors, and other laboratory and industrial radiation instruments.

GRID CHAMBER

Intertechnique, Division Nucléaire, 81, rue Escudier, Boulogne, Seine, France

Alpha spectrometry with grid chamber allows a very good resolution on large surface sources.

The Intertechnique chamber claimed a resolution of 1 % in Pu^{239} and to accept 50 mm diameter sources.

Low noise preamplifier and all gas filling accessoires are included.